MODELLING OF THE PERFORMANCE OF STIRRED MEDIA MILLS IN REGRINDING CIRCUITS

KARIŞTIRMALI BİLYALI DEĞİRMENLERİN ARA ÜRÜN ÖĞÜTME DEVRELERİNDE PERFORMANSININ MODELLENMESİ

SERKAN DİKMEN

Submitted to
HACETTEPE UNIVERSITY
THE INSTITUTE FOR GRADUATE STUDIES
IN SCIENCE AND ENGINEERING
in partial fulfillment of the requirements for the degree of
PHYLOSOPHY OF DOCTORATE
in
MINING ENGINEERRING

2008

Fen Bilimleri Enstitüsü Müdürlüğü'ne,

Bu çalışma jürimiz tarafından **MADEN MÜHENDİSLİĞİ ANABİLİM DALI'nda DOKTORA TEZİ** olarak kabul edilmiştir.

Başkan	:...
	Prof. Dr. Ali İhsan AROL
Üye (Danışman)	: ....
	Prof. Dr. Ş. Levent ERGÜN
Üye	: ....
	Prof. Dr. Özcan Y. GÜLSOY
Üye	: ....
	Prof. Dr. Zafir EKMEKÇİ
Üye	: ....
	Doç. Dr. A. Hakan BENZER

ONAY

Bu tez / / 2008 tarihinde Enstitü Yönetim Kurulunca belirlenen yukarıdaki jüri üyeleri tarafından kabul edilmiştir.

..... / ..... / 2008

Prof. Dr. Erdem YAZGAN
FEN BİLİMLERİ ENSTİTÜSÜ MÜDÜRÜ

ÖZ

KARIŞTIRMALI BİLYALI DEĞİRMENLERİN ARA ÜRÜN ÖĞÜTME DEVRELERİNDE PERFORMANSININ MODELLENMESİ

Serkan Dikmen

Bu tez çalışmasında, karıştırmalı bilyalı değirmenlerin (KBD) öğütme performansının cevher hazırlama tesislerinde ara ürün öğütme devrelerinde kullanılan bilyalı değirmenlerle karşılaştırılmasına imkan verecek bir metodolojinin geliştirilmesi amaçlanmaktadır.

Bu amaçla gerçekleştirilen deneysel çalışmalar üç grup altında toplanabilir. Bunlar sırasıyla, laboratuvar ölçekli KBD testleri, pilot ölçekli KBD testleri ve Çayeli Bakır İşletmeleri (ÇBİ) flotasyon tesisinde yürütülen örnek alma çalışmalarıdır.

Kesikli öğütme testlerinde net hacmi 1,7 litre olan laboratuvar ölçekli KBD kullanılmış ve bu değirmende karıştırma hızı, öğütücü ortam boyu, öğütücü ortam dolum oranı, besleme malzemesi katı oranı ve farklı öğütücü ortamların (çelik bilya, çakıl ve zirkon bilya) ürün inceliği üzerindeki etkileri incelenmiştir. Pilot ölçekli KBD testlerinde net hacmi 19,8 litre olan değirmen kullanılmıştır. Pilot ölçekli değirmen ÇBİ flotasyon tesisinde belirlenen akımlara bağlanarak değirmenin açık devre öğütme performansı belirlenmiştir. Testler sırasında değirmen üzerinde bulunan torkmetre yardımıyla değirmen gücü ölçülmüştür. Bu testlerde, karıştırma hızı, besleme hızı, besleme inceliği, öğütücü ortam dolum oranı ve öğütücü ortam tipi (çelik bilya ve çakıl) gibi işlem değişkenlerinin ürün inceliği ve değirmen gücü üzerindeki etkisi incelenmiştir. ÇBİ flotasyon tesisinde yapılan örnek alma çalışmaları ile bakır flotasyon devresinde bulunan mevcut ara ürün öğütme devresinin performansı ve flotasyon tesisinde işlenen iki farklı cevher tipi (Spec ve Non- Spec cevher) için tüm tesis performansı belirlenmiştir. Ayrıca, flotasyon tesisindeki bazı akışlarda mineralojik çalışma yapılarak bu akışların tekrar öğütme gereksinimleri ortaya konmuştur. Bu veriler aynı zamanda mevcut ara ürün öğütme devresinin modellenmesi amacıyla da kullanılmıştır.

Sistematik laboratuvar testleri değirmende öğütme üzerindeki en etkin değişkenin karıştırma hızı olduğunu ortaya koymuştur. Testlerde değirmen içerisinde iri boyların tercihli olarak kırıldığı da gözlenmiştir. Bununla birlikte, farklı öğütme koşulları için ürün

tane boyu dağılımlarının tahmin edilebilmesi amacıyla self-similariteden yararlanılarak ampirik bir model başarıyla oluşturulmuştur.

Pilot ölçekli test sonuçları, laboratuvar ölçekli testlerden elde edilen verileri doğrular nitelikte olduğu görülmüştür. Pilot testlerde, değirmen gücünü ve ürün inceliğini etkileyen en önemli değişkenin değirmenin karıştırma hızı olduğu gözlenmiştir. Bununla beraber, öğütücü ortam yoğunluğunun ve öğütücü ortam dolum oranının da değirmenin çektiği güç üzerinde önemli bir etkilerinin olduğu belirlenmiştir. Flotasyon tesisinde KBD'nin farklı akışlara bağlanarak yapılan açık öğütme testlerinde bilyalı değirmenlerde ulaşılan öğütme sınırından daha ince ürün elde edilebilmesinin de mümkün olduğu görülmüştür.

Mükemmel karışım modeli, pilot KBD'nin modellenmesinde başarıyla uygulanmıştır. Modelleme çalışmasının sonuçları, hesaplanan r/d değerlerinin değirmenin çektiği güç ile normalize edilebileceğini ve bunun da farklı boyuttaki değirmenler de elde edilebilecek ürün tane boyu dağılımlarının belirlenmesinde kullanılabileceğini göstermektedir.

Tesiste yapılan örnek alma çalışmaları ile ÇBİ flotasyon tesisinde tekrar öğütme gereksinimi ile ilgili aşağıdaki yargılara varılmıştır:

- Bakır tekrar öğütme devresinde yapılan altı (6) örnek alma çalışması, tekrar öğütme devresinin performansının flotasyon devresi besleme tonajı, tenörü ve tesiste işlenen cevher tipine göre dalgalandığını göstermektedir.
- Devreden yük oranının düşük olduğu gözlenmiştir. Devreden yük oranı yükseltilerek değirmende enerji verimi arttırılabilecektir. Fakat, mevcut siklon besleme sampının kapasitesi arttırılmalıdır. Bu ayrıca siklon beslemesindeki dalgalanmalarıda önleyecektir.
- Flotasyon tesisinde iri boylarda bulunan bağlı taneler metal kaçağının ana nedenini oluşturmaktadır. Yüksek tonaj nedeniyle birincil öğütme devresinde istenen inceliğe ulaşılamaması bu kaçak miktarını arttırmaktadır.
- Bakır flotasyon devresinde, kaba süpürme devresi atığı içerdiği iri boydaki bağlı taneler nedeniyle ana metal kaybının gerçekleştiği akış olarak belirlenmiştir. Aynı zamanda, örnek alma çalışmaları sırasında pek çok hücrenin de boş olduğu gözlenmiştir. Bu nedenle, bakır kaba flotasyon devresi atığının mevcut ara ürün

öğütme devresinde öğütülerek süpürme aşamasına beslenmesinin verim artışına neden olacağı düşünülmektedir. Bu değişiklik aynı zamanda çinko flotasyon devresine beslenen malzemenin serbestleşme derecesini de yükseltecektir.

- Çinko flotasyon devresinde, kolon atığının tekrar öğütülmesi bu akıştaki serbestleşmeyi etkileyeceğinden kolon süpürme devresinin verimini artacağı ve bu aşamanın atığında gerçekleşen metal kaçaklarını azaltacaktır.

Sonuç olarak, deneysel ve modelleme çalışmalarının sonucunda, bir tesisteki farklı akışların, üzerinde güç ölçümünün yapılabileceği torkmetre bulunan KBD ile öğütülmesi, değirmenin öğütme performansının belirlenmesinde kullanılacak verilerin alınmasını sağlayacaktır. Boyut dağılımları ve güç ölçümleri herhangi bir uygulama için model geliştirilmesinde kullanılabilecektir. Son olarak, model değişkenleri özgül enerji tüketiminden yararlanılarak ölçeklendirilebilecektir. Geliştirilen bu model de ana işlem değişkenlerinin ürün tane boyu dağılımı üzerindeki etkilerinin hesaplanmasını sağlayacak kapasitede olacaktır.

Anahtar Kelimeler: Karıştırmalı Bilyalı Değirmen, İnce Öğütme, Modelleme ve Simülasyon
Danışman: Prof. Dr. Ş. Levent ERGÜN, Hacettepe Üniversitesi, Maden Mühendisliği Bölümü, Cevher Hazırlama Anabilim Dalı

ABSTRACT

MODELLING OF THE PERFORMANCE OF THE STIRRED MEDIA MILLS IN REGRINDING CIRCUITS

Serkan Dikmen

The aim of this study was to develop a methodology which can be used to determine the grinding performance of stirred ball mills at operating plants to compare and/or replace their existing ball mills.

Experimental studies were into laboratory scale stirred media mill tests, pilot scale stirred media mill tests and sampling surveys performed at ÇBİ's flotation plant.

In the batch tests, laboratory scale stirred media mill having 1.7 liter net volume was used. The effect of impeller speed, ball size, ball charge, %solids of the pulp and different grinding media types (steel balls, river pebble and zircon balls) on product fineness were investigated. Then, pilot scale stirred media mill having 19.8 liter net volume was installed at ÇBİ's flotation plant and the tests were conducted as open circuit on various streams in flotation plant. This mill has a torquemeter which allows measurement of power draw. In these tests, the effects of impeller speed, feed rate, feed fineness, ball charge and grinding media type (steel balls and river pebble) were investigated. Plant sampling surveys were accomplished to evaluate the performance of existing copper regrinding and whole flotation circuit for two different ore types (Spec and Non-Spec ore) processed in the plant. Mineralogy of the various samples in flotation circuit were studied to define regrinding requirements and limits. These data were also used to model the existing regrinding circuit.

Systemmatical laboratory tests showed that stirring speed of the mill was the dominating variable for size reduction. Preferential grinding of coarse particles was evident in all tests. An empirical model was successfully developed using the self similarity of size distributions produced under different conditions.

The results of the pilot scale tests verified the findings obtained from laboratory scale tests. The major operating parameter affecting the power draw and product fineness was the impeller speed of the mill. The density of grinding media and the media load had also

significant effect on power draw. The tests performed on various streams showed that it is possible to obtain finer products which are below the grinding limit of ball mill.
Perfect mixing mill model was successfully applied to the pilot scale stirred mill data obtained from various streams in ÇBİ's flotation plant. The results of modelling studies indicated that r/d*(the ratio of breakage and discharge rate of particles inside the mill) values can be normalized with power draw of the mill which enables to predict the product size distribution for any size mill.

Regarding to the regrinding requirements in ÇBİ flotation plant, the following conclusions were drawn:

- Six surveys carried out at the ÇBİ copper regrinding circuit showed that Cu regrinding circuit was operating at varying conditions due to changes in fresh feed tonnage and grade and ore type.
- Circulating load was found to be very low indicating possibility of increasing energy efficiency. However, the capacity of existing cyclone feed sump should be increased. This was also found to be necessary to avoid fluctuations in cyclone feeding.
- Locked particles at coarse sizes constituted the main reason of metal loss at the flotation plant. High metal loss at coarse fractions occured because the desired fineness was not achieved in primary grinding due to the high flowrate
- In copper flotation circuit, rougher scavenger tailing was found to be responsible for the main losses particularly due to the locked particles at coarse sizes. At the same time, most of the cells were idle during the surveys. Therefore, grinding of copper rougher tailing in the existing regrinding circuit and then feeding to scavenger cells would improve the recovery. Regrinding requirement should be evaluated after implementation of these modifications. This modification would also improve the liberation of zinc flotation feed.
- In zinc flotation circuit, column tail seemed the most promising stream for regrinding in the existing circuit. This application would improve the liberation in the column scavenger cells and may reduce the losses through scavenger tails.

After detailed experimental and modelling studies, it was concluded that grinding tests with a mill having a torquemeter on various streams in an operating plant would provide the required data to predict performance of stirred milling. Size distributions and power

measurements will than be used to develop a model for that particular application. Finally, model parameters can be scaled up by using specific energy consumption. The model will be capable of calculating the effects of main operating variables on size distribution.

Keywords: Stirred Media Mills, Ultra-fine Grinding, Modelling and Simulation

Advisor: Prof. Dr. Ş. Levent ERGÜN, Hacettepe University, Mining Engineering Department, Mineral Processing Division

ACKNOWLEDGMENTS

I wish to express my gratitude to Prof. Dr. Ş Levent Ergün for his assistance, valuable advice and constant encouragement which contributed immensely to the success of this investigation.

Prof. Dr. Zafir Ekmekçi and Prof. Dr. Özcan Gülsoy deserve special recognition for their suggestions made in the regular meetings we dedicated to the analysis of this research.

I would also like to express my most sincere appreciation to Dr. Namık Aydoğan and Doç. Dr. Hakan Benzer for their guidance, interest and contributions throughout the course of the research program.

I would also like to acknowledge the assistance, advice and friendship of E.Caner Orhan, A. Seyfi Erdem and Ömürden Genç on this study and other related subjects.

Finally, I wish to express my grateful appriciation to my parents for their understanding, interest and encouragement during my schooling.

TABLE OF CONTENTS

ÖZ... i
ABSTRACT iv
TABLE OF CONTENTS viii
INDEX OF FIGURES x
INDEX OF TABLES xv
1. INTRODUCTION 1
2. STIRRED MEDIA MILLS 5
    2.1. Fundamentals of Stirred Media Milling 13
        2.1.1. Flow patterns in stirred media mills 14
        2.1.2. Motion of A Single Grinding Media 21
    2.2. Important Grinding Mechanisms in Stirred Media Mills 25
        2.2.1. Estimation of Stress Intensity 28
        2.2.2. Estimation of Number of Stress Events 32
    2.3. Important Parameters Affecting the Comminution Performance in Stirred Media Milling 35
        2.3.1. Design Parameters 36
        2.3.2. Operating Parameters 36
            2.3.2.1. Mill Speed 37
            2.3.2.2. Media Size, Density and Filling Ratio 37
            2.3.2.3. Pulp Density 38
    2.4. Modelling Studies of Stirred Media Mills 39
    2.5. Case Studies 40
        2.5.1. McArthur River Mining (MRM) 40
        2.5.2. George Fisher Orebody 41
3. EXPERIMENTAL STUDIES AND RESULTS 43
    3.1. Laboratory Scale Stirred Media Mill Tests 43
        3.1.1. Tests carried out in Hacettepe University's laboratory 45
        3.1.2. Tests carried out in CBI's laboratory 50
    3.2. Pilot Scale Stirred Ball Mill Tests 52
4. EFFECT OF OPERATIONAL PARAMETERS ON GRINDING PERFORMANCE OF STIRRED MEDIA MILLS 59
    4.1. Laboratory Scale Stirred Media Tests 59
    4.2. Pilot Scale Stirred Media Tests 66
5. MODELING OF COMMINUTION PERFORMANCE OF STIRRED MEDIA MILLING 74
    5.1. Modelling of Batch Grinding Tests 74
        5.1.1. The Relationships Between the Operating Conditions and d_{50} 77

5.2. Modeling of Continuous Grinding Tests (Pilot Scale Stirred Media Mill) 92
5.3. Scale-Up of Stirred Media Mills 102
6. SAMPLING STUDIES CARRIED OUT AT CAYELI FLOTATION PLANT 105
6.1. Mass Balance Calculations 110
6.2. Copper Regrinding Circuit Surveys 112
6.2.1. 31/07/2006 Copper Regrinding Survey 113
6.2.2. 04/08/2006 Copper Regrinding Survey 116
6.2.3. 08/08/2006 Copper Regrinding Survey 119
6.2.4. 09/08/2006 Copper Regrinding Survey 122
6.3. Copper and Zinc Flotation Circuit Surveys 125
6.3.1. 28/08/2006 Copper and Zinc Flotation Circuit Survey – Spec Ore 126
6.3.2. 06/09/2006 Copper and Zinc Flotation Circuit Survey – Non-Spec Ore 130
6.4. Performance Evaluation of Copper Regrinding Circuit 133
6.5. Mineralogical Studies 137
6.5.1. Metallurgical Evaluations 143
6.6. Evaluation of Alternative Circuit Design in CBI Flotation Plant 145
7. CONCLUSIONS AND RECOMMENDATIONS 150
REFERENCES 152
8. APPENDICES 158
8.1. Appendix 1 158
8.2. Appendix 2 170
8.3. Appendix 3 179
RESUMÈ 193

INDEX OF FIGURES

Figure 1-1. A comparison of the effectiveness of vibratory, tumbling and stirred ball mill (Sepulveda, 1981) 2
Figure 2-1. Picture of Perl Mill 7
Figure 2-2. Schematic representation of CoBall® mill 8
Figure 2-3. Picture of MaxxMill® 9
Figure 2-4. Schematic representaion of Vertimill® 10
Figure 2-5. Picture of SMD® 12
Figure 2-6. Schematic representation of IsaMill® 13
Figure 2-7. Geometry of the stirred ball mill 15
Figure 2-8. Power characteristic of the stirred ball mill 16
Figure 2-9. Axial profiles of the tangential velocity, Re=2000 17
Figure 2-10. Radial and axial velocities, Re=10 18
Figure 2-11. Radial and axial velocities, Re=2000 18
Figure 2-12. Isolines of the energy density, Re=10 19
Figure 2-13. Isolines of the energy density, Re=2000 20
Figure 2-14. Part of the grinding chamber volume with high energy density and part of the entire energy input dissipated there 21
Figure 2-15. Influence of the radius ratio between ball and disk on the location of the stationary ball trajectory for ρ_b/ρ=2.5 and Re=2000 23
Figure 2-16. Influence of the density ratio between ball and fluid on the location of the stationary ball trajectory for R_b/R_d=1/120 and Re=2000 23
Figure 2-17. Influence of the Reynolds number on the location of the stationary ball trajectory for R_b/R_d=1/120 and ρ_b/ρ=2.5 24
Figure 2-18. Active volume 27
Figure 2-19. Ratio d_{act}/y as function of ratio d_{GM}/x for different á 28
Figure 2-20. Influence of the stress intensity on median size for a specific energy input of 1000 kJ/kg 32
Figure 2-21. Product fineness as a function of the stress intensity and the specific enery input 32
Figure 2-22. Influence of the stress intensity on the stress frequency 35
Figure 2-23. Zinc recovery increase from Isamilling 41
Figure 2-24. Mt. Isa Pb/Zn concentrator flow sheet 42
Figure 3-1. Comparison of size distributions of both feed materials used in the experiments 45
Figure 3-2. Particle size distributions of the products obtained from experiments (1-8) carried out in Hacettepe University's laboratory 47
Figure 3-3. Particle size distributions of the products obtained from experiments (9-16) carried out in Hacettepe University's laboratory 48
Figure 3-4. Particle size distributions of the products obtained from experiments (17-24) carried out in Hacettepe University's laboratory 49

Figure 3-5. Particle size distributions of the products obtained from experiments (25-28) carried out in Hacettepe University's laboratory ... 50
Figure 3-6. Particle size distributions of the products obtained from experiments (1-6) carried out in CBI's laboratory ... 51
Figure 3-7. Particle size distributions of the products obtained from experiments (7-9) carried out in CBI's laboratory ... 52
Figure 3-8. Particle size distributions of the products obtained from pilot scale tests (2-7)54
Figure 3-9. Particle size distributions of the products obtained from pilot scale tests (8-15) ... 55
Figure 3-10. Particle size distributions of the products obtained from pilot scale tests (16-23) ... 56
Figure 3-11. Particle size distributions of the products obtained from pilot scale tests (24-31) ... 57
Figure 3-12. Particle size distributions of the products obtained from pilot scale tests (32-36) ... 58
Figure 4-1. The change in the amount of material in each size fraction with grinding time ... 60
Figure 4-2. Changes of d_{50} values of products obtained from different grinding time ... 60
Figure 4-3. Effect of various impeller speeds on product fineness ... 61
Figure 4-4. Effect of changes in ball size on product fineness with various impeller speeds ... 62
Figure 4-5. Effect of %solid on product fineness ... 63
Figure 4-6. Effect of ball load on product fineness ... 64
Figure 4-7. Effect of material filling ratio on product fineness ... 65
Figure 4-8. Size distributions of products after stirred media milling with three different grinding medias ... 66
Figure 4-9. The relation between the impeller speed and power ... 68
Figure 4-10. Effect of different stirring speeds at 557 kg/h on product fineness ... 69
Figure 4-11. Effect of different stirring speeds at 765 kg/h on product fineness ... 69
Figure 4-12. Effect of different stirring speeds at 916 kg/h on product fineness ... 70
Figure 4-13. Effect of different feed rates at 1400 rpm on product fineness ... 71
Figure 4-14. The effect of ball charge to the mill on product fineness ... 71
Figure 4-15. The relation between media load and power ... 72
Figure 4-16. Effect of different grinding media on product fineness ... 73
Figure 5-1. Normalized particle size distribution ... 75
Figure 5-2. Comparison of the normalized particle size distributions ... 76
Figure 5-3. The calculated and measured normalized particle size distributions ... 76
Figure 5-4. The change in d_{50} with impeller speed for different media sizes ... 77
Figure 5-5. The change in d_{50} with media size for different impeller speeds ... 78
Figure 5-6. The change in d_{50} with solids content of the pulp for different impeller speeds ... 79
Figure 5-7. The change in d_{50} with media charge for different impeller speeds ... 80
Figure 5-8. The change in d_{50} with material load for different impeller speeds ... 80

Figure 5-9. The change in d_{50} with grinding media density for different impeller speeds.. 81
Figure 5-10. Variation of d_{50} with grinding time for 3 different impeller speeds and media sizes (steel balls) ... 83
Figure 5-11. Relationship between the variable a in the equation and the impeller speed for various ball sizes ... 84
Figure 5-12. Comparison of the calculated and measured particle size distributions ... 84
Figure 5-13. Variation of d_{50} with grinding time for 3 different impeller speeds and solids content of the pulp ... 86
Figure 5-14. Relationship between the variable a and %solid for different impeller speeds ... 86
Figure 5-15. Comparison of the calculated and measured particle size distributions ... 87
Figure 5-16. Variation of d_{50} with grinding time for 3 different impeller speeds and various media loads to the mill ... 88
Figure 5-17. Relationship between the variable a and media load for different impeller speeds ... 89
Figure 5-18. Comparison of the calculated and measured particle size distributions ... 89
Figure 5-19. Variation of d_{50} with grinding time for various materials used as grinding media ... 90
Figure 5-20. Relationship between the variable b and the density of grinding media ... 91
Figure 5-21. Relationship between the variable a and the impeller speed for different grinding media ... 91
Figure 5-22. Comparison of the calculated and measured particle size distributions ... 92
Figure 5-23. The effect of the impeller speed on r/d* function (zinc column scavenger tail stream) ... 94
Figure 5-24. The effect of feed flowrate on r/d* function (zinc column scavenger tail stream) ... 95
Figure 5-25. The effect of the impeller speed on r/d* function (copper cleaner 4 tail) ... 95
Figure 5-26. The effect of the media load on r/d* function (copper cleaner 4 tail) ... 96
Figure 5-27. The effect of the media density on r/d* function (copper cleaner 4 tail) ... 97
Figure 5-28. Comparison of particle size distributions of the streams fed to pilot stirred media mill ... 98
Figure 5-29. Normalized r/d* values ... 98
Figure 5-30. The relationship between the mill content and power draw for different impeller speeds ... 99
Figure 5-31. The relationship between the impeller speed and the slopes of the lines (C) in Figure 5-30 ... 100
Figure 5-32. Predicted and measured power ... 100
Figure 5-33. Energy-size reduction relationship for the attrition mill (Sepulveda, 1981) 102
Figure 5-34. Energy-size reduction relationship for the IsaMill (Weller et al., 1999)... 103
Figure 5-35. Energy-size reduction relationship for the pilot scale stirred media mill... 104
Figure 6-1. Locations of the sampling points for copper and zinc flotation circuit ... 108
Figure 6-2. Locations of the sampling points for copper regrinding circuit ... 110
Figure 6-3. Overall comparison of the raw and adjusted assays ... 111

Figure 6-4. Frequency distribution of the residuals in mass balance calculations 112
Figure 6-5. The result of mass balance calculation around regrinding circuit 114
Figure 6-6. Calculated and experimental particle size distributions around regrinding circuit 114
Figure 6-7. Mass balancing result of 31/07/2006 Cu Regrinding circuit survey 115
Figure 6-8. Efficiency curves of cyclones sampled on 31/07/2006 116
Figure 6-9. The result of mass balance calculation around regrinding circuit 117
Figure 6-10. Calculated and experimental particle size distributions around regrinding circuit 117
Figure 6-11. Mass balancing result of 04/08/2006 Cu Regrinding circuit survey 118
Figure 6-12. Efficiency curves of cyclones sampled on 04/08/2006 119
Figure 6-13. Mass balancing result of 08/08/2006 Cu Regrinding circuit survey 120
Figure 6-14. The result of mass balance calculation around regrinding circuit 121
Figure 6-15. Calculated and experimental particle size distributions around regrinding circuit 121
Figure 6-16. Efficiency curves of cyclones sampled on 08/08/2006 122
Figure 6-17. The result of mass balance calculation around regrinding circuit 123
Figure 6-18. Mass balancing result of 09/08/2006 Cu Regrinding circuit survey 124
Figure 6-19. Calculated and experimental particle size distributions around regrinding circuit 125
Figure 6-20. Efficiency curves of cyclones sampled on 09/08/2006 125
Figure 6-21. 28/08/2006 - mass balancing result of spec ore survey at copper and zinc flotation circuit 127
Figure 6-22. The result of mass balance calculation around regrinding circuit 128
Figure 6-23. Calculated and experimental particle size distributions around regrinding circuit 129
Figure 6-24. Efficiency curves of cyclones sampled on 28/08/2006 129
Figure 6-25. 06/09/2006 - Mass balancing result of non-spec ore survey at copper and zinc flotation circuit 131
Figure 6-26. Calculated and experimental particle size distributions around regrinding circuit 132
Figure 6-27. Calculated and experimental particle size distributions around regrinding circuit 132
Figure 6-28. Efficiency curves of cyclones sampled on 06/09/2006 133
Figure 6-29. Comparison of the size distribution of streams around the regrinding cyclones obtained from 6 sampling periods 135
Figure 6-30. Actual efficiency curves of regrinding cyclones obtained from 6 sampling periods 136
Figure 6-31. Corrected efficiency curves of regrinding cyclones obtained from 6 sampling periods 136
Figure 6-32. Comparison of particle size distributions of recirculating streams in Cu Regrind circuit and Cu RG Cyclone O/F 145
Figure 6-33. Simulated tonnages and %solids of the streams around regrinding circuit .. 146

Figure 6-34. Simulated particle size distributions of the streams around regrinding circuit 147
Figure 6-35. The comparison between the coarsest and the finest particle size distribution of regrind hydrocyclone overflow obtained from sampling surveys and the particle size distributions of several streams in flotation circuit after ground in pilot stirred ball mill 148
Figure 6-36. Overall liberation figures of Cu Rougher concentrate before and after grinding in stirred media mill 148

INDEX OF TABLES

Table 2-1. Performance of McArthur River since commissioning 40
Table 3-1. Specifications of laboratory scale stirred ball mill 44
Table 3-2. Size distributions of steel balls used in the experiments 44
Table 3-3. Parameters tested in experiments in Hacettepe University's Laboratory 46
Table 3-4. Parameters tested in experiments in CBI's laboratory 51
Table 3-5. Specifications of pilot scale stirred ball mill 52
Table 3-6. Parameters tested in the pilot stirred ball mill 53
Table 4-1. Specific energy consumption in the tests 67
Table 5-1. Relationship between the variable a and operating conditions 83
Table 5-2. Relationship between the variable b and the impeller speed 85
Table 5-3. Relationship between the variable a and %solid for different impeller speeds . 85
Table 5-4. Relationship between the variable b and the impeller speed 88
Table 5-5. Relationship between the variable a and media load for different impeller speeds 88
Table 5-6. Relationship between the variable b and the density of grinding media 90
Table 5-7. Tests' conditions and predicted-measured power draws 101
Table 6-1. Sampling points for copper and zinc flotation circuit 107
Table 6-2. Sampling points for copper regrinding circuit 109
Table 6-3. Geometrical parameters of regrinding cyclones in the cluster 113
Table 6-4. Parameters recorded in the control room during the survey 113
Table 6-5. Parameters recorded in the control room during the survey 116
Table 6-6. Parameters recorded in the control room during the survey 119
Table 6-7. Parameters recorded in the control room during the survey 122
Table 6-8. Parameters recorded in the control room during the survey 126
Table 6-9. Parameters recorded in the control room during the survey 130
Table 6-10. Mass-balanced flowrates and figures relating to the separation efficiency of cyclones 133
Table 6-11. The streams where samples were taken for mineralogical analysis 137
Table 6-12. The results of mineralogical analysis of each stream for Non-Spec ore 137
Table 6-13. The results of mineralogical analysis of each stream for Spec ore 140
Table 6-14. The comparison between the values P_{95} and P_{80} of the available finest and coarsest regrinding hydrocyclone overflow and the stirred media mill product 147
Table 6-15. Results from a test program and literature 149

1. INTRODUCTION

Due to the progress in technology, the demands for fine and ultrafine materials in several industries such as plastic, ceramics, paint, food, pharmaceutical, cosmetics etc. have been steadily increasing. In mining industry, depletion of high grade and easy to process deposits, the beneficiation of the low grade complex ores which can be liberated at very fine sizes is inevitable. On the other hand, current metal prices force companies to grind finer and finer to recover values even from tailings. Although the definition of fine grinding varies for different industries, in this study, grinding of particles to a size finer than P_{80} of 20 μm is referred.

Size reduction is well known for being an energy inefficient and energy intensive process. Considerable work has been done in the past in an attempt to find ways to improve the efficieny of this operation. In this regard, several types of wet and dry size reduction devices have been developed to meet the needs of industry for fine and ultrafine grinding. Stirred ball mills and tower mills are used in mineral processing while jet mills, planetery mill and vibrating ball mills are used in ceramics, paint, plastics etc. Although each equipment has its own advantages and disadvantages, application of stirred ball mills in mineral porcessing plants have been increasing especially at regrinding circuits where fine grinding is necessary. The fact that the amount of energy dissipated in unit time and unit volume inside the mill chamber is very much higher than those of tumbling ball mills and vibrating ball mills. This makes the specific energy consumption of this kind of equipment lower. A comparison of the effectiveness of vibratory, tumbling and stirred ball mill for producing ultrafine products from a chalcopyrite concentrate has shown that the stirred ball mill is capable of producing a finer product with a smaller energy input. These data are shown in Figure 1-1, as can be seen from the figure it is observed that for energy inputs exceeding 200 kWh/t the stirred ball mill continues to grind into the submicron range when size reduction in the other equipment has almost stop. In addition, in the micron range the capacity of the stirred ball mill is high relative to the other equipment because of the exceptionally high power input per unit volume of grinding chamber (Sepulveda, 1981).

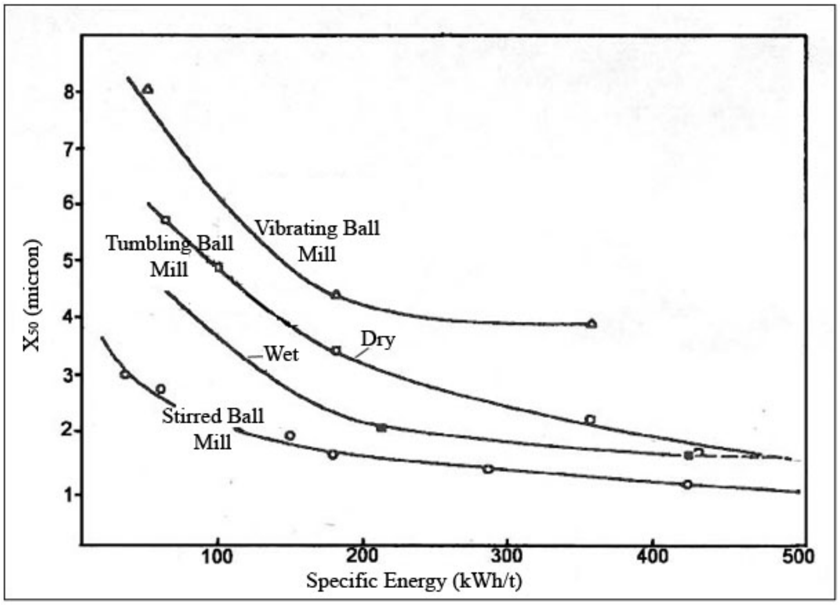

Figure 1-1. A comparison of the effectiveness of vibratory, tumbling and stirred ball mill (Sepulveda, 1981)

There are three main reasons why size reduction continues in stirred ball mill to submicron range as long as energy is provided. Stirred ball mill is free of the obstacles that limits the performance of tumbling ball mills. These are;

- Size of the grinding media,
- Media charge to the mill,
- Rotational speed of the mill.

Since the power delivered in tumbling ball mills is limited by the number of revolutions at which the grinding media are centrifugated at the chamber wall, the power density is relatively small. Thus, for the production of fine and ultrafine powders very long comminution times are necessary. To improve the efficiency in fine grinding, a mill with a vertical stationary grinding chamber is proposed in 1928, in which spherical grinding media are moved by a slowly rotating agitator. Such low-speed stirred media mills, also called ‘‘attritors’’, with circumferential speeds up to approximately 6 m/s are still built and used, mainly for fine grinding of minerals and ceramic materials. Parallel to further improvement of this mill (e.g., increase in length/diameter ratio of the vertical chamber) high-speed stirred media mills were developed, which were operated with circumferential stirrer speeds of 8 to 20 m/s and with smaller grinding media. While the first high-speed stirred media mills were vertically placed and had an open top with a sieve cage, today, mainly closed-type stirred media mills are in use. The grinding chamber of these closed stirred media mills can be arranged horizontally or vertically and is equipped usually with a water-jacket for cooling purposes. Usually 70 up to 85% of the free grinding chamber volume is filled with grinding media. Depending on the feed size and the feed material different grinding media sizes (usually between 200 and 4000 μm) and different grinding media materials (e.g., glass, steel, ceramic, pebble etc.) are employed. The grinding media are moved by a stirrer with circumferential speeds of up to 20 m/s, so that centrifugal accelerations of more than 50 times the acceleration due to gravity can be gained. Today, closed-type stirred media mills are built with grinding chamber volumes from less than 1 liter (laboratory scale) up to more than 10 m^3 and with drive powers of more than 2.6 MW.

An understanding of mechanisms behind any technology is the key to develop it further and this has become a subject of many researches trying to reveal how comminution takes place and how the parameters (design and operating) affect the comminution result in stirred media milling. CFD and DEM techniques enabled the researchers to determine the energy distribution and media motions in the grinding chamber and the correctness of these calculations were verified by high tech devices such as PET Scan. The results of these studies showed that there were two high energy intensive zones which are responsible to efficient size reduction in the stirred media milling. The parameters (design and operating) thought to be effective on grinding performance should be adjusted so that the grinding media can pass through these high energy intensive zones as much as possible. This situation leads the researchers to desing different mills in an attempt to optimize the media motion in the grinding chamber of the mills (Lane, 1999; Baker et al., 1999; Baker et al., 2001; Sinnott et al., 2006(a); 2006(b)). Several researchers have also made extensive work on determining the grinding mechanisms prevailing in the stirred media mills. They came up with the idea of stress intensity (the amount of energy consumed in each media collision) and stress number (the total number of media collisions), the product of stress intensity and stress number is the total amount of energy consumed in the grinding chamber. They also have tried to relate this energy with the comminution result to develop the model of the mill and predict the comminution result. Other researchers have used the population balance model to describe the change of the particle size distribution of the product with time or with the specific energy input (Heim and Leszczyniecki, 1985; Woodburn and Skentzos, 1987; Tüzün et al., 1995; Berthiaux et al., 1996; Varinot et al., 1997; 1999; Shinobara, 1999; Wang and Forssberg, 2000; Yue and Kline, 2004). All these studies were carried out laboratory scale devices and it is not the intent of this work to replicate these studies. However, in mineral processing plant, application of different stirred media mills have been prominent recently especially in the regrinding circuits where fine grinding is necessary to achieve sufficient liberation of valuable minerals. There are several equipments available on the market and VertiMill, SMD and IsaMill have found more applications. Especially, the IsaMills were first applied to McArthur River and George Fisher ore and allowed economic grinding to 80% passing 7 μm. The benefits of the usage of these mills were so profound in recovery and grade together with the appropirate regulations in the flotation stage.

Although the application of stirred media mills have been increasing, most of the industrial data have been published by the equipment manufacturers. On the other hand, many flotation plants around the world use conventional ball mills for regrinding purposes. Especially, quantitative comparison of the performance of conventional ball mills and stirred media mills is missing.

The aim of this study is to develop a methodology which can be used to determine the grinding performance of stirred ball mills at operating plants to compare and/or replace their existing ball mills. With this respect, by taking ÇBİ's(Çayeli Bakır İşletmeleri A.Ş.) flotation plant as an experimental site, detailed experimental studies were performed. Performance of existing copper regrinding circuit was evaluated by the data obtained through six surveys at the plant. Laboratory scale stirred ball mill tests were conducted to evaluate the effect of major operating parameters on the grinding performance. Continuous pilot scale stirred media mill tests were also performed on various streams at the plant with a mill having torquemeter which allows measurement of power draw. Mineralogy of the various samples in flotation circuit were studied to define regrinding requirements and limited laboratory flotation tests were conducted on selected streams before and after regrinding.

2. STIRRED MEDIA MILLS

A large number of different types of stirred media mills were developed by the industry, especially in the last 20 years. The various mill designs differ above all in their chamber and stirrer geometry as well as in the separation device, which allows free discharge of the product, but prevents the grinding media from leaving the mill. Usually, the grinding media are held back in the grinding chamber by a screen (e.g., flat screens, screen cartridges, rotating or stationary cylindrical screens) or by a rotating gap. In principle, the width of the rotating gap or the mesh width of the screen should be less than half the size of the grinding media. Since increasingly grinding media with sizes of a few hundred microns are used, screens are increasingly used instead of rotating gaps. They are usually designed and fixed in a manner, that they cause no dead zones in the grinding chamber and that they can be changed without emptying the grinding chamber (screen cartridges) and/or that a contact of the media with the screen can be mostly avoided by using the centrifugal force inside the mill or even by using a special kind of rejector wheel classifier.

One of the earliest device is a shot mill in which fluidization of the grinding media is obtained by several discs located along the impeller shaft. The shot mill uses a grinding media ranging from 0.5 mm to 2 mm and features a rotating filter mounted on and rotating with the shaft which protects the discharge area from grinding media and unground material. In the late 30's the USBM (U.S Bureau of Mines) developed an "attritor" with the purpose of conditioning minerals by removing surface contaminants for froth flotation. The attritor turned out to be a very efficient grinding device. It was later modified and patented by the USBM and by Union Process Inc. as the Szegvari attritor system. The USBM attritor consists of a cage like rotor turning inside a cage-like stator, both of which are held in a cylindrical water-jacketed container. Simpler in design is the Szegvari attritor which consists of a cylindrical water-jacketed vessel containing the grinding media which is fluidized with a central branched shaft. Descriptions of the use of the USBM attritor as a grinding device for grinding coarse kaolins to 2 μm particle size range were first published in 1960 (Feld et al., 1960). This study of "attrition grinding" of kaolin was continued by running both continuous open-circuit and closed-circuit tests, and later by investigating the operating variables of the process and large scale performance (Stanczyk and Feld, 1963; 1965; 1968; Davies et al., 1973). A summary of the grinding practice with the USBM attritor mills for different solid materials including autogeneous grinding of olevine and mica in both batch and continuous tests was published in 1980 (Davis et al., 1980). However, there is no information related to the operating characteristics of the Szegvari attritor in the open literature. Most of the information available consists of patents on this device granted to its inventor, Andrew Szegvari. The first one granted in 1956 describes several design characteristics of this stirred mill and gives three examples of typical application: grinding 60 μm ultramarine blue pigment to a product of 4 μm, producing and suspending finely divided particles in liquid, and grinding titanium dioxide alkyd paste to 6 μm (Szegvari, 1956). Suggested improvements to the original design were reported by Szegvari in the following years (Szegvari, 1961; 1964a; 1964b; 1969).

Very similar to the Szegvari attritor is the tower mill developed and marketed in Japan for over 40 years, the main difference being the use of an impeller with a screw shape. The mill, manufactured by the Japan Tower Mill Co. Ltd., is offered in two different kinds of models for both wet and dry operation. In order to reduce wear, the interior of the grinding vessel and the screw agitator are lined with abrasion-proof rubber, which at the same time makes the mill acid resistant and makes it possible to carry out chemical reactions while grinding.

Similar to the Tower mill in height to diameter ratio but having evolved from Szegvari attritors and Sand mill, Perl mills® of Draiswerke Inc. (see Figure 2-1) are characterized by the tall and comparatively small diameter grinding chambers fitted with high speed agitators. The agitators of various designs can be notably perforated discs or stationary pins fixed on both the rotor and chamber wall. Perl mills having nominal capacities up to 1000 liters are available. The grinding chamber in the Perl mill is oriented either horizontally or vertically. There are several other stirred media mills such as UFG Mill manufactured by RSG Inc. and Netszch Mill manufactured by Netszch Feinmahltechnik GmbH sharing the same operating principle of high stirring action of grinding media with agitator on which pins or discs are mounted in either horizontally or vertically oriented grinding chamber (Zheng, 1997).

Figure 2-1. Picture of Perl Mill

The Szego mill is a recent introduction to the field of comminution and it falls in the catagory of ring-roller mills. The mill consists of a stationary cylindrical grinding surface (stator), in which is housed a rotor. The rotor consists of helically grooved rollers which are suspended on flexible wire rope shafts fixed to the rotor. The mill can be top driven or bottom driven. The stator is water-jacketed. The material to be ground is fed by gravity, or pumped to the top of the mill. The particles upon entering the grinding zone are repeatedly crushed between the rollers and the stator. The primary forces acting on the particles are the shearing and crushing forces, caused by rotational and centrifugal motion of the rollers. The helical grooves on the rollers aid in the transport of material through the mill. The mill has a number of design variables which can be utilised to meet specific product requirements (Koka and Trass, 1985).

CoBall mills are different from the others because of their incorporation of stirring devices (see Figure 2-2). The grinding zone is created in the gap between a conical working vessel (stator) and a conicol rotor. The gap is in the range of 6.5 to 13 mm, depending on the model selected. The movement of the rotor creates radial movement of the grinding media. Momentum amplifies the outward motion, so that the product shear force increases steadily during the milling operation. Product is fed to the grinding chamber by an external variable flow pump. Grinding media and product are separated at the end of the cycle by a sieve located at the outfeed. Grinding media are automatically re-introduced into the product flow as it enters the grinding chamber, so that continuous circulation of the media in the grinding chamber is achieved (CoBall® Brochure).

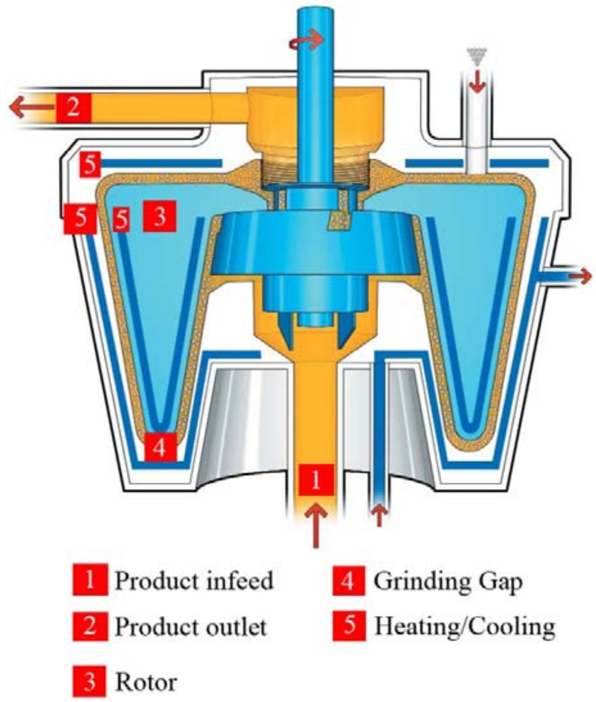

Figure 2-2. Schematic representation of CoBall® mill

The MaxxMill® is a newly developed stirred media mill of Maschinenfabrik Gustav Eirich GmbH&Co KG (see Figure 2-3). Its main components are the rotating grinding chamber, one or more agitator(s), and the stationary material deflector with integrated feed pipe. Each agitator is positioned eccentrically relative to the center of the grinding chamber. Depending on the comminution task, the agitator may rotate in the same or opposite direction as the chamber. The grinding chamber is filled with grinding media of 2 to 10 mm up to a volume of max. 90%. The grinding ball size used depends on the particle size of the raw material and on the desired product fineness. The MaxxMill® operates continuously in both dry and wet grinding processes. The grinding effect in the chamber is produced by the energy input via the agitator, the variable compression of the grinding ball filling in the agitator area, the compressive stress close to the bottom, and the generation of the shearing forces in front of the material deflector. The comminuted product is extracted continuously from the top of the ball layer by means of an extraction pipe with a big cross section installed in the upper part of the machine, where the grinding media, due to the gravitational force, are prevented from being discharged (Dürr, 2002; Wang, 2004).

Figure 2-3. Picture of MaxxMill®

Above mentioned machines, although they are being used effectively in both dry and wet grinding processes, have small dimensions and capacities. However, in mineral processing plants, the streams which needs further grinding especially for achieving the desired liberation of valuable minerals, have much higher capacities and need heavy duty machines. Stirred milling technology may be regarded as relatively new in minerals processing. However, it is a mature and extensively used technology in the ceramic, food, paint and pharmaceutical industries. One may say that stirred mills used today in mining and minerals processing are equivalent to the early models of stirred mills used in parallel industries. The most commonly used stirred mills in mining and minerals processing are the Vertimill®, Stirred Media Detritor (SMD®) and ISAMill®.

The predecessor of today's Vertimill® (see Figure 2-4) is the Tower Mill which was introduced in 1953 by the Nichitsu Mining Industry Co., Ltd. It was invented by a chemical engineer, Iwasaki Iskoichi, and developed further with input from others. In the beginning, different stirrer designs were tested, with the screw type stirrer being chosen as the standard for use as a consequence of this testing. After Iwasaki's death in 1954, a new company Nippon Funsaiki (Japan Crushing Machines) in Tokyo was founded to exclusively produce the Abrasive Toushiki (steeple-like) Crusher. Hereafter, as the crusher become widely used, it was named "Tower Mill" and in 1965 the Japan Tower Mill Co., Ltd was established. In 1983, Kubota Ironworks Co. purchased the Japan Tower Mill Co., Ltd, and it supplied the technology as Kubota Tower mills. The latest "owner" of Tower mill is Nippon-Eirich. In 1979, two Tower mills were supplied to the American Hoosier Power station, sparking interest in the technology by various American grinding equipment manufacturers. The Koppers Company, Inc. located in York Pennsylvania adopted the new fine grinding technology in the early 80's (Hively and Jons, 1983) after which the Tower mill was manufactured by MPSI under a license agreement with the Japanese. In 1991, the license expired and Svedala Industries, Inc obtained all rights to the technology, except the name which was changed to Vertimill®. Svedela Industries (now trading under the banner of Metso Minerals Ltd) have installed over 250 of these units around the world (Jankovic and Valery, 2005).

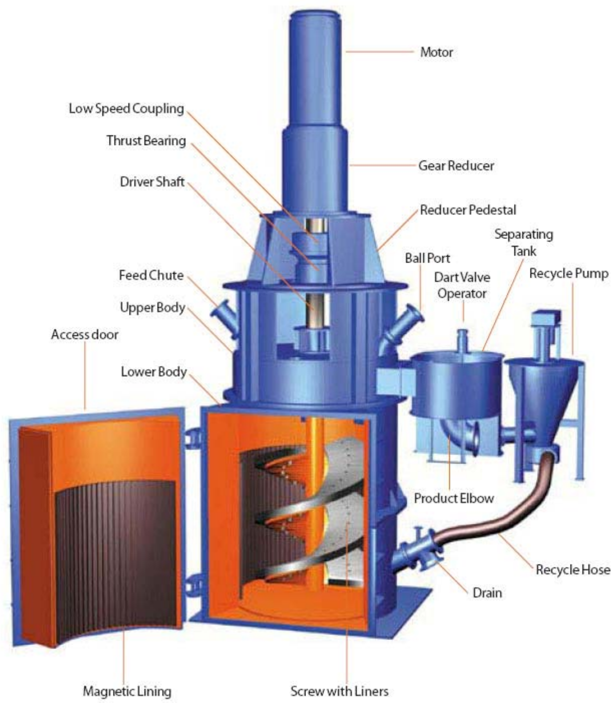

Figure 2-4. Schematic representaion of Vertimill®

The Vertimill® can grind feed material having up to 6 mm top size to produce product size ranges 74 to 2 µm or finer. It can be used in continuous and batch applications in open and closed circuit. Available motor power ranges from 20 to 1250 HP with capacities of up to 100 tph. In the Vertimill®, grinding media, such as steel balls or ceramic or natural pebbles, is stirred by an overhung double helix screw (or charge agitator). Feed material and water enter through an opening at the top of the grinding chamber. An external recycle pump provides a predetermined uprising velocity which causes a classification of particles in the upper portion of the mill body. Preclassification and removal of product sized feed reduces overgrinding and increases efficiency. The small particles rise, while the large particles are drawn into the media and ground. Grinding efficiency is enhanced by the relatively high pressure between the media and particles to be ground. The lower portion of the mill body is packed with media except for a small place directly below the screw flights. When steel balls are used, typical media depth is 160 to 200 cm. Grinding media rises within the screw flights and falls downward in the space between the flight tips and the inside diameters of the mill body. Pulp overflows from the mill body into a splitter box. The splitter box is equipped with a dart valve and control devices which split the pulp into a process stream and a recycle stream. The recycle stream is controlled to produce an optimum uprising velocity in the mill body for the specific grinding application. The process stream is either finished product or feed for an external classifying system (VertiMill® Brochure).

English China Clays developed an attrition stirred sand mill during the 1960's and in 1969 the first production scale machines were installed in a kaolin plant. Currently ECC, now Imerys, operate more than 200 attrition sand mills in their kaolin and calcium carbonate plants around the world. In 1996, Svedala and ECC signed a license agreement enabling attrition sand mills to be supplied for the Century Zinc Project. In the following year, this licence was expanded, enabling Svedala ,(and now Metso Minerals Ltd) to manufacture and supply the Stirred Media Detritor (SMD®) globally for all applications other than the white pigment industry (Figure 2-5). After extensive testing, four SMD® mills were installed at Pasminco's Elura operation in 1998 and 18 machines were installed in the Century Zinc concentrator in July 1999. Since 1998, 45 units have been installed in base metal concentrators all around the world (Jankovic and Valery, 2005).

Figure 2-5. Picture of SMD®

SMD® mills are available in a wide range of sizes, currently ranging up to 1100 kW machines, with the typical machine rating at 200 to 500 kW installed. The feed size to the SMD® mill depends on the product requirements but feeds up to 15 mm are common. This feed size would typically produce a product with a top size of 75 µm. This would then either be a product or would be suitable to act as the feed to further stages of SMD® mills producing products with d_{80}'s of 5 µm or less. SMD® mills consist of an octagonal body which supports the suspended internal multi-armed impeller. The impeller is driven by an electric motor through a single stage gear reducer. Both of these are supported by the top of the mill body. Feed slurry enters through a port in the top of the detritor. The impellers thoroughly intermix the feed slurry and the media. A predominantly axial flow regime throughout the grinding charge provides intense interparticle abrasion. This action utilizes the applied energy and maximizes grinding efficiency. The axial flow within the charge constantly circulates particles across the media retention screens. Milled product discharges through these screens which are located around the top half of the unit. The launder collects the product as it flows through the screen. The number of exit screens depends on the grinding requirements and the required feed flow rate (SMD® Brochure).

The IsaMill® (see Figure 2-6) was developed by Mt Isa Mines Limited and Netszch-Feinmahltechnik GmbH in the 1990s. By the end of 1994, this technology had become an integral part of the Lead/Zinc concentrator flowsheet. During 1995, the concentrator at McArthur Mining Limited commenced operation with a large 3 m^3 volume 1.1 MW IsaMill® (Enderle et all, 1997). IsaMill® is in fact a large version of the Netszch horizontal stirred mill which was being used for various ultrafine grinding applications in various chemical processing industries. To make this horizontal mill suitable for use in the mining industry, the mechanical engineering challenges involved in expanding the volume by a factor of 6 (the largest mill at that time being 0.5 m^3 in volume) were addressed. The most distinctive feature of the IsaMill® is its media separation system that enables slurry to exit the mill but prevents the grinding media from leaving the mill. Since this time, the IsaMill® technology has been implemented at several mining operations and undergone further development. The latest development is a 2.6 MW, 10 m^3 unit installed and operating in the Merensky Platinum Tailings retreatment process (Jankovic and Valery, 2005).

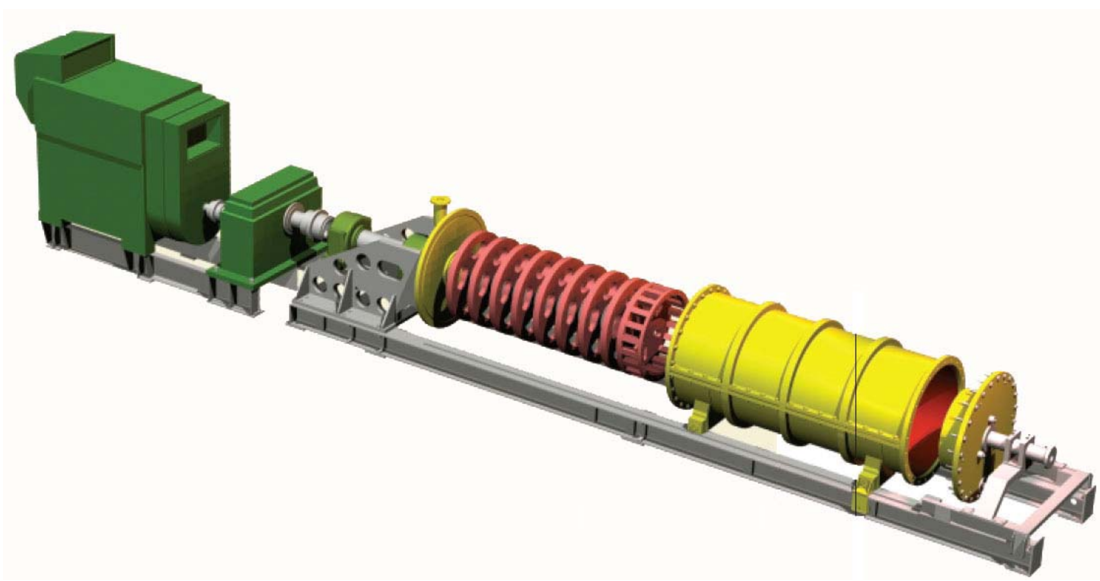

Figure 2-6. Schematic representation of IsaMill®

2.1. Fundamentals of Stirred Media Milling

For development and refinement of any technology, an understanding of its fundamental processes is required. Stirred milling development work in the mining industry up until this time has been limited to that related to simply adopting the technology and making it work in high throughput, low value product conditions: larger mill sizes, low cost grinding media, wear protection, etc. Only limited work on the fundamentals has been undertaken and there therefore remains many important issues of stirred milling operation which are not well understood by the industry.

Stirred media mills are used successfully for fine and ultrafine grinding of several products. Basically the stirred media mills consist of a stirrer placed in the center of a fixed grinding cylinder. The grinding chamber is filled with grinding media and a suspension containing the product particles. The filling rate of the grinding media (bulk volume related to the net volume of the grinding chamber) normally varies between 70 and 85%. By stirring the product-fluid-grinding media mixture a characteristic flow pattern and a grinding effect is generated in the grinding chamber. The respective kind of flow determines the spatial distribution of zones with high comminution intensity as well as the predominant type of comminution mechanisms and their composition.

Investigations have shown that the specific energy input (net energy input into the grinding chamber related to the mass or the volume of the product) is the main parameter which determines the comminution result. The specific energy describes the influence of mill size, circumferential speed of the stirrer, solids concentration of the suspension and density of the grinding media on the comminution result for a wide range. Thus, respective value of the specific energy characterizes the efficiency of comminution mechanisms which are mainly dependent on the motion of the grinding media and suspension. Further investigations show that beside the specific energy, the size of the grinding media strongly affects the comminution result. Thus, the combination of specific energy input and media size is very important for the prediction of the comminution result. Because the flow field in the grinding chamber determines the motion of the grinding media as well as the specific energy consumption, the physical connection between media size, specific energy and comminution result can be deduced by more detailed information about the physical events in the grinding chamber (Blecher et al., 1996; Blecher and Schwedes, 1996; Theuerkauf and Schwedes, 1999).

2.1.1. Flow patterns in stirred media mills

The mechanisms of motion of the stirred product-media-fluid mixture in the grinding chamber are very complex. According to Mölls and Hörnle, they are affected by 44 parameters and can only be calculated by means of an appropriate limitation of the problem with regards to a realizable mathematical method (Blecher et al., 1996). Therefore, the calculations regarding to determination of flow pattern and the specific energy distribution (related to the volume) are based on a laminar stirred, homogeneous Newtonian fluid (in the absence of media). Experimental investigations concerning the entire power consumption of a stirred media mill indicate that there should be a similar flow pattern in the grinding chamber both with and without media. The flow pattern of the stirred Newtonian fluid is calculated using CFD program. Furthermore, the distribution of the specific energy in the grinding chamber is calculated directly from the flow pattern previously determined. Finally, the motion of individual spherical balls exposed to the flow pattern of the stirred fluid is investigated. In all investigations, steady state stirring of the Newtonian fluid and discontinuous processing is provided (Blecher et al., 1996; Blecher and Schwedes, 1996; Theuerkauf and Schwedes, 1999; Lane, 1999; Kwade, 1999(a)).

The mill used in these investigations was a commercial stirred ball mill. Since the geometry is symmetrical in circumferential direction and due to the assumption that the endfaces of the mill have no effect on the flow pattern, the area to be calculated can be restricted to the domain shown in Figure 2-7 (Blecher et al., 1996; Blecher and Schwedes, 1996)

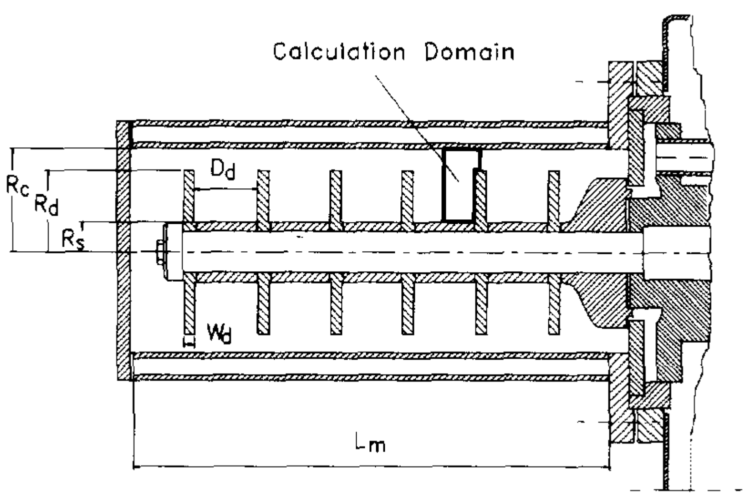

Figure 2-7. Geometry of the stirred ball mill

Figure 2-8 shows one of the experimental results of Weit characterizing the entire power consumption of the mill in terms of the Newton and the Reynolds number. Depending on the Reynolds number, three different ranges of power input which can be approximated using correlations known from stirring technology. Range I can be approximated by the power input of a cylindrical agitator operating in laminar state. The two other ranges are approximated by power inputs of disk stirrers operating in laminar (Range II) or turbulent (Range III) states. For the three ranges three completely different flow patterns in the grinding chamber with different energy distributions can be expected. The results confirm this assumption for the laminar ranges I and II. The turbulent range III has not been investigated yet (Blecher and Schwedes, 1996).

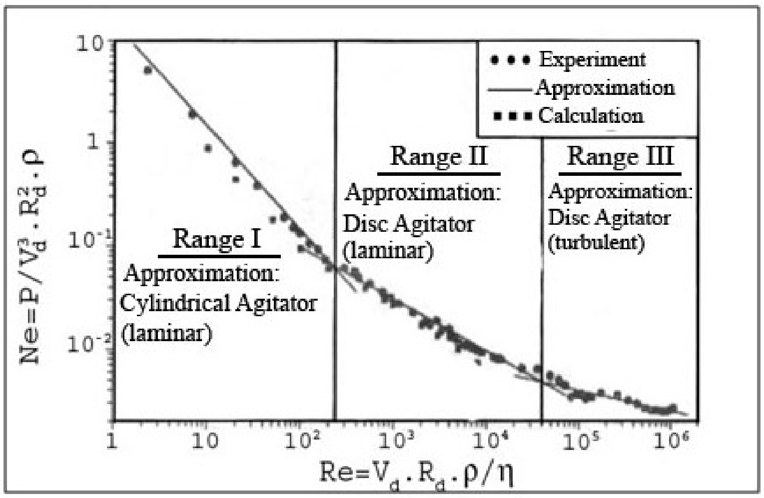

Figure 2-8. Power characteristic of the stirred ball mill

Figure 2-9 shows flow profiles of the non-dimensional tangential velocity calculated for Re=2000. The plot displays the calculation domain shown in Figure 2-7 which is located in the non-dimensional r-z plane. The left side of the calculation domain in Figure 2-9 is restricted by the agitator shaft whereas the right side is limited by the chamber wall. The bottom and the top limitations of the diagram are given by the lines of symmetry existing in the middle of the agitator disk and between two disks respectively. The direction of the tangential velocity is normal to the plane of representation.

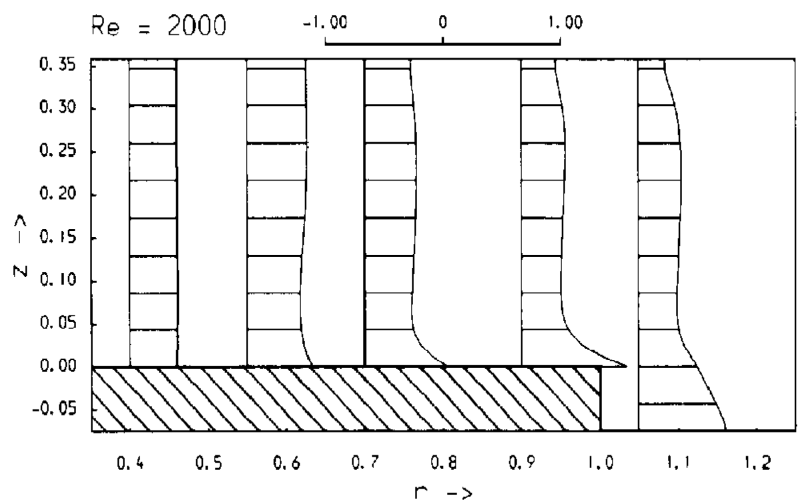

Figure 2-9. Axial profiles of the tangential velocity, Re=2000

In the vicinity of the shaft, the fluid is rotating like a solid body. Thus, for an identical radius the tangential velocity of the fluid corresponds to the velocity of the rotating disk. With increasing radial distance to the shaft a velocity profile develops with decreasing values in z-direction. The highest velocity gradients are located at the disk surface. Another porfile with a similar course can be found above the non-dimensional outer disk radius at r=1.05. Due to the no-slip condition at the disk surface maximum speed values of υ=1 occur at the outer radius of the disk. The shape of the velocity profiles in Figure 2-9 are characteristic for all investigated Reynolds number. By increasing the Reynolds number significant qualitative modifications of the flow profile just occur in the vicinity of the disk, where the gradients in axial direction become higher (Blecher et al., 1996; Blecher and Schwedes, 1996).

A characteristic results of the velocity distribution in the calculation domain for range I (Re=10) and range II (Re=2000) are shown in Figure 2-10 and Figure 2-11,respectively.

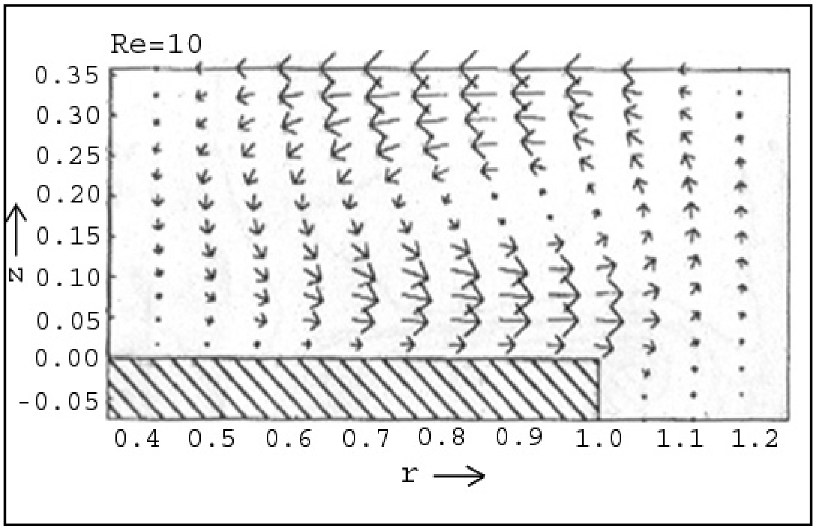

Figure 2-10. Radial and axial velocities, Re=10

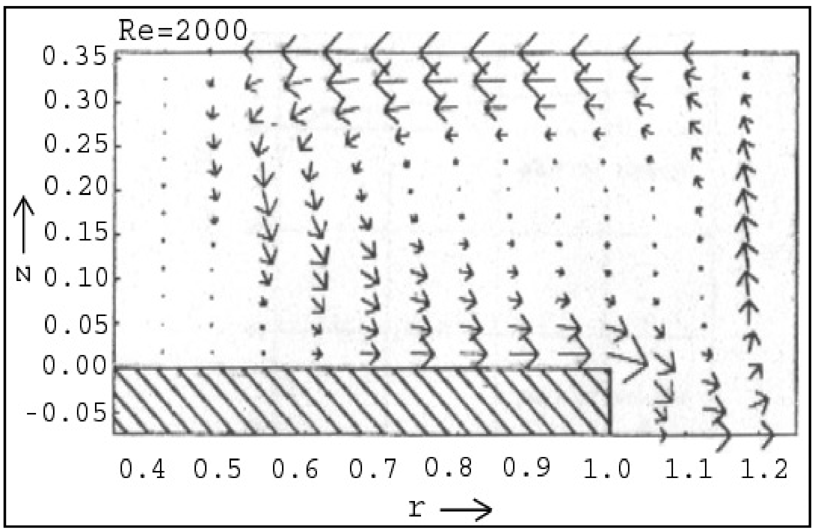

Figure 2-11. Radial and axial velocities, Re=2000

In Figure 2-10, velocity vectors which are composed of the radial and axial velocity components (secondary velocities) are represented. This figure proves that a cyclic flow exists in the r-z plane. The cyclic flow is caused by the driven outwards by the rotating disk (centrifugal effect). Having been driven outwards, the fluid is diverted at the chamber wall. In order to satisfy the continuity equation the fluid has to flow back to the direction of the shaft from where it is driven outwards again. The order of the magnitude of the secondary velocities is very low (see the scale at the right hand side of figures). This is a typical result for calculations carried out in range I of power input. In the vicinity of the outer disk radius and on the symmetry line between two disks the velocity reaches maximum values of about 8% of the circumferential speed of the agitator disk. Therefore, compared to the tangential velocities the secondary velocities are negligibly small. Thus, they do not contribute much to the specific energy consumption which is considerable responsible for the product fineness that can be achieved. Representing a typical calculation result in range II of power input Figure 2-11 shows the flow pattern of the secondary velocities that develops for Re=2000. Due to the centrifugal effect of the rotating disk a cyclic flow in the r-z plane also exists, but its location, its shape and the order of magnitude of the velocities differ from that shown in Figure 2-10. Higher velocities particularly occur in the periphery of the cyclic flow (vicinity of the disk surface, symmetry field between two disks, vicinity of the grinding chamber wall). Furthermore, the fluid flows more intensively through the area between the edge of the disk and the grinding chamber wall. This area as well as those in the direct vicinity of the grinding chamber wall and the disk surface are characterized by high gradients of the secondary velocities. In these areas the velocity vectors composed of the (non-dimensional) radial and axial velocities can come to maximum values of 20% of the circumferential velocity of the agitator disk. Thus, in range II the secondary and the tangential velocities are of the same order of magnitude and contribute to the same extent to the energy consumption. The basically different flow patterns in range I and II cause different distributions of the specific energy in the grinding chamber.

Figure 2-13 and Figure 2-13 shows isolines of the energy density for the Reynolds number 10 and 2000, respectively.

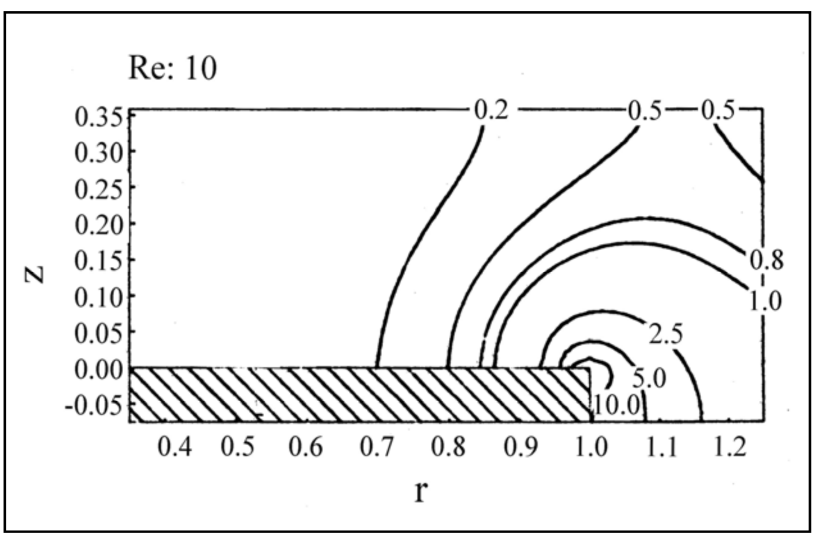

Figure 2-12. Isolines of the energy density, Re=10

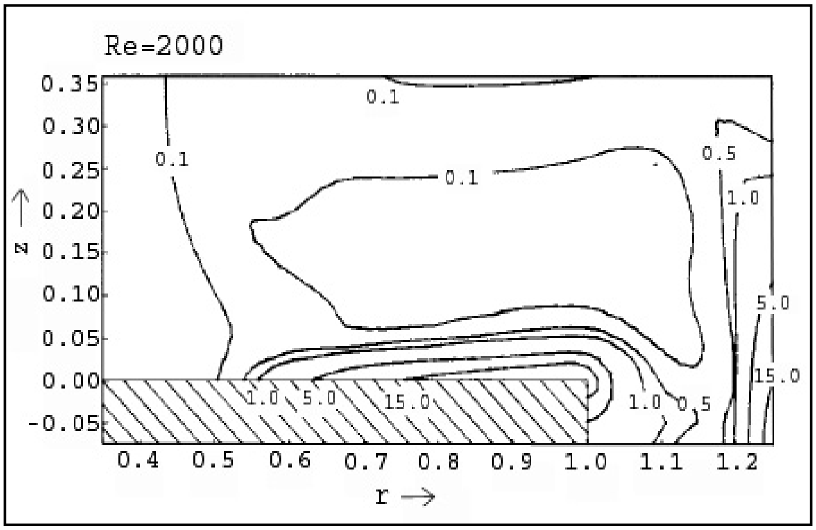

Figure 2-13. Isolines of the energy density, Re=2000

The energy density is defined as the ratio of the local to the mean specific energy which is calculated from the total amount of energy dissipated in the grinding chamber divided by the net volume of the grinding chamber. The isoline with the value of 1 in Figure 2-13 is of great importance. It separates the grinding chamber into different characteristic zones. In these zones the local specific energy is larger (high energy density) or smaller (low energy density) than the mean specific energy. For range I of the power input (see Figure 2-8) the isolines connecting the points of high energy densities (≥ 1) run normal from the disk surface, follow a semicircular way around the edge of the disk and end at the grinding wall. Only one single zone characterized by a high energy density exists. This zone basically extends from the edge of the disk up to the grinding chamber wall. Since high energy densities are indispensible for a successful comminution process this zone donates the area of the chamber where the comminution is most successful. The energy dissipation in this area is especially caused by the gradients of the tangential velocity. A different energy distribution is found for range II in Figure 2-13. In this case, two zones characterized by a high energy density exist. The first zone extends around the disk and runs very close to it. It arises from the high gradients of the tangential velocity and from the very high gradients of the radial velocity which are caused by the centrifuged fluid. The second zone is located near the grinding chamber wall. It results from gradients caused by the axial return transport of the centrifuged fluid which is directed to the top symmetry line. For Re=2000 (range II) the total area with high densities is much smaller than for Re=10 (range I). Hence, the specific energy distribution for range I is much more homogeneous than for range II. Figure 2-14 quantifies the last statement. It shows the volume percent of the entire grinding chamber with a high energy density (higher than the mean specific energy) as a function of the respective Reynolds number. The second curve indicates the portion of the entire energy consumption which is dissipated within this volume part. For small Reynolds numbers (range I) the volume percent increases slightly with increasing Reynolds numbers. For Re=100 it reaches its maximum of about 32%. This point marks a transition region from range I to range II. For Reynolds numbers greater than 100 the volume percent decreases continuously over the whole investigated range. For Re=8000 the volume part of the grinding chamber with a high energy density is just about 10%. But within this small subvolume about 90% of the entire energy is dissipated. Therefore, the zones where effective comminution takes place should be very small for range II. In order to achieve optimum comminution action it must be ensured that the product as well as the balls permanently pass these zones (Blecher et al., 1996; Blecher and Schwedes, 1996).

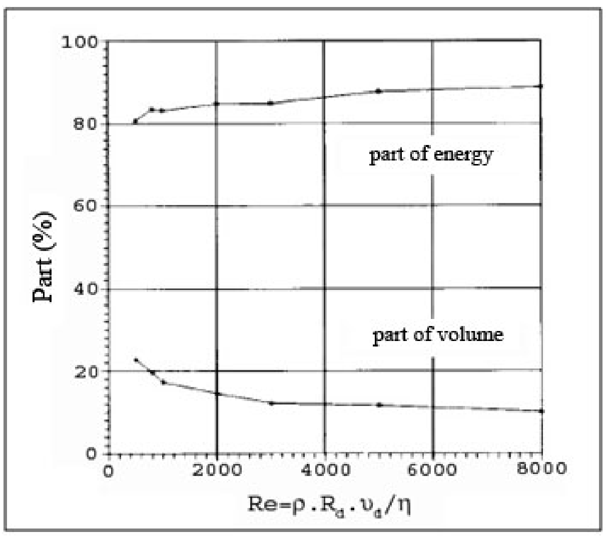

Figure 2-14. Part of the grinding chamber volume with high energy density and part of the entire energy input dissipated there

2.1.2. Motion of A Single Grinding Media

The main part of the entire energy is converted in the two small zones of high energy density. Therefore, optimum comminution results can be expected if grinding ball pass permanently through these zones. The calculated results concerning the motion of a single ball will show which kind of grinding balls lead to optimum comminution. All calculated results have shown that a single ball which is exposed to the flow field in the grinding chamber tends to follow a stationary trajectory. The moment when the ball reaches this trajectory depends on the starting conditions (position and ball velocity). The course of the stationary trajectory is determined by the radius (radius of ball R_b and stirrer disk R_d) and density ratio (density of ball ρ_b and pulp ρ) as well as the Reynolds number.

In Figure 2-15, four different stationary trajectories representing four different radius ratios R_b/ R_d are depicted. The density ratio of $\rho_b/\rho=2.5$ is kept constant. The trajectories are projected into the non-dimensional r-z plane. Therefore, the ball motion in circumferential direction cannot be seen. A graphical indicator for the tangential motion is given by the squares which are plotted at the graphical starting position as well as every time the ball passes a complete cycle of 360° in the grinding chamber. The distance between two adjacent spherical symbols on a trajectory which are calculated for regular non-dimensional time intervals is an indicator of the ball velocity in the r-z plane. Besides the motion in circumferetial direction, all balls move in a counter-clockwise direction along their individual trajectory located in the r-z plane. The smallest balls ($R_b/R_d=1/240$ and $R_b/R_d=1/120$) follow almost the same stationary trajectory which leads them through both zones of high energy density. On their way along these trajectories, both balls almost follow the streamlines of the stirred fluid. For increasing radius ratios the stationary trajectories are constricted and shifted towards the top symmetry line. The largest ball ($R_b/R_d=1/30$) does not reach the zones of high energy density when following its trajectory. As the ball moves along the top symmetry line down to the shaft, a ball exchange between the two adjacent mill domains now takes place. A ball leaving the calculation domain is replaced graphically by another one entering at a corresponding angle. The course back to the grinding chamber wall runs closer to the top symmetry line. In so-doing the ball moves partially against direction of the fluid flow. The complete trajectory is located in regions where low energy densities are predominant.

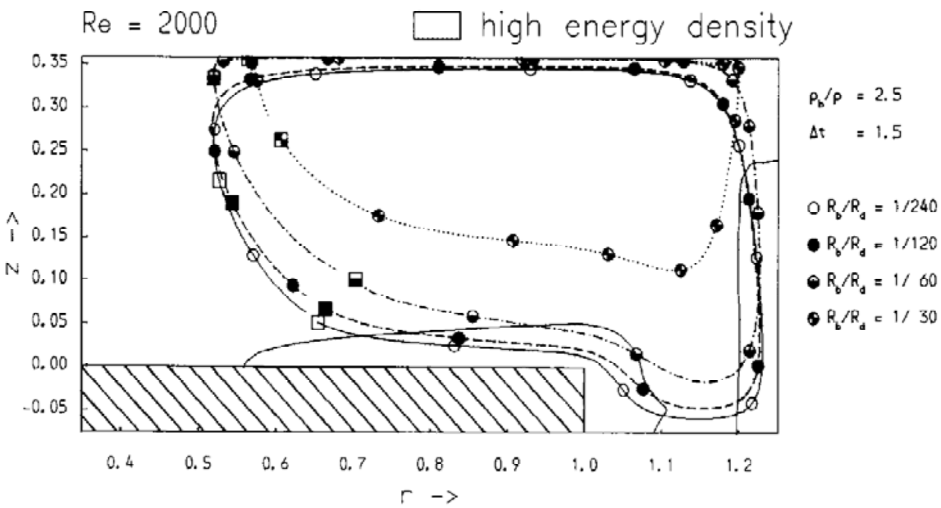

Figure 2-15. Influence of the radius ratio between ball and disk on the location of the stationary ball trajectory for ρ_b/ρ=2.5 and Re=2000

Figure 2-16 indicates the influence of the density ratio on the location of stationary trajectories. The radius ratio of R_b/R_d=1/120 is kept constant. An increase of the density ratio from 2.5 to 7.6 leads to a displacement of the stationary trajectory to the top symmetry line. The ball moving along this trajectory only passes the zone of high energy density located at the grinding chamber wall. The course of the trajectory does not always correspond to the streamlines of the stirred fluid.

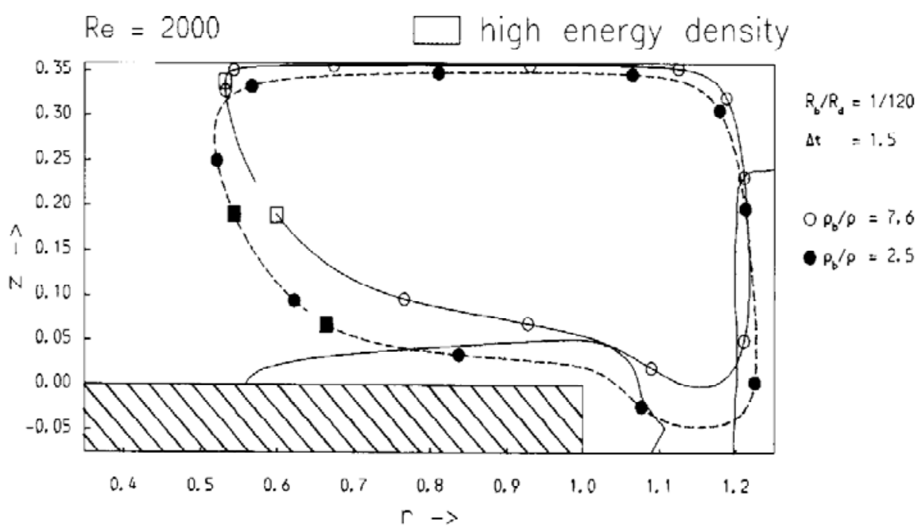

Figure 2-16. Influence of the density ratio between ball and fluid on the location of the stationary ball trajectory for R_b/R_d=1/120 and Re=2000

Finally, Figure 2-17 shows the influence of the Reynolds number on the stationary trajectory. The results have been obtained using a constant radius ratio of $R_b/R_d=1/120$ and a constant density ratio of $\rho_b/\rho=2.5$. The zones of high energy density are not plotted in Figure 2-17 because their extension (but not their location) varies slightly for the different Reynolds numbers. For Reynolds numbers of 800 and 2000 both trajectories run through the regions next to the disk surface and close to the grinding chamber wall where high energy densities exist. Balls moving along these trajectories basically follow the fluid flow. For increasing Reynolds number (Re=8000) the trajectory is constricted and shifted towards the top symmetry line where low energy densities are predominant.

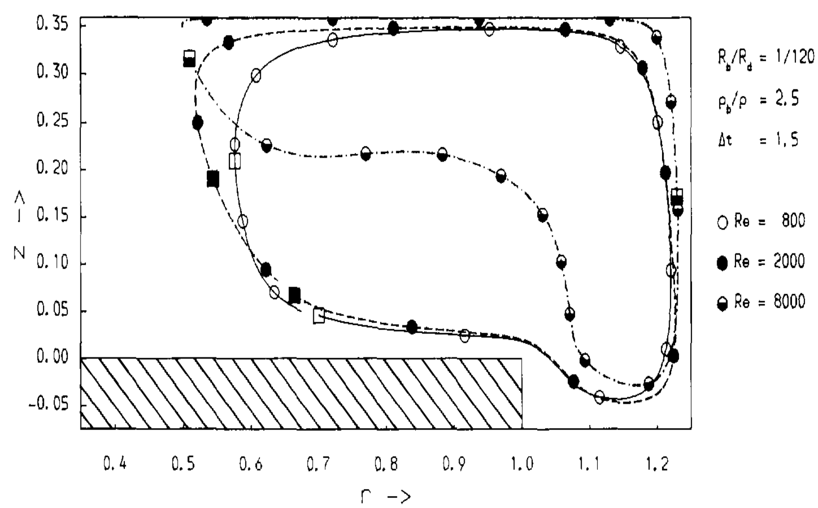

Figure 2-17. Influence of the Reynolds number on the location of the stationary ball trajectory for $R_b/R_d=1/120$ and $\rho_b/\rho=2.5$

Calculations concerning the prediction of trajectories of single ball have shown that the influence of the radius ratio of ball to disc, the density ratio of ball to fluid and the Reynolds number on the ball motion can be described by the so-called motion index given in Eq. 2-1 below.

$$M_{sb} = [R_b^3 \times (\rho_b - \rho) \times \vartheta_d^2] \times \left(\frac{1}{R_d}\right) \times \left(\frac{\rho}{\eta^2}\right) \qquad \text{Eq. 2-1}$$

Where,

R_b ball radius, m
R_d disc radius, m
υ stirring speed, m/s
ρ_b ball density, kg/m^3
ρ fluid density, kg/m^3
η dynamic viscosity, Pa.s

At small values of the motion index, the ball motion is dominated by the drag force so that the ball basically follows the fluid flow and passes the zones of high energy density. Above a transition region, high values of the motion index describe a ball motion that is dominated by inertia forces. Then the ball does not follow the fluid flow and tends to move in the vicinity of the top symmetry line where low energy densities exist. Using a bulk of balls, a small motion index which ensures ball transport dominated by the drag force indicates a favourable operating conditionof the mill because all balls basically follow the streamlines of the stirred fluid. Therefore, for small motion indeces, a homogeneous ball distribution over the entire grinding chamber can be expected and thus enough balls come into the zones of high energy density. Here they contribute most effectively to comminution. For a fixed operating point of a stirred media mill, this situation can mainly be adapted by the choice of sufficiently small balls. In contrast, a high motion index, which describes a ball motion dominated by inertia forces, indicates an inhomogeneous ball distribution over the grinding chamber, whereas the highest ball concentration will be found in the zone extending around the top symmetry line. Only a few balls are found in the zones of high energy density and consequently the comminution result becomes worse (Blecher et al., 1996).

2.2. Important Grinding Mechanisms in Stirred Media Mills

It is known that the stirred media mills are capable to produce a product fineness in the micron and submicron range. But it is not still clear, where in the mill and in which way the particles are stressed and broken. Two conditions have to be fulfilled in order to break a sufficient quantity of product particles in a certain time (Kwade et al., 1996; Kwade, 1999(a); 1999(b); Kwade and Schwedes, 2002).

These are;

- The number of stress events in the mill per unit time, i.e., the number grinding media collisions per unit time, has to be strong enough,
- The intensity at a high percentage of the stress events must be sufficient to break the feed particles and the resulting fragments.

Crystalline particles can only be broken when they are stressed between two grinding media or between a grinding medium and the chamber wall. An important condition that particles are stressed between two grinding media is that the particles are captured by the grinding media and are not carried out by the displaced fluid. According to the number of captured particles, three cases can be distinguished as follows (Kwade, 1999(b)).

- Only one particle is captured, which is stressed with the entire energy or force, respectively (single particle stressing),
- More than one particle is captured between two media, all particles have contact to both media during the stress event and all particles are stressed independent of each other. In this case, at first the particle is captured, which has the largest size and/or which has the smallest distance to the connection line of both media center. This particle is stressed with the maximum energy or force. The particles, which are captured between the two media after the first particle, are stressed with a considerable reduced energy or force,
- A particle bed is captured and stressed between two grinding media.

The number of captured particles depends among others on the solid concentration of the suspension and the size of the particles and can be evaluated by the ratio between the diameter of the active volume between two grinding media (d_{act}), and the average distance between two particles in the suspension (y) (Figure 2-18). Based on this, Eq. 2-2 can be given for the ratio d_{act}/y.

$$\frac{d_{act}}{y} = \sqrt[3]{\frac{6 \times C_v}{\pi}} \cdot \sqrt{2 \cdot (1 - \dot{a}) \cdot \frac{d_{GM}}{x} + 1 - \dot{a}^2} \quad ; \quad \dot{a} = \frac{a}{x} \qquad \text{Eq. 2-2}$$

Where,

C_v : the solids volume concentration of the suspension
a : the minimum distance of the grinding media, m
d_{GM} : diameter of grinding media, m
x : the particle size, m

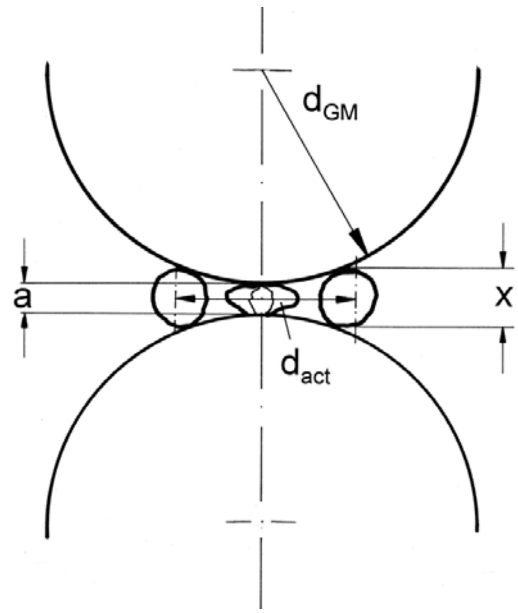

Figure 2-18. Active volume

The ratios d_{act}/y, which are obtained for different relative distances *á* at a solids concentration of 20% by volume are shown in Figure 2-19 as a function of the ratio between media and particle size. The ratio d_{act}/y required for capturing more than one particle increases with decreasing particle size. Since on the other hand at constant media diameters the ratio d_{GM}/x increases with decreasing particle size x, overall the probability that more than one particle is captured should increase with decreasing particle size. Moreover, at a solids concentration of 20% by volume and at a average particle size below 2 μm the suspension viscosity increases and thus, the freedom of motion decreases. Therefore, in the particle size range below 2 μm probably more than one particle can be captured and stressed between two grinding media. But only at very high product fineness (average particle size below 1 μm) it seems possible that a particle bed is stressed between two media (Kwade et al., 1996; Kwade, 1999(a); 1999(b); Kwade and Schwedes, 2002).

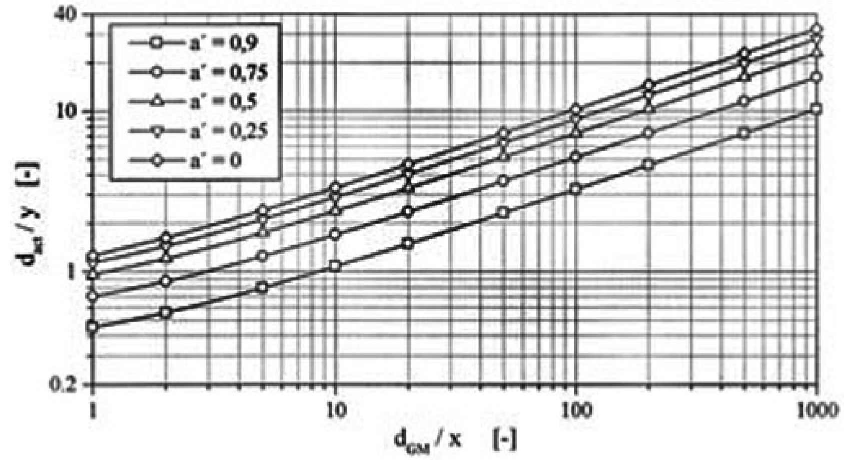

Figure 2-19. Ratio d_{act}/y as function of ratio d_{GM}/x for different á

2.2.1. Estimation of Stress Intensity

Relations for the stress intensity can only be derived, if it is known, where and how comminution takes place in stirred media mills. Information about the stress events in stirred media mills can be deducted from the motion of grinding media in the mill. Reseachers suggested three different grinding mechanisms which cause particle breakage in stirred ball mills (Kwade, 1999(a); 1999(b); Kwade, 2004).

- Product particles can be stressed by grinding media which are accelerated from the stirrer shaft towards the grinding chamber wall and thus take up kinetic energy, which can be used for stressing particles,
- Product particles can be stressed by grinding media which are pressed against the chamber wall because of the centrifugal accelerration. The particles are stressed by the pressure acting between the grinding media,
- Product particles can be stressed by grinding media which move in tangential direction with high velocities and collide with grinding media with lower velocities. Thus, they loose a part of their kinetic energy which can be used for comminution.

The intensity of grinding media mills can be described either by the force acting on a grinding medium or by the kinetic energy of a grinding medium. In stirred media mills, usually only one particle is stressed intensively between two grinding media as long as the particles are not much smaller than 1μm and/or the solids concentration is not extremely high. Therefore, the stress intensity acting on a particle between two grinding media can be described either by the energy related to the particle volume or by the force related to the cross-sectional area. In case of mechanism A, the media is accelerated in the vicinity of the disc from the stirrer shaft towards the grinding chamber wall. Thereby, the media take up kinetic energy, which can be used for comminution when the media collides with media which are based on the chamber wall and, thus, which have no or nearly no radial velocity. This process is comparable to the one in a tumbling ball mill, in which grinding media are dropped from the upper part of the grinding cylinder and fall on the bulk media in the lower part of the grinding cylinder. In this case, the stress intensity is determined by the kinetic energy of the medium and the volume of the captured product particle. The specific energy $E_{V,GM}$ which is related to the volume V_p of the captured particle, can be calculated (Eq. 2-3):

$$E_{V,GM} = \frac{1}{2} \cdot \left[1 - \left(\frac{d_S}{d_D}\right)^2\right] \cdot \left(\frac{d_{GM}}{x}\right) \cdot \left(\rho_{GM} - \rho_{susp}\right) \cdot \vartheta_{GM}^2 \qquad \text{Eq. 2-3}$$

Where,

d_S : diameter of the stirrer shaft, m
d_D : diameter of the disc, m
d_{GM} : diameter of the grinding media, m
x : mean particle size, m
ρ_{GM} : density of the grinding media, kg/m^3
ρ_{susp} : density of the suspension, kg/m^3
υ_{GM} : the tangential velocity of the grinding media, m/s

In case of mechanism B, the grinding media in the vicinity of the chamber wall have no radial velocity. Because of the centrifugal force they are based on the grinding chamber wall. Comminution takes place by a combined normal and shear force between the grinding media. As a measure for the stress intensity the centrifugal force, F_C, related to the cross-sectional area of the captured particle, A_p, can be used. For the calculation, the centrifugal force at the outer circumference of the disc was taken (Eq. 2-4):

$$\frac{F_C}{A_p} = \frac{4}{3} \cdot \left(\frac{d_{GM}}{x}\right)^2 \cdot \left(\frac{d_{GM}}{d_D}\right) \cdot \left(\rho_{GM} - \rho_{susp}\right) \cdot \vartheta_{GM}^2 \qquad \text{Eq. 2-4}$$

Where,

d_D : diameter of the disc, m
d_{GM} : diameter of the grinding media, m
x : mean particle size, m
ρ_{GM} : density of the grinding media, kg/m^3
ρ_{susp} : density of the suspension, kg/m^3
υ_{GM} : the tangential velocity of the grinding media, m/s

In case of mechanism C, grinding media with different velocities collide. Since the tangential velocities are usually much higher than the axial and radial velocities, only the tangential direction is considered. Two grinding media, which move with different tangential velocities $\upsilon_{GM,1}$ and $\upsilon_{GM,2}$ ($\upsilon_{GM,1} > \upsilon_{GM,2}$), have different kinetic energies. For the evaluation of the stress intensity, it is assumed that the impacts are straight and inelastic and that the faster medium is decelerated from the velocity $\upsilon_{GM,1}$ to the velocity of the slower medium, $\upsilon_{GM,2}$. The difference between the energies of the faster medium before and after the collision, ΔE_{kin}, is used for stressing the captured particle (Eq. 2-5):

$$\Delta E_{kin} = \frac{1}{2} \cdot \left(\frac{d_{GM}}{x}\right)^3 \cdot \rho_{GM} \cdot \left(\vartheta_{GM,1}^2 - \vartheta_{GM,2}^2\right) \qquad \text{Eq. 2-5}$$

Where,

d_{GM} : diameter of the grinding media, m
x : particle size, m
ρ_{GM} : density of the grinding media, kg/m^3
$\upsilon_{GM,1}$ and $\upsilon_{GM,2}$: the tangential velocity of the grinding media, m/s

The importance of the three grinding mechanisms A, B and C for the comminution result can be evaluated based on the theoretical considerations and the comparison of theoretical with experimental results. The considerations regarding the stress intensity show that by grinding media which are pressed against the chamber wall because of the centrifugal acceleration even with large grinding media only particles sufficiently smaller than 10 mm can be broken completely (mechanism B). Moreover, the velocity gradients in tangential direction are clearly smaller at the chamber wall than near the disk. Therefore, because of the clearly higher stress intensity the zone near the stirrer disc is much more important than the zone at the chamber wall, especially if particles larger than 10 mm have to be ground. When a grinding medium moves through the zone of high power density near the disc, the medium is accelerated in radial direction taking up kinetic energy and collides with a medium which is based on the chamber wall. Therefore, usually mechanism A occurs only once during a complete revolution in the radial–axial plane. Against that media collisions because of velocity gradients in tangential direction can occur several times during one revolution and, thus, during one passage through the zone near the disc (mechanism C). Therefore, most of the particles are broken by mechanism C in the zone near the stirrer disc, especially if coarser feed particles have to be ground (Kwade et al., 1996; Kwade, 1999(b)).

Above given equations, using for the calculation of stress intensity (SI) of the grinding media for different grinding mechanisms occured in the stirred media mill, have three parameters in common. These are circumferential velocity of the stirrer as well as the density and the size of the grinding media. These parameters can be summoned up in one equation which can be used to determine the stress intensity of the grinding media in the stirred media mill (Eq. 2-6).

$$SI = d_{GM}^3 \cdot \left(\rho_{GM} - \rho_{susp}\right) \cdot \vartheta_{GM}^3 \qquad \text{Eq. 2-6}$$

Where,

d_{GM} : diameter of the grinding media, m
ρ_{GM} : density of the grinding media, kg/m^3
ρ_{susp} : density of the suspension, kg/m^3
$\upsilon_{GM,}$: the tangential velocity of the grinding media, m/s

Figure 2-20 shows that for a constant specific energy input the stress intensity SI determines the product fineness. Small stress intensities are not always sufficient to break particles, so that multiple stressing or more energy are required. With increasing stress intensity the median size decreases until a minimum is reached. At this point the stress intensity has an optimum value. When the stress intensity is further increased, the product becomes coarser again. For different specific energy inputs different relationships between the stress intensity and the product fineness exist. In Figure 2-21, curves for six different specific energy inputs are presented. Each curve has an optimum value of the stress intensity. With increasing specific energy input and therefore increasing product fineness, the optimum stress intensity decreases, because with decreasing particle size smaller energies and smaller forces of pressure are necessary.

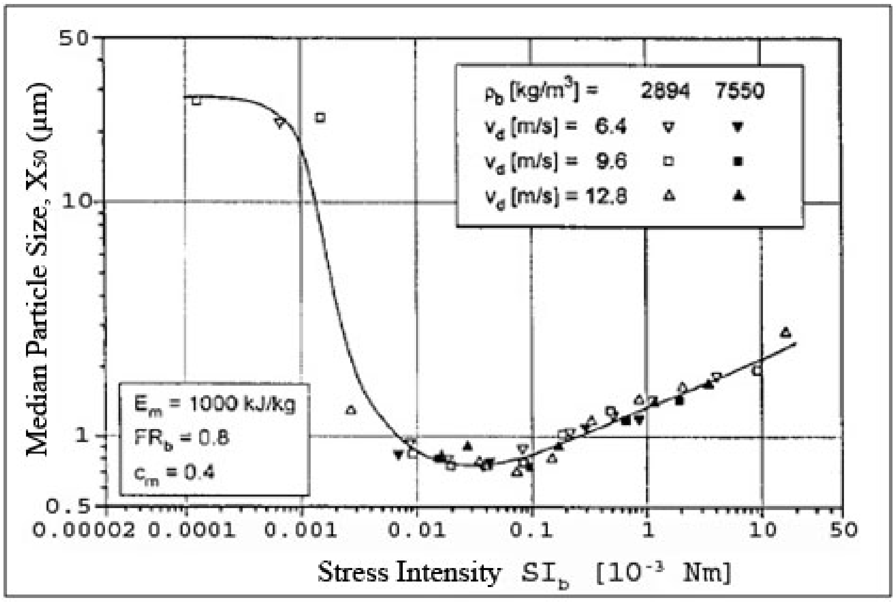

Figure 2-20. Influence of the stress intensity on median size for a specific energy input of 1000 kJ/kg

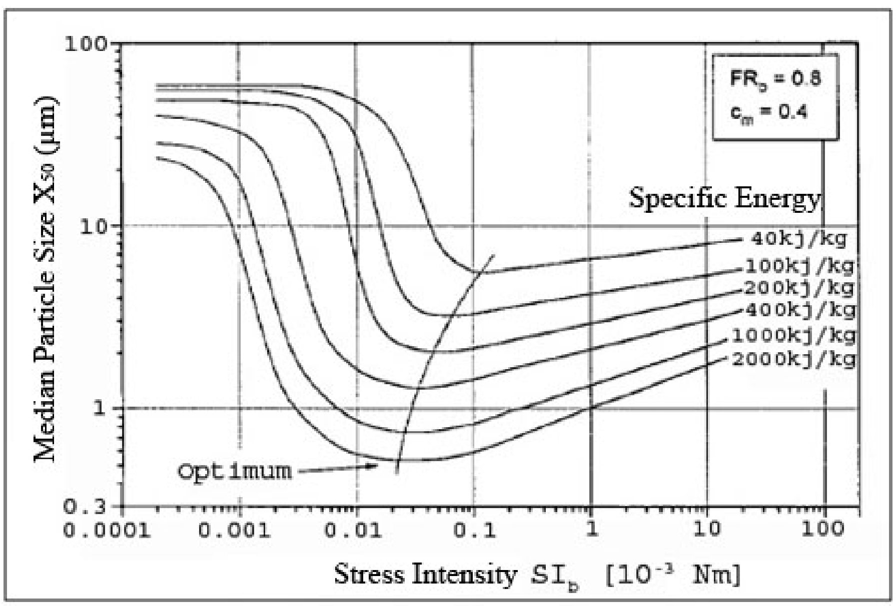

Figure 2-21. Product fineness as a function of the stress intensity and the specific enery input

2.2.2. Estimation of Number of Stress Events

The result of a comminution process is essentially a function of the specific energy input and the stress intensity of the grinding media. Since the specific energy is proportional to the product of the number of stressing events and the energy consumed at one stressing event and, therefore to the product of stress frequency (SN) and stress intensity (SI), the result of the comminution process can also be correlated with the stress frequency (SN) (Eq. 2-7).

$$E \propto SI \cdot SN \qquad \text{Eq. 2-7}$$

In batch grinding, the average number of stress events of each product particle, SN, is determined by the number of media contacts, N_C, by the probability that a particle is caught and sufficiently stressed at a media contact, P_S, and by the number of product particles inside the mill, N_P (Eq. 2-8).

$$SN = \frac{N_C \cdot P_S}{N_P} \qquad \text{Eq. 2-8}$$

The number of media contacts, N_C, can be assumed to be proportional to the number of revolutions of the stirrer and the number of grinding media. Based on this, the number of media contacts can be described as follows (Eq. 2-9):

$$N_C \propto n \cdot t \cdot \frac{V_{GC} \cdot \varphi_{GM} \cdot (1-\varepsilon)}{\frac{\pi}{6} \cdot d_{GM}^3} \qquad \text{Eq. 2-9}$$

Where,

n : the number of revolutions of the stirrer per unit time, s^{-1}
t : comminution time, s
V_{GC} : the volume of the grinding chamber, m^3
φ_{GM} : the filling ratio of the grinding media
ε : the porosity of the bulk of grinding media
d_{GM} : the diameter of the grinding media, m

The probability, that a particle is caught and sufficiently stressed at a media contact, depends among others on the type of the grinding process. In case of grinding crystalline materials, the probability is proportional to the active volume between two grinding media, which is proportional to the diameter of the grinding media (Eq. 2-10):

$$P_S \propto d_{GM} \qquad \text{Eq. 2-10}$$

d_{GM} : the diameter of the grinding media, m

The number of product particles is proportional to the overall volume of the product particles, which can be given as follows (Eq. 2-11):

$$N_P \propto V_{GC} \cdot \frac{\left(1 - \varphi_{GM} \cdot (1 - \varepsilon)\right) \cdot C_v}{\frac{\pi}{6} \cdot x^3} \qquad \text{Eq. 2-11}$$

Where,

V_{GC} : the volume of the grinding chamber, m^3
φ_{GM} : the filling ratio of the grinding media
ε : the porosity of the bulk of grinding media
C_v : solids concentration of the suspension, v/v%
x : average particle size, m

Combining the equations above, the following proportionality can be derived for the stress number (Eq. 2-12):

$$SN \propto n \cdot t \cdot \frac{\varphi_{GM} \cdot (1 - \varepsilon)}{\left(1 - \varphi_{GM} \cdot (1 - \varepsilon)\right) \cdot C_v} \cdot \frac{x^3}{d_{GM}^2} \qquad \text{Eq. 2-12}$$

Where,

n : the number of revolutions of the stirrer per unit time, s^{-1}
t : comminution time, s
φ_{GM} : the filling ratio of the grinding media
ε : the porosity of the bulk of grinding media
C_v : solids concentration of the suspension, v/v%
x : average particle size, m

It can be seen from Figure 2-22 that the stress frequency increases with a decreasing value of stress intensity. For very small values of stress intensity, the curve tends towards a limit because nearly no comminution takes place if the stress intensities are smaller than the stress intensity which is at least necessary to break a product particle (Kwade et al., 1996; Kwade, 1999(a); 1999(b)).

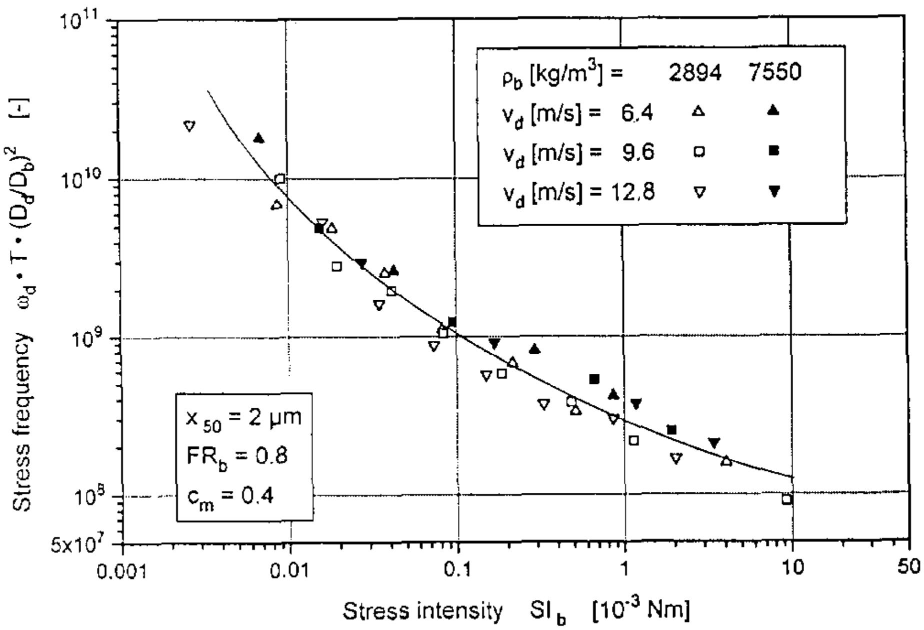

Figure 2-22. Influence of the stress intensity on the stress frequency

According to the above mentioned arguments, a comminution process is determined by the stress number and the stress intensity, i.e. the result in product fineness is always the same as long as the operating parameters are chosen in a way that stress number and stress intensity are constant. The stress intensity can be seen as the specific energy consumed at a single stress event, i.e. the energy transferred to the stressed particle related to the particle mass (or volume). If all particles in the mill are taken into account, the product of the stress number and the stress intensity is proportional to the total specific energy, which is the total energy input related to the total mass (or volume) of the feed material. In order to achieve an identical product quality two of the three parameters—*stress number*, *stress intensity*, and s*pecific energy*—have to be constant (Kwade and Schwedes, 2002).

2.3. Important Parameters Affecting the Comminution Performance in Stirred Media Milling

In stirred media milling, parameters affecting the comminution result can be divided into two major categories, namely, design parameters and operating parameters.

2.3.1. Design Parameters

This group of parameters covers the design features of the equipment such as diameter-length ratio of the mill, type of impeller (disc or pin), the number and the location of impellers in the grinding chamber, the number of discs or pins on the impeller, the distance between each pin or disc, the size of pin and disc and their orientation on the impeller etc. In addition, some equipment have the auxillary components which are suggested to improve the comminution result in the mill. For instance, Maxxmill® has a rotating chamber and a stationary reflector in the grinding chamber (Dürr, 2002). Similarly, Perlmill has a stationary pins vertically oriented inwards on the grinding chamber wall. And, all of these changes in the design of the mills aim at optimizing the flow profiles which consequently affects the media motion in the grinding chamber to obtain better grinding performance (Tüzün, 1994).

Grinding performance of mostly used stirred media mills such as VertiMill, SMD and IsaMill in minerals processing plants, were compared by Nesset et al. (2006). The result of the study showed that IsaMill and SMD technologies proved to be equivalent in terms of specific energy (kWh/t) needed for size reduction and in terms of the spread of the particle size distribution created (P_{80}/P_{20} ratio). The VertiMill technology showed a 43% lower energy requirement than the other technologies, and may reflect a more efficient use of grinding energy in these devices. However, the major difference was in the power density, the IsaMill having 400 kW/m^3 compared to the SMD at 150 kW/m^3 and the VertiMill at 4 kW/m^3. This would influence the feed rate per unit, the number of units required and the size of the footprint in the plant.

2.3.2. Operating Parameters

In the literature, there are number of studies investigating the effect of operating parameters on the grinding performance of stirred media mills (Mankosa et al., 1986; Gao and Forssberg, 1993; Persson and Forssberg, 1994; Tüzün et al., 1995; Zheng et al., 1996; 1997; Kapur et al., 1996; Belaroui et al., 1999; Bernhardt et al., 1999; Bel Fadhel et al., 1999; Kwade, 1999(a); Bel Fadhel and Frances, 2001; Jankovic, 2003).

2.3.2.1. Mill Speed

The mill speed is believed to be one of the most important factor in stirred media milling. As mill speed is increased, both product fineness and energy input increase but energy efficiency declines. This finding that higher speed results in lower energy efficiency, is in accordance with the results reported by Mankosa et al. (1989), Gao and Forssberg (1993) and Zheng et al. (1996). However, if the objective is to obtain finer product in a given grinding time, then higher speed is needed.

Actually, the selection of an optimum mill speed depends on what is required. A lower speed enables the mill to use energy more efficiently. A much reduced milling capacity is however accomplished. A higher mill speed should be a better choice. It increases the milling capacity to a great extent and also achieves reasonable energy efficiency.

2.3.2.2. Media Size, Density and Filling Ratio

Generally speaking, using small media leads to obtain finer product from the stirred media mill. This tendency continues until the media size becomes too small to cause particle fracture effectively. The use of finer media also results in reduced energy input due to increased fluidity.

Mankosa et al. (1986) suggested that the breakage between balls in a stirred media mill could be likened to breakage between the rolls of a roll crusher, one important criterion for breakage would be the angle of nip which is defined as the critical angle at which a particle can be pulled down between two rolls rotating in opposite directions at equal speed. The result of this study showed that there was an optimum ball-particle size ratio at which the breakage rate was maximum and the optimum ratio was 20:1. However, there are several other studies recommending various values ranging from 7:1 to 20:1 for the optimum ratio, possibly due to different minerals and media used in the studies. Tüzün (1994) observed that there was a mutual interaction between mill speed and media size and suggested that large balls were more effective on grinding performance at low speeds while finer balls could be employed at high mill speeds.

The most of the energy consumed in the stirred media mills is used for displacing the media. Therefore, a way can be found to reduce the media density without affecting the grinding performance of the mill, this leads to significant reduction in energy consumption. For this reason, the effect of media density on comminution result has been become a subject of various studies (Gao et al., 2000; Pease et al., 2006; Graves and Boehem, 2007). Low density (glass, ceramic, pebble etc.) is less efficient than high density media when they are employed in the mill grinding coarse material at low speeds. However, if iron contamination is not demanded in the product, different materials can be used as grinding media. In recent years, Magotteaux International announced that a ceramic grinding media (Keramax MT1) was developed for specifically applying to high intensity stirred media milling in the minerals industry. In cooperation with Xstrata Technology, the performance and cost effectiveness of the Keramax MT1 grinding media has beed tested and verified using laboratory, pilot and full scale IsaMills. MT1 offers a way of lowering capital and operating costs for large scale stirred milling projects. The footprint of IsaMill installations can be decreased because of the lower installed power requirement and smaller media handling system (Curry and Clermont, 2005).

Moreover, Tüzün (1994) investigated the effect of ball charge on the grinding performance of the mill. In his experimental conditions, he found that for same specific energy consumption, ball charge has no significant effect on the product fineness but increases power draw of the mill linearly. In addition, Jankovic (2001) indicated that stress intensity equation should bear the effect of gravitational force which is linearly related to the amount of balls in the stirred media mills.

2.3.2.3. Pulp Density

The solids content of the pulp is very important factor in wet grinding systems because of its direct influence on the ground product fineness. The results of the studies showed that it is possible to get finer products from the pulp having high solids concentration. But, if the solids concentration of the pulp exceeds 75% by weight, the breakage rate of the particles decreases due to high viscosity caused by very fine particles. This case is more pronounced when the particle size distribution of the feed is already fine (Gao and Forssberg; 1993; Tüzün, 1994; Zheng et al., 1996; Belaroui et al., 1999; Bernhardt et al., 1999). In order to eliminate of negative effect of high viscosity caused by very fine particles, various type of grinding aids (chemicals) are employed. These chemicals are absorbed to the surface of the particles to increase the charge density on the surface and to reduce the apperant viscosity of the pulp. These reactives used as grinding aids are especially employed to enhance the fluidity of the pulp having high solids concentration so that the capacity of the mill can be increased (Kapur et al., 1996; Zheng et al., 1997; Bernhardt et al., 1999).

2.4. Modelling Studies of Stirred Media Mills

In the last decades, several papers dealt with the simulation of the grinding process in stirred media mills. In most of the papers the population balance model is used to describe the change of the particle size distribution of the product with time (Orumwense, 1992) or with the specific energy input (Sepulveda, 1981; Stehr et al., 1987). As well known from other mills the problem of using the population balance model is to obtain the values for the selection function (grinding rate) and the breakage function. In older papers often feed with narrow particle size distributions (narrow sieve cut) is used to identify the model parameters. But this cannot be done in the micron range. Further problems in modelling fine and ultrafine grinding processes are that usually the selection and the breakage function are a function of the stress number or grinding time, respectively and, thus, are not constant. Therefore, often only the beginning of the grinding process the first minutes could be simulated satisfactory. Recently backcalculation of the model parameters is used increasingly. As an example, Berthiaux et al.(1996) and Varinot et al.(1997; 1999) used a backcalculation method proposed by Kapur and Agrawal (1970) to identify values of the breakage and selection functions. For example, their results showed that with increasing solids concentration of the product suspension and with increasing grinding media diameter the breakage function is displaced to larger particle sizes. Moreover, they showed that the grinding rate increases with increasing stirrer speed and with decreasing solids concentration as well as decreasing grinding media diameter.

The practical application of the published models and model results is limited because in general it is not possible to calculate the change of the product particle size distribution for values of the operating parameters, which are not used in an experiment before. Works focus on, how comminution results can be predicted for any values of the operating parameters based only on a few grinding tests. The stress number can be used as variable instead of the grinding time and the stress intensity can be applied to calculate the breakage and the selection function for values of the operating parameters which are not used in grinding tests (Kwade, 1999(a)).

2.5. Case Studies

2.5.1. McArthur River Mining (MRM)

The McArthur River lead-zinc deposit was the driving force behind the development of IsaMills. The orebody was discovered in 1955. It had a resource of 227 Mt at 9.2% Zn and 4.1%Pb, however no existing technology could economically treat the extremely fine grained minerals. The development of the IsaMill was truly enabling for this orebody. It allowed economic regrinding to 80% passing 7 µm, fine enough to reduce silica in bulk concentrate to marketable levels. Note that at this size there is not adequate galena-sphalerite liberation to allow separate lead and zinc concentrates. The plant started mid 1995 with 4 IsaMills regrinding rougher concentrate. Media for the mills was provided by screening a fraction of ore gravel from the SAG mill discharge. Two more mills were installed to increase production ans recovery. In 2004 the media was changed from ore gravel to screened sand. Higher efficiency of the sand increased mill capacity and reduced wear on mill components at the higher throughputs. Table 2-1 shows production performance at MRM. Very high concentrate grades and recoveries are achieved in spite of the ultrafine minerals (Harbort et al., 1999; Clark and Burford, 2004; Pease et al., 2004).

Table 2-1. Performance of McArthur River since commissioning

MINING			METALLURGY			
	Tonnes	Head Grade	Tonnes	Zn Recovery	Concentrate Grade	
					Zn %	Pb %
1995/96	707,994	12.9%	759,519	66.4%	39.3%	11.2%
1996/97	1,035,222	14.4%	1,026,150	73.5%	43.5%	11.0%
1997/98	1,127,000	16.1%	1,139,000	74.3%	43.3%	11.9%
1998/99	1,222,238	16.4%	1,220,957	79.5%	45.0%	12.7%
1999/00	1,254,227	16.3%	1,262,639	80.9%	46.9%	12.0%
2000/01	1,226,499	15.4%	1,270,319	82.4%	46.8%	11.2%
2001/02	1,398,109	14.9%	1,404,539	82.7%	46.8%	11.1%
2002/03	1,505,306	12.7%	1,511,856	82.4%	46.6%	10.5%
2003/04	1,523,243	13.2%	1,579,762	80.1%	47.1%	10.4%

2.5.2. George Fisher Orebody

The IsaMill technology for MRM was developed in the lead-zinc concentrator at Mt. Isa. It was clear that the technology would have benefites for the Mt. Isa lead-zinc orebodies, and it was to prove enabling for the George Fisher orebodies north of Mt. Isa. While not as fine grained as MRM, components of George Fisher require a 7 µm grind to achieve acceptable concentrate grades and recoveries. A circuit was designed to treat the mixture of ores from George Fisher, Hilton, and Mt. Isa lead-zinc orebodies. The circuit included eight 1 MW IsaMills, grinding rougher concentrate and intermediate zinc streams as shown in Figure 2-24. The principles of the circuit design can be summarized as (Young and Gao, 2000):

- Only grind minerals you want – this needs a thorough understanding of size by size mineralogical performance throughout the circuit. Recover what minerals you can at coarser sizes, then apply successively finer grinding and flotation stages to recover the finer grained minerals.
- Float in narrow size distributions and tailor the flotation conditions to suit – this is achieved in the staged grind and float circuit in Figure 2-24, with separate zinc recovery stages for 37 µm, 15 µm and 7µm particles. A vital principle is to avoid recirculating loads.

In fact, the benefits of the inert grinding and the staged flotation design were so profound.

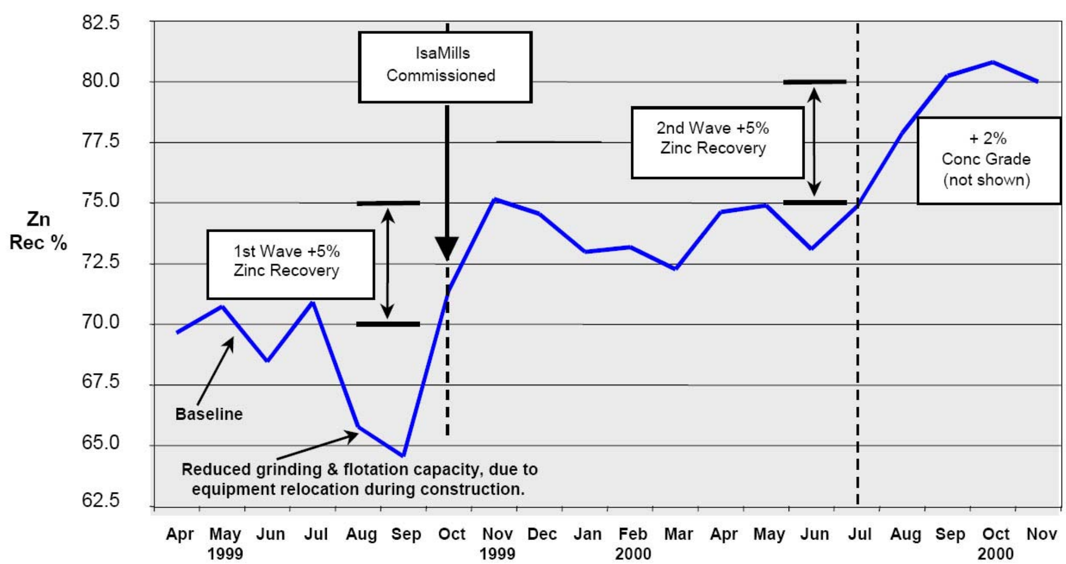

Figure 2-23. Zinc recovery increase from Isamilling

Figure 2-23 shows the immediate 5% Zn recovery gain after installing. This was the gain due to extra liberation of sphalerite. The second wave of even higher benefits happened when the clean surfaces from inert milling and the staged flotation circuit, fundamentally changed mineral surfaces. The net impact of the circuit changes was:

- Lead recovery increased by 5% and lead concentrate grade increased by 5%
- Zinc recovery increased by 10% and zinc concentrate grade increased by 2%
- Unit cost per tonne of ore was unchanged in spite of 6 MW of extra grinding power.

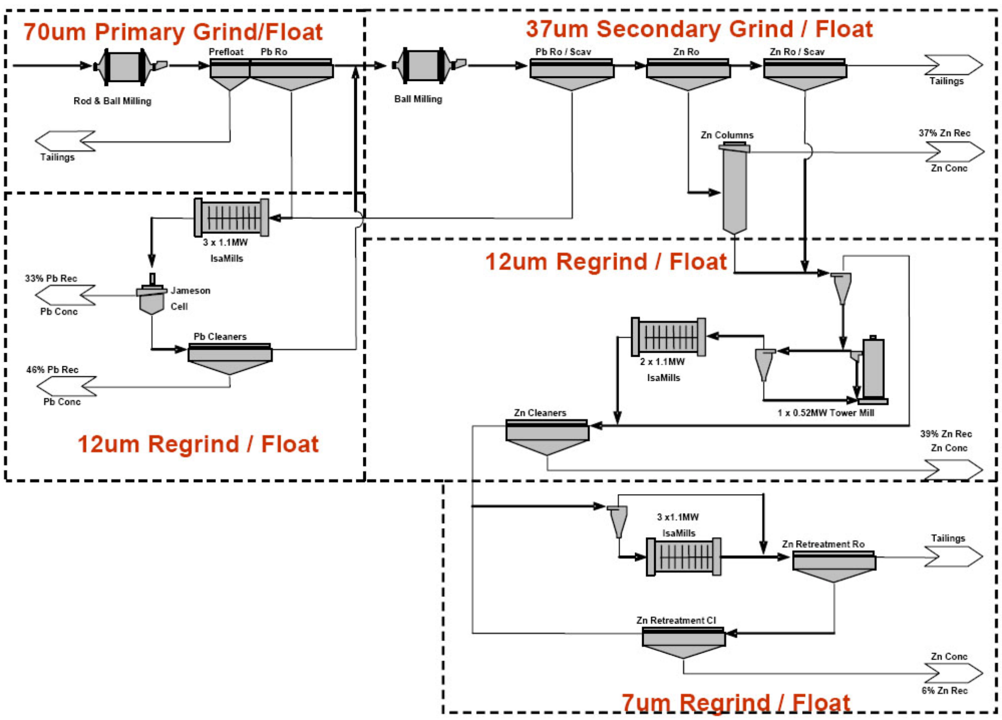

Figure 2-24. Mt. Isa Pb/Zn concentrator flow sheet

3. EXPERIMENTAL STUDIES AND RESULTS

Experimental studies carried out can be divided into three steps, namely, laboratory scale stirred media mill tests, pilot scale stirred media mill tests and sampling surveys performed at CBI's flotation plant.

In the batch test, laboratory scale stirred media mill manufactured by Hacettepe University were used. Major aim was to investigate the effect of main operating parameters such as impeller speed, ball size, ball charge, %solids of the pulp and different grinding media types (steel balls, river pebble and zircon balls) on product fineness. Related experiments were performed in both Hacettepe University and CBI laboratories. Then, pilot scale stirred media mill manufactured again by Hacettepe University was transferred and installed to various streams around the circuit at CBI's flotation plant. The grinding performance of the mill was investigated while the mill was running in an open circuit. Investigated parameters were the impeller speed, feed rate, feed fineness, ball charge and grinding media type (steel balls and River pebble). Plant sampling surveys were accomplished to evaluate the performance of existing copper regrinding and whole flotation circuit for two different ore types (Spec and Non-Spec ore) processed in the plant. These data were also used to model the existing regrinding circuit.

3.1. Laboratory Scale Stirred Media Mill Tests

For laboratory tests carried out at both Hacettepe University and CBI's laboratories with the same laboratory scale stirred media mill manufactured by Hacettepe University. Specifications of this mill is given in Table 3-1. Four different impeller speeds (1030, 710, 480, 330 rpm) can be arranged by means of belt and pulley system installed on the motor and there are eight pins vertically mounted on the impeller shaft which provide the effective stirring action inside the mill chamber.

Table 3-1. Specifications of laboratory scale stirred ball mill

SBM Specifications	
Diameter, cm	11
Length, cm	20
Shaft diameter, cm	3
Shaft length, cm	16
Pin diameter, cm	1
Pin length, cm	7
Total volume, cm^3	1900
Net volume, cm^3	1700
Motor power, kW	5.5

Steel balls in three different sizes used as grinding media in the experiments were purchased from Çelik Granül Sanayii A.Ş. and their size distributions are given in Table 3-2. The density of the steel ball is 7.00 g/cm^3.

Table 3-2. Size distributions of steel balls used in the experiments

Screen Aperture (mm)	Code Numbers		
	S780	S550	S460
2.83	%100		
2.38			
2.00	min. %85	%100	%100
1.68	min. %97		max. %5
1.41		min. %85	
1.19		min. %97	min. %85
1.00			min. %97

Zirconium ball used as grinding media was purchased from Asil Kimya ve Boya Sanayii Ticaret A.Ş. The balls have the density of 4.00 g/cm^3 and their sizes are -3.00+2.40 mm. In addition, river pebble having the size of -4.75+3.35 mm was also employed as grinding media in the experiments. The density of river pebbles used in the grinding tests are 2.75 g/cm^3.

Two different feed material were used in the batch grinding tests. Feed material used in the experiments at Hacettepe University was CBI's copper regrinding hydrocyclone underflow while that used at CBI's laboratory was the tailing from the 3rd cleaning stage in copper flotation circuit. Comparison of the size distributions of both feed material used in the experiments is given in Figure 3-1.

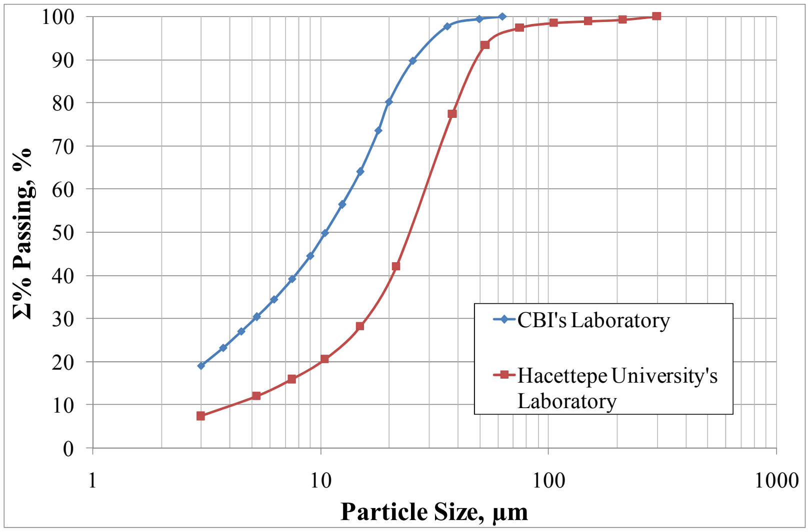

Figure 3-1. Comparison of size distributions of both feed materials used in the experiments

All laboratory scale stirred media mill tests were carried out as batch mode. In each experiment, appropriate amount of ball, material and water were fed to the mill and the mill was started to stir up the pulp at various speeds. Products at different grinding times (0.5, 1, 2, 3 and 5 minutes) were collected and the size distributions of the products were determined by the combination of wet sieving and Sympatech Laser Sizer.

3.1.1. Tests carried out in Hacettepe University's laboratory

Tests carried out in HU laboratory focused on the effect of impeller speed, ball size, ball charge, media type (steel ball and zirconium ball), %solid and filling ratio of the material on product fineness. Samples taken from the stream of copper regrinding hydrocyclone underflow were used as feed material for all tests. Two different materials were used as grinding media, namely steel ball and zirconium ball. Products at different grinding times (0.5, 1, 2, 3 and 5 minutes) were collected in each experiment. Size distributions of the products were determined down to 75 µm by wet sieving while -75 µm material was sized with Sympatech Laser Sizer in wet mode. Sodium hexa metaphosphate was added to suspension as a dispersant in order to avoid agglomeration of particles during laser sizing. Experimental design is given in Table 3-3. The particle size distributions of the products obtained from each experiment are presented in Figure 3-2, Figure 3-3, Figure 3-4 and Figure 3-5.

Table 3-3. Parameters tested in experiments in Hacettepe University's Laboratory

	Impeller speed (rpm)	Ball size (mm)	Ball charge (v/v)	%solid (w/w)	Filling Ratio (v/v)
Exp. 1	1030	2.00	50	50	100
Exp. 2	480	2.00	50	50	100
Exp. 3	710	2.00	50	50	100
Exp. 4	1030	2.83	50	50	100
Exp. 5	1030	1.68	50	50	100
Exp. 6	480	2.83	50	50	100
Exp. 7	710	2.83	50	50	100
Exp. 8	480	1.68	50	50	100
Exp. 9	710	1.68	50	50	100
Exp. 10	480	2.83	50	35	100
Exp. 11	480	2.83	50	65	100
Exp. 12	480	2.83	50	80	100
Exp. 13	480	2.83	35	50	100
Exp. 14	480	2.83	65	50	100
Exp. 15 (Zr ball)	480	-3.00+2.40	50	50	100
Exp. 16 (Zr ball)	710	-3.00+2.40	50	50	100
Exp. 17 (Zr ball)	1030	-3.00+2.40	50	50	100
Exp. 18	480	2.83	50	50	75
Exp. 19	480	2.83	50	50	50
Exp. 20	710	2.83	50	35	100
Exp. 21	710	2.83	50	65	100
Exp. 22	710	2.83	50	80	100
Exp. 23	710	2.83	35	50	100
Exp. 24	710	2.83	65	50	100
Exp. 25	1030	2.83	50	35	100
Exp. 26	1030	2.83	50	65	100
Exp. 27	1030	2.83	35	50	100
Exp. 28	1030	2.83	65	50	100

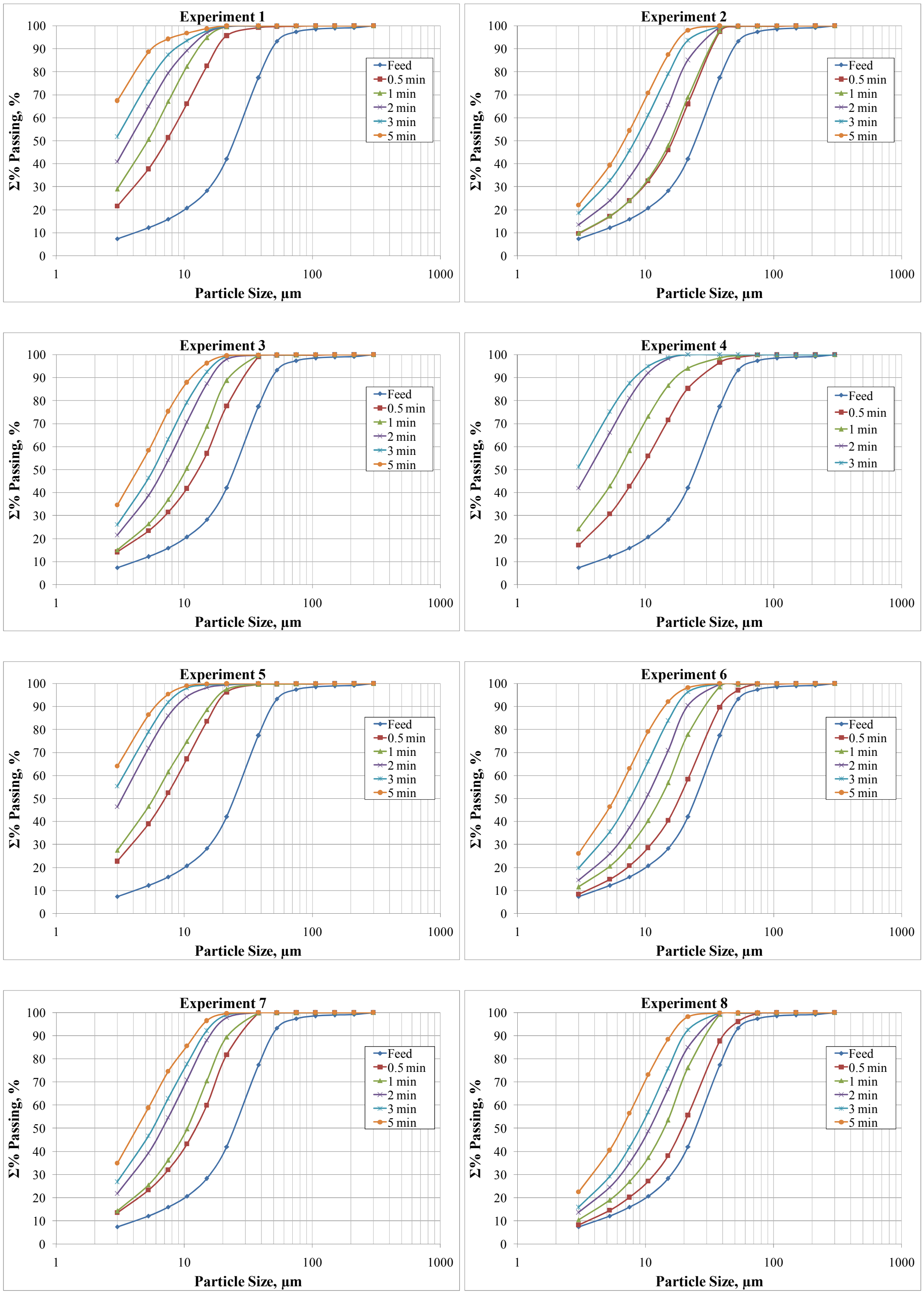

Figure 3-2. Particle size distributions of the products obtained from experiments (1-8) carried out in Hacettepe University's laboratory

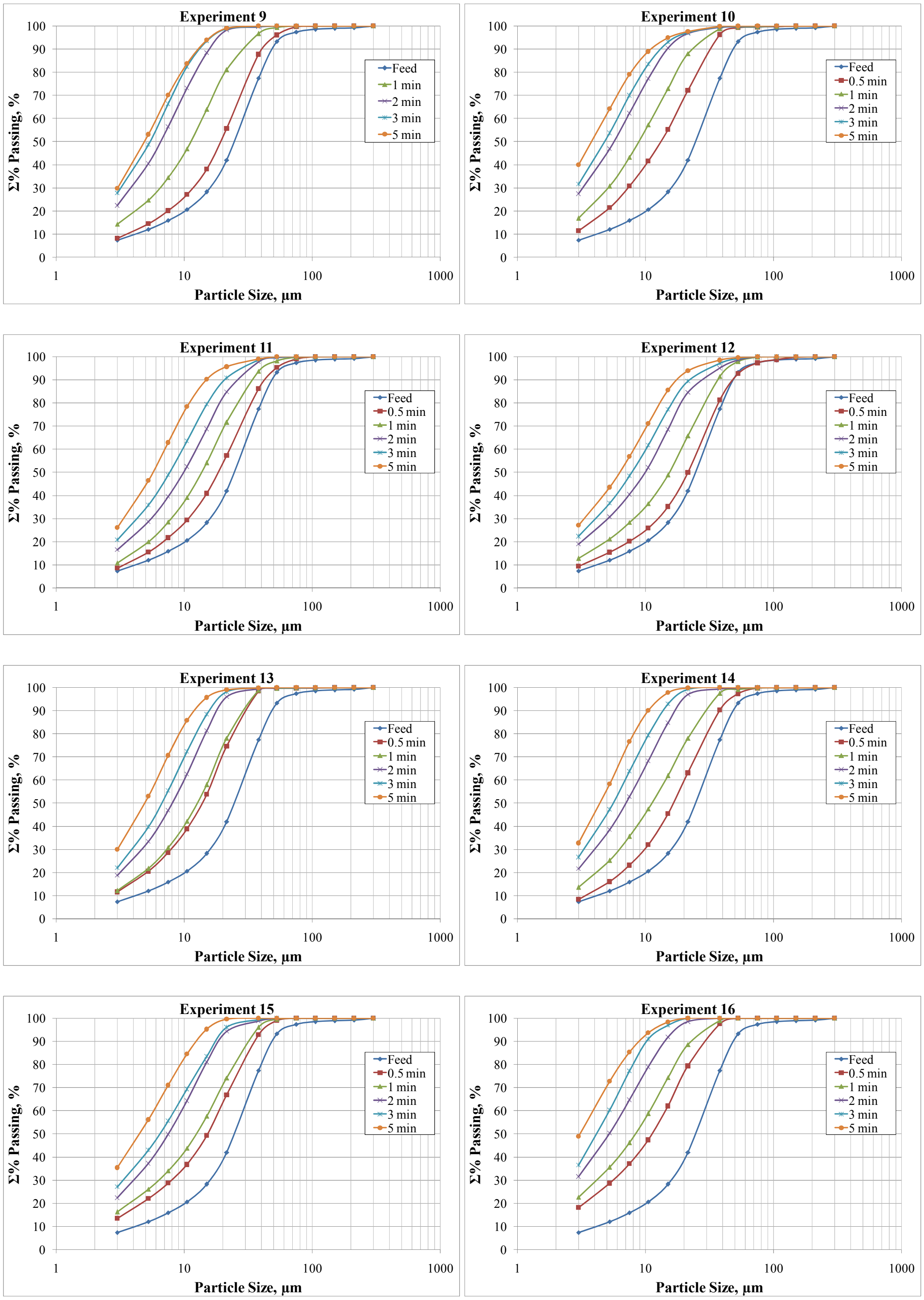

Figure 3-3. Particle size distributions of the products obtained from experiments (9-16) carried out in Hacettepe University's laboratory

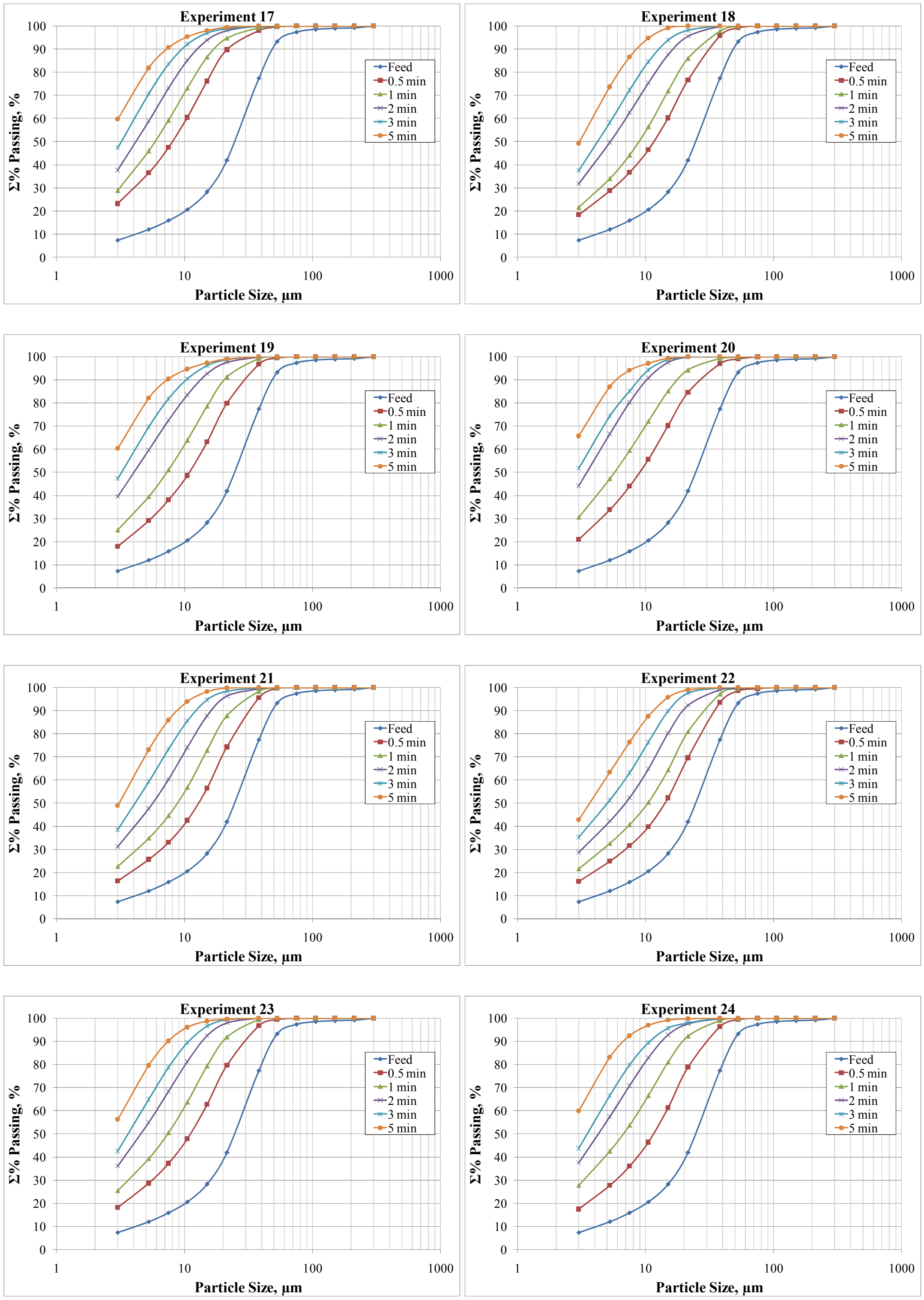

Figure 3-4. Particle size distributions of the products obtained from experiments (17-24) carried out in Hacettepe University's laboratory

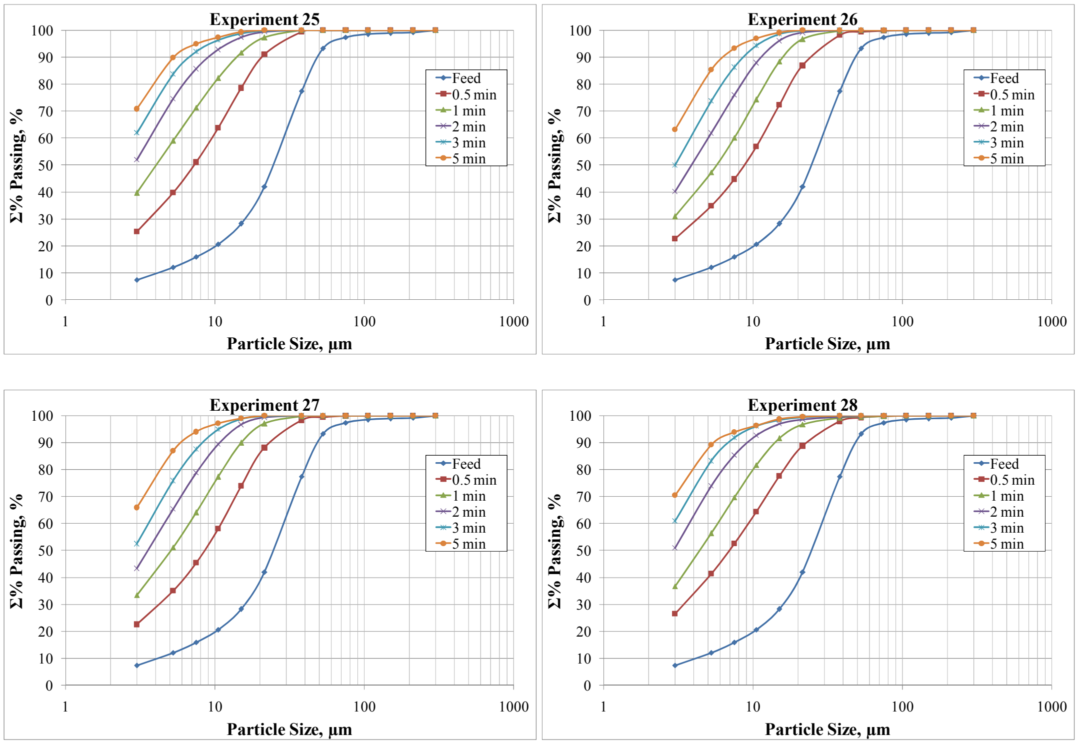

Figure 3-5. Particle size distributions of the products obtained from experiments (25-28) carried out in Hacettepe University's laboratory

3.1.2. Tests carried out in CBI's laboratory

In CBI's laboratory, further experiments investigating the effect of different grinding media used in the stirred ball mill with various impeller speeds on product fineness were performed. Samples taken from the stream of Cu Cl 3 Tail were used as feed material for all tests. Three different materials were used as grinding media, namely steel ball (2.83 mm), river pebble (-4.75+3.35 mm) and zirconium ball (-3.00+2.40 mm). Products at different grinding times (0.5, 1, 2, 3 and 5 minutes) were collected in each experiment. Size distributions of the products were determined down to 36 µm by wet sieving while -36 µm material was sized with Sympatech Laser Sizer in wet mode. Sodium hexa metaphosphate was added to suspension as a dispersant in order to avoid agglomeration of particles during laser sizing. Experimental design is given in Table 3-4. The particle size distributions of the products obtained from each experiment are presented in Figure 3-6 and Figure 3-7.

Table 3-4. Parameters tested in experiments in CBI's laboratory

Experiment No	Grinding media	Impeller speed (rpm)
1	Steel ball	1030
2	Steel ball	710
3	Steel ball	480
4	Pebble	1030
5	Pebble	710
6	Pebble	480
7	Zircon ball	1030
8	Zircon ball	710
9	Zircon ball	480

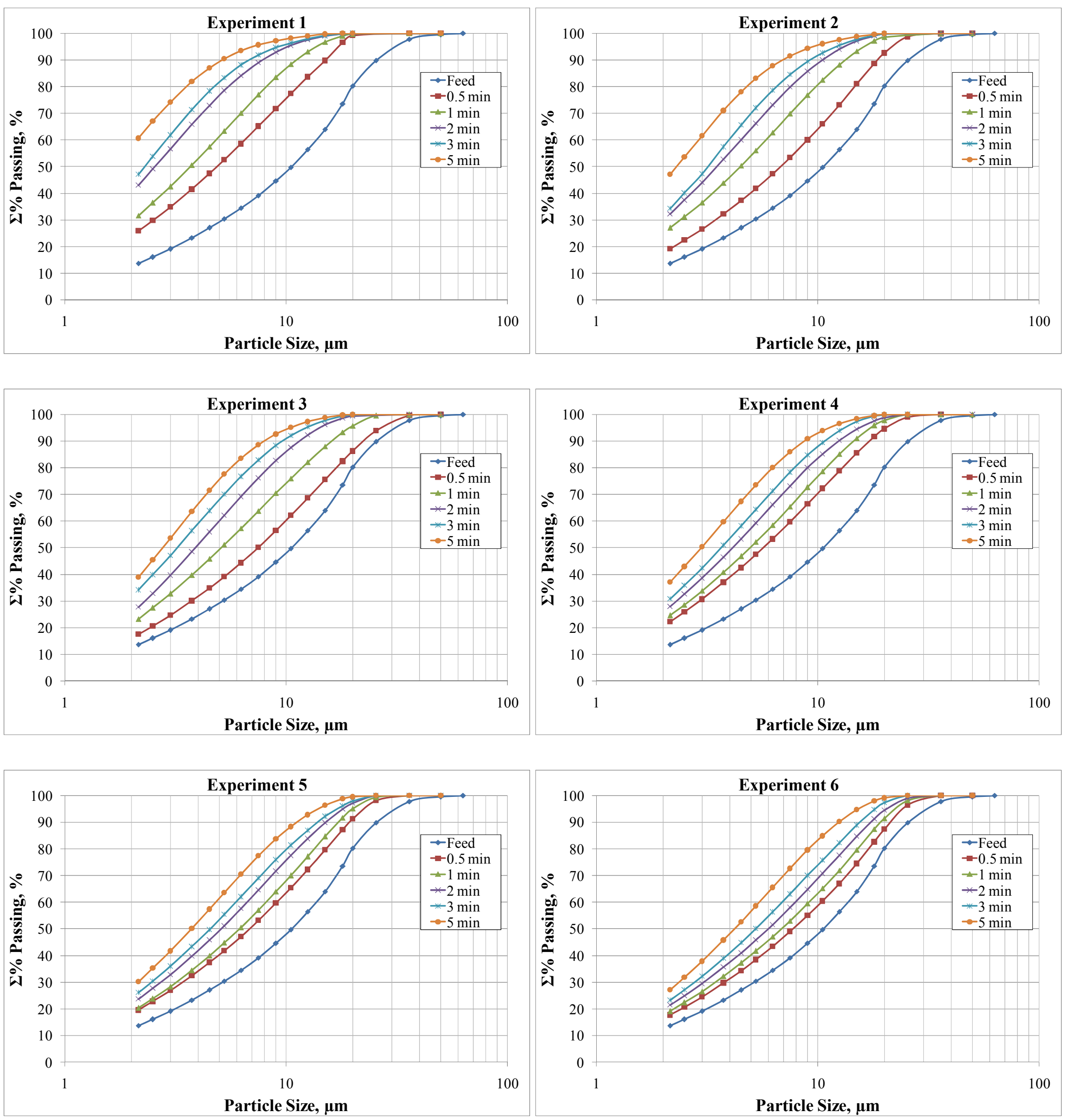

Figure 3-6. Particle size distributions of the products obtained from experiments (1-6) carried out in CBI's laboratory

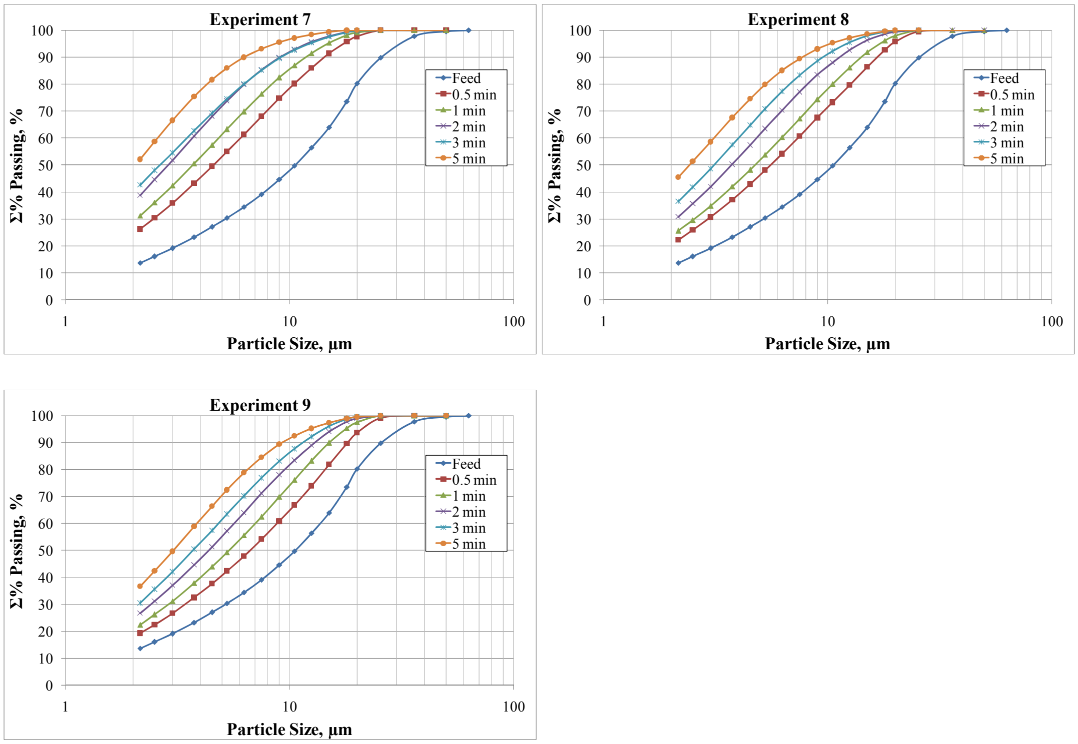

Figure 3-7. Particle size distributions of the products obtained from experiments (7-9) carried out in CBI's laboratory

3.2. Pilot Scale Stirred Ball Mill Tests

For these tests, a pilot scale vertical stirred media mill was installed in the plant. Specification of this mill is given in Table 3-5. Pilot mill also has a torquemeter which enables to measure the energy transferred to the mill during operation. All the tests were performed as an open circuit.

Table 3-5. Specifications of pilot scale stirred ball mill

SBM Specifications	
Diameter, cm	20
Length, cm	70
Shaft diameter, cm	5.5
Shaft length, cm	62
Pin diameter, cm	2
Pin length, cm	18
Total volume, cm^3	22000
Net volume, cm^3	19800
Motor power, kW	11

In order to evaluate the performance of this mill in an open circuit grinding, one stream (Zn Column Scavenger Concentrate) in the circuit was chosen as feed stream to the mill and the effect of major operating parameters such as stirrer speed, feed rate, ball charge and media type on product fineness were tested. Experimental desing and the streams ground in the mill are given in Table 3-6. Table 3-6 also contains the torque measurement in each test. Once the operating conditions that gave the finest product were determined, various streams around the circuit were ground in the mill. Feed material from these selected streams were conveyed to the mill by means of hose and peristaltic pump. Steel balls and river pebbles were employed as grinding media in the mill. During the course of grinding, torque values were also recorded. Product samples were collected after 15 minutes of grinding which is thought to be sufficient to reach the steady state condition. Size distributions of the products were determined down to 36 µm by wet sieving while -36 µm material was sized with Sympatech Laser Sizer in wet mode.

Table 3-6. Parameters tested in the pilot stirred ball mill

	Name of the Stream	**Impeller speed (rpm)**	**Feed rate (kg/h)**	**Ball charge (v/v)**	**Media type**
Exp. 1	Zn Column Scav Conc	1000	765	46	Steel ball
Exp. 2	Zn Column Scav Conc	1200	765	46	Steel ball
Exp. 3	Zn Column Scav Conc	1400	765	46	Steel ball
Exp. 4	Zn Column Scav Conc	600	765	46	Steel ball
Exp. 5	Zn Column Scav Conc	800	765	46	Steel ball
Exp. 6	Zn Column Scav Conc	1400	916	46	Steel ball
Exp. 7	Zn Column Scav Conc	1200	916	46	Steel ball
Exp. 8	Zn Column Scav Conc	1000	916	46	Steel ball
Exp. 9	Zn Column Scav Conc	800	916	46	Steel ball
Exp. 10	Zn Column Scav Conc	600	916	46	Steel ball
Exp. 11	Zn Column Scav Conc	1400	557	46	Steel ball
Exp. 12	Zn Column Scav Conc	1200	557	46	Steel ball
Exp. 13	Zn Column Scav Conc	1000	557	46	Steel ball
Exp. 14	Zn Column Scav Conc	800	557	46	Steel ball
Exp. 15	Zn Column Scav Conc	600	557	46	Steel ball
Exp. 16	Cu RG Cyclone U/F	1400	259	46	Steel ball
Exp. 17	Cu RG Cyclone U/F	1200	259	46	Steel ball
Exp. 18	Cu RG Cyclone U/F	1000	259	46	Steel ball
Exp. 19	Cu Cleaner 4 Tail	1000	193	46	Steel ball
Exp. 20	Cu Cleaner 4 Tail	1200	193	46	Steel ball
Exp. 21	Cu Cleaner 4 Tail	1400	193	46	Steel ball
Exp. 22	Cu Cleaner 4 Tail	1000	193	53	Steel ball
Exp. 23	Cu Cleaner 4 Tail	1200	193	53	Steel ball
Exp. 24	Cu Cleaner 4 Tail	1000	193	60	Steel ball
Exp. 25	Cu Cleaner 4 Tail	1200	193	60	Steel ball
Exp. 26	Cu Cleaner 4 Tail	1000	193	67	Steel ball
Exp. 27	Cu Cleaner 4 Tail	1000	193		Pebble

Table 3-6. (Continuing). Parameters tested in the pilot stirred ball mill

Exp. 28	Cu Cleaner 4 Tail	1200	193		Pebble	27
Exp. 29	Cu Cleaner 4 Tail	1400	193		Pebble	33
Exp. 30	Zn Col Scav Tail	1400	66	46	Steel ball	78
Exp. 31	Zn Col Tail	1400	231	46	Steel ball	77
Exp. 32	Zn Cleaner 1 Tail	1400	122	46	Steel ball	79
Exp. 33	Cu Cleaner 1 Scav Tail	1400	267	46	Steel ball	78
Exp. 34	Cu Rougher Conc	1400	426	46	Steel ball	80
Exp. 35	Cu Cleaner 3 Tail	1400	182	46	Steel ball	78
Exp. 36	Cu RG Cyclone O/F	1400	327	46	Steel ball	79

The particle size distributions of the products obtained from each tests are given in Figure 3-8, Figure 3-9, Figure 3-10, Figure 3-11, and Figure 3-12.

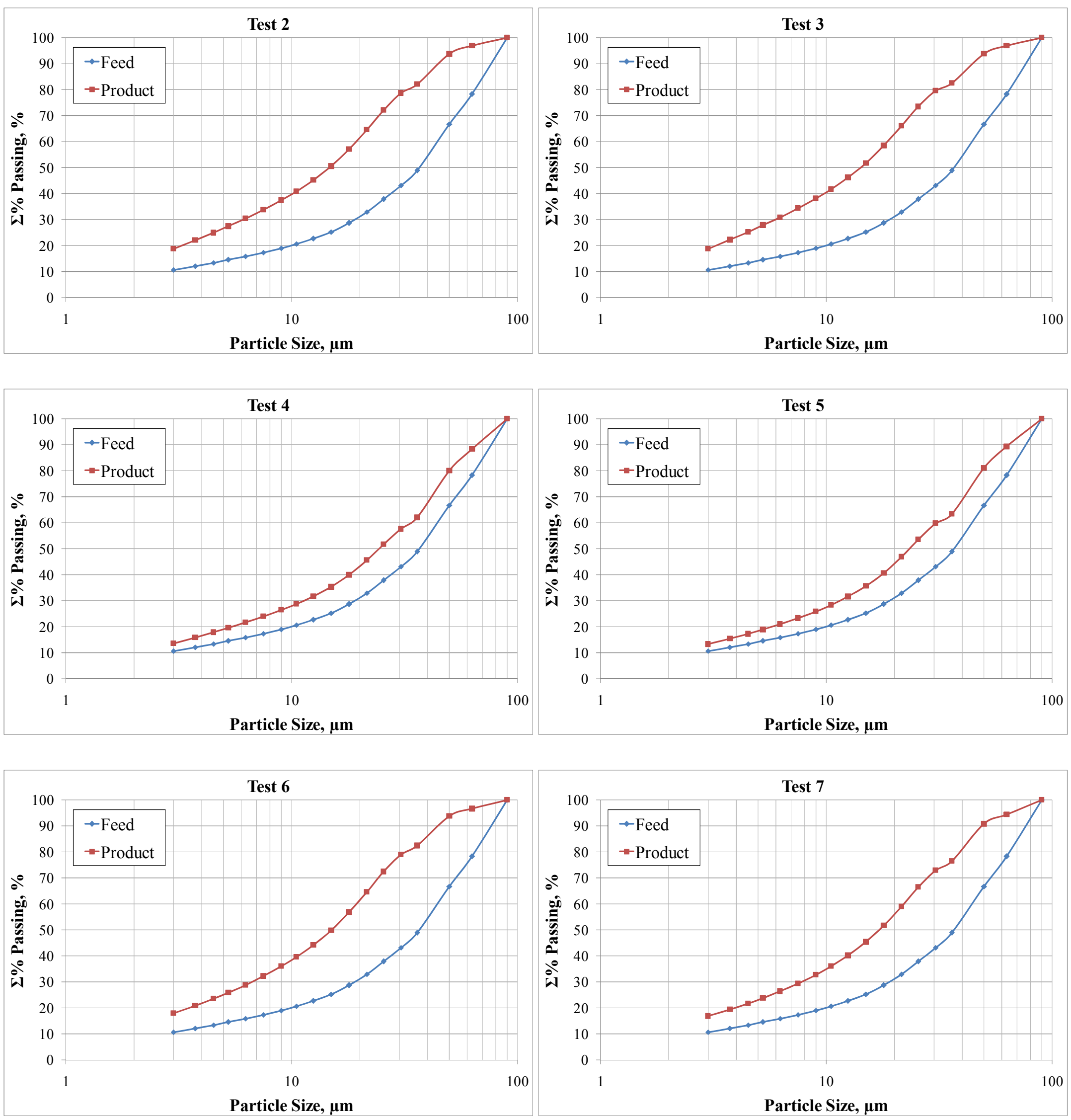

Figure 3-8. Particle size distributions of the products obtained from pilot scale tests (2-7)

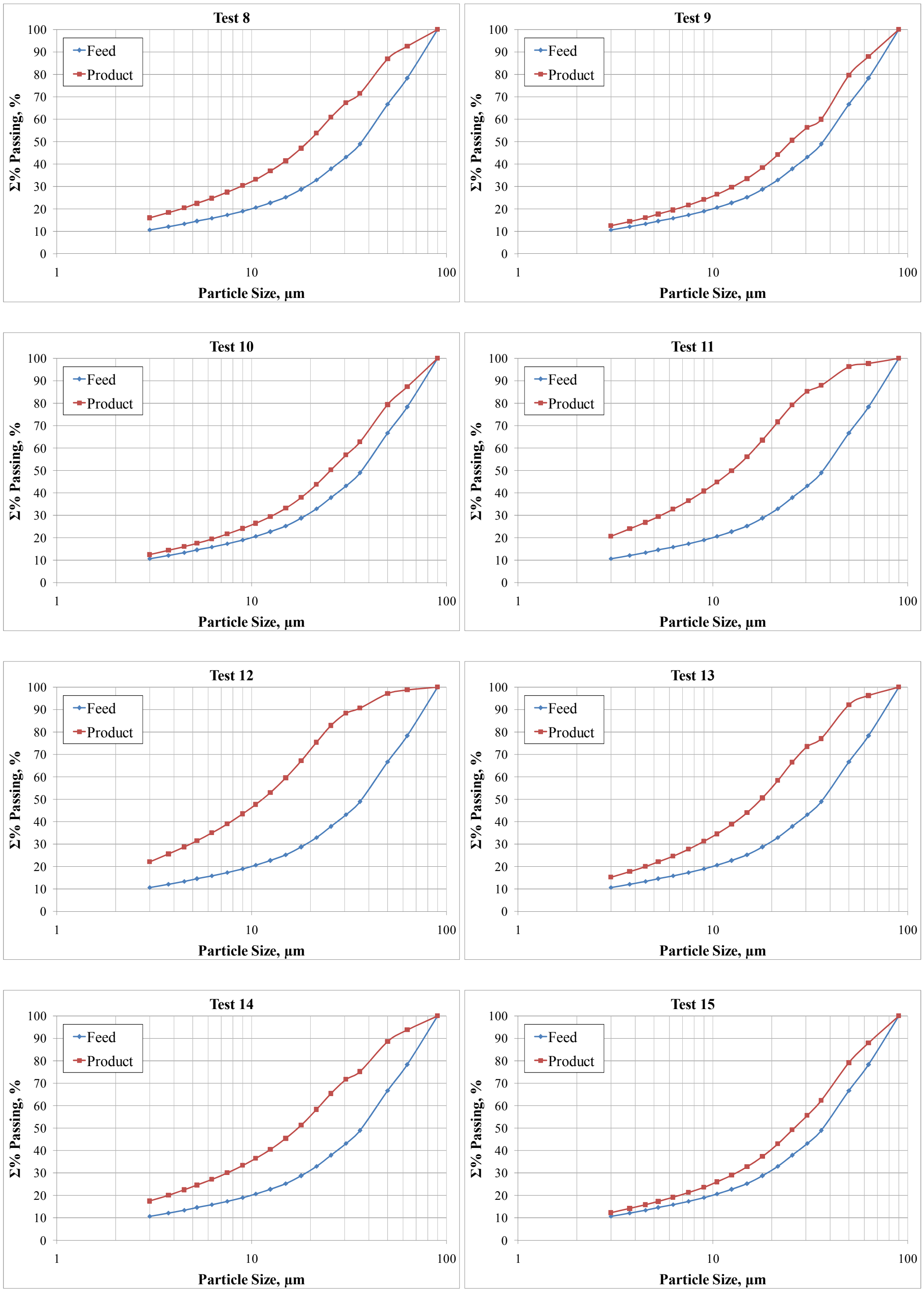

Figure 3-9. Particle size distributions of the products obtained from pilot scale tests (8-15)

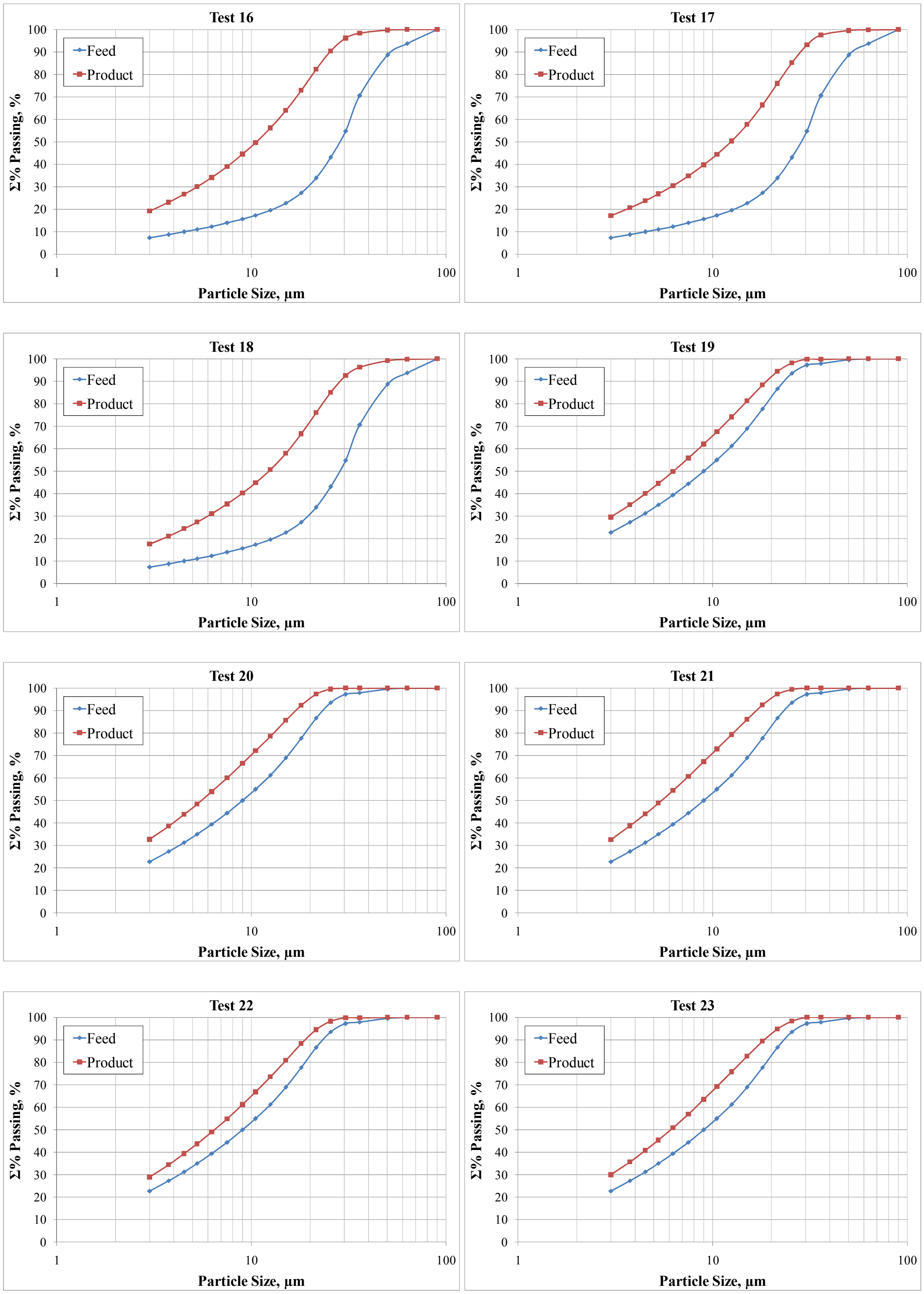

Figure 3-10. Particle size distributions of the products obtained from pilot scale tests (16-23)

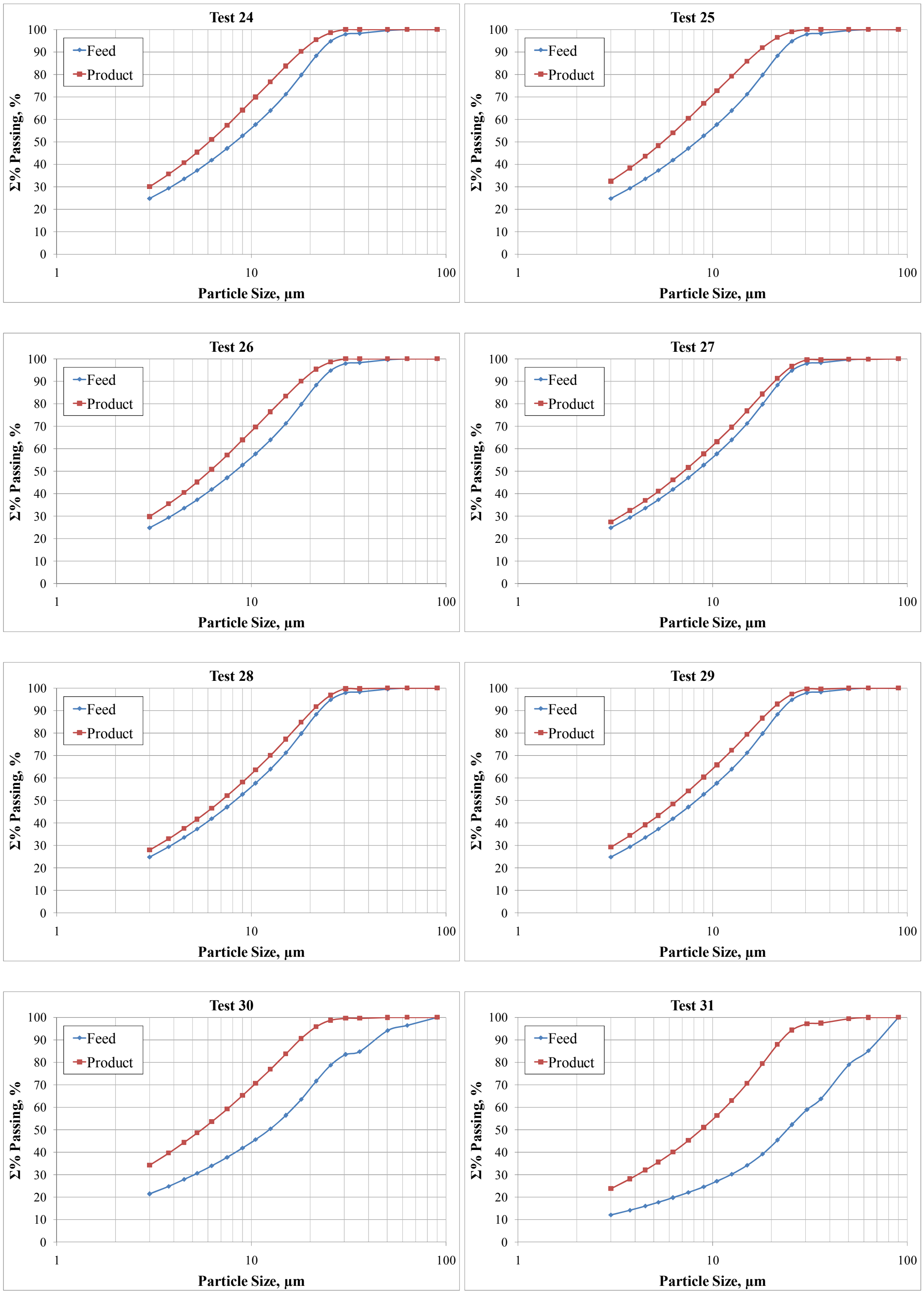

Figure 3-11. Particle size distributions of the products obtained from pilot scale tests (24-31)

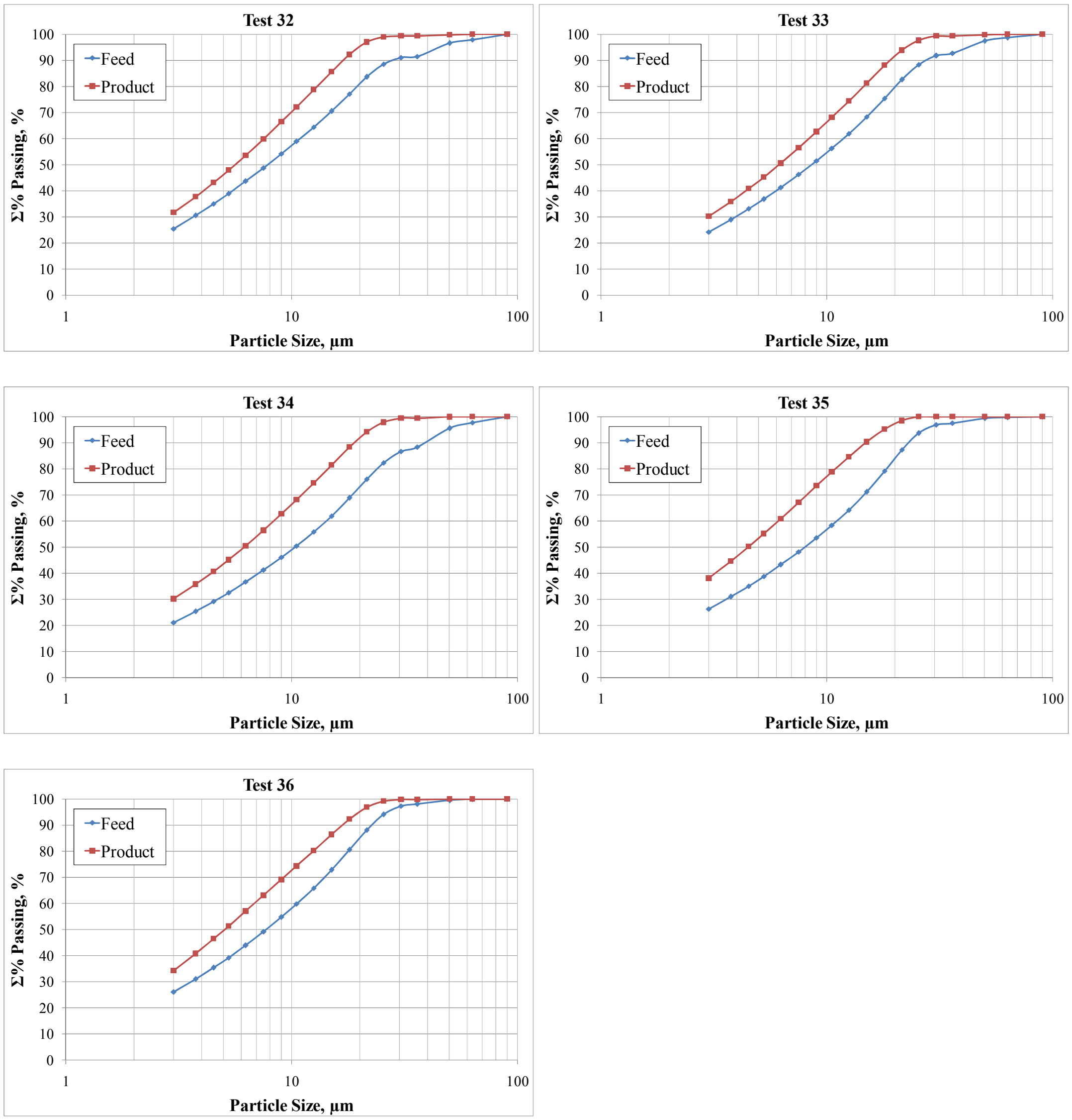

Figure 3-12. Particle size distributions of the products obtained from pilot scale tests (32-36)

4. EFFECT OF OPERATIONAL PARAMETERS ON GRINDING PERFORMANCE OF STIRRED MEDIA MILLS

The effect of operating parameters on grinding performance of stirred media milling were investigated by performing laboratory scale and pilot scale tests. In laboratory scale tests carried out at both Hacettepe University and CBI laboratory, major operating parameters such as impeller speed, media size, media density, solids content of the pulp, media charge to the mill were under investigation in batch grinding mode. In pilot scale tests, the effect of impeller speed, feed rate, media density and media charge to the mill on the product fineness and energy consumption of the mill were studied while the pilot mill was running in an open circuit.

4.1. Laboratory Scale Stirred Media Tests

The particle size distributions of the products obtained from laboratory scale stirred ball mill tests were given in Figure 3-2, Figure 3-3, Figure 3-4, Figure 3-5, Figure 3-6 and Figure 3-7. Those graphs show that the curves at different grinding times shift parallel to each other and the size distribution curve of the feed. The results obtained by batch grinding of a brittle material in stirred ball mill is as typical as those obtained by batch grinding in a ball mill, where the size distribution is getting finer and finer for longer periods of time of grinding (Austin et al., 1984). The results also indicate that there is a preferential elimination of the coarse sizes. This can be explicitly displayed by observing the change in the amount of material in each size fraction (Figure 4-1). This situation would be beneficial in terms of energy efficiency, liberation and overgrinding. In addition, variation of d_{50} values of each size distribution curve with grinding time is a good indicator about the grinding action inside the mill. In Figure 4-2, it is shown that d_{50} values are linearly changed in the early periods of grinding whereas changes in d_{50} is reduced with further grinding and tends to towards a limiting size. Obviously, the finer the particles, the lesser chance of cracks and defaults in the volume of particle, hence the stronger the particles become. Finally, a limit size is reached. This extreme fineness corresponds to a dynamic equilibrium. The fines produced by grinding aggregate to each other leading to coarse particle production, this is balanced by subsequent down. For longer period of grinding, the curves of d_{50} versus time related to the different operating conditions will meet and tend towards the same limit fineness (Bel Fadhel and Frances, 2001).

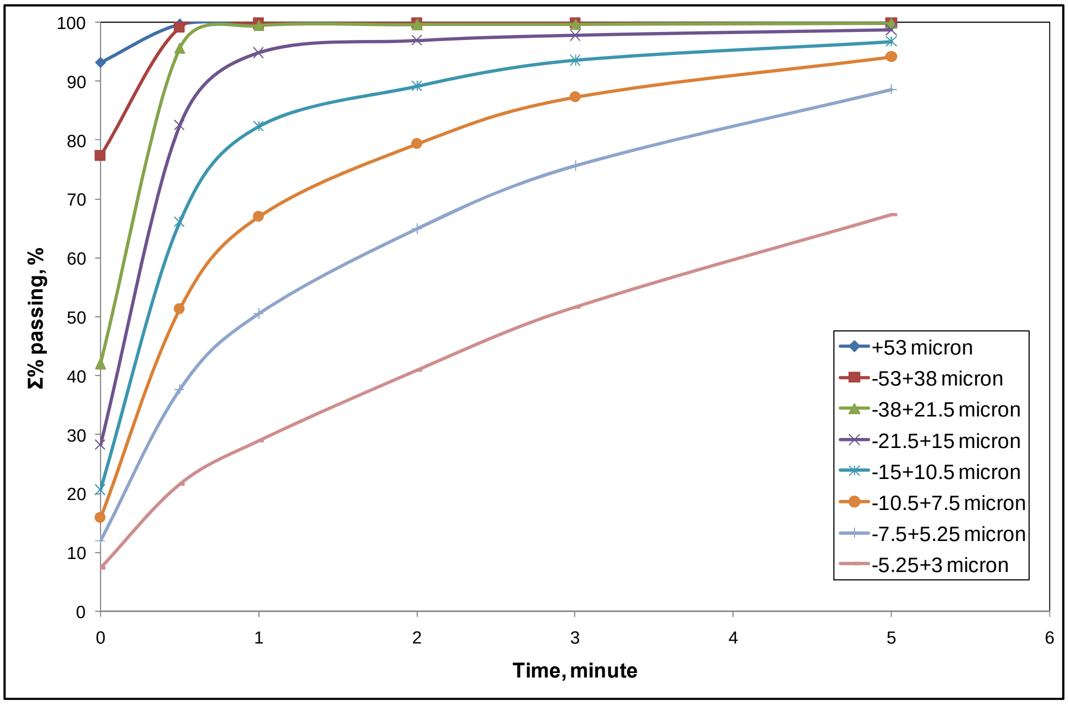

Figure 4-1. The change in the amount of material in each size fraction with grinding time

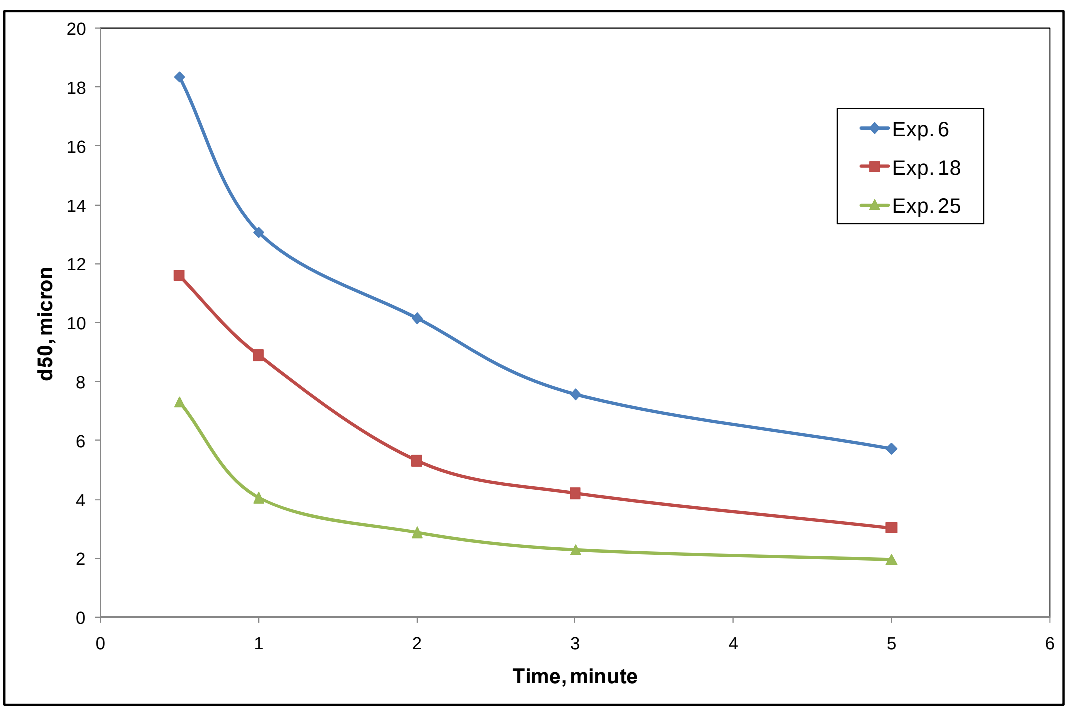

Figure 4-2. Changes of d_{50} values of products obtained from different grinding time

It is also found that the impeller speed has more pronounced effect on the product fineness than the other operating parameters. Because impeller speed is directly related to the energy transferred to the mill. This effect can be clearly seen when comparing the size distributions of the products of different experiments having the same grinding time (Figure 4-3). As seen in Figure 4-3, increasing the impeller speed significantly reduces the particle size of the products. The same effect is true for the other grinding times tested in the experiments. However, in the literature, it is reported that the energy efficiency is much higher at low stirring speeds because of the fact that the increased energy input is not entirely used for size reduction. Instead, to reach a higher speed, the mill consumes much energy to activate the motor, overcome the mechanical diffuculties and to generate more heat (Sepulveda, 1981; Mankosa et al., 1989; Gao and Forssberg, 1993; Zheng et al., 1996; Jankovic, 2003). Figure 2-14 also shows that the specific energy distribution in the mill chamber for low Reynold's number, i.e. low stirring speeds, is more homogeneous than for high Reynold's number. Therefore, the zones where effective comminution takes place should be very small for high stirring speeds. This leads to low energy utilization at high stirring speeds (Blecher et al., 1996; Blecher and Schwedes, 1996).

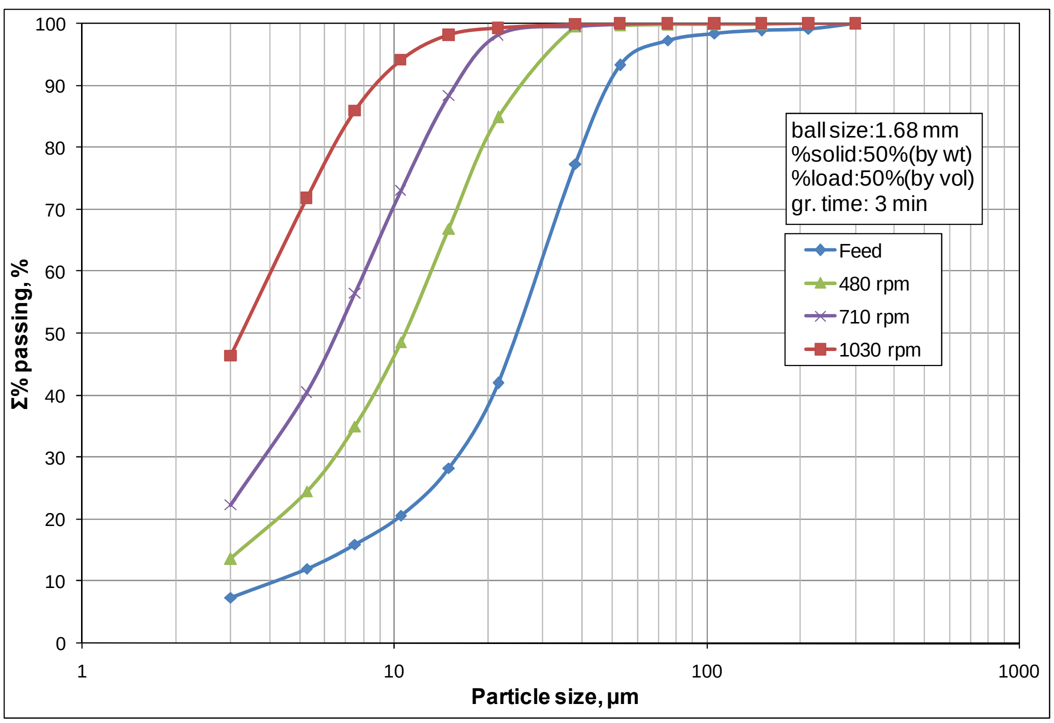

Figure 4-3. Effect of various impeller speeds on product fineness

Figure 4-4 shows the effect of different ball sizes on product fineness at 480 and 1030 rpm. It is observed that it is possible to reach finest product with balls having the diameter of 2.83 mm at 480 rpm while finest product can be obtained at 1030 rpm with balls having the diameter of 1.68 mm. This situation can be explained in a way that the large balls have higher kinetic energy consumed for breakage inside the mill than small balls at lower stirring speeds. This finding is in accordance with the results reported by Tüzün (1994). Jankovic (2003) indicates that the transfer of momentum from the stirrer to the bulk of the media charge reduces as the ball size decreases. Therefore, there must be a media size for a particular stirrer speed below which further decrease in media size will have a deleterious effect on grinding performance.

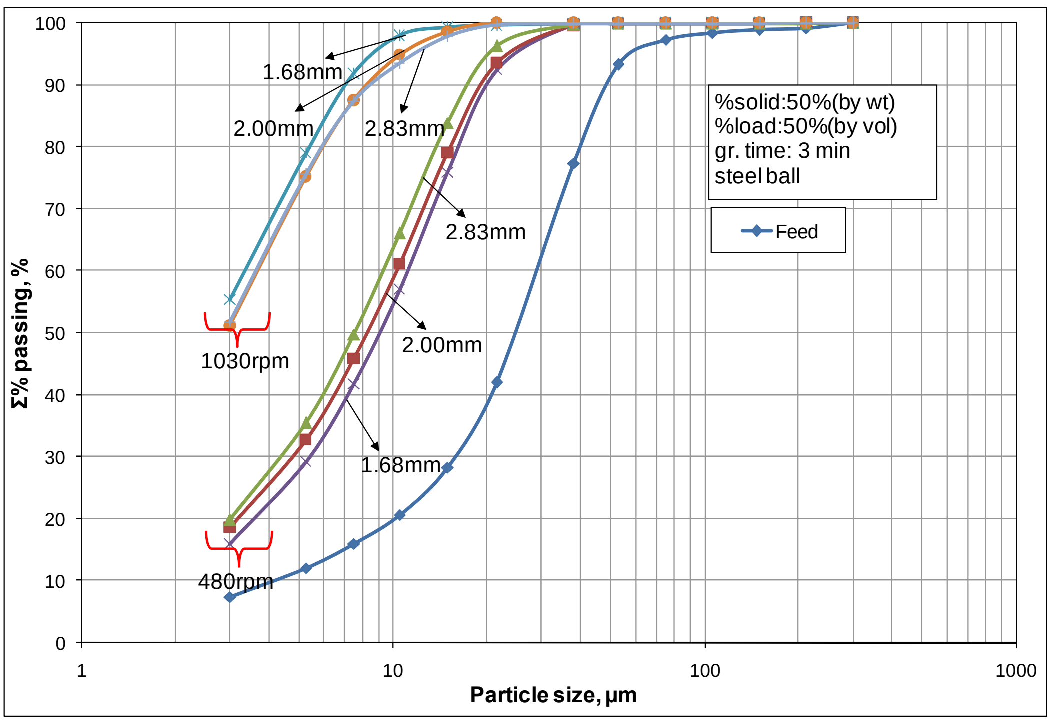

Figure 4-4. Effect of changes in ball size on product fineness with various impeller speeds

Figure 4-5 shows the effect of solids content of the pulp on product fineness. As can be seen from the graph, finest product was obtained with the pulp having low solids content (35%) while no significant change in the product size distribution was observed over the range of 50 to 80% solids although at 50% solids, the elimination of coarse size was more pronounced. This finding is similar to what has been reported by Sepulveda (1981). At higher %solids, the decrease in grinding efficiency may be attributed to the pulp viscosity.

Since the product fineness significantly increases with grinding time, the rheological properties tend to predominate in the system (Bernhardt et al., 1999; Zheng et al., 1997; Klimpel, 1999). Inter-particle and electrostatic forces lead to the formation of agglomeration and aggregation. This results changes in rheological property in fine grinding operations. The effect of pulp viscosity becomes particularly important. The optimization of the rheological behaviour of a pulp can enhance the energy efficiency and throughput in fine grinding operations. Therefore, the addition of a grinding aid to a feed pulp permits a higher solids concentration of a ground pulp (Gao and Forssberg, 1993; Zheng et al., 1996; Yue and Klein, 2004; He et al., 2006; He and Forssberg, 2007). Although finest product can be obtained with low density pulps, working with such a material significantly reduces the capacity of the equipment from the operational point of view.

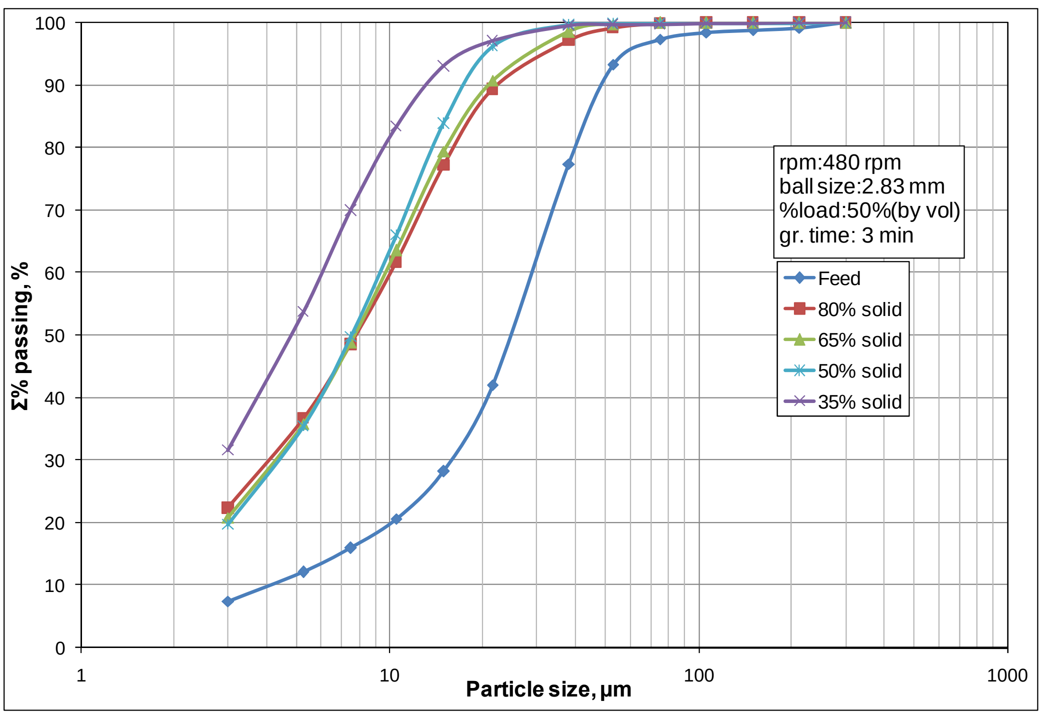

Figure 4-5. Effect of %solid on product fineness

Figure 4-6 show the effect of ball load on product fineness. In Figure 4-6, it is shown that higher ball loads to the mill is advantageous in terms of not only product fineness but also capacity because the higher charges allows to process higher feedrates. The motor power increases with increase in ball load in the mill. However, in the literature, same adverse effect regarding to low energy efficiency due to the increased energy input is reported since much more energy is consumed to stir up the grinding media in the mill.

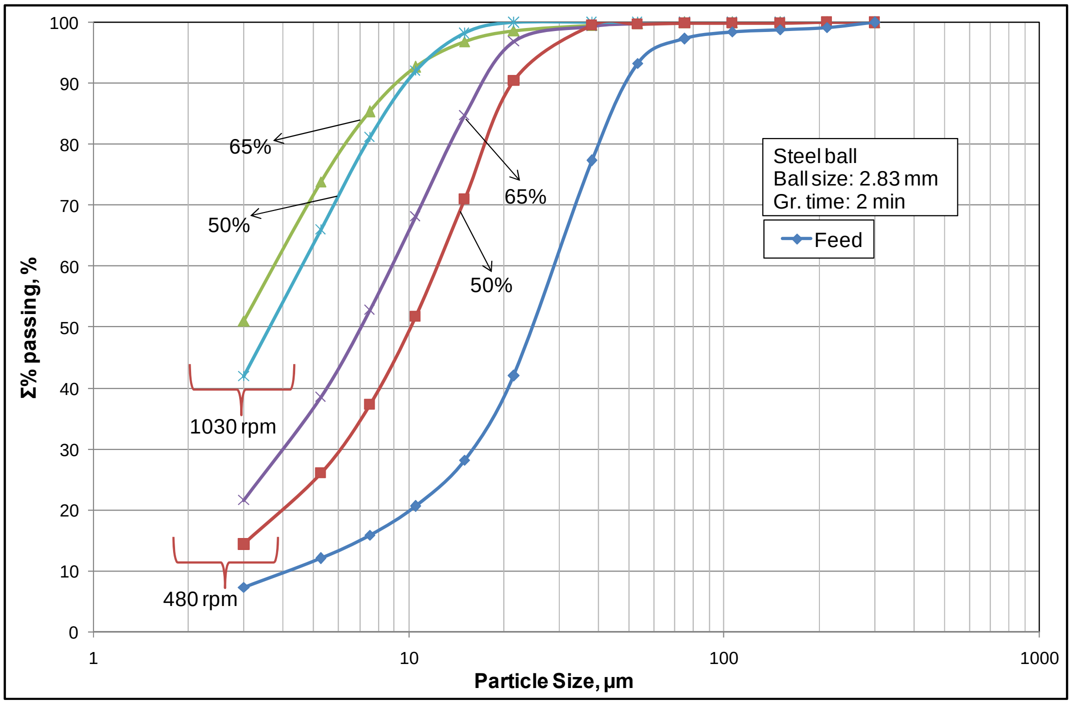

Figure 4-6. Effect of ball load on product fineness

In Figure 4-7, the effect of amount of material in the voids between the grinding media can be observed. It is also a good indication of how the particle size distribution of the product will be changed with various feedrates. In an open or closed circuit grinding, the amount of material held up in the mill is changed with feedrate. In other words, the higher the feedrate, the higher the amount of material in the mill. As can be seen from the graph, at the same operating conditions, it is possible to obtain finer product when hold-up material is low in the mill. However, from the operational point of view, not only does it lead to lower feedrates but it also causes higher wear rate as ball to ball collisions become prominent in the mill.

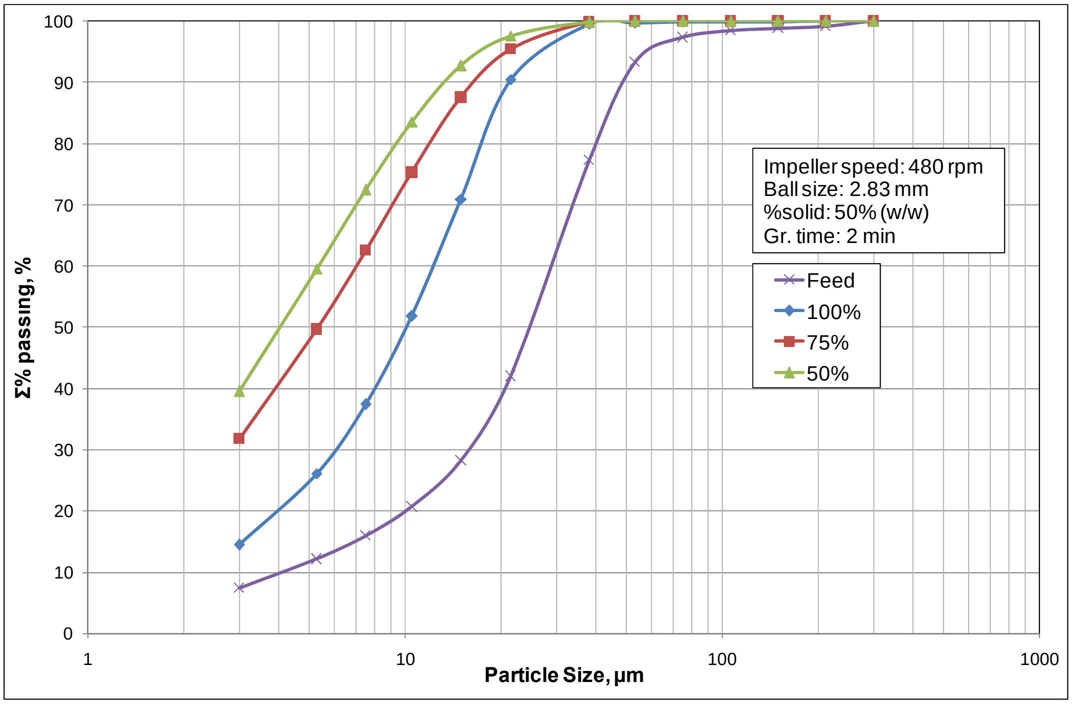

Figure 4-7. Effect of material filling ratio on product fineness

The results obtained in this study show that stirred ball mills should be operated at highest possible impeller speed, ball charge and %solid with small balls in order to obtain finest product with acceptable capacity.

Tests carried out in HU laboratory had indicated that major operating parameter affecting the product fineness was the impeller speed. Therefore, tests carried out at CBI's laboratory were especially done to observe the effect of different material used as grinding media on fineness with various impeller speeds. As shown in Figure 4-8, denser grinding media is capable of producing finer product. Densities of steel balls, zirconium balls and river pebbles are 7.8, 4.0 and 2.8 g/cm^3, respectively. Although it is possible to reach finest product with using steel balls in stirred media mill, steel balls may have adverse effect on flotaton due to the precipitation of iron oxides on mineral surfaces (Gao et al., 2000; Pease et al., 2006; Graves and Boehem, 2007). This problem could be ceased by using inert material such as river pebble.

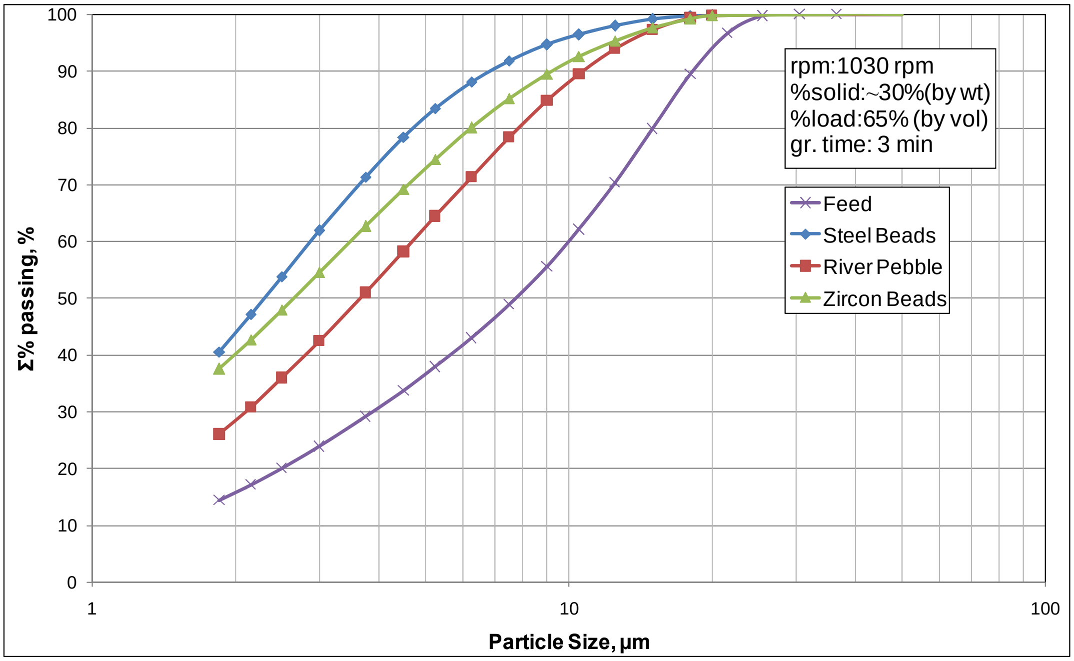

Figure 4-8. Size distributions of products after stirred media milling with three different grinding medias

4.2. Pilot Scale Stirred Media Tests

In pilot scale stirred media mill tests, experiments were done to investigate the effect of different stirring speeds, feed rates, media load and media type (steel balls and river pebbles) on grinding performance of the pilot stirred media mill. Furthermore, the effect of changes in particle size distribution of feed material to the mill was also investigated by grinding the different streams around the circuit. The first 15 experiments in which the tests were focused on the effects of impeller speed and feedrate were carried out on Zn Column Scavenger concentrate. Cu Cleaner 4 tail was used as feed material in the tests in which the effects of media load and type were primary concern. The streams on which the tests were carred out were summarized in Table 3-6 together with the tests' conditions. In pilot scale tests, torque values were also recorded with the aid of torquemeter installed between the motor and the impeller shaft of the mill. These torque values were used to calculate the specific energy consumption of the mill in each test according to Eq. 4-1.

$$E(\frac{kWh}{t}) = \frac{1.04E^{-4} \times torque(Nm) \times impeller\ speed(rpm)}{Feedrate(tph)}$$ Eq. 4-1

Specific energy consumptions of the mill in 15 tests are given in Table 4-1.

Table 4-1. Specific energy consumption in the tests

	Impeller Speed (rpm)	Feedrate (kg/h)	Media Load (v/v)	Torque (Nm)	Power (kW)	Specific Energy (kWh/t)
Exp. 1	1000	765	46	56	5.85	7.64
Exp. 2	1200	765	46	66	8.27	10.81
Exp. 3	1400	765	46	81	11.84	15.48
Exp. 4	600	765	46	34	2.13	2.78
Exp. 5	800	765	46	44	3.68	4.81
Exp. 6	1400	916	46	82	11.99	13.09
Exp. 7	1200	916	46	64	8.02	8.76
Exp. 8	1000	916	46	53	5.53	6.04
Exp. 9	800	916	46	42	3.51	3.83
Exp. 10	600	916	46	33	2.07	2.26
Exp. 11	1400	557	46	81	11.84	21.26
Exp. 12	1200	557	46	65	8.15	14.62
Exp. 13	1000	557	46	54	5.64	10.12
Exp. 14	800	557	46	43	3.59	6.45
Exp. 15	600	557	46	34	2.13	3.82
Exp. 16	1400	259	46	82	11.99	46.29
Exp. 17	1200	259	46	63	7.89	30.48
Exp. 18	1000	259	46	54	5.64	21.77
Exp. 19	1000	193	46	53	5.53	28.68
Exp. 20	1200	193	46	61	7.64	39.61
Exp. 21	1400	193	46	80	11.70	60.60
Exp. 22	1000	193	53	59	6.16	31.92
Exp. 23	1200	193	53	70	8.77	45.45
Exp. 24	1000	193	60	68	7.10	36.79
Exp. 25	1200	193	60	80	10.03	51.94
Exp. 26	1000	193	67	72	7.52	38.96
Exp. 27	1000	193	46	25	2.61	13.53
Exp. 28	1200	193	46	27	3.38	17.53
Exp. 29	1400	193	46	33	4.82	25.00
Exp. 30	1400	66	46	78	11.40	172.78
Exp. 31	1400	231	46	77	11.26	48.73
Exp. 32	1400	122	46	79	11.55	94.67
Exp. 33	1400	267	46	78	11.40	42.71
Exp. 34	1400	426	46	80	11.70	27.46
Exp. 35	1400	182	46	78	11.40	62.66
Exp. 36	1400	327	46	79	11.55	35.32

Particle size distribution of the feed and products obtained from different stirring speeds at 557, 765 and 916 kg/h are given Figure 4-10, Figure 4-11 and Figure 4-12. Since the particle size distributions obtained at 1400-1200 rpm and 800-600 rpm were close to each other, only those obtained at 1400 and 600 rpm are presented in the graphs. In Figure 4-9, the relation between the power drawn by the motor and the impeller speed is given. As can be seen from the figure, the power drawn by the motor changes exponentially with the impeller speed.

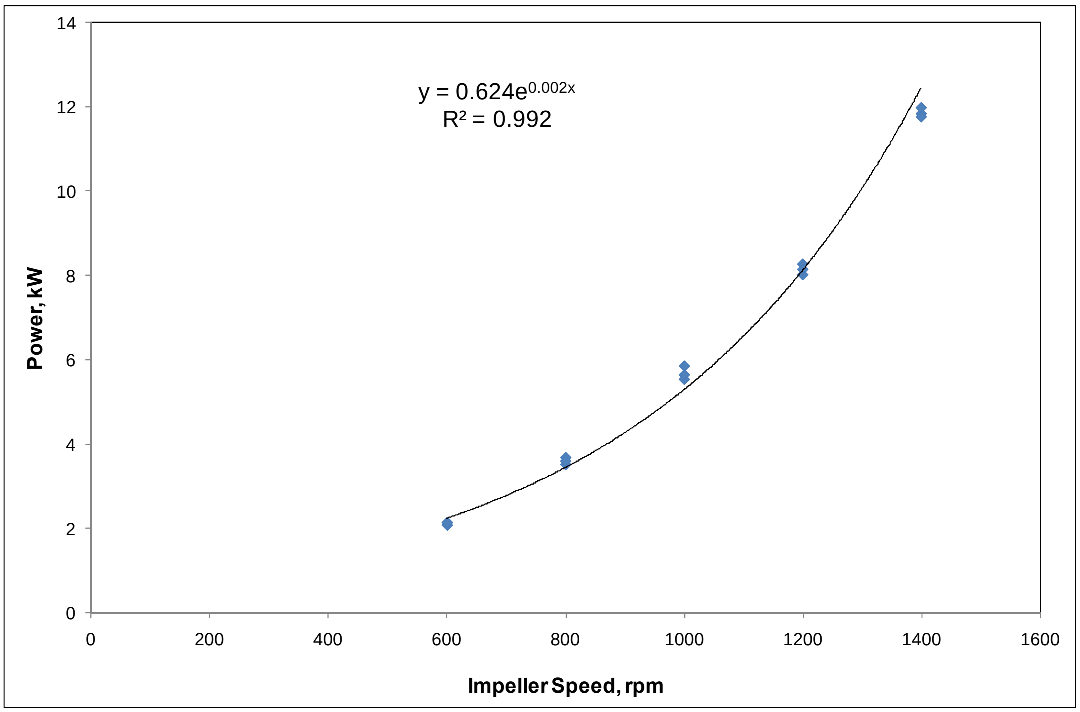

Figure 4-9. The relation between the impeller speed and power

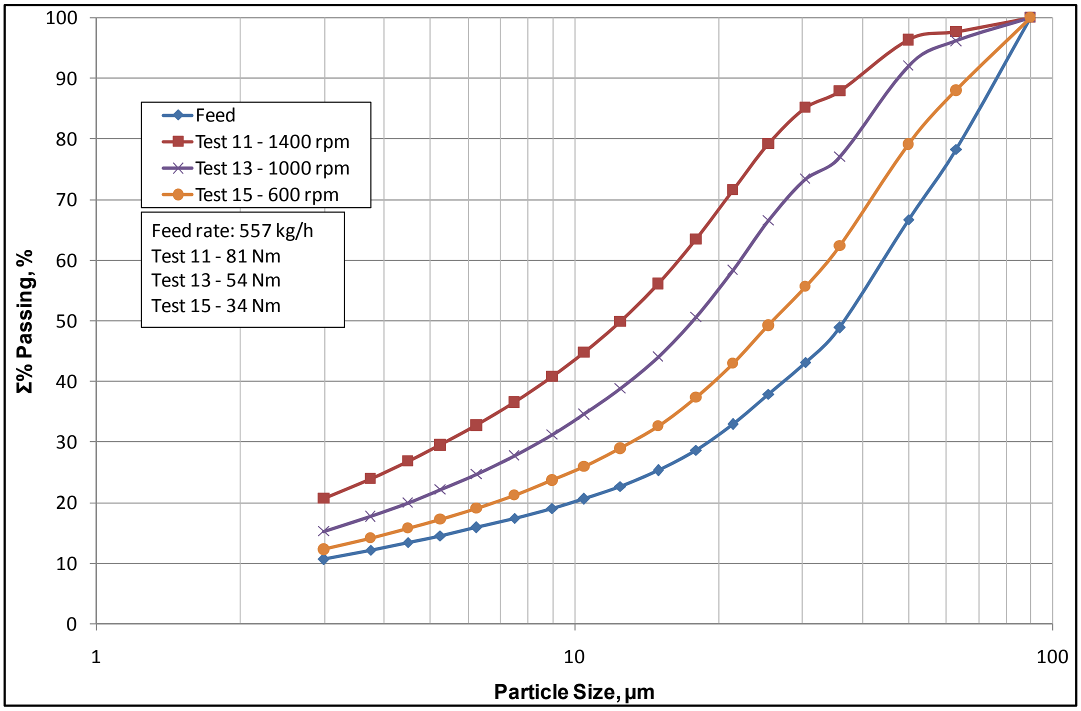

Figure 4-10. Effect of different stirring speeds at 557 kg/h on product fineness

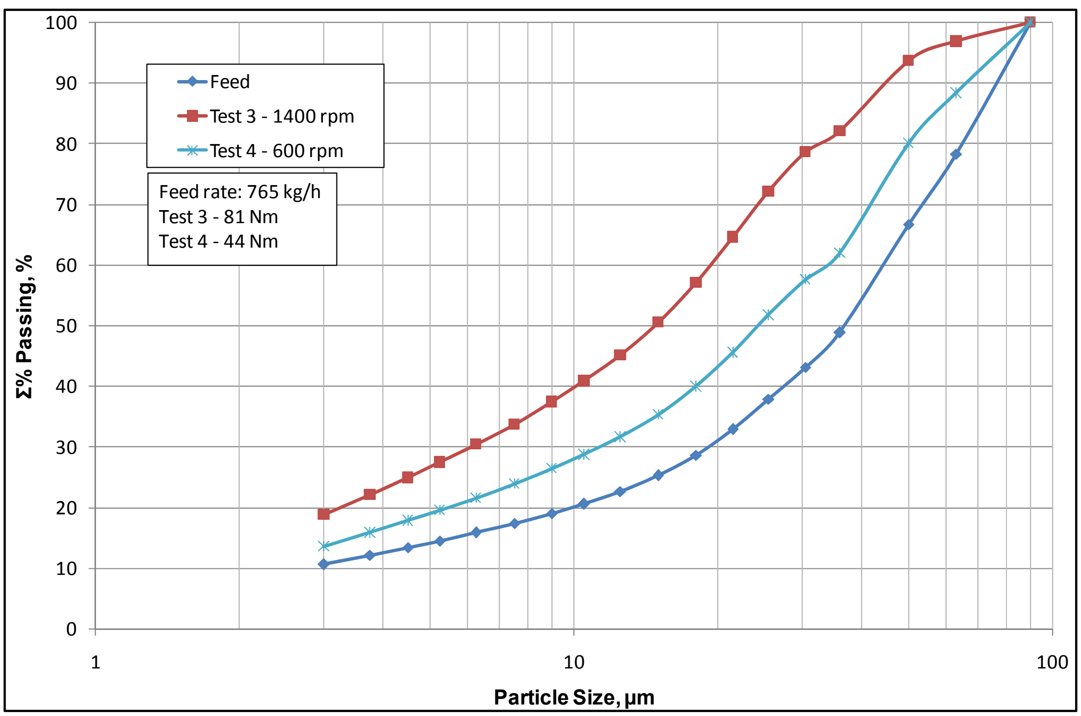

Figure 4-11. Effect of different stirring speeds at 765 kg/h on product fineness

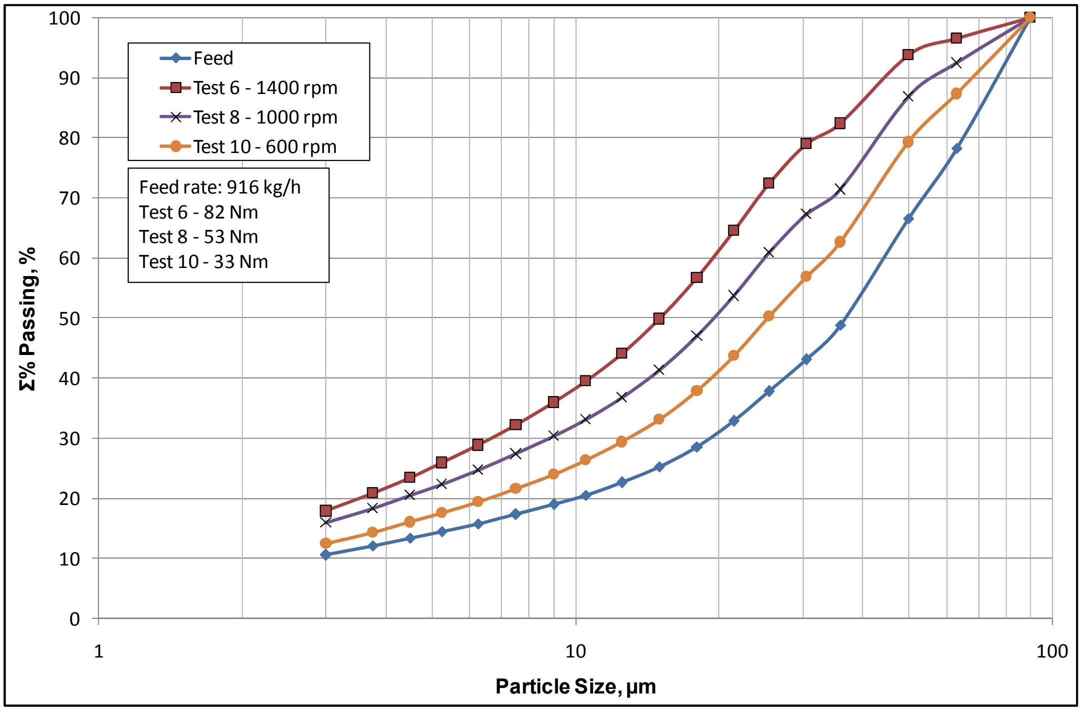

Figure 4-12. Effect of different stirring speeds at 916 kg/h on product fineness

As can be seen from the graphs above, increase in stirring speed caused significant size reduction especially at coarse sizes. This situation verifies the result of laboratory scale stirred ball mill tests which indicated the preferential elimination of coarse sizes in the mill.

Particle size distribution of feed and the products obtained from different feedrates at 1400 rpm are given in Figure 4-13. As can be seen from the particle size distributions obtained at different feedrates at 1400 rpm, the product fineness increases with decrease in feed rate due to the increase in residence time of particles in the mill. However, the power drawn by the mill remained the same as the torque observed at different feedrates were almost the same.

During the tests, ball charge of the mill was gradually increased by adding make-up balls. Figure 4-14 shows the effect of ball charge on product fineness. As can be seen from the graph below, adding more grinding media slightly increases the product fineness. In Figure 4-15, the relation between the media load and the power drawn is given. As can be seen, the power drawn linearly changes with the amount of grinding media in the mill.

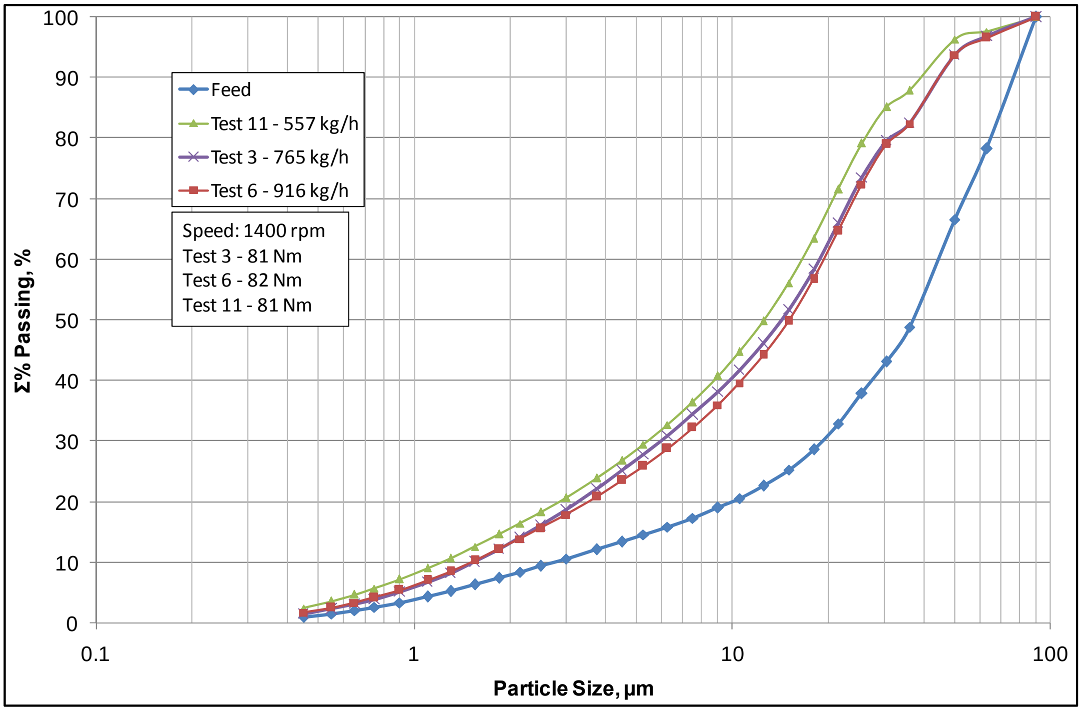

Figure 4-13. Effect of different feed rates at 1400 rpm on product fineness

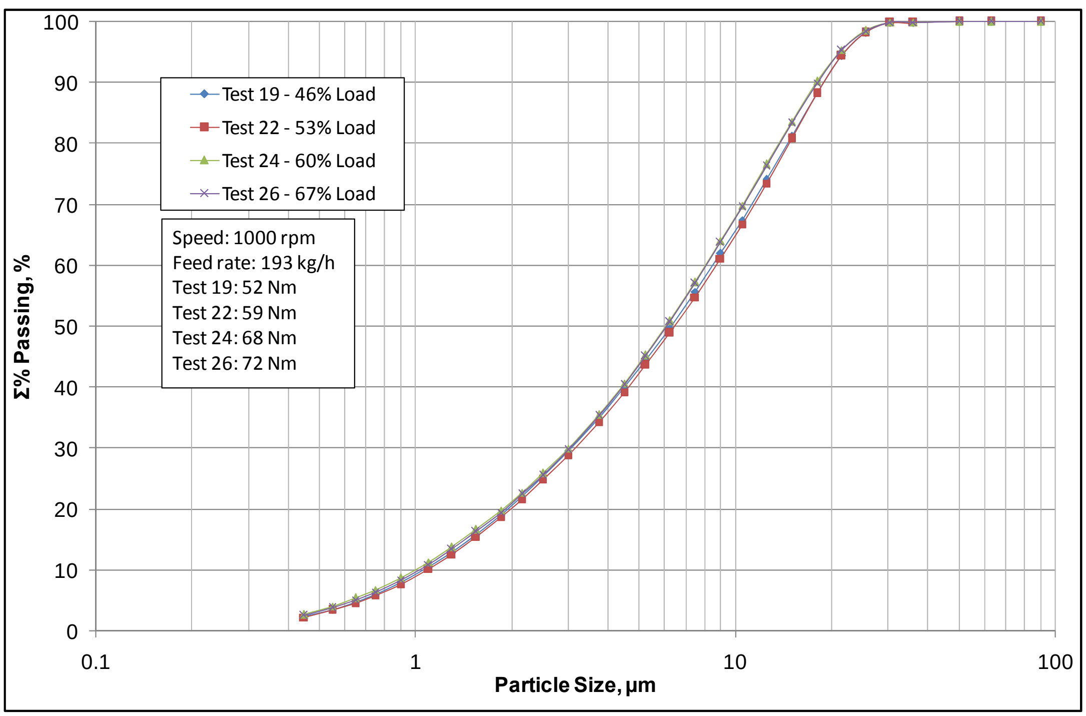

Figure 4-14. The effect of ball charge to the mill on product fineness

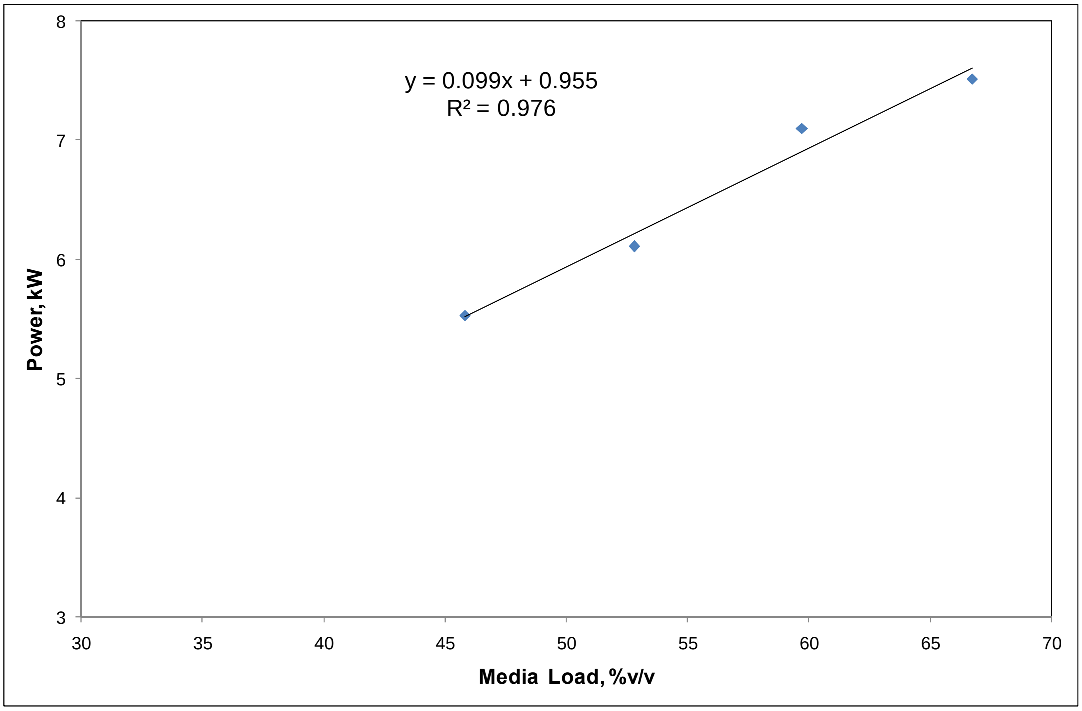

Figure 4-15. The relation between media load and power

The result of flotation tests after grinding with different grinding media in laboratory stirred ball mill indicated that the inert media such as river pebbles has enhanced the flotation to some degree considering its flotation obtained with steel balls. Apart from the advantages of river pebbles in flotation, lower specific gravity causes low energy consumption in the mill. Figure 4-16 shows the effect of different grinding media such as steel ball and river pebble on product fineness. As can be seen from the graph, at same stirring speed, it is possible to obtain finer particles with steel balls. However, considering the torque value, an indication of energy consumption in the mill, recorded for steel ball, it is much higher than that for river pebbles. Difference in fineness can be justified by applying higher stirring speeds for river pebbles or any other material with lower density. The ratio of density ($\rho_{steel}/\rho_{pebble}$=7/2.8) is 2.50 while the ratio of the power drawn (P_{steel}/P_{pebble}=11.70/4.82) is 2.42. This situation enables to comment that the power drawn changes linearly with the density of material used as grinding media in the mill.

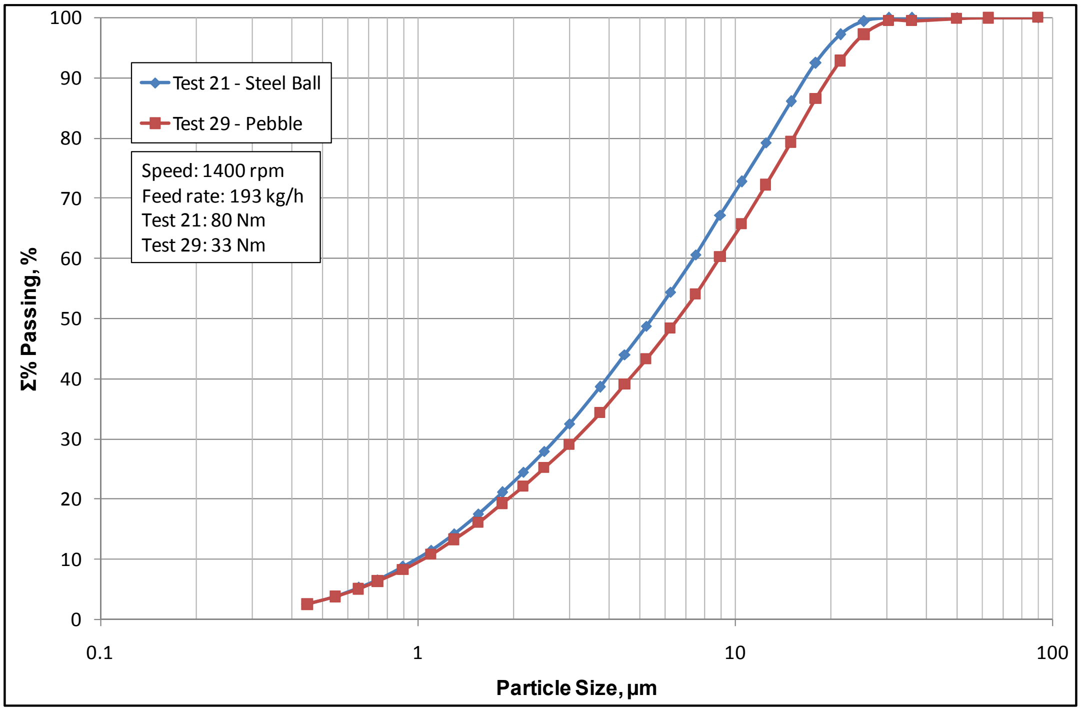

Figure 4-16. Effect of different grinding media on product fineness

After the operating conditions that gave finest product were determined, several other streams in the circuit were ground in the mill. These streams were Zn Column Scavenger tail, Zn Column tail, Zn Cleaner 1 tail, Cu Cleaner 1 Scavenger tail, Cu Rougher concentrate, Cu Rougher Cyclone U/F, Cu RG Cyclone O/F, Cu Cleaner 3 tail and Cu Cleaner 4 tail. The particle size distributions of feed and products of each stream after grinding were graphically presented in Figure 3-10, Figure 3-11 and Figure 3-12. As can be seen in the graphs, significant size reduction can be achieved in an open circuit stirred milling. However, size reduction at fine size fractions is not as much as that at the coarse size fractions. This situation provides the production of fine material without increasing the amount of very fines. Therefore, the size reduction in the mill is more pronounced when the feed is coarse or classified. It indicates that in plant operation, feed material should be classifed before introducing to the mill.

5. MODELING OF COMMINUTION PERFORMANCE OF STIRRED MEDIA MILLING

After having investigated the effects of major operating parameters on the grinding efficiency of stirred media mills operating in both batch and continuous tests, the attempt was made to find out the relation between the operating parameters and the particle size distribution of product. For this reason, an amprical approach based on the normalization of particle size distributions according to d_{50} was used for batch laboratory scale tests while for pilot scale continuos tests, population balance model was used.

5.1. Modelling of Batch Grinding Tests

After having determined all the particle size distributions of the products obtained from different grinding conditions in laboratory scale stirred media mill, it is observed that the product particle size distributions can be normalized according to the d_{50} value of each particle size distribution to form a self similar curve in spite of different operating conditions. With respect to self similarity, Kapur et al.(1996) also indicated this characteristic property. In his study, it was concluded that the self similar curve remains invariant and the energy-reduction ratio also does not vary materially. Recently, Rao and Datta (2006) showed the self similarity of product particle size distributions which were normalized with respect to d_{50}. The self similar curve obtained from the results of this syudy is given in Figure 5-1. Moreover, the self similar curve calculated from the particle size distributions of the products obtained from the tests carried out in CBI's laboratory was found to be represented by the same curve given in Figure 5-1 in spite of the difference in particle size distributions of the feed materials used in these tests (Figure 3-1). Two normalized curves are given in Figure 5-2.

Self similarity enables to represent this normalized curve with a mathmetical expression. Due to the fact that the shape of the curve is very much similar to hydrocyclone efficiency curve according to overflow, the Whiten equation given below was used to represent this curve.

$$\Sigma\%oversize = C \times \frac{\exp(A) - 1}{\exp(A \times D) + \exp(A) - 2} \qquad \text{Eq. 5-1}$$

Where,

D: d/d_{50}
A: parameter related to the slope of the curve
C: the amount of material finer than the last sieve in the row, %

With the aid of SPSS statistics software, the measured values were fitted the equation. As a result of this, the variables in the equation were found to be as follows; **C: 99.568** and **A: 1.007**. The sum of squares was found to be 0.996 which also indicates that the predicted values are in good agreement with the measured ones. The calculated and measured normalized particle size distribution curves are given in Figure 5-3.

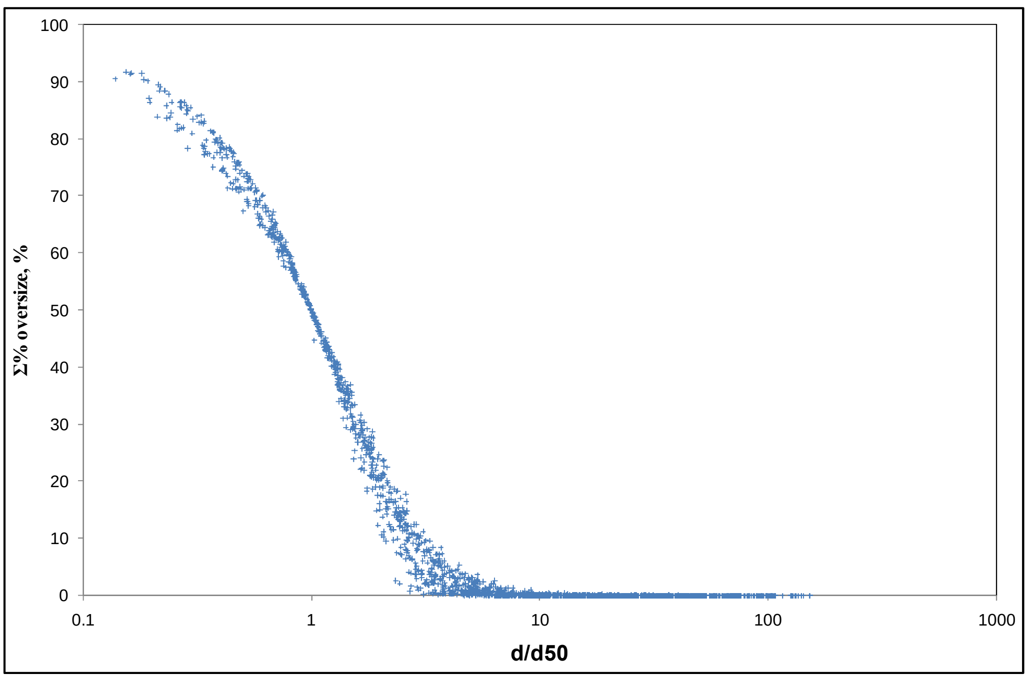

Figure 5-1. Normalized particle size distribution

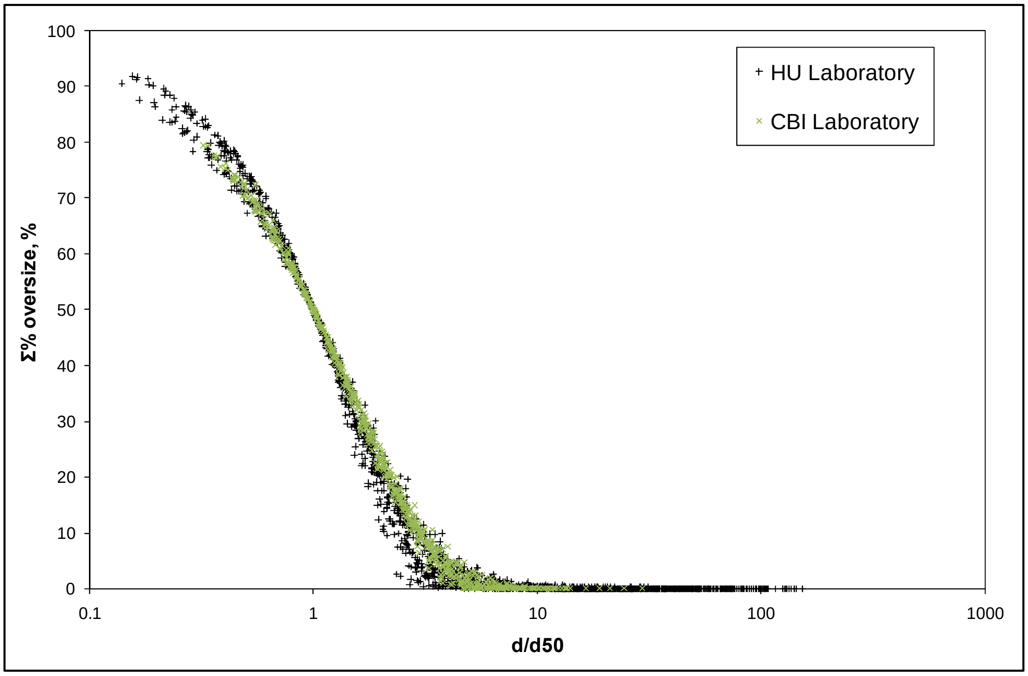

Figure 5-2. Comparison of the normalized particle size distributions

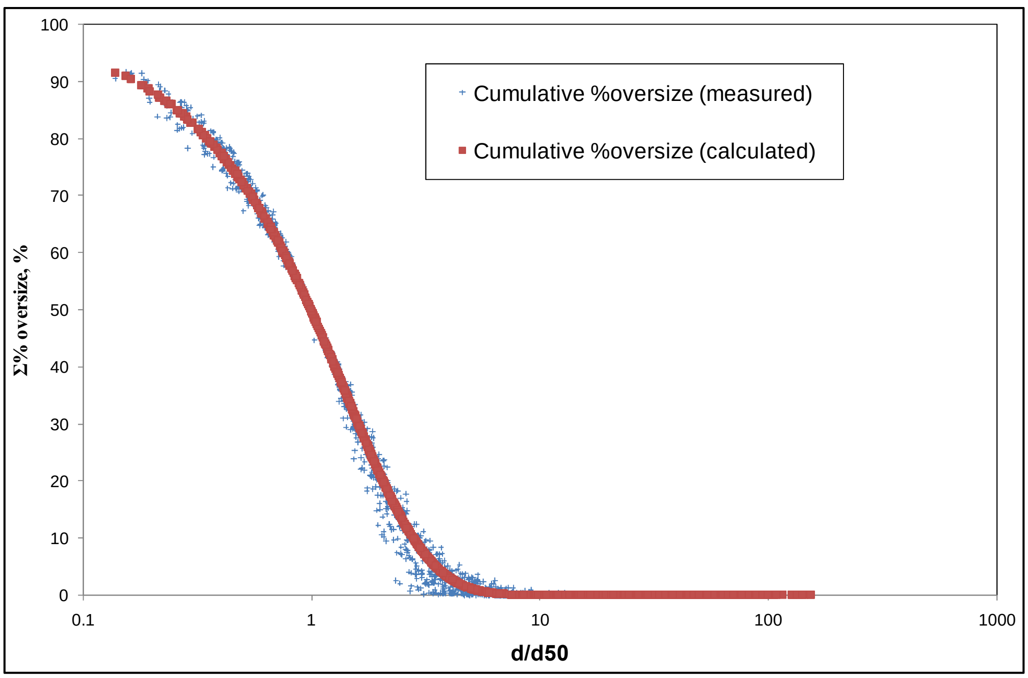

Figure 5-3. The calculated and measured normalized particle size distributions

Fitting the curve into the equation enables to predict the particle size distribution of the product if the d_{50} value is known. For this reason, the relationships between d_{50} and the operating conditions such as impeller speed, media size, media charge and media density were investigated.

5.1.1. The Relationships Between the Operating Conditions and d_{50}

So far, the effects of major operating parameters of stirred media mill on the particle size distribution of product in both batch and continuous operation have been given. In addition, it was also observed that independent of the operating conditions, all the particle size distibutions of products can be normalized according to the value of d_{50} in a way that forms a self similar curve which can be expressed with a mathematical equation. This equation enables us to predict the particle size distribution of product if the value of d_{50} is estimated. In order to this, the relationships between the operating conditions and d_{50} were investigated with available results of batch grinding tests.

It was shown that the most important operating parameters among the others was the impeller speed of the stirred media mill. It is possible to obtain finer product by increasing the impeller speed of the mill. Figure 5-4 shows the changes in the value of d_{50} with impeller speed for different media sizes of steel balls. In these tests, media load to the mill was kept constant at 50% v/v and solids content of the pulp was 50% w/w. As can be seen from the graph, d_{50} value of the product steadily reduces with increasing impeller speed for all ball sizes tested in the experiments.

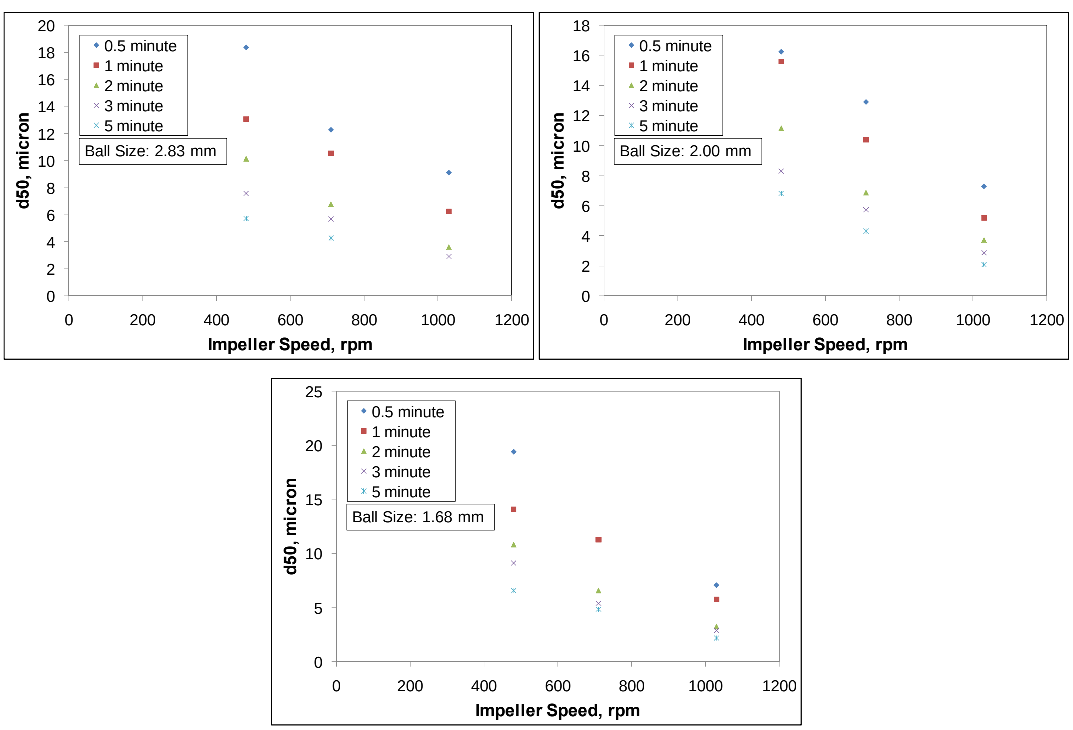

Figure 5-4. The change in d_{50} with impeller speed for different media sizes

Figure 5-5 shows the changes in d_{50} values with media size for different impeller speeds. In these tests, media load to the mill was kept constant at 50% v/v and solids content of the pulp was 50% w/w. As can be seen from the graph, there is no significant change in d_{50} values of the products in spite of the fact that particle size distributions of the products were found to be altered with media size. This situation was given in Figure 4-4. This finding clearly emphasizes the negative sides of all ampirical approaches in which the single size was used to represent whole particle size distribution. However, in order to build an ampirical approach, it was assumed that the media size did not have any influence on d_{50} value of the product.

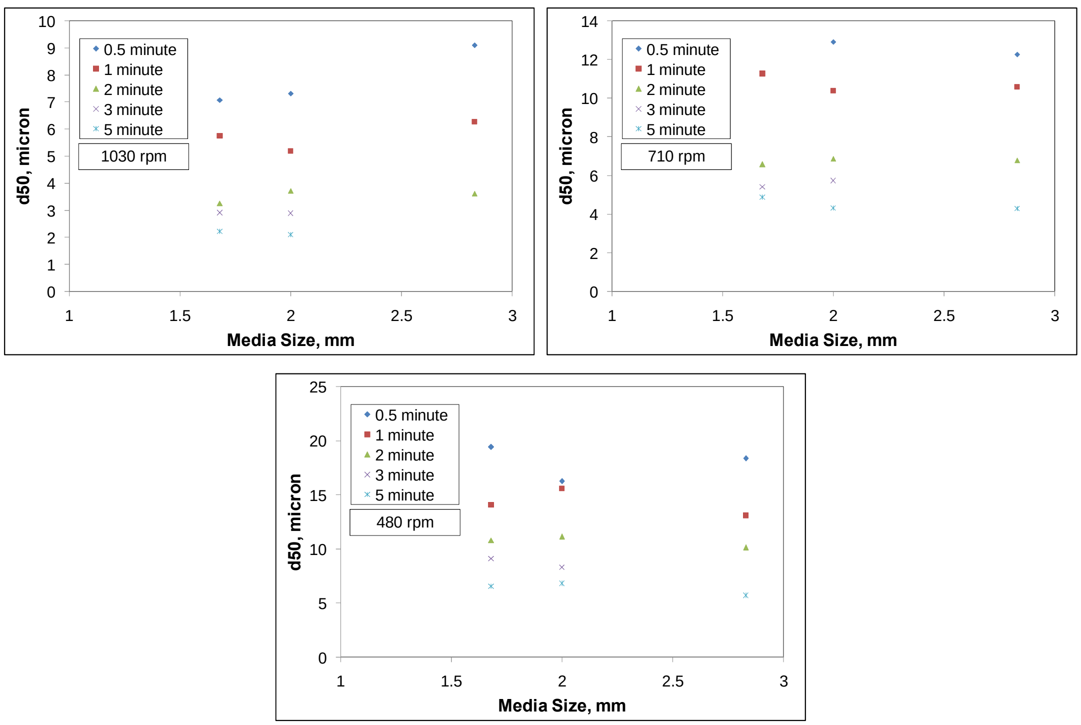

Figure 5-5. The change in d_{50} with media size for different impeller speeds

Figure 5-6 shows the effect of solids content of the pulp on d_{50}. In these tests, media load to the mill was kept constant at 50% v/v and size of the steel balls was 2.83 mm. As can be seen from the graph, there is a general trend in which the d_{50} value of the product increases with an increase in solids content of the pulp in the mill although particle size distributions of the products obtained from the tests in which the solids content of the pulp is higher than 50% are similar to each other (Figure 4-5). When considering the pilot stirred media milling, the power drawn by the mill drastically increases with the pulp having low solids content as the amount of material passing through the mill reduces. Therefore, for better energy efficieny, the stirred media mill should be operated at high solids content.

Figure 5-7 shows the effect of amount of grinding media in the mill on the d_{50} value of the product at various impeller speeds. In these tests, steel balls having the diameter of 2.83 mm were employed as grinding media and solids content of the pulp was 50% w/w. As can be seen from the graph, when 35% of total volume of the mill is filled with grinding media, it is possible to obtain the product as fine as when 65% of total volume of the mill is filled with grinding media. However, low media load will result in reduced capacity. Thus, in operational point of view, media load as high as possible should be preferred.

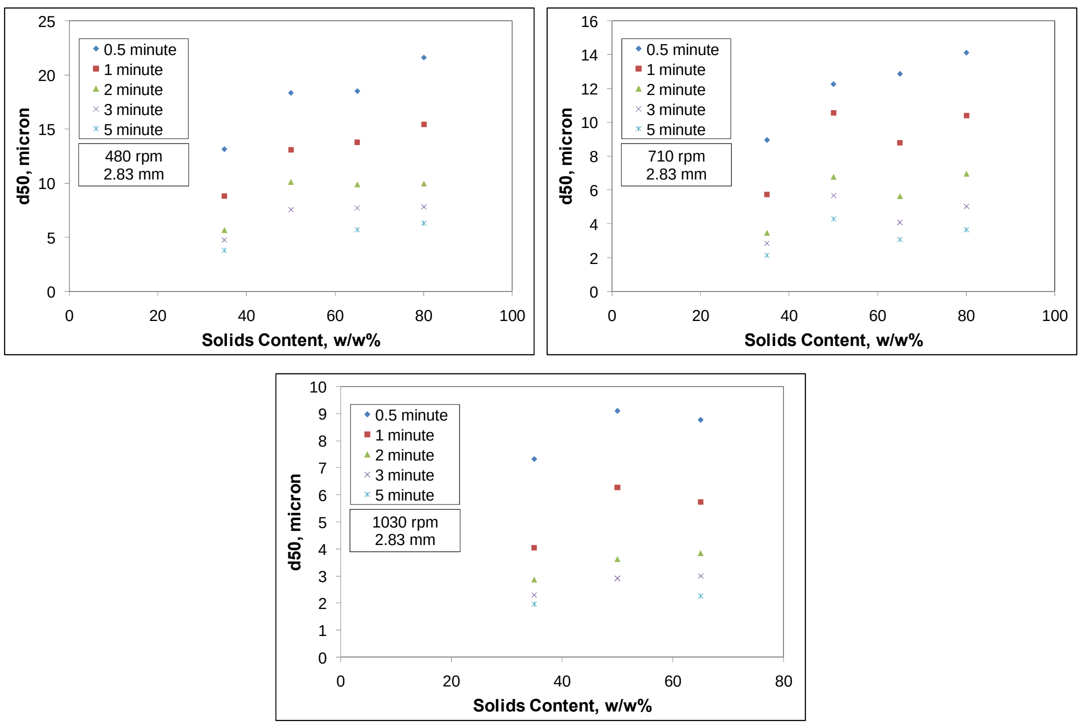

Figure 5-6. The change in d_{50} with solids content of the pulp for different impeller speeds

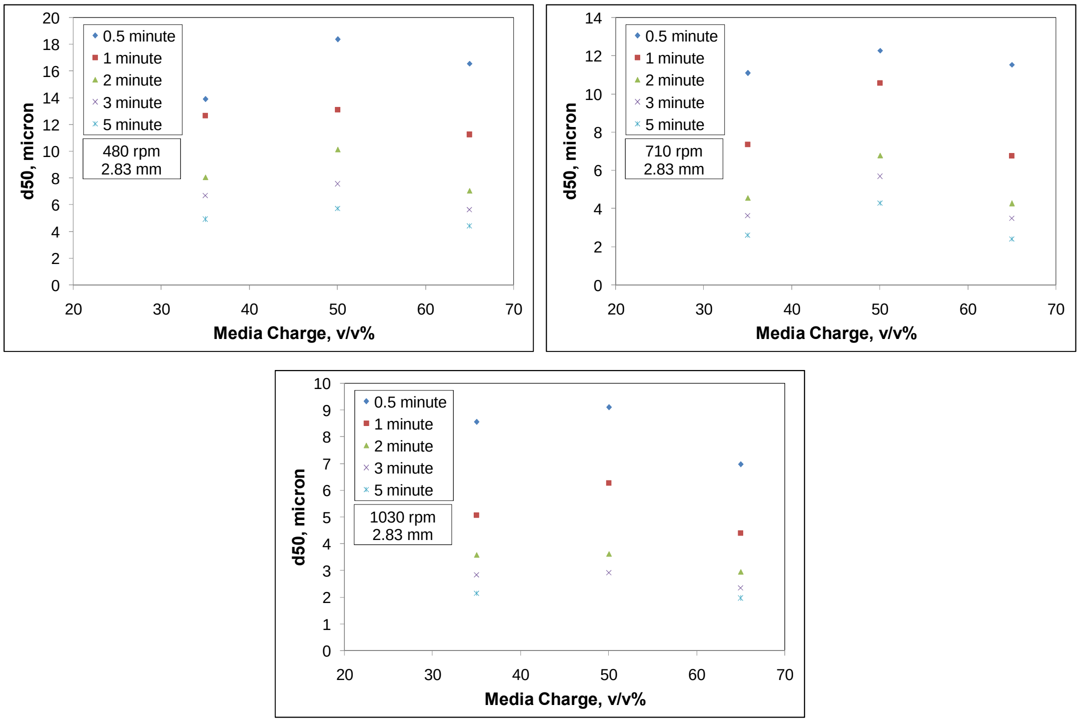

Figure 5-7. The change in d_{50} with media charge for different impeller speeds

Figure 5-8 shows the effect of the amount of material held up in the mill on the d_{50} value of the product at 480 rpm. The amount of hold-up material in the mill was calculated according to the volumetric percentage of the voids between the grinding media. In these tests, solids content of the pulp was kept constant at 50% w/w while 50% of the mill total volume was filled with grinding media having the diameter of 2.83 mm. As can be seen from the graph, it is possible to get finer product when the mill is underfilled. However, in operational point of view, this situation causes lower capacity and higher wear rates inside the mill because of the increased probability of ball to ball collision.

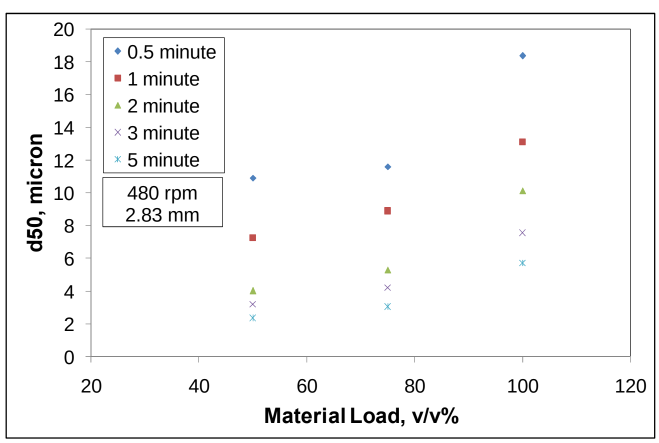

Figure 5-8. The change in d_{50} with material load for different impeller speeds

Figure 5-9 shows the effect of the density of grinding media used in the mill on the fineness of the product at various impeller speeds. In these tests, three different grinding media, namely steel balls, river pebble and zirconium balls, were employed. The sizes of steel balls, river pebble and zirconium beads were 2.83 mm, -4,76+3,35 mm and -3.00+2.40 mm, respectively. Solids content of the pulp was kept constant at 50% w/w while 50% of the mill total volume was filled with grinding media uner investigation. As can be seen from the graph, the denser the grinding media, the finer the final product. However, using of lighter grinding media significantly reduces the power drawn by the mill. This situation enables us to stir up the pulp with higher impeller speeds which eventually cause finer product with low density grinding media. Another consideration which should be taken into account in selecting grinding media is the possible adverse effect of material used as grinding media on subsequent processes in the flowsheet.

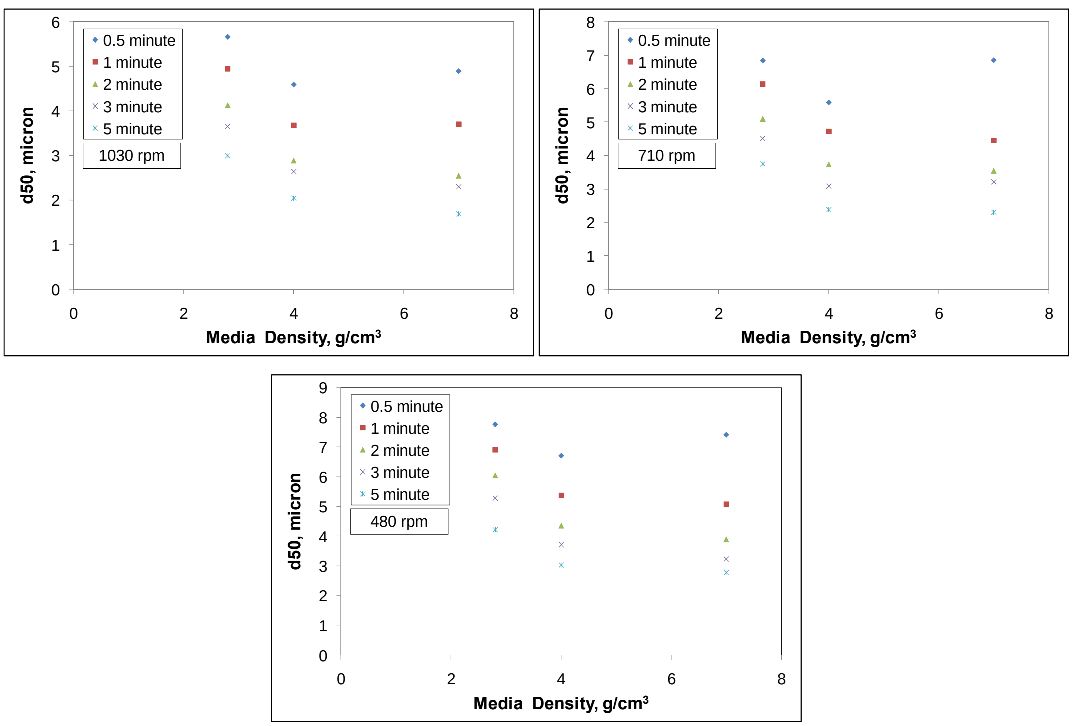

Figure 5-9. The change in d_{50} with grinding media density for different impeller speeds

Up to this point, the effects of major operating parameters of stirred media mill on the fineness of final product were investigated. As a result of this, it should be suggested that the stirred media mill should be operated at high impeller speed with the pulp having high solids content in order to get acceptable capacity. Moreover, grinding media load to the mill should be as high as possible. However, the size of the grinding media depends strictly on the top size of the feed material. The type of grinding media should be picked considering its effect on the subsequent processes in the flowsheet.

As mentioned above, the most important operating parameter for stirred media milling is the impeller speed of the mill. In addition to this, the effect of media size was assumed to be insignificant regarding to the d_{50} values of the products (Figure 5-5). If the variation of the d_{50} values of the products obtained from the tests in which the different impeller speeds and media size (steel balls) were invesigated at constant ball charge (50% v/v) and solids content of the pulp (50% w/w), with the grinding time was drawn, the graphs in the Figure 5-10 were obtained. In these tests, three different ball sizes (1.68, 2.00 and 2.83 mm) and three different impeller speeds (480, 710 and 1030 rpm) were used. As can be seen from the graphs, three distinct series were obtained according to the various impeller speeds although the ball sizes were different. In this graph, grinding time can be considered as energy given to the mill as the energy will be increased with grinding time in batch tests. Furthermore, each serie can be represented by the equation given in Eq. 5-2.

$$d_{50} = a \times \frac{1}{(gr.time)^b} \qquad \text{Eq. 5-2}$$

The equations defining each curve in these graphs have common variable b, which is 0.5156 while the variable a changes with the operating consitions investigated in the tests. Table 5-1 shows the value of variable a in Eq. 5-2 for different impeller speeds and ball sizes. However, it is assumed that the size of the ball has no significant effect on the product fineness, then variable a is only related to the impeller speed in this case. Figure 5-11 also shows the relationship between the variable a in Eq. 5-2 and the impeller speed. This linear relationship is given in Eq. 5-3.

$$a = -0.014 * (rpm) + 20.51 \qquad \text{Eq. 5-3}$$

As a result, Eq. 5-2 and Eq. 5-3 can be combined in order to calculate the d_{50} value for any grinding time, again, within the range (Eq. 5-4).

$$d_{50} = (-0.014 * (rpm) + 20.51) * (gr.time)^{-0.5156} \quad \text{Eq. 5-4}$$

By substituting the calculated d_{50} into Eq. 5-1, whole particle size distribution of the product can be calculated after having calculated d_{50}. Figure 5-12 shows comparison of the calculated and measured particle size distributions of the products for three different impeller speeds. As can be seen from the graph, the calculated particle size distributions can be said to be in good agreement with the measured ones.

Table 5-1. Relationship between the variable a and operating conditions

Impeller Speed (rpm)	Ball Size, mm		
	1.68	**2.00**	**2.83**
480	14.188	13.422	13.155
710	10.527	9.588	9.383
1030	5.135	5.141	6.089

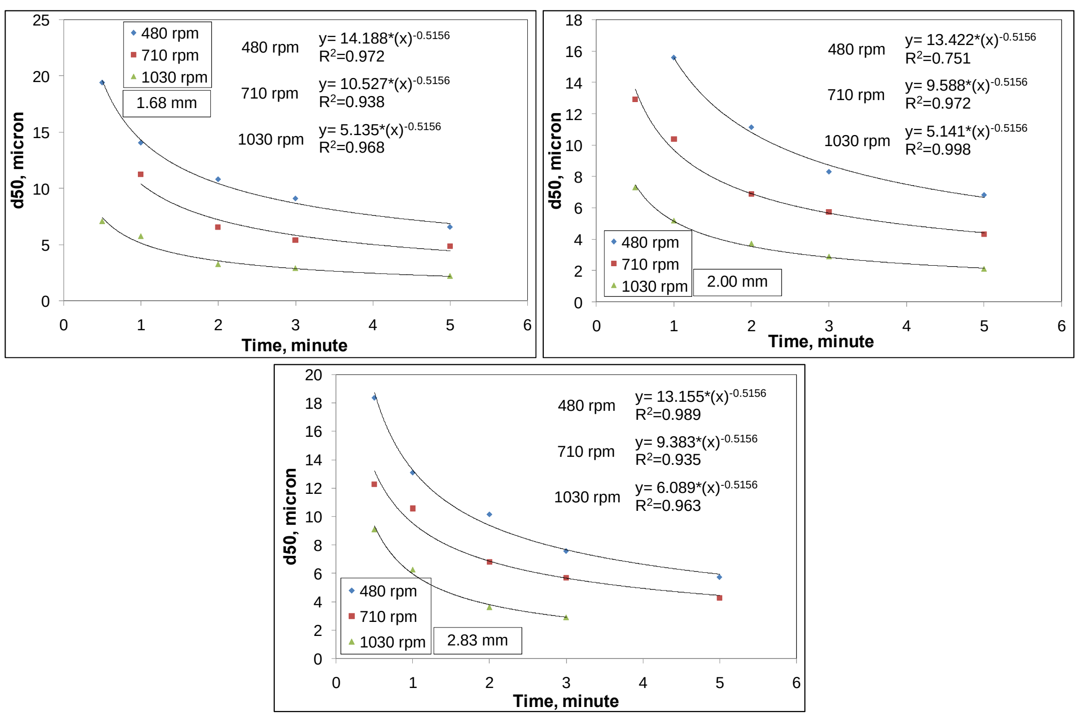

Figure 5-10. Variation of d_{50} with grinding time for 3 different impeller speeds and media sizes (steel balls)

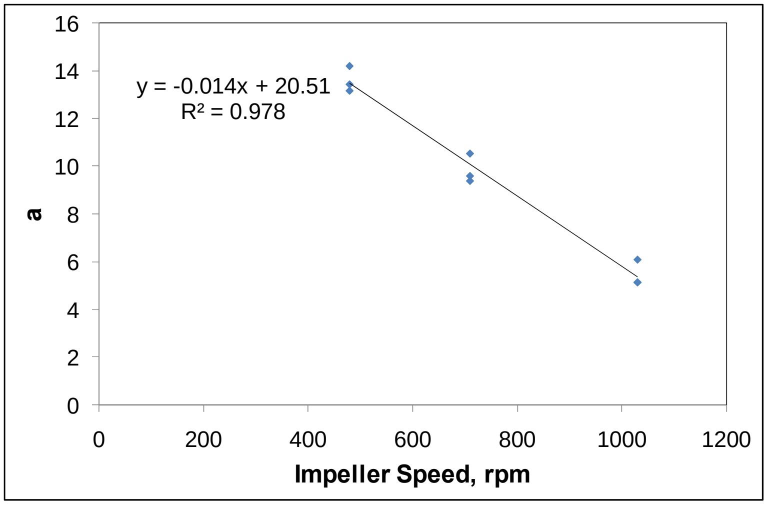

Figure 5-11. Relationship between the variable a in the equation and the impeller speed for various ball sizes

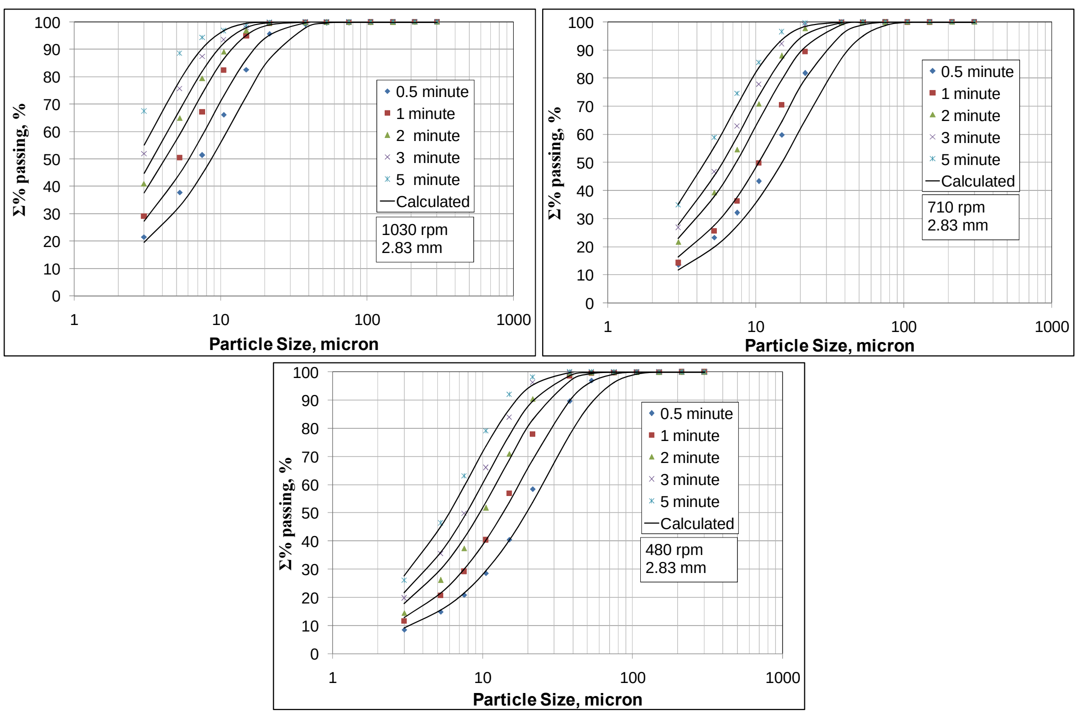

Figure 5-12. Comparison of the calculated and measured particle size distributions

Figure 5-13 shows the variation of the d_{50} values of the products obtained from the tests in which the different impeller speeds and solids contents of the pulp were investigated at constant ball charge (50% v/v) with steel balls having the diameter of 2.83 mm, with the grinding time. In these tests, three different solids contents of the pulp (35, 65 and 80% w/w) and three different impeller speeds (480, 710 and 1030 rpm) were used. It was observed that the communition performance of the stirred media mill showed different behaviour for the pulps having solids content lower and higher than 50%. This situation can be clearly seen in Figure 4-5 where particle size distributions of the materials ground in higher pulp densities were close to each other while the particle size distribution of the product obtained from low pulp density was much finer. Thus, each curve in the graphs in Figure 5-13 can be represented, again, with Eq. 5-2. The variable b in this equation changes with the impeller speed and has constant value for each impeller speed (Table 5-2). In addition to this, for each impeller speed, the variable a is related to the solids content of the pulp (Table 5-3). Figure 5-14 also shows this relationship graphically. As a result, variables in Eq. 5-2 (a and b) can be determined from these relationships to calculate the d_{50} value of the product for any solids content of the pulp within the range at various impeller speeds again within the range. By putting the calculated d_{50} into Eq. 5-1, whole particle size distribution of the product can be calculated. Figure 5-15 shows comparison of the calculated and measured particle size distributions of the products for various solids content of the pulp at three different impeller speeds. As can be seen from the graph, the calculated particle size distributions are in good agreement with the measured ones.

Table 5-2. Relationship between the variable b and the impeller speed

Impeller Speed (rpm)	**b**
480	-0.533
710	-0.613
1030	-0.570

Table 5-3. Relationship between the variable a and %solid for different impeller speeds

	Impeller Speed, rpm		
% solid	**480**	**710**	**1030**
35	8.886	5.758	4.606
65	13.334	8.507	5.816
80	14.93	9.728	----

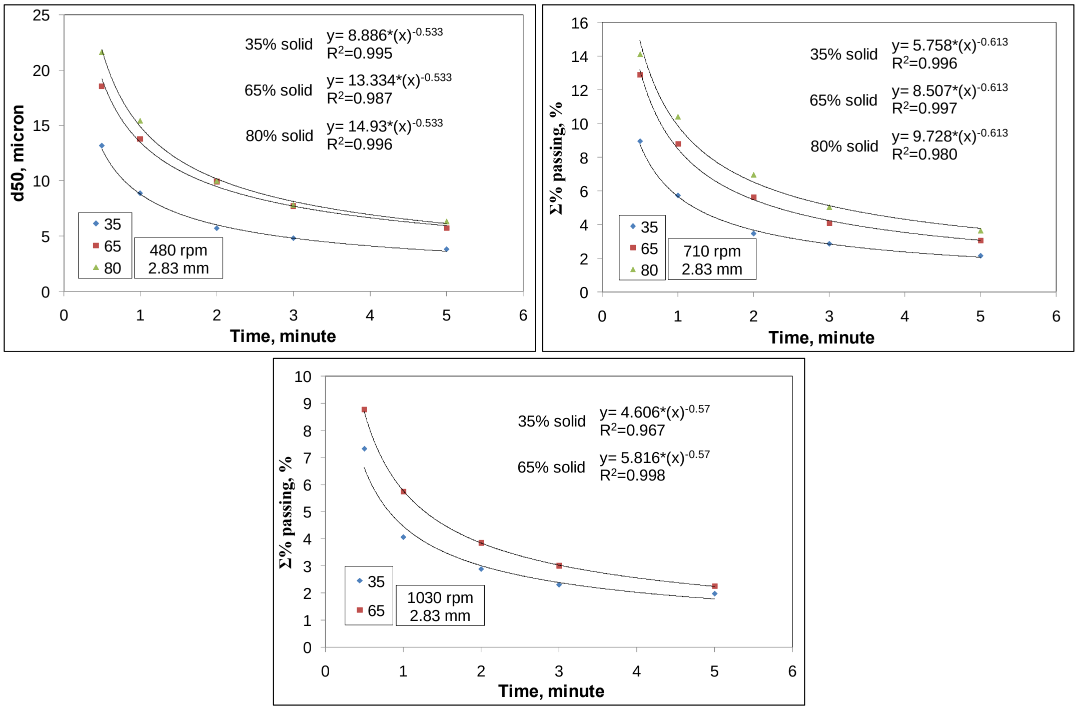

Figure 5-13. Variation of d_{50} with grinding time for 3 different impeller speeds and solids content of the pulp

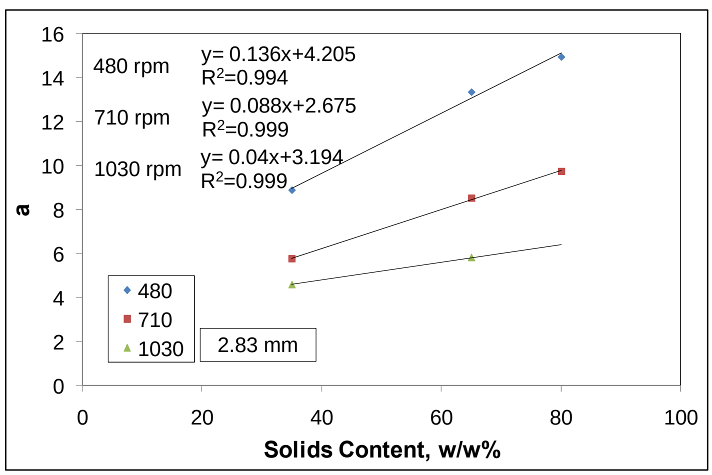

Figure 5-14. Relationship between the variable a and %solid for different impeller speeds

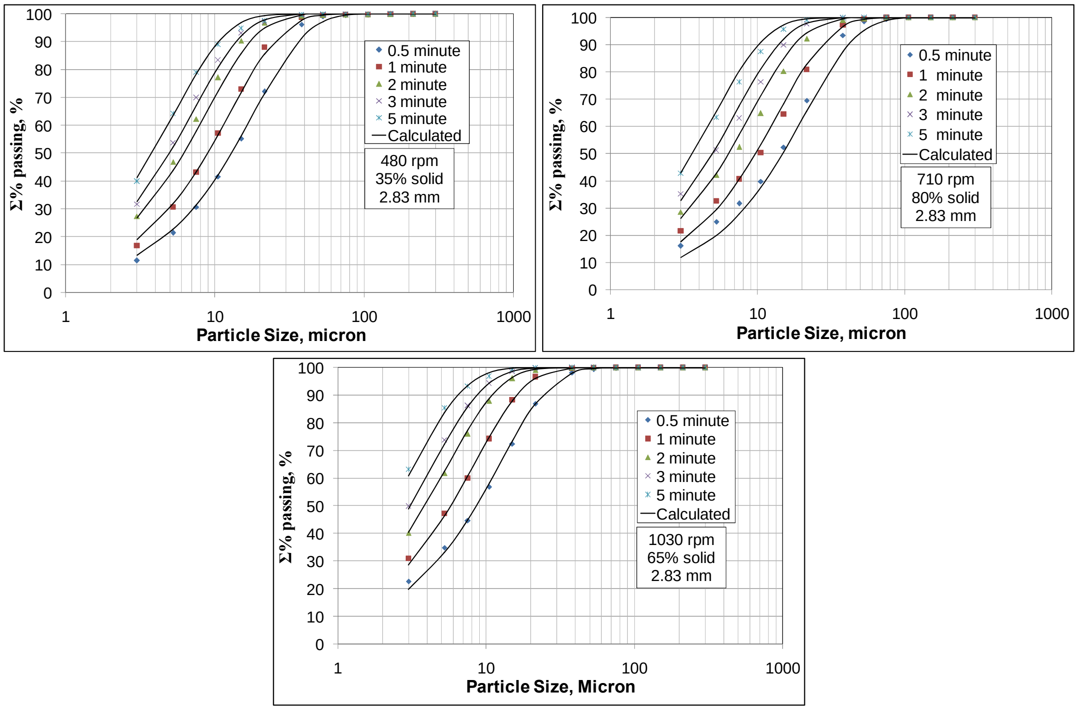

Figure 5-15. Comparison of the calculated and measured particle size distributions

Figure 5-16 shows the variation of the d_{50} values of the products obtained from the tests in which the different impeller speeds and mill loads were investigated at constant solids content of the pulp (50% w/w) with steel balls having the diameter of 2.83 mm, with the grinding time. In these tests, three different media loads to the mill (35 and 65% v/v) and three different impeller speeds (480, 710 and 1030 rpm) were used. Following the same approach, the curves were represented by the same equation in Eq. 5-2. It was found that the variable b in the equation changes with the impeller speed and had a constant value for each impeller speed. The relationship between the variable b and the impeller speed was given in each graph in Figure 5-16 and tabulated in Table 5-4. In addition to this, for each impeller speed, the variable a is related to the media load to the mill (Table 5-5). Figure 5-17 also shows this relationship graphically.

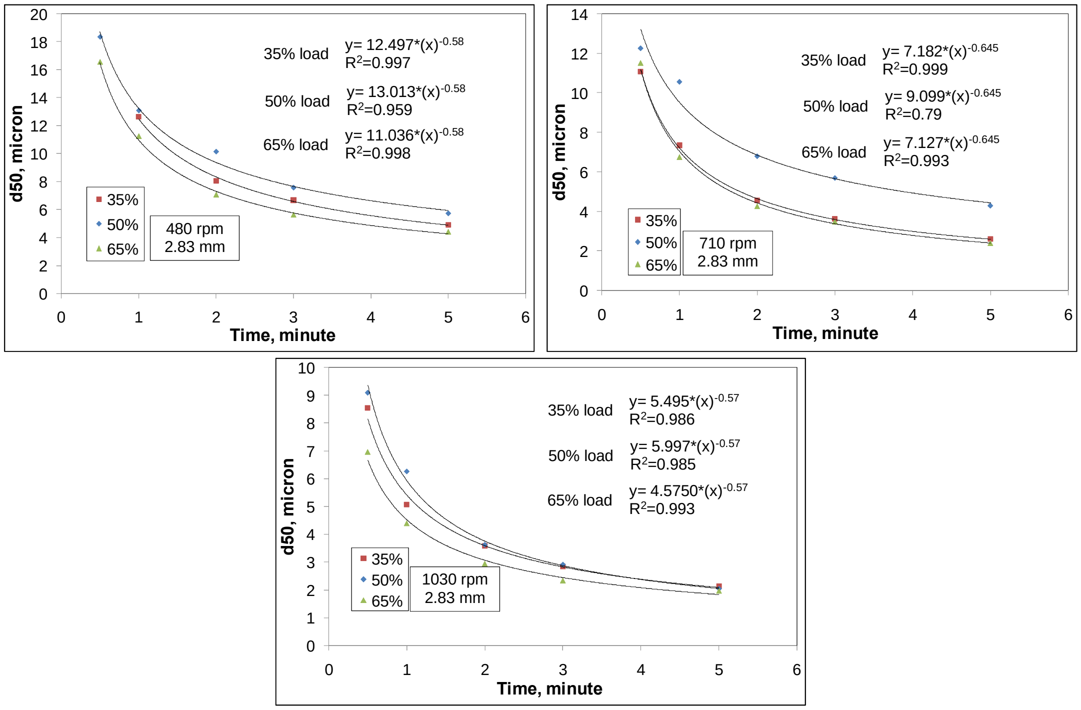

Figure 5-16. Variation of d_{50} with grinding time for 3 different impeller speeds and various media loads to the mill

Table 5-4. Relationship between the variable b and the impeller speed

Impeller Speed (rpm)	b
480	-0.580
710	-0.645
1030	-0.570

Table 5-5. Relationship between the variable a and media load for different impeller speeds

	Impeller Speed, rpm		
% load	**480**	**710**	**1030**
35	12.497	7.182	5.495
65	11.036	7.127	4.575
80	13.013	9.099	5.997

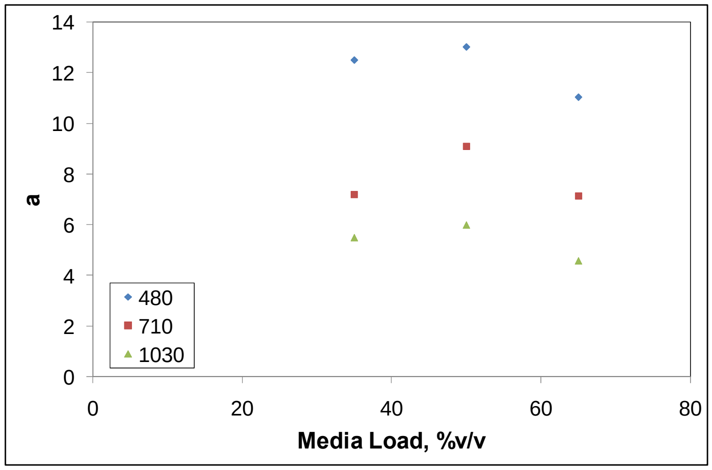

Figure 5-17. Relationship between the variable a and media load for different impeller speeds

As a result, the variables in Eq. 5-2 (a and b) can be determined from these relationships to calculate the d_{50} value of the product for any media load within the range at various impeller speeds again within the range. By putting the calculated d_{50} into Eq. 5-1, whole particle size distribution of the product can be calculated. Figure 5-18 shows comparison of the calculated and measured particle size distributions of the products for various solids content of the pulp at three different impeller speeds. As can be seen from the graph, the calculated particle size distributions are in good agreement with the measured ones.

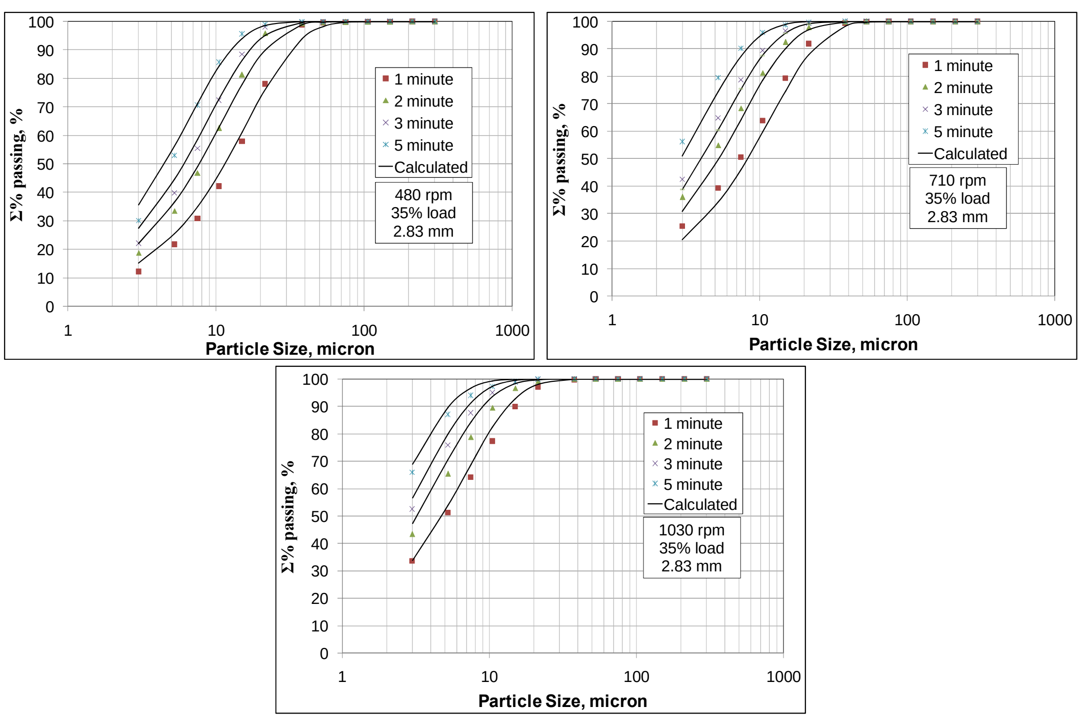

Figure 5-18. Comparison of the calculated and measured particle size distributions

Figure 5-19 shows the variation of the d_{50} values of the products obtained from the tests in which different grinding media were employed at constant solids content of the pulp (50% w/w) and mill load (50% v/v), with the grinding time. In these tests, three different material used as grinding media (steel ball (7 g/cm^3), river pebble (2.80 g/cm^3) and zircon beads (4.00 g/cm^3)) and three different impeller speeds (480, 710 and 1030 rpm) were used. Following the same approach used to define the previous relationships, the curves were represented by the equation in Eq. 5-2. It was found that the variable b in the equation changes with the density of material used as grinding media and had a constant value for each material. The relationship between the variable b and the density of grinding media was given in each graph in Figure 5-20 and tabulated in Table 5-6. In addition to this, for each grinding media, the variable a is related to the impeller speed (Table 5-6).

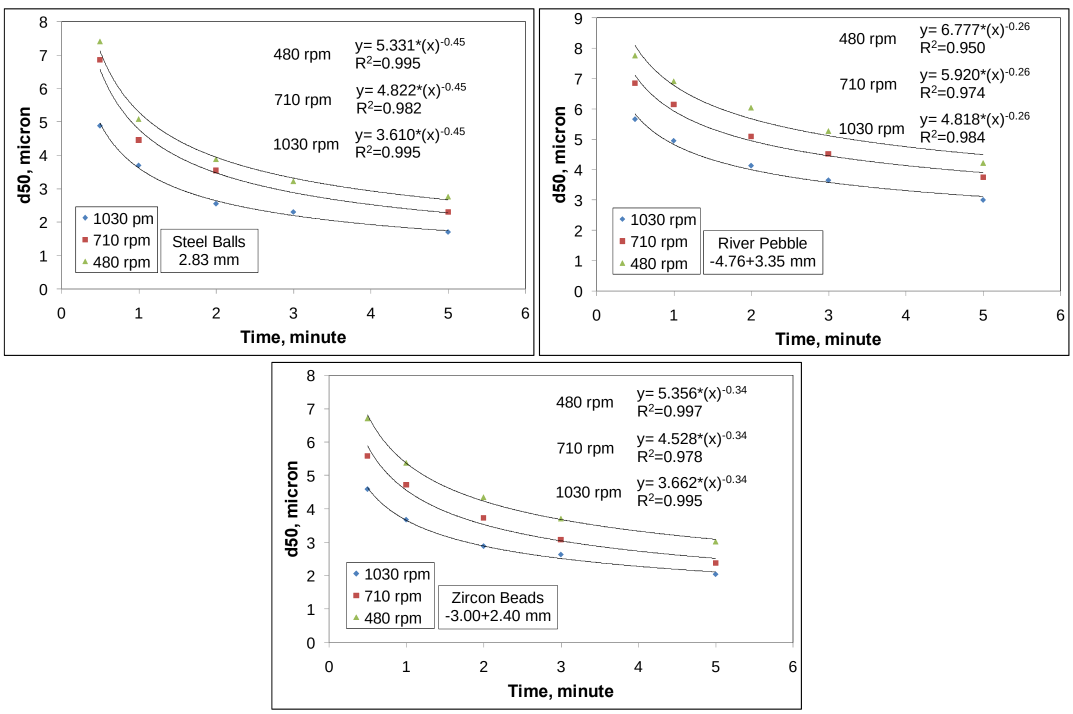

Figure 5-19. Variation of d_{50} with grinding time for various materials used as grinding media

Table 5-6. Relationship between the variable b and the density of grinding media

Density of Grinding Media g/cm^3	**b**
River Pebble, 2.8	-0.26
Zircon Beads, 4.0	-0.34
Steel Balls, 7.0	-0.45

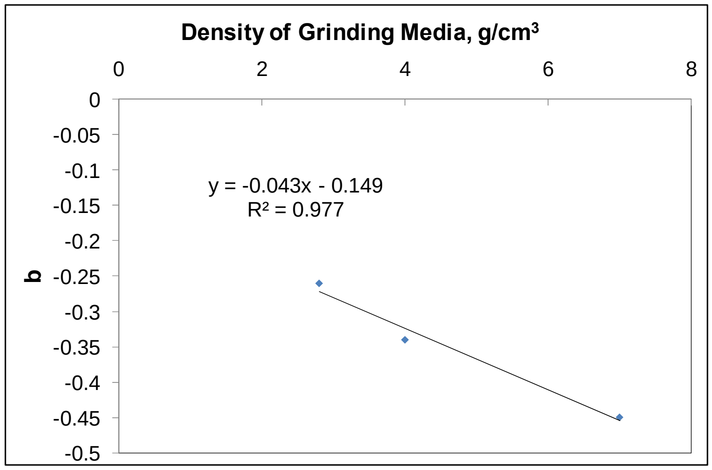

Figure 5-20. Relationship between the variable b and the density of grinding media

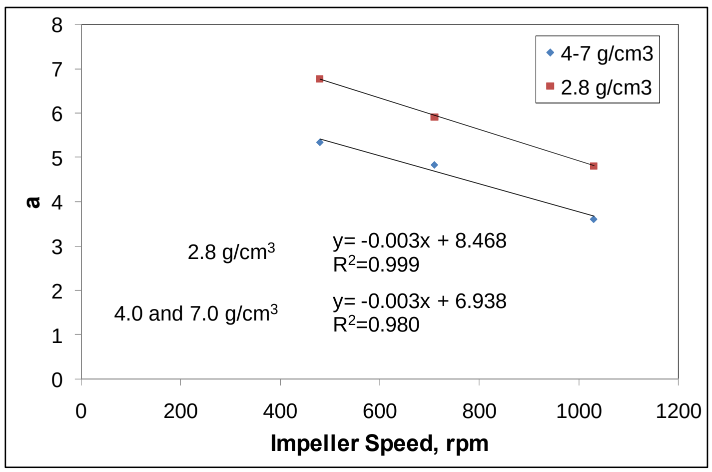

Figure 5-21. Relationship between the variable a and the impeller speed for different grinding media

As a result, the variables in Eq. 5-2 (a and b) can be determined from above relationships to calculate the d_{50} value of the product for any grinding media used in the tests at various impeller speeds within the range. By putting the calculated d_{50} into Eq. 5-1, whole particle size distribution of the product can be calculated. Figure 5-22 shows comparison of the calculated and measured particle size distributions of the products for various solids content of the pulp at three different impeller speeds. As can be seen from the graph, the calculated particle size distributions are in good agreement with the measured ones.

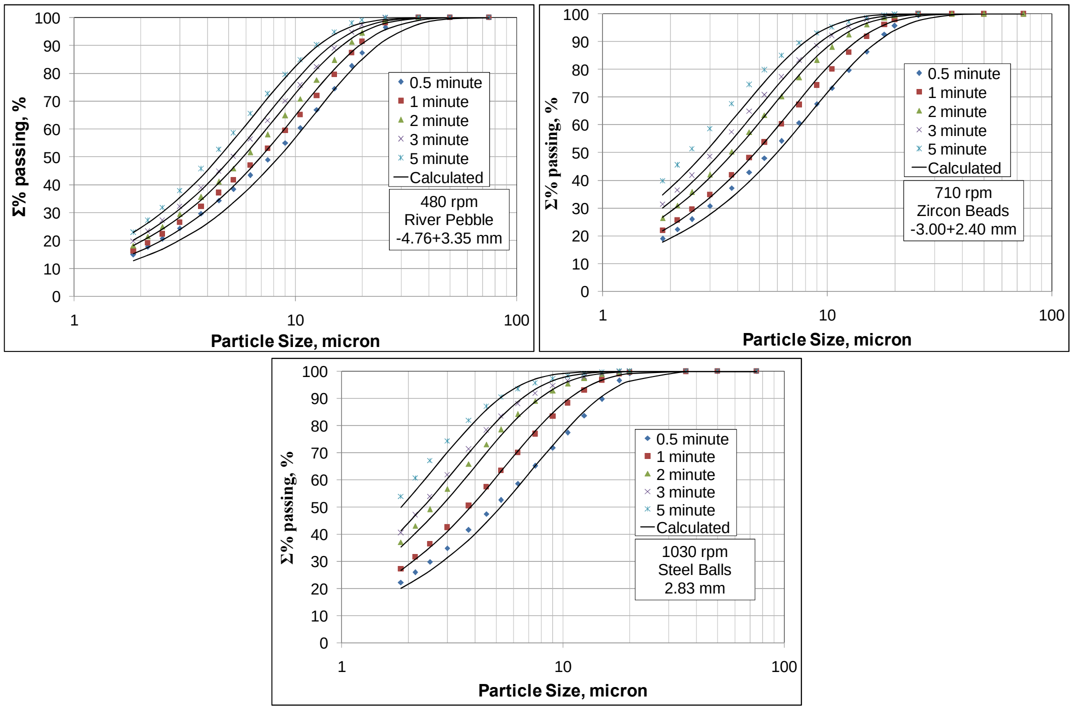

Figure 5-22. Comparison of the calculated and measured particle size distributions

5.2. Modeling of Continuous Grinding Tests (Pilot Scale Stirred Media Mill)

In perfect mixing ball mill model, a ball mill is considered as a perfectly stirred tank. Then, the process can be described in terms of transport through the mill and breakage within the mill.

f s p

f, s and p are size distribution vectors in units of tph of t. Because the mill is perfectly mixed, a discharge rate, d_i, for each size fraction completely defines the product (Eq. 5-5):

$$p_i = d_i \times s_i \qquad \text{Eq. 5-5}$$

That is, if we know the mill contents (in each size fraction) and a rate of discharge for each size fraction, we can multiply the two to get a product vector in tonnes per hour. If the mill is at steady state, then the sum (mill feed – material selected for breakage

+ material from breakage of coarser particles – mill discharge)

must be equal to zero. In symbols, for size i (Eq. 5-6):

$$f_i - r_i.s_i + \Sigma_{j=1}^{i} a_{ij}.r_i.s_i - d_i.s_i = 0 \qquad \text{Eq. 5-6}$$

Where, a_{ij} represents breakage from size j into size i and $r_i a_{ij}$ the rate of breakage within that size fraction. Remembering that

$$p_i = d_i.s_i \qquad \text{or} \qquad s_i = \frac{p_i}{d_i} \qquad \text{Eq. 5-7}$$

Then,

$$f_i - r_i.\frac{p_i}{d_i} + \Sigma_{j=1}^{i} a_{ij}.r_i.\frac{p_i}{d_i} - p_i = 0 \qquad \text{Eq. 5-8}$$

Now we only need a measured feed and product size distributions, and a breakage function to find r_i/d_i and so describe the mill. If the assumptions are satisfied, it is not necessary to measure the mill contents.

In case of stirred media mill, r/d function can be used to describe the mill as well. Moreover, change in this function can give information about the grinding performance of the mill. In order to calculate r/d functions for different grinding conditions, JKSimMet software was used. As a breakage function, the standart Broadbent and Callcott breakage function was used. For all the tests investigating the effects of major operating parameters on pilot scale stirred media milling, r/d functions were determined. Tests carried out on the stream of Zn Column Scavenger concentrate were focused on the effects of the impeller speed and feed flowrate while tests carried out on the stream of Cu Cleaner 4 tail were done to observe the effects of mill load and the density of material used as grinding media in the mill.

Figure 5-23 shows the effect of impeller speed on r/d* function at constant flowrate of 916 kg/h. As can be seen from the graph, an increase in the impeller speed of the mill increases the breakage rate of the particles in each size fraction entering the mill when considering that the discharge rate of each fraction remains the same. Thus, finer product can be obtained.

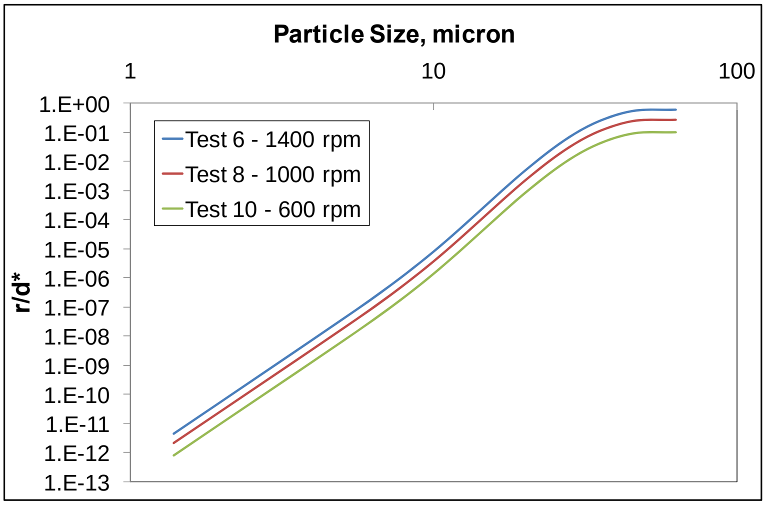

Figure 5-23. The effect of the impeller speed on r/d* function (zinc column scavenger tail stream)

Figure 5-24 also shows the effect of feed flowrate on r/d* function at constant impeller speed of 1400 rpm. As can be seen from the graph, the amount of material passing through the mill in unit time slightly changes r/d* values. That's, low r/d* values is observed for higher tonnages which increases the discharge rate of the particles in each size fraction. It is assumed that the breakage rate of each size fraction will not be changed because of constant impeller speed, an increase in the discharge rate will cause lower r/d* values for higher feed flowrates. This was observed in the tests investigating the feed flowrate effect on r/d* values.

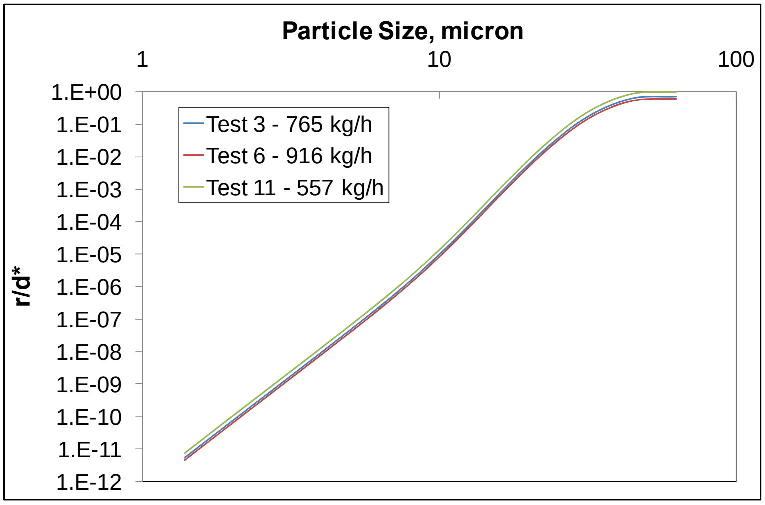

Figure 5-24. The effect of feed flowrate on r/d* function (zinc column scavenger tail stream)

Cu cleaner 4 tail stream was fed to the pilot mill in order to evaluate the effects of various media loads and media densities on r/d* values. For this stream, the effect of impeller speed on grinding performance was also investigated. Figure 5-25 shows the effect of different impeller speeds on r/d* values. As can be seen from the graph, the calculated r/d* for Cu cleaner 4 tail values are in accordance with the results obtained from the stream of Zn Column Scavenger concentrate. An increase in the impeller speed of the mill increases the breakage rate of the particles in each size fraction entering the mill when considering that the discharge rate of each fraction remains the same.

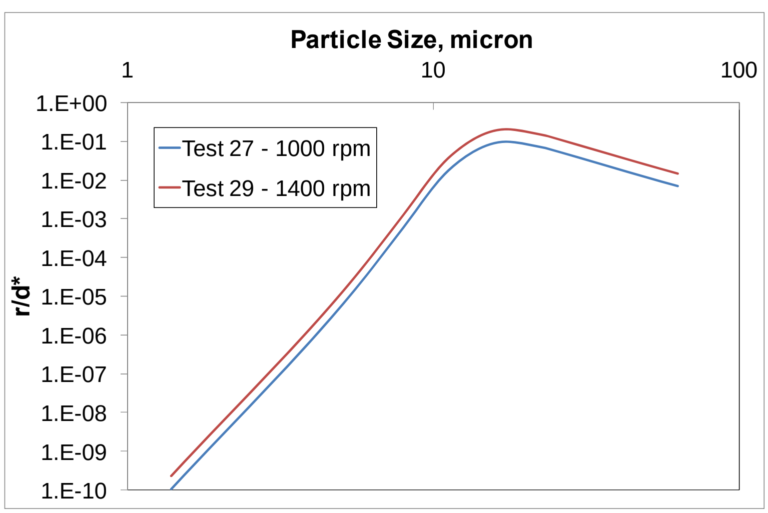

Figure 5-25. The effect of the impeller speed on r/d* function (copper cleaner 4 tail)

Figure 5-26 shows the effect of media charge to the mill on grinding performance of the mill. An increase in the amount of grinding media in the mill increases the power drawn by the mill from 5.53 to 7.52 kW at constant impeller speed of 1000 rpm and constant feed rate of 193 kg/h. Thus, this increase in power leads to increase in the breakage rates of the particles in each size fraction when considering that the discharge rate of the particles of each size fraction remains constant because of same feed flowrate. As can be seen from the graph, r/d* values calculated for higher media load was found to be greater than that for lower media load.

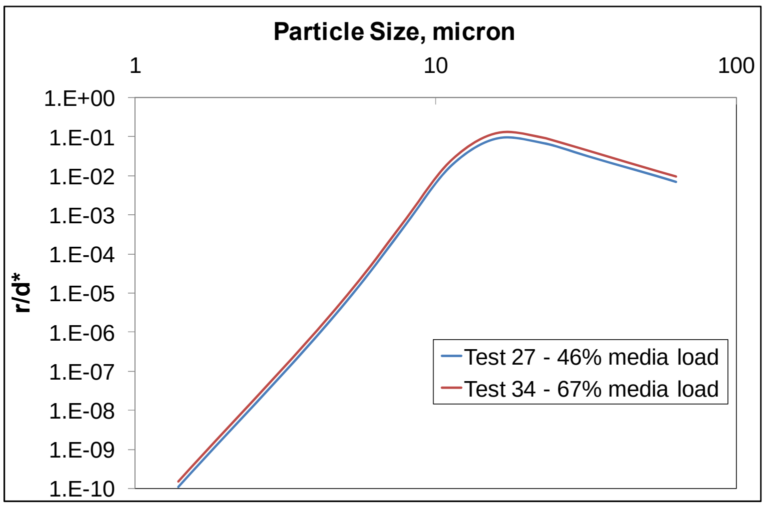

Figure 5-26. The effect of the media load on r/d* function (copper cleaner 4 tail)

Figure 5-27 shows the effect of media types having different density on the grinding performance of the stirred media mill. The power drawn by the mill varies in case of employing different grinding media in the mill. For grinding media having higher density such as steel ball (7.00 g/cm^3), the power was measured as 5.53 kW while for grinding media having lower density such as river pebble (2.80 g/cm^3), the power was measured as 2.61 kW. Thus, this increase in power leads to increase in the breakage rates of the particles in each size fraction when considering that the discharge rate of the particles of each size fraction remains constant because of same feed flowrate. As can be seen from the graph, r/d* values calculated for steel balls was found to be greater than that for river pebble.

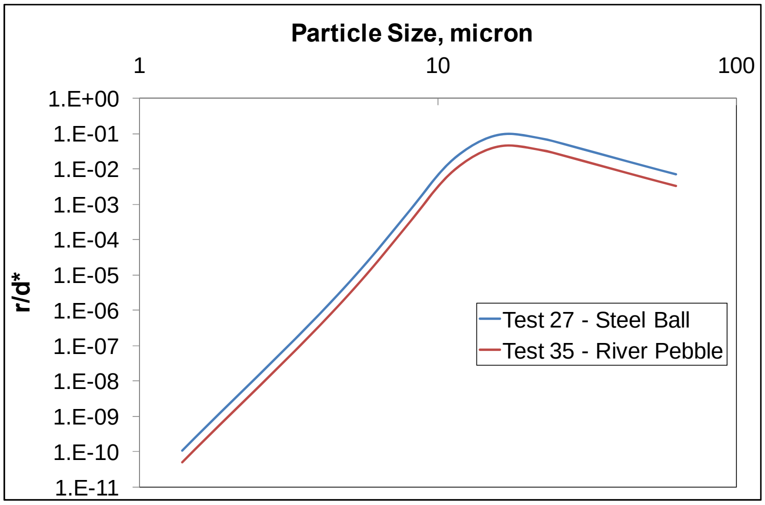

Figure 5-27. The effect of the media density on r/d* function (copper cleaner 4 tail)

After having calculated r/d* values for each test investigating the effects of major operating parameters of stirred media mill installed two streams at the plant, it was found that the calculated r/d* values can be normalized with the power drawn by the mill in each test. Figure 5-29 shows the normalized r/d* values for the streams on which the tests were carried out. The difference in normalized r/d* values is caused by the different material characteristics of each stream in terms of different mineral composition which leads to different grindability and breakage. In addition to mineral composition of the streams, the particle size distributions of these streams are also significantly different (Figure 5-28). However, the standart breakage function and grindability were used in the calculation of r/d* values for all tests. In order to overcome this situation, the suitable method for determining the grindability and breakage function should be developed for fine particles. In the literature, the grinding table was used to determine the breakage function of fine materials. Jankovic and Morrell (1998) indicated that the breakage function is not only dependent on material but also strongly on the particle size. The results shown in Figure 5-29 are in accordance with the results of the study done by Jankovic and Morrell (1998). In this study, the effect of material characteristics in terms of grindability and particle size distribution on r/d* values were ignored and for this reason, calculated r/d* values contain the error resulting from this situation. Nevertheless, calculated r/d* values are good indication of how the stirred media mill will perform under various operating conditions. When it comes back to Figure 5-29, it enables us to predict r/d* values for any power drawn by the mill. Once r/d* is predicted, it can be used to calculate the particle size distribution of the product.

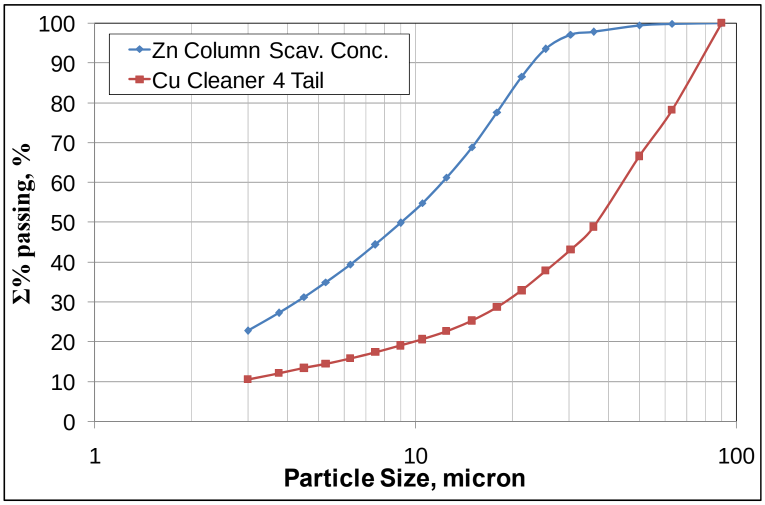

Figure 5-28. Comparison of particle size distributions of the streams fed to pilot stirred media mill

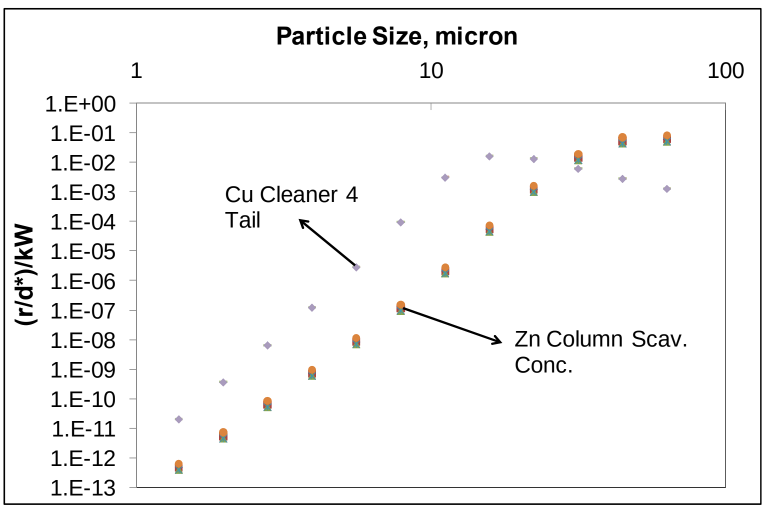

Figure 5-29. Normalized r/d* values

In order to take advantage of the normalized r/d* values shown in Figure 5-29, the power drawn by the mill should have to be predicted correctly. It is found that the power drawn is the function of the impeller speed and the amount of grinding media in the mill. The relationship is given in Eq. 5-9.

$$P \propto (\psi, \phi)$$ Eq. 5-9

Where,

Ψ : the impeller speed, rpm

Φ : mill content

The mill content can be calculated according to the equation given below (Eq. 5-10).

$$\phi = 0.6 \times mill\ volume \times gr.media\ load\ fraction \times density\ of\ gr.media$$ Eq. 5-10

The relationship between the mill content and power draw for different impeller speeds can be shown in Figure 5-30. As can be seen from the graph, power varies linearly with the mill content. The slopes of the lines (C) are related to the changes in the impeller speed.

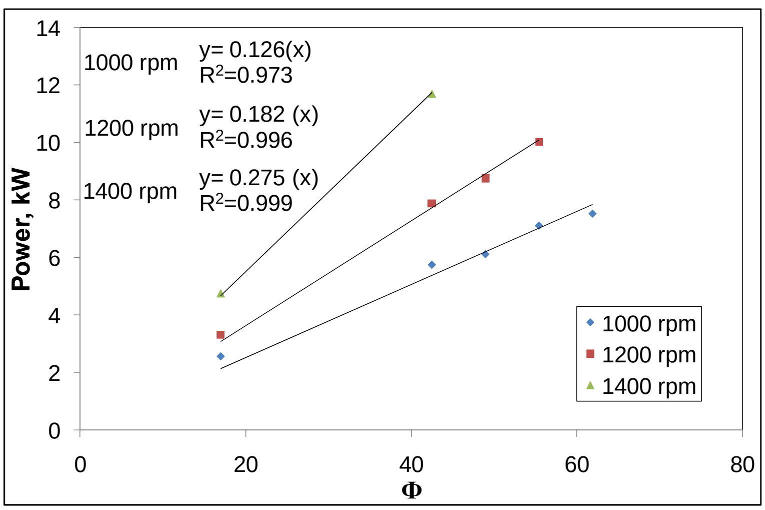

Figure 5-30. The relationship between the mill content and power draw for different impeller speeds

Figure 5-31 shows the variation of the slopes of lines (C) in Figure 5-30 with the impeller speed.

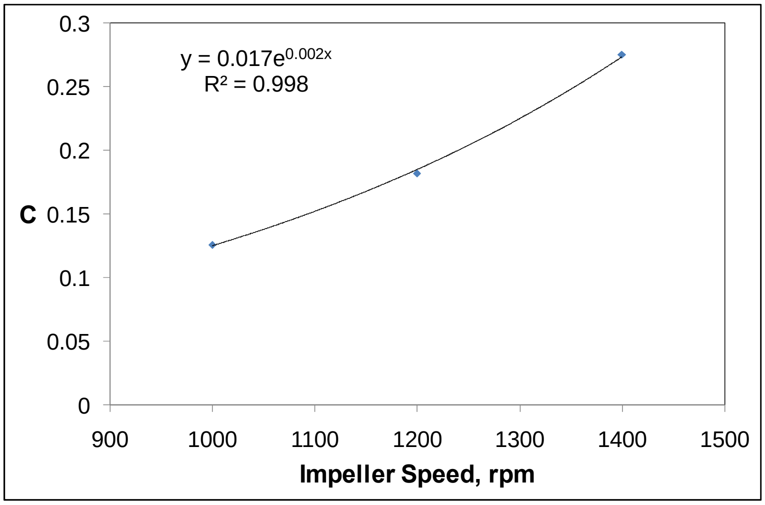

Figure 5-31. The relationship between the impeller speed and the slopes of the lines (C) in Figure 5-30

In this condition, power draw can be calculated by using Eq. 5-11

$$P\ (kW) = 0.017 \times \phi \times e^{(0.002 \times impeller\ speed)} \qquad \text{Eq. 5-11}$$

Power draw calculated according to Eq. 5-11 in each test is given in Table 5-7 and also illustrated in Figure 5-32. As can be seen from the graph, the predicted power draws are in good agreement with the measured ones.

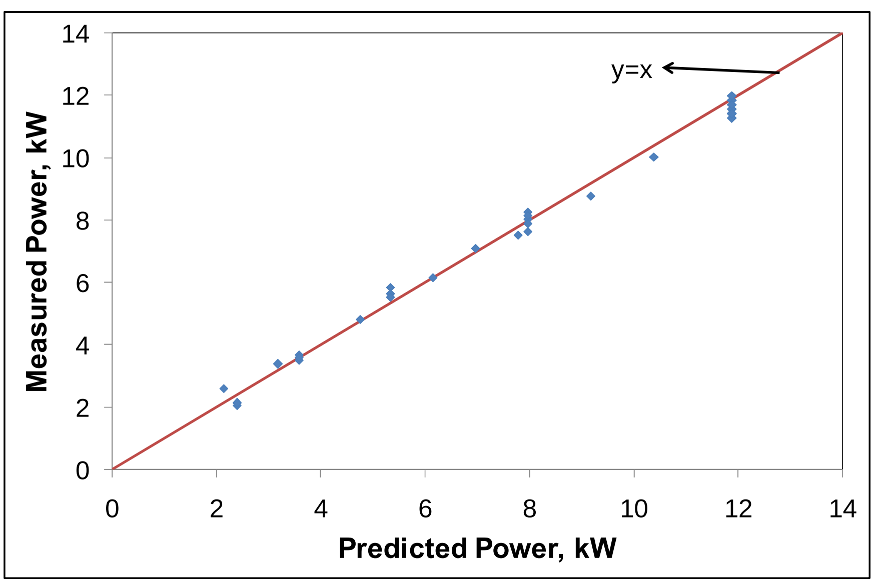

Figure 5-32. Predicted and measured power

Table 5-7. Tests' conditions and predicted-measured power draws

	Impeller Speed (rpm)	Feedrate (kg/h)	Media Density g/cm^3	Media Load (v/v)	ϕ	Power predicted kW	Power measured (kW)
Test 1	1000	765	7	46	42.504	5.34	5.85
Test 2	1200	765	7	46	42.504	7.96	8.27
Test 3	1400	765	7	46	42.504	11.88	11.84
Test 4	600	765	7	46	42.504	2.40	2.13
Test 5	800	765	7	46	42.504	3.58	3.68
Test 6	1400	916	7	46	42.504	11.88	11.99
Test 7	1200	916	7	46	42.504	7.96	8.02
Test 8	1000	916	7	46	42.504	5.34	5.53
Test 9	800	916	7	46	42.504	3.58	3.51
Test 10	600	916	7	46	42.504	2.40	2.07
Test 11	1400	557	7	46	42.504	11.88	11.84
Test 12	1200	557	7	46	42.504	7.96	8.15
Test 13	1000	557	7	46	42.504	5.34	5.64
Test 14	800	557	7	46	42.504	3.58	3.59
Test 15	600	557	7	46	42.504	2.40	2.13
Test 16	1400	259	7	46	42.504	11.88	11.99
Test 17	1200	259	7	46	42.504	7.96	7.89
Test 18	1000	259	7	46	42.504	5.34	5.64
Test 19	1000	193	7	46	42.504	5.34	5.53
Test 20	1200	193	7	46	42.504	7.96	7.64
Test 21	1400	193	7	46	42.504	11.88	11.7
Test 22	1000	193	7	53	48.972	6.15	6.16
Test 23	1200	193	7	53	48.972	9.18	8.77
Test 24	1000	193	7	60	55.44	6.96	7.1
Test 25	1200	193	7	60	55.44	10.39	10.03
Test 26	1000	193	7	67	61.908	7.78	7.52
Test 27	1000	193	2.8	46	17.0016	2.14	2.61
Test 28	1200	193	2.8	46	17.0016	3.19	3.38
Test 29	1400	193	2.8	46	17.0016	4.75	4.82
Test 30	1400	66	7	46	42.504	11.88	11.4
Test 31	1400	231	7	46	42.504	11.88	11.26
Test 32	1400	122	7	46	42.504	11.88	11.55
Test 33	1400	267	7	46	42.504	11.88	11.4
Test 34	1400	426	7	46	42.504	11.88	11.7
Test 35	1400	182	7	46	42.504	11.88	11.4
Test 36	1400	327	7	46	42.504	11.88	11.55

5.3. Scale-Up of Stirred Media Mills

Herbst and Sepulveda (1978) showed that there is a relationship between specific energy and the median particle size of the product on a log-log plot and shows a straight line over the range of particle size considered for the four different mill sizes under their investigation (Figure 5-33). The study carried out on IsaMills by Weller et al. (1999) verified this finding. A parallel test was arranged both on 4 liter Netzsch horizontal mill and 4000 liter IsaMill. Figure 5-34 compares the energy efficiency of the two mills with a volume ratio of 1000. It can be seen that the energy versus product P_{80} relations of the two mills fell on the same straight line on a log-log scale. This result show that testing in the small 4 litre mill using media proposed for the large scale gives an accurate estimate of the specific energy needed to prepare a chosen product size in a large scale mill.

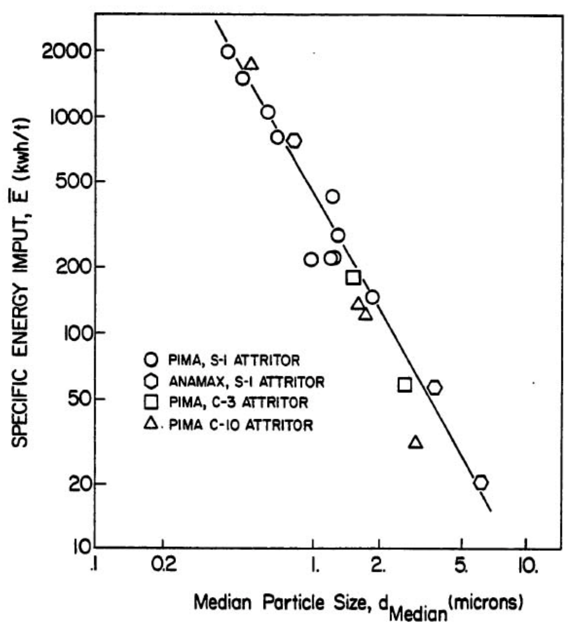

Figure 5-33. Energy-size reduction relationship for the attrition mill (Sepulveda, 1981)

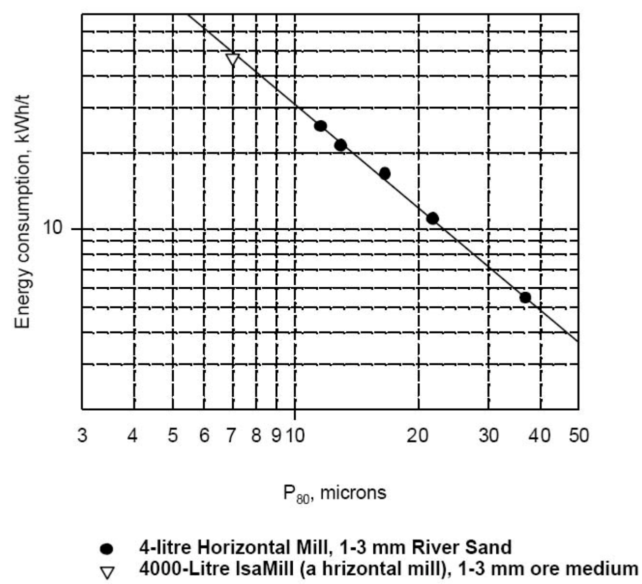

Figure 5-34. Energy-size reduction relationship for the IsaMill (Weller et al., 1999)

In this study, by using the data obtained from pilot scale stirred media mill tests, similar finding was observed. Figure 5-35 shows the relation between specific energy and d_{50} values for different grinding conditions. Herbst and Sepulveda (1978) defined this relation with Charles' law which may be expressed in Eq. 5-12.

$$Ecs = A \times (d_{50})^{-n} \qquad \text{Eq. 5-12}$$

Where,

Ecs : Specific Energy, kWh/t
A : Constant for a given material
n : slope of the line
d_{50} : median size, micron

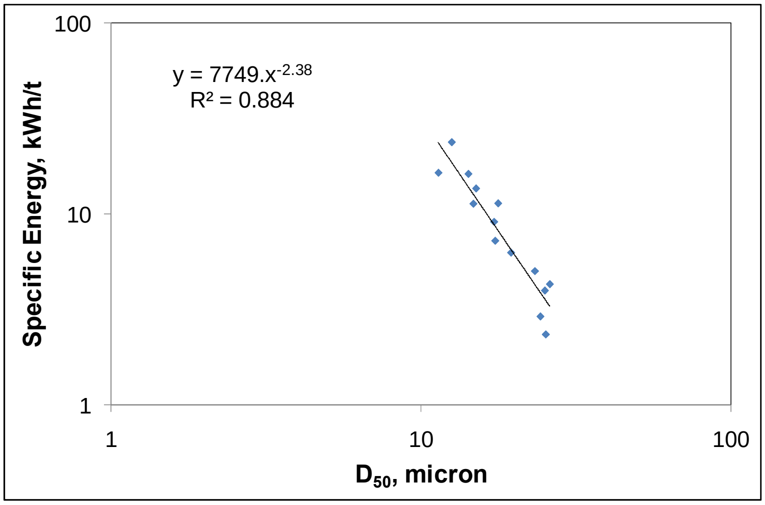

Figure 5-35. Energy-size reduction relationship for the pilot scale stirred media mill

According to Eq. 5-12, the line given in Figure 5-35 can be expressed in Eq. 5-13.

$$Ecs = 7749 \times (d_{50})^{-2.38} \qquad \text{Eq. 5-13}$$

By using Eq. 5-13, the stirred media mill in this study can be scaled-up to a larger size under the assumption that the specific energy consumption will remain constant for different mill sizes for a given material. The motor power can be determined based on the amount of material ground in the mill.

6. SAMPLING STUDIES CARRIED OUT AT CAYELI FLOTATION PLANT

Plant surveys were accomplished for two major objectives. First objective is the performance evaluation and modeling of existing copper regrinding circuit. The other one is to evaluate the performance of whole flotation circuit for spec and non-spec ore when the plant was run at 150 tph.

In the sampling studies, pulp samples were taken from the required flows in the flotation circuit of ÇBİ copper flotation plant and copper regrinding circuit. The locations of the sampling points were determined considering the importance of the flows for mineralogical evaluation of the copper and zinc flotation circuit and for the evaluation of copper regrinding circuit. Physical conditions for proper sampling were also considered for locating the sampling points in the plant. All the facilities required for proper sampling operation were provided by ÇBİ stuff. Many streams were sampled by an existing automatic sampling system (multiplexer). Therefore, these automatically taken samples were collected in separate buckets during the sampling surveys. The other flows were sampled by a specially designed sampling device. In the copper regrinding circuit, a cutter was used to take samples from mill discharge and cyclone underflow.

In whole plant surveys, some of the streams such as Cu Rougher Cleaner 1 tail and concentrate, Cu Rougher Cleaner 1 Scavenger concentrate and Cu Cleaner 2 tail were not sampled. Multi cleaning stages containing recircuilation flows were converted to a one feed-two products point in order to eliminate the effect of recycling on the mineralogical evaluation. In this case, regrinding cyclone overflow was accepted as the feed of the first two copper cleaning stages. Therefore, Cu Cleaner 2 concentrate was the concentrate and Cu Rougher Cleaner 1 Scavenger tail was the tailing of these two cleaning stages. In the zinc flotation circuit, two Zn column stages were considered as single column stage. Since Zn Column 1 and Column 2 concentrates were combined as Zn final concentrate, this combined flow was sampled and accepted as the concentrate of this column flotation stage. Also combined concentrate of Zn Column Scavenger 1 and Scavenger 2 concentrates was sampled and accepted as the concentrate of Zn Column Scavenger concentrate. The sampling points were illustrated in Figure 6-1. The samples taken from multiplexer are represented by “SP” and the other streams by capital letters. All the samples taken from the circuit are defined in Table 6-1.

In the sampling campaign for copper regrinding circuit, the locations of the sampling points in copper flotation circuit were determined in order to calculate the tonnage of regrinding cyclone overflow. In case of preventing the overflowing of sump which feeds the regrinding cyclones, some part of Cu Rougher concentrate is bypassed to Cu Cleaner circuit especially at high tonnages of flotation feed. In these cases, additional streams in copper flotation circuit had to be sampled. The basic sampling points were illustrated in Figure 6-2. Additional sampling points were indicated in red color if there was any bypassed stream during the sampling survey. All the samples taken from the circuit are defined in Table 6-2. Table 6-2 also included the additional sampling points in red in case of bypassing in the circuit.

During the sampling surveys, the amount of plant feed was changed to required value. Before starting the sampling surveys, the operational parameters were monitored for 4-5 hours to ensure steady state operation during the survey.

All the samples were collected in separate buckets. The required amount of samples taken were estimated using the approximate size distribution of each stream from previous records.

Table 6-1. Sampling points for copper and zinc flotation circuit

Sample code	Sampling point	Sampling system
SP1	Cu Concentrate	Multiplexer
SP2	Cu Regrinding Cyclone Overflow	Multiplexer
SP4	Cu Cleaner 3 Con	Multiplexer
SP5	Flotation Feed	Multiplexer
SP6	Cu Rougher Concentrate	Multiplexer
SP7	Column Feed	Multiplexer
SP8	Cu Rougher Tail	Multiplexer
SP9	Zn Rougher Feed	Multiplexer
SP10	Zn Cleaner 1 Tail	Multiplexer
SP11	Zn Rougher Concentrate	Multiplexer
SP12	Zn Column Tail	Multiplexer
SP13	Cu Rougher Cleaner&Scavenger Tail	Multiplexer
SP14	Final Tail	Multiplexer
SP15	Cu Rougher Scavenger Tail	Multiplexer
SP16	Zn Concentrate	Multiplexer
SP17	Zn Column Scavenger Tail	Multiplexer
SP18	Zn Rougher Tail	Multiplexer
A	Cu Rougher Scavenger Concentrate	Sampler
B	Cu Cleaner 2 Concentrate	Sampler
C	Cu Cleaner 3 Tail	Sampler
D	Cu Cleaner 4 Tail	Sampler
E	Cu Cleaner 4 Concentrate	Sampler
F	Cu Cleaner 5 Tail	Sampler
G	Cu Regrinding Cyclone Underflow	Cutter
H	Cu Regrinding Mill Discharge	Cutter
I	Cu Regrinding Cyclone Feed	Cutter
J	Zn Cleaner 1 Concentrate	Sampler
K	Zn Col Scav 1 Concentrate + Zn Col Scav 2 Concentrate	Sampler

Figure 6-1. Locations of the sampling points for copper and zinc flotation circuit

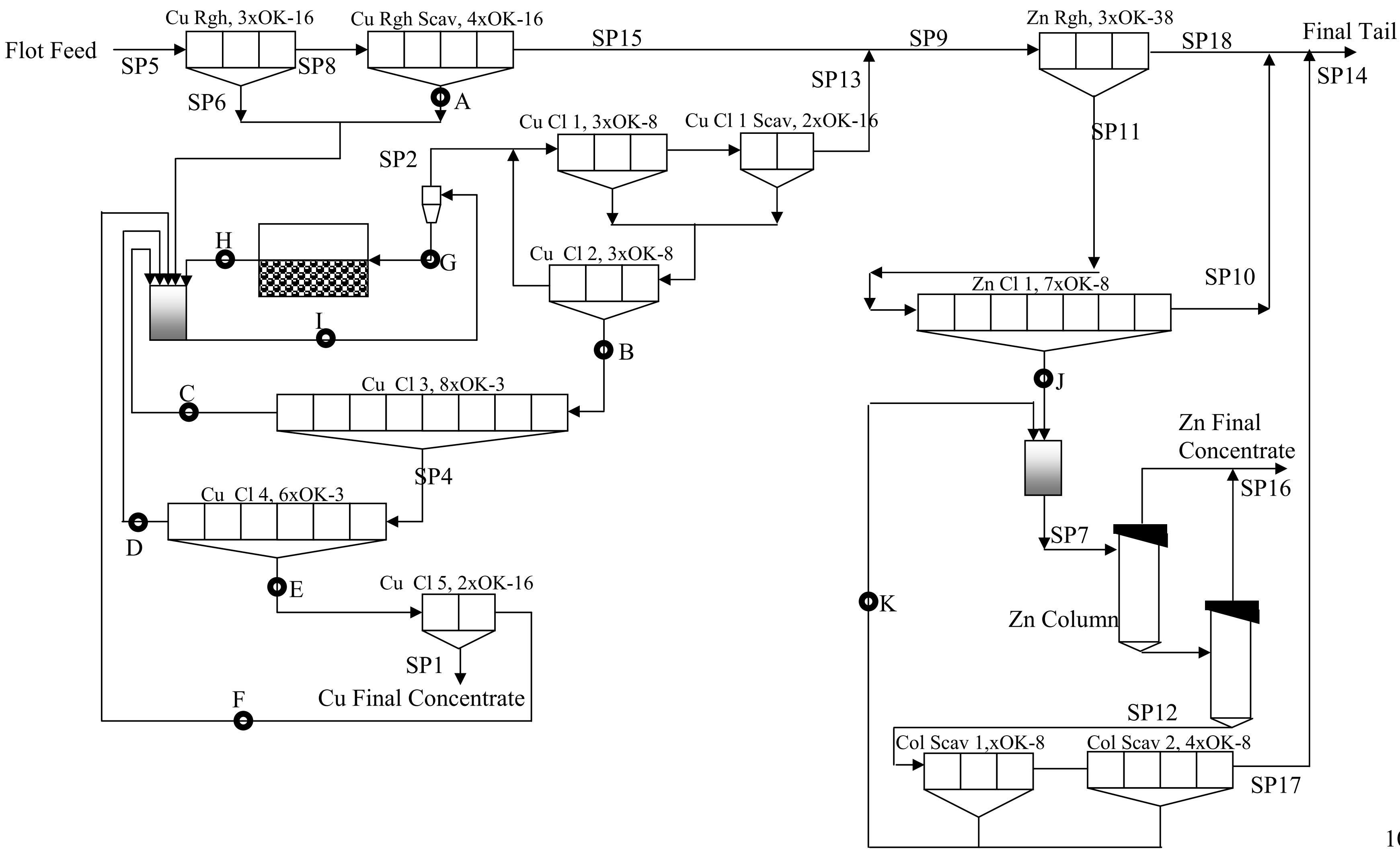

Table 6-2. Sampling points for copper regrinding circuit

Sample code	Sampling point	Sampling system
SP1	Cu Concentrate	Multiplexer
SP2	Cu Regrinding Cyclone Overflow	Multiplexer
SP5	Flotation Feed	Multiplexer
SP6	Cu Rougher Concentrate	Multiplexer
SP9	Zn Rougher Feed	Multiplexer
SP13	Cu Rougher Cleaner&Scavenger Tail	Multiplexer
SP15	Cu Rougher Scavenger Tail	Multiplexer
A	Cu Cleaner 2 Concentrate	Sampler
B	Cu Regrinding Cyclone Underflow	Cutter
C	Cu Regrinding Mill Discharge	Cutter
D	Cu Regrinding Cyclone Feed	Cutter
E	Cu Rougher Concentrate + Cu Regrinding Cyclone Overflow + Cu Cleaner 2 Concentrate	Sampler
F	Cu Cleaner 2 Concentrate	Sampler
G	Cu Cleaner 1 Concentrate + Cu Cleaner 1 Scavenger Concentrate	Sampler

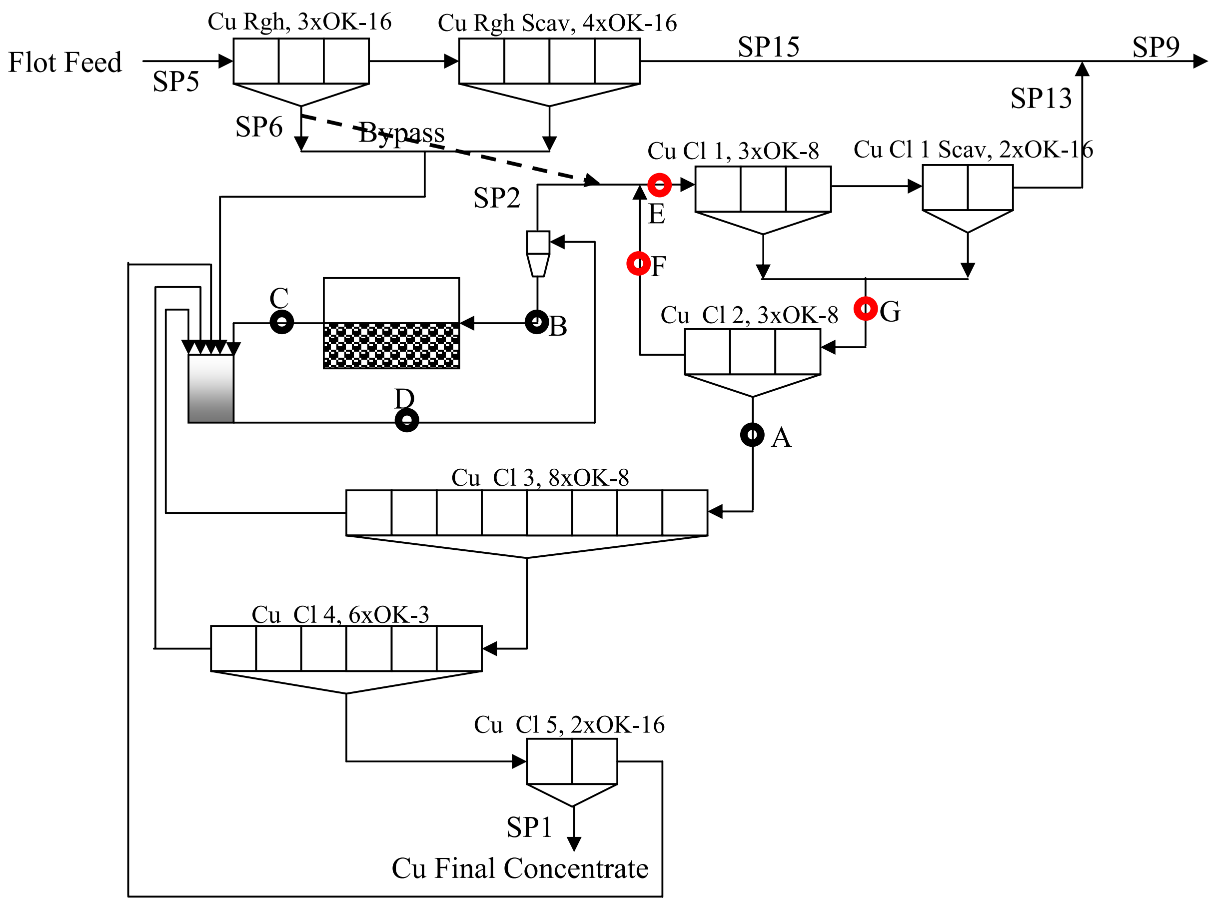

Figure 6-2. Locations of the sampling points for copper regrinding circuit

6.1. Mass Balance Calculations

In any sampling operation, some errors are inevitable. These errors result from the dynamic nature of the system, the physical conditions at a particular point, random errors, measurement errors and human errors.

Mass balancing involves statistical adjustment of raw data to obtain best fit estimates of flowrates. Whenever a stream is split into two or more streams, or two or more streams are combined to form one or more flows, or there is closed circuit processing, mass balancing software is required to estimate the flowrates in each stream. Then, it is possible to evaluate the performance of a circuit or an equipment.

During sampling surveys, excess data were collected in some points. This is important to obtain reliable solution and provides a cross check. After having Cu, Zn and Fe assays and size distributions of the samples, mass balancing studies were commenced. Then, using mass flow rate of the fresh feed and chemical assays of the stream, flowrates and copper, zinc and pyrite recoveries in each stream were calculated. Mass balancing was carried out by using a step by step approach. Mass balances were obtained around various nodes and finally a whole flotation plant. Therefore, calculations were checked and verified for different routes (*Convergence limits in all iterations were chosen as* 10^{-6} *mass balancing of the raw data was performed by using JKSimMet software*).

After mass balancing, raw assays vs adjusted assays are given in Figure 6-3. Frequency distribution of the standardized residuals (as percentage of measured assays) are shown in Figure 6-4.

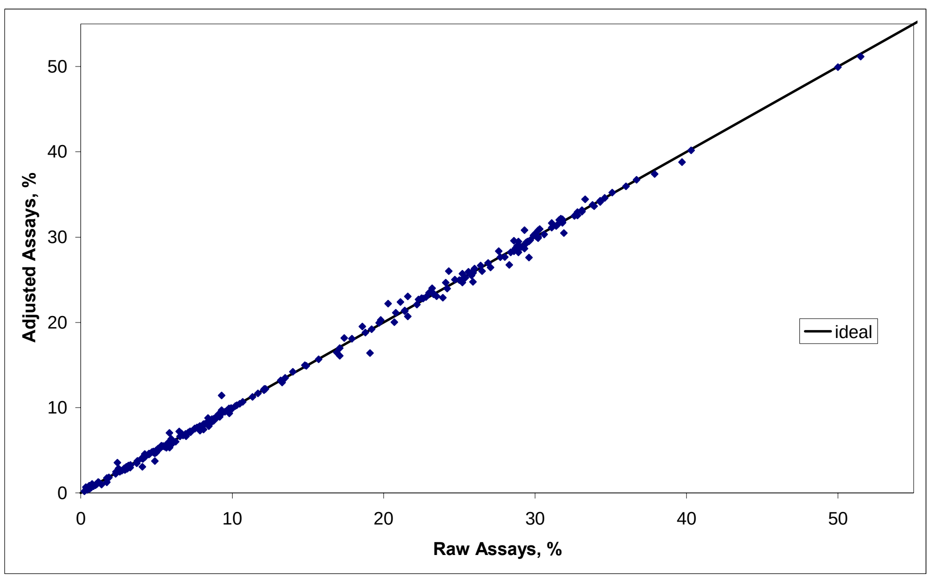

Figure 6-3. Overall comparison of the raw and adjusted assays

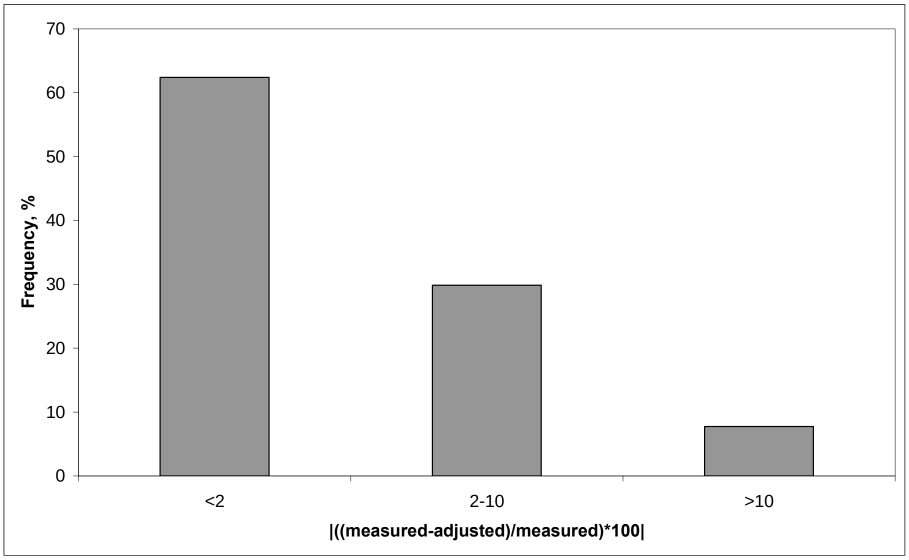

Figure 6-4. Frequency distribution of the residuals in mass balance calculations

As can be seen from the figure, 95% of the adjustments in the measured values is less than 10% showing that the raw and adjusted assays were in good agreement. This also showed that sampling was performed without significant errors.

6.2. Copper Regrinding Circuit Surveys

Using the size distributions, % solids and chemical assays of some streams, flow rates of the streams were calculated and overall performance of regrinding circuit was evaluated. This progress report covers the results of mass balancing of four sampling surveys around Cu Regrind circuit.

Before commencing sampling surveys, all cyclones in the regrinding cyclone cluster were replaced by new ones. Table 6-3 gives the geometrical parameters of the cyclones in the cluster.

Ball charge in the ball mill was determined as 29.17% and was kept constant during all sampling surveys by adding make-up balls.

After sampling, all samples were weighted, then filtered, dried and weighed again to determine % solid of each stream. Then, representative samples were taken for chemical analysis and sizings.

Table 6-3. Geometrical parameters of regrinding cyclones in the cluster

Cyclone number	Cyclone diameter mm	Apex diameter mm	Vortex diameter mm	Inlet diameter mm
1	151.48	24.78	51.00	32.38
2	152.14	25.00	49.62	33.32
3	150.90	24.79	48.90	31.00
4	151.62	24.92	50.50	31.00
5	151.68	25.30	50.30	30.22
6	152.24	25.10	50.20	30.20
7	151.96	25.22	50.20	31.24
8	151.90	25.00	50.38	30.60
9	151.32	26.22	50.14	30.28
10	150.40	24.54	51.12	31.76
11	151.68	25.00	51.54	30.82
12	151.86	25.00	50.08	31.26

6.2.1. 31/07/2006 Copper Regrinding Survey

This survey was carried out when the fresh feed to the plant was 150 wmtph. Cyclone pressure was adjusted to 1.45 bar and kept constant during the survey. The observed parameters recorded in the control room are presented in Table 6-4.

Table 6-4. Parameters recorded in the control room during the survey

	Feed Tonnage (wet)	Cu Concentrate		Flotation Feed		Zn Concentrate		Final Tail	
		Cu%	Zn%	Cu%	Zn%	Cu%	Zn%	Cu%	Zn%
13:00	150.70	25.97	3.43	3.90	5.90	2.38	50.08	0.45	0.82
14:00	148.20	27.01	3.10	4.04	5.99	2.44	50.19	0.47	0.82
15:00	151.05	26.56	3.14	4.00	5.79	2.60	49.19	0.45	0.82

Since some part of Cu Rougher concentrate was bypassed to Cu Cleaner circuit during the survey, samples were taken from the points (including red ones in this case) shown in Figure 6-2. Mass balancing by using chemical assays in copper flotation circuit was done to calculate the flow rate of Cu Regrinding cyclone overflow. Flow rates and adjusted assays after mass balancing were given in Figure 6-7. The pyrite recoveries are presented instead of Fe recoveries for a better representation of performance.

As can be seen from Figure 6-7, overall copper recovery was around 85%. Zinc grade in copper concentrate was 3.27% which referred to 7.3% zinc loss. Copper metal losses occured from two streams, Cu Rougher Scavenger tail which was responsible from 6.54% copper loss and Cu Cleaner 1 Scavenger tail which was responsible from 9.04% copper loss. After having determined the flow rate of Cu regrinding cyclone overflow, by using particle size distribution and %solids of the streams around regrinding ball mill and cyclone mass balance study was performed to determine the mass and water flow rates of each stream. Calculated flowrates and particle size distributions after mass balancing is given in Figure 6-5 and Figure 6-6, respectively. By using mass balance results, efficiency curve and some important parameters of hydrocyclones was calculated and given in Figure 6-8.

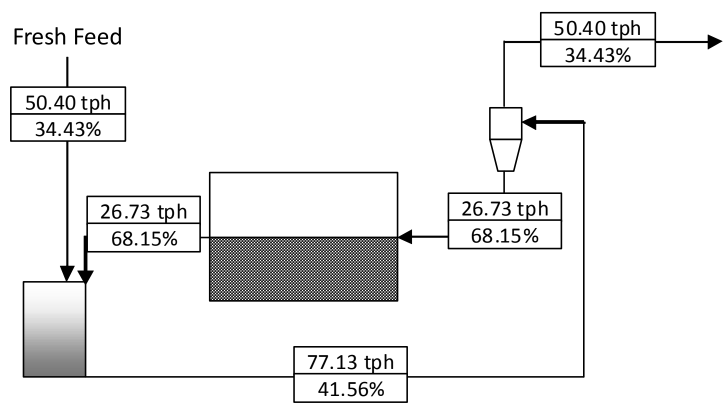

Figure 6-5. The result of mass balance calculation around regrinding circuit

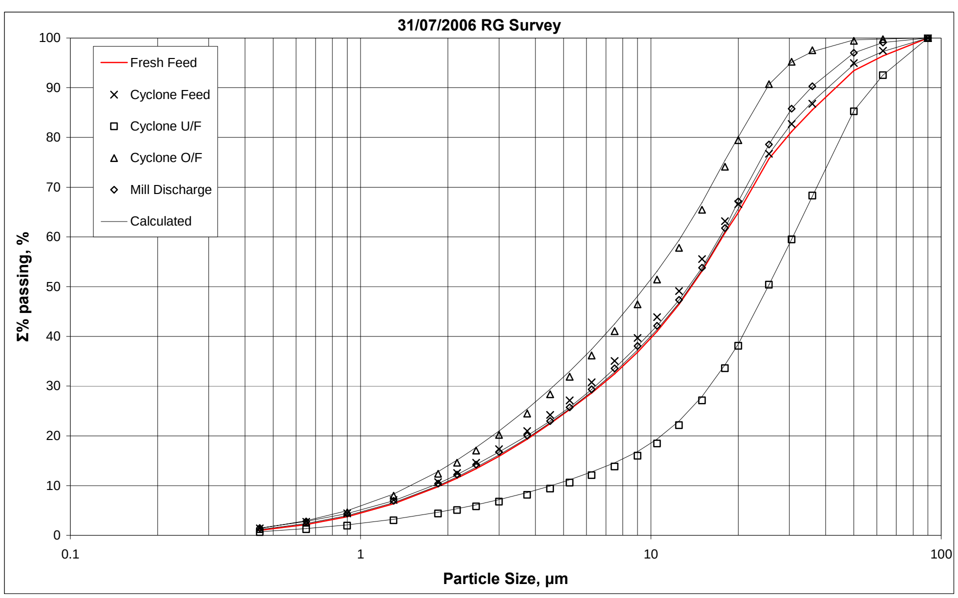

Figure 6-6. Calculated and experimental particle size distributions around regrinding circuit

Figure 6-7. Mass balancing result of 31/07/2006 Cu Regrinding circuit survey

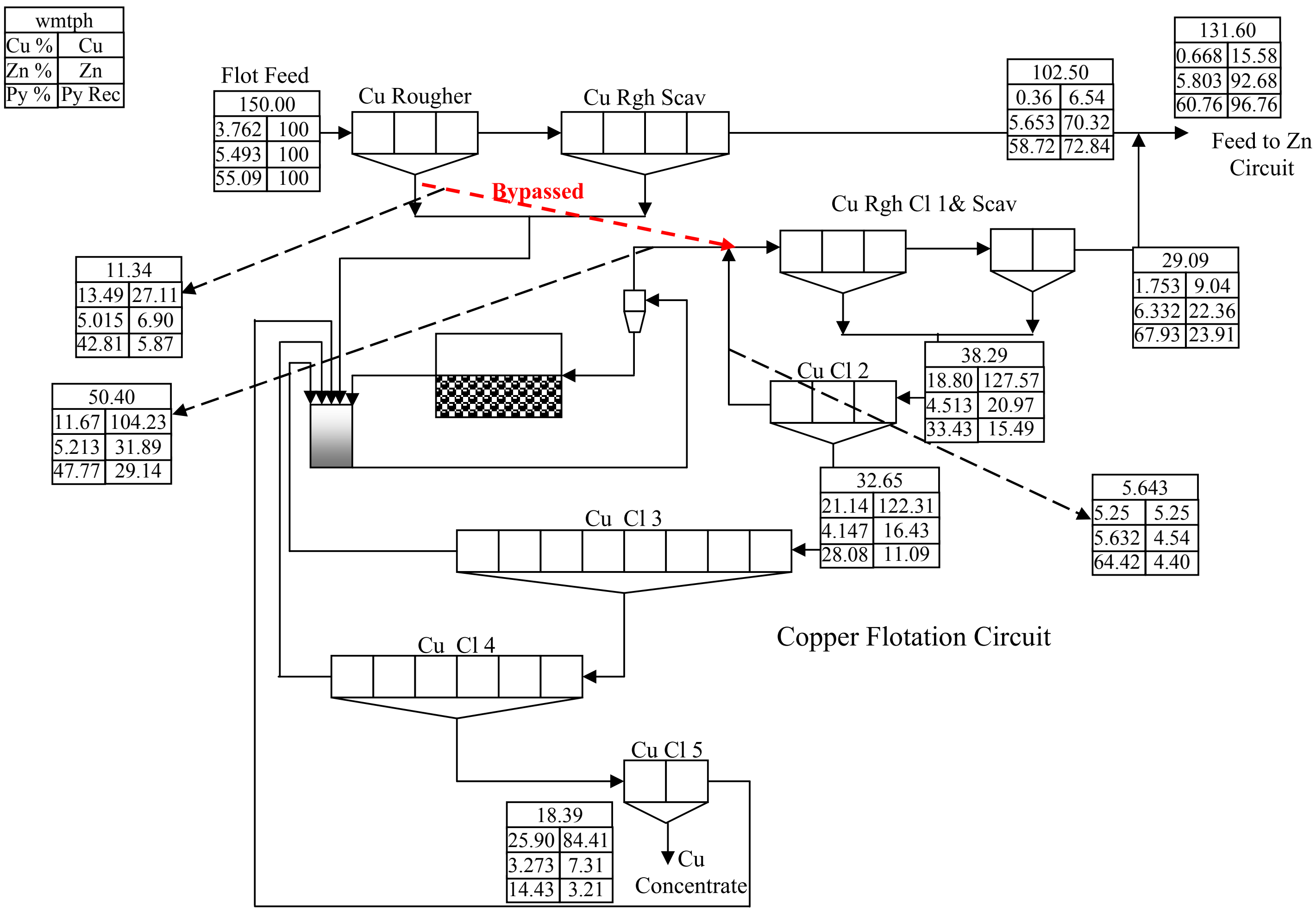

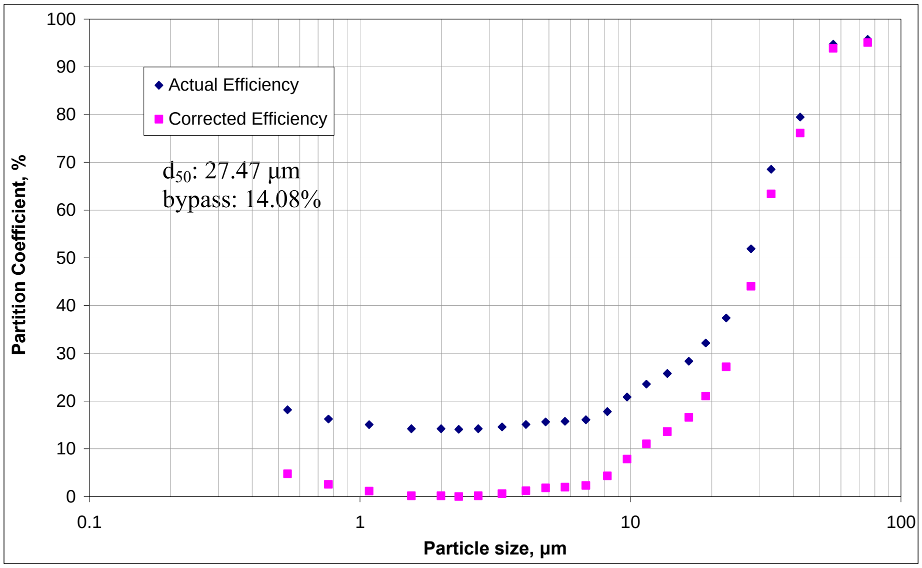

Figure 6-8. Efficiency curves of cyclones sampled on 31/07/2006

6.2.2. 04/08/2006 Copper Regrinding Survey

This survey was carried out when the fresh feed to the plant was 120 wmtph. Cyclone pressure was adjusted to 1.20 bar and kept constant during the survey. The observed parameters recorded in the control room are presented in Table 6-5.

Table 6-5. Parameters recorded in the control room during the survey

	Feed Tonnage (wet)	Cu Concentrate		Flotation Feed		Zn Concentrate		Final Tail	
		Cu%	Zn%	Cu%	Zn%	Cu%	Zn%	Cu%	Zn%
14:00	121.23	29.07	4.23	4.15	7.70	3.21	52.95	0.95	1.43
15:00	118.95	26.75	6.10	4.34	6.89	2.90	53.72	0.76	1.16
16:00	120.23	25.05	7.03	4.02	4.12	3.12	50.56	0.73	1.16

There was no bypassed stream in the circuit. Mass balancing by using chemical assays in copper flotation circuit was done to calculate the flow rate of Cu Regrinding cyclone overflow. Flow rates and adjusted assays after mass balancing were given in Figure 6-11. The pyrite recoveries are presented instead of Fe recoveries for a better representation of performance.

As can be seen from Figure 6-11, overall copper recovery was around 80%. Zinc grade in copper concentrate was 6.1% which referred to 11.74% zinc loss. Copper metal losses were occured from two streams, Cu Rougher Scavenger tail which was responsible from 8.66% copper loss and Cu Cleaner 1 Scavenger tail which was responsible from 11.46% copper loss. After having determined the flow rate of Cu regrinding cyclone overflow, by using size distribution and %solids of the streams around regrinding ball mill and cyclone mass balance study was performed to determine the mass and water flow rates of each stream. Calculated flowrates and particle size distributions after mass balancing is given in Figure 6-9 and Figure 6-10, respectively. By using mass balance results, efficiency curve and some important parameters of hydrocyclones was calculated and given in Figure 6-12.

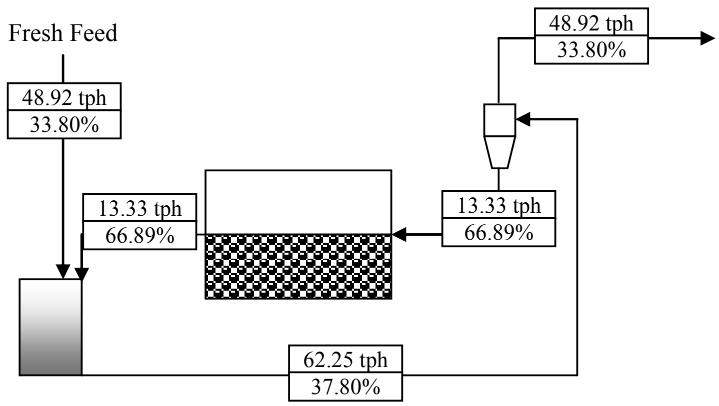

Figure 6-9. The result of mass balance calculation around regrinding circuit

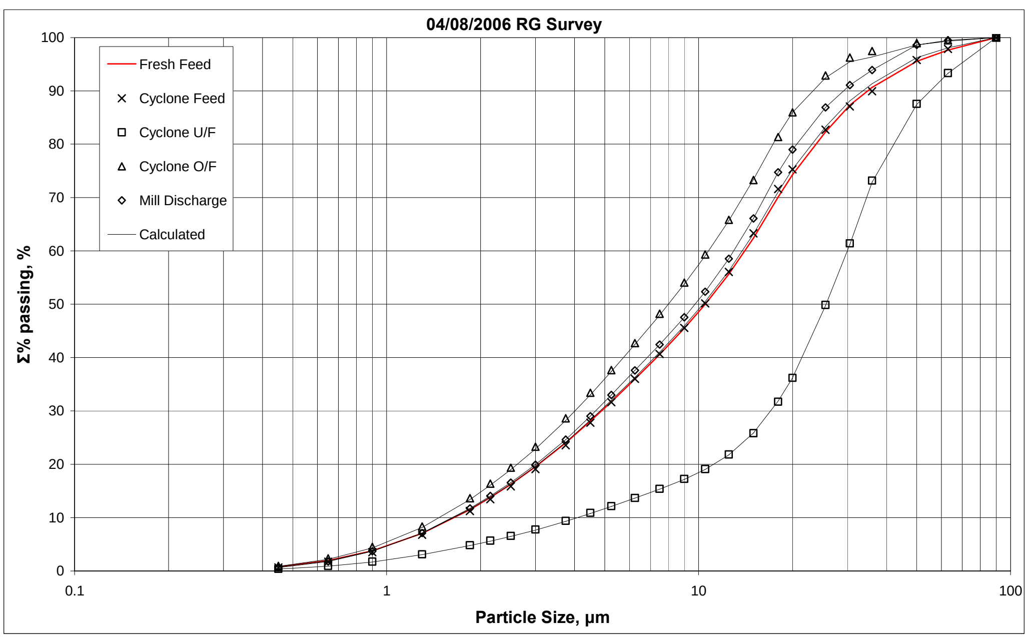

Figure 6-10. Calculated and experimental particle size distributions around regrinding circuit

Figure 6-11. Mass balancing result of 04/08/2006 Cu Regrinding circuit survey

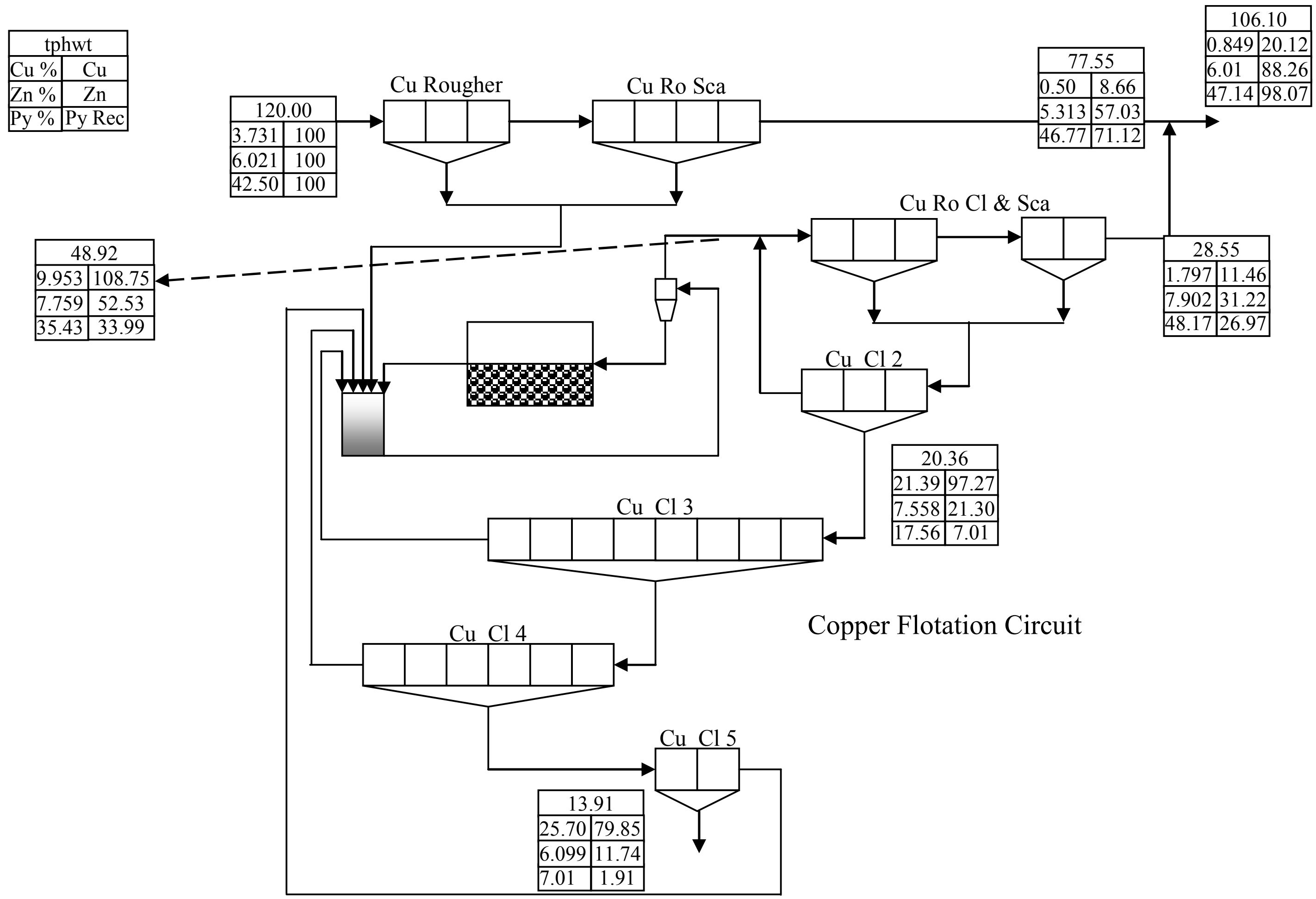

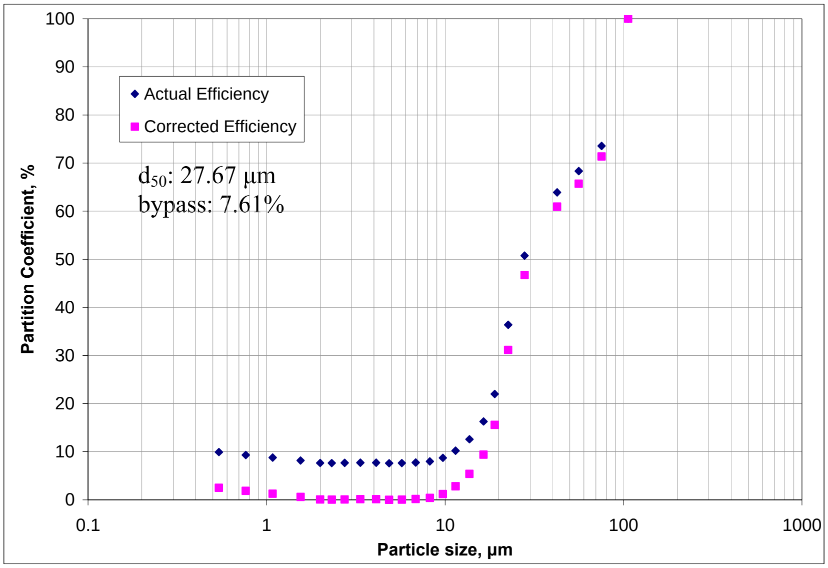

Figure 6-12. Efficiency curves of cyclones sampled on 04/08/2006

6.2.3. 08/08/2006 Copper Regrinding Survey

This survey was carried out when the fresh feed to the plant was 140 wmtph. Cyclone pressure was adjusted to 1.85 bar and kept constant during the survey. The observed parameters recorded in the control room are presented in Table 6-6.

Table 6-6. Parameters recorded in the control room during the survey

	Feed Tonnage (wet)	Cu Concentrate		Flotation Feed		Zn Concentrate		Final Tail	
		Cu%	Zn%	Cu%	Zn%	Cu%	Zn%	Cu%	Zn%
14:00	140.46	21.72	7.69	2.79	8.21	2.58	48.27	0.70	1.62
15:00	138.47	23.06	6.09	2.95	8.16	2.63	48.55	0.66	1.40
16:00	140.77	23.85	5.31	2.94	8.21	2.71	48.86	0.80	1.47

There was no bypassed stream in the circuit. Mass balancing by using chemical assays in copper flotation circuit was done to calculate the flow rate of Cu Regrinding cyclone overflow. Flow rates and adjusted assays after mass balancing were given in Figure 6-13. The pyrite recoveries are presented instead of Fe recoveries for a better representation of performance.

Figure 6-13. Mass balancing result of 08/08/2006 Cu Regrinding circuit survey

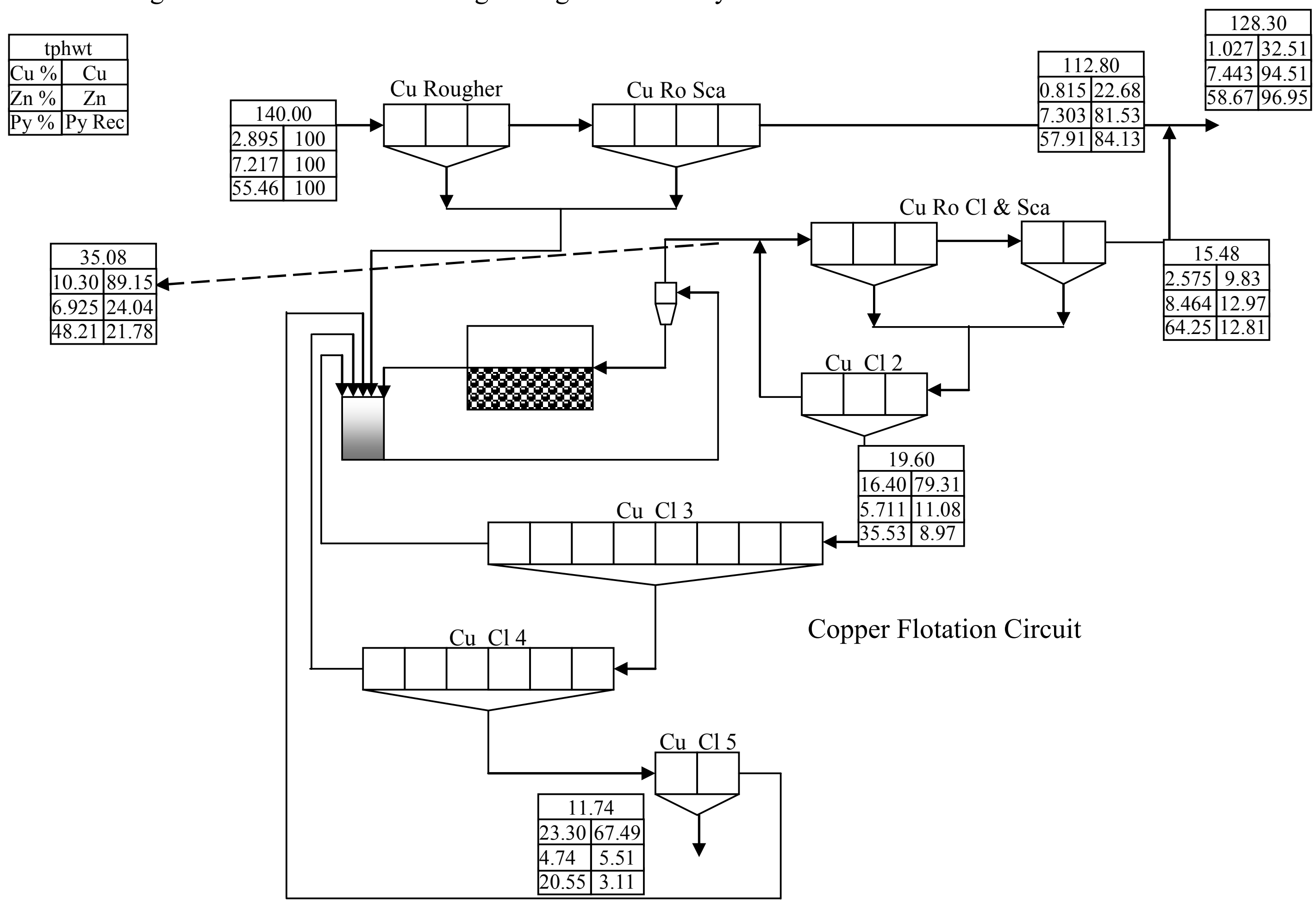

As can be seen from the figure, overall copper recovery was around 68%. Zinc grade in copper concentrate was 4.74% which referred to 5.51% zinc loss. Copper metal losses were occured from two streams, Cu Rougher Scavenger tail which was responsible from 22.68% copper loss and Cu Cleaner 1 Scavenger tail which was responsible from 9.83% copper loss. After having determined the flow rate of Cu regrinding cyclone overflow, by using particle size distribution and %solids of the streams around regrinding ball mill and cyclone mass balance study was performed to determine the mass and water flow rates of each stream. Calculated flowrates and particle size distributions after mass balancing is given in Figure 6-14 and Figure 6-15, respectively. By using mass balance results, efficiency curve and some important parameters of hydrocyclones was calculated and given in Figure 6-16.

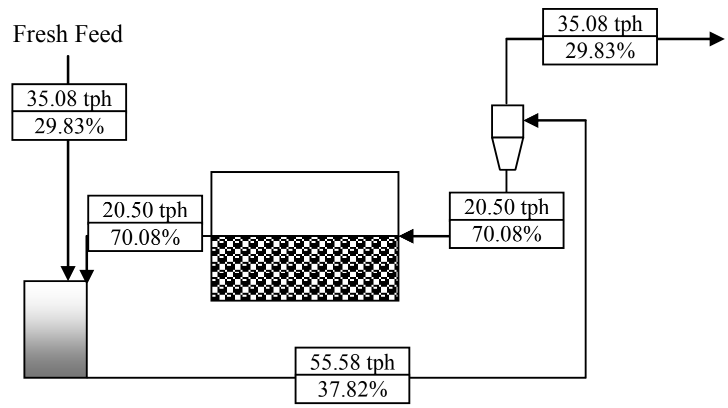

Figure 6-14. The result of mass balance calculation around regrinding circuit

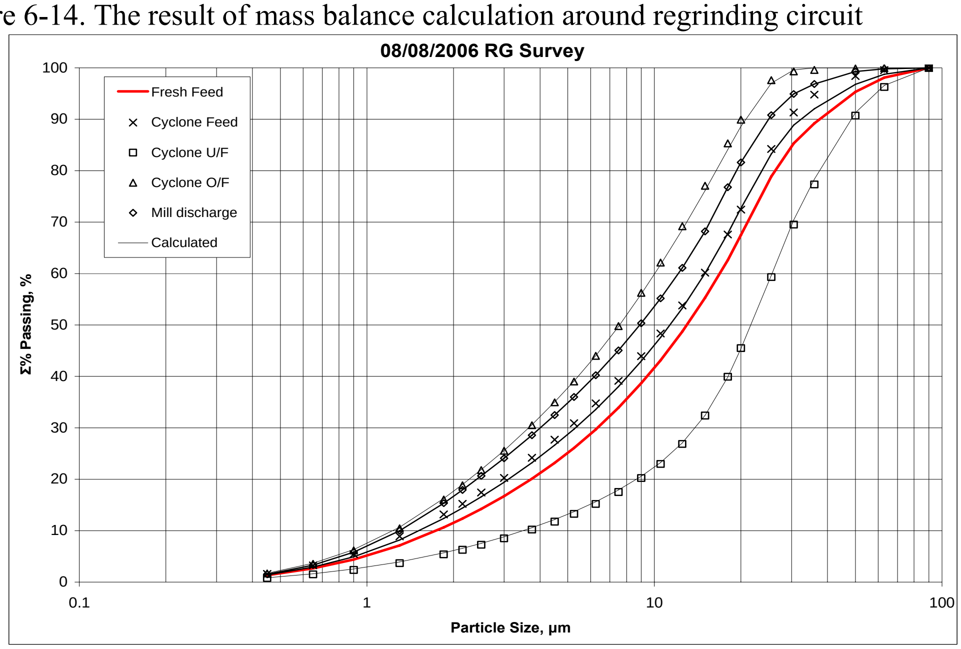

Figure 6-15. Calculated and experimental particle size distributions around regrinding circuit

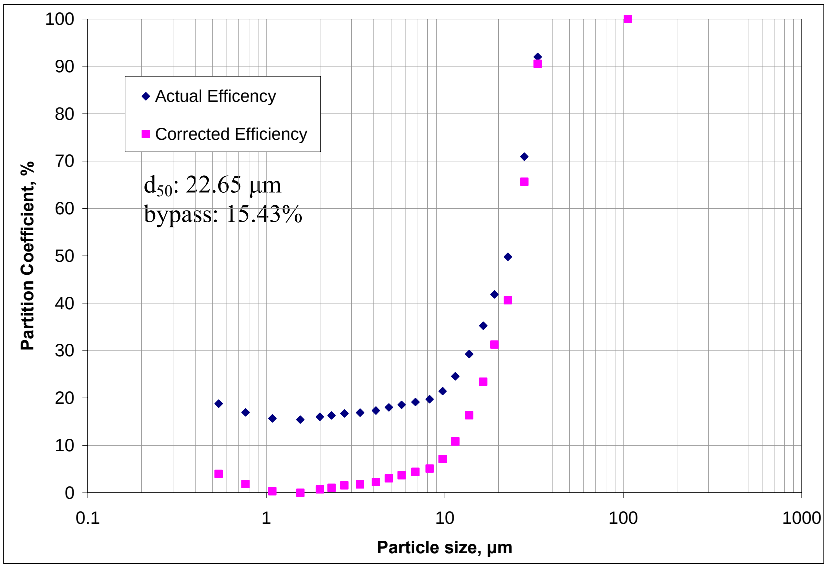

Figure 6-16. Efficiency curves of cyclones sampled on 08/08/2006

6.2.4. 09/08/2006 Copper Regrinding Survey

This survey was carried out when the fresh feed to the plant was 140 wmtph. Cyclone pressure was adjusted to 0.85 bar and kept constant during the survey. The observed parameters recorded in the control room are presented in Table 6-7.

Table 6-7. Parameters recorded in the control room during the survey

	Feed Tonnage (wet)	Cu Concentrate		Flotation Feed		Zn Concentrate		Final Tail	
		Cu%	Zn%	Cu%	Zn%	Cu%	Zn%	Cu%	Zn%
14:00	140.08	20.78	6.96	3.72	6.97	2.75	50.74	0.84	1.55
15:00	140.01	21.66	6.40	3.62	7.65	2.89	49.09	0.82	1.34
16:00	140.07	21.26	6.79	3.67	7.67	2.97	49.48	0.83	1.12

Since some part of Cu Rougher concentrate was bypassed to Cu Cleaner circuit during the survey, samples were taken from the points (including the red ones in this case) shown in Figure 6-2. Mass balancing by using chemical assays in copper flotation circuit was done to calculate the flow rate of Cu Regrinding cyclone overflow. Flow rates and adjusted assays after mass balancing were given in Figure 6-18. The pyrite recoveries are presented instead of Fe recoveries for a better representation of performance.

As can be seen from the figure, overall copper recovery was around 69.70%. Zinc grade in copper concentrate was 6.65% which refers to 10.62% zinc loss. Copper metal losses were occured from two streams, Cu Rougher Scavenger tail which was responsible from 13.30% copper loss and Cu Cleaner 1 Scavenger tail which was responsible from 17.03% copper loss. After having determined the flow rate of Cu regrinding cyclone overflow, by using particle size distribution and %solids of the streams around regrinding ball mill and cyclone mass balance study was performed to determine the mass and water flow rates of each stream. Calculated flowrates and particle size distributions after mass balancing is given in Figure 6-17 and Figure 6-19, respectively. By using mass balance results, efficiency curve and some important parameters of hydrocyclones was calculated and given in Figure 6-20.

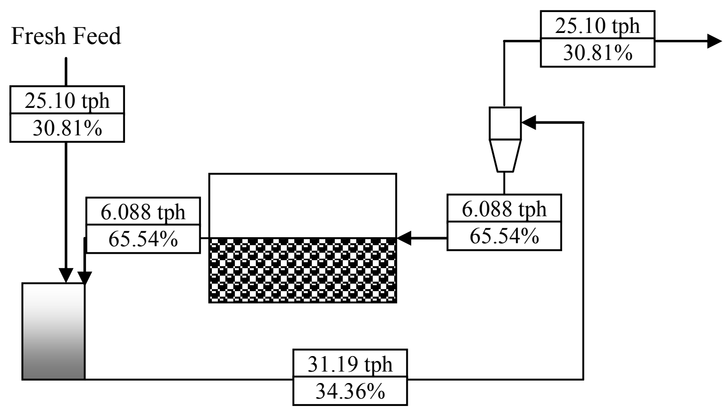

Figure 6-17. The result of mass balance calculation around regrinding circuit

Figure 6-18. Mass balancing result of 09/08/2006 Cu Regrinding circuit survey

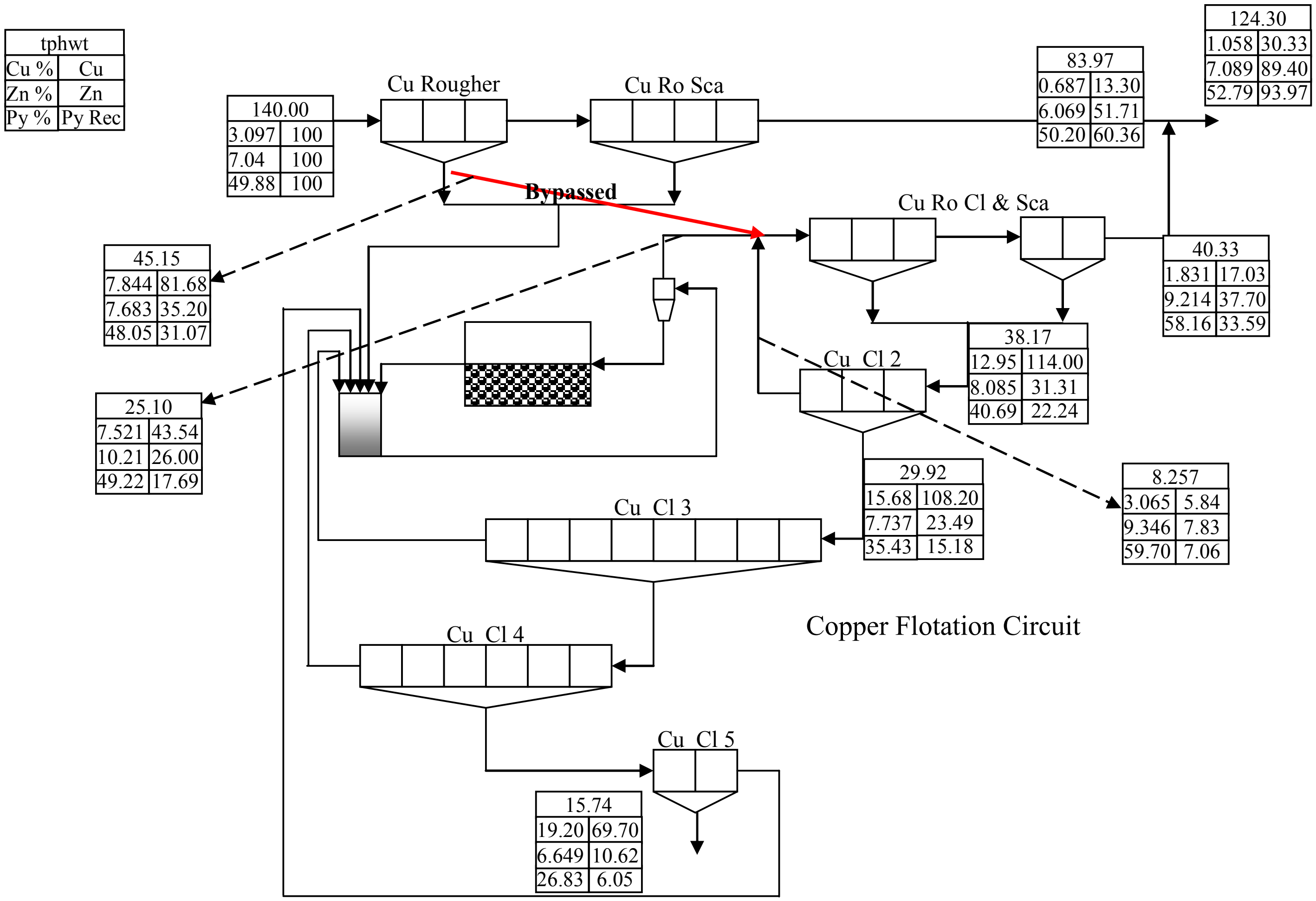

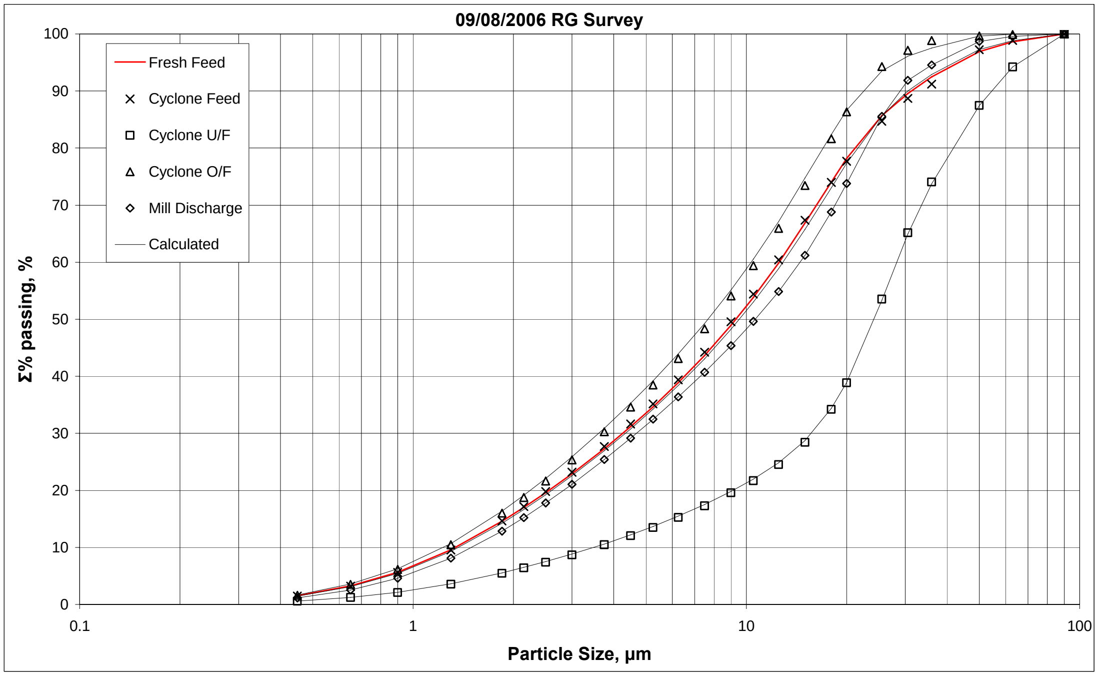

Figure 6-19. Calculated and experimental particle size distributions around regrinding circuit

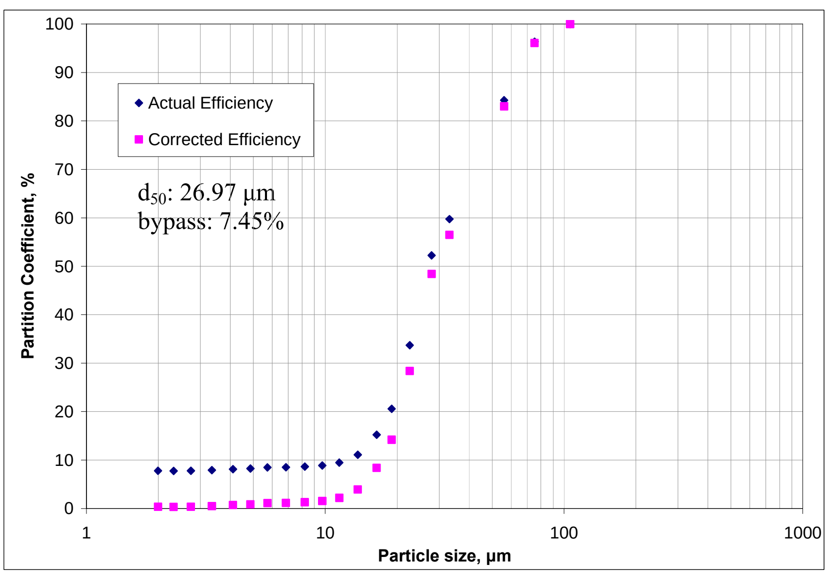

Figure 6-20. Efficiency curves of cyclones sampled on 09/08/2006

6.3. Copper and Zinc Flotation Circuit Surveys

This study covers the results of two mass balance studies of sampling surveys carried out in copper and zinc flotation circuit. One of the survey was performed when the plant was processing spec ore while the other survey was performed for non-spec ore. For both ore types, flowrate of fresh feed to plant was adjusted to 150 wmtph. And there was no bypassed stream in both circuit.

6.3.1. 28/08/2006 Copper and Zinc Flotation Circuit Survey – Spec Ore

This survey was carried out when the fresh feed to the plant was 150 wmtph. Cyclone pressure was adjusted to 1.31 bar and kept constant during the survey. The observed parameters recorded in the control room are presented in Table 6-8.

Table 6-8. Parameters recorded in the control room during the survey

	Feed Tonnage (wet)	Cu Concentrate		Flotation Feed		Zn Concentrate		Final Tail	
		Cu%	Zn%	Cu%	Zn%	Cu%	Zn%	Cu%	Zn%
11:00	150.06	26.03	2.53	4.16	3.73	3.66	49.66	0.58	0.68
12:00	150.05	24.50	2.99	4.04	4.16	3.81	49.16	0.56	0.69
13:00	150.44	22.93	3.88	3.81	3.75	3.50	50.58	0.54	0.69

Mass balancing by using chemical assays in copper and zinc flotation circuit was done to calculate the flow rate of each stream. Flow rates and adjusted assays after mass balancing were given in Figure 6-21. The pyrite recoveries are presented instead of Fe recoveries for a better representation of performance.

Figure 6-21. 28/08/2006 - mass balancing result of spec ore survey at copper and zinc flotation circuit

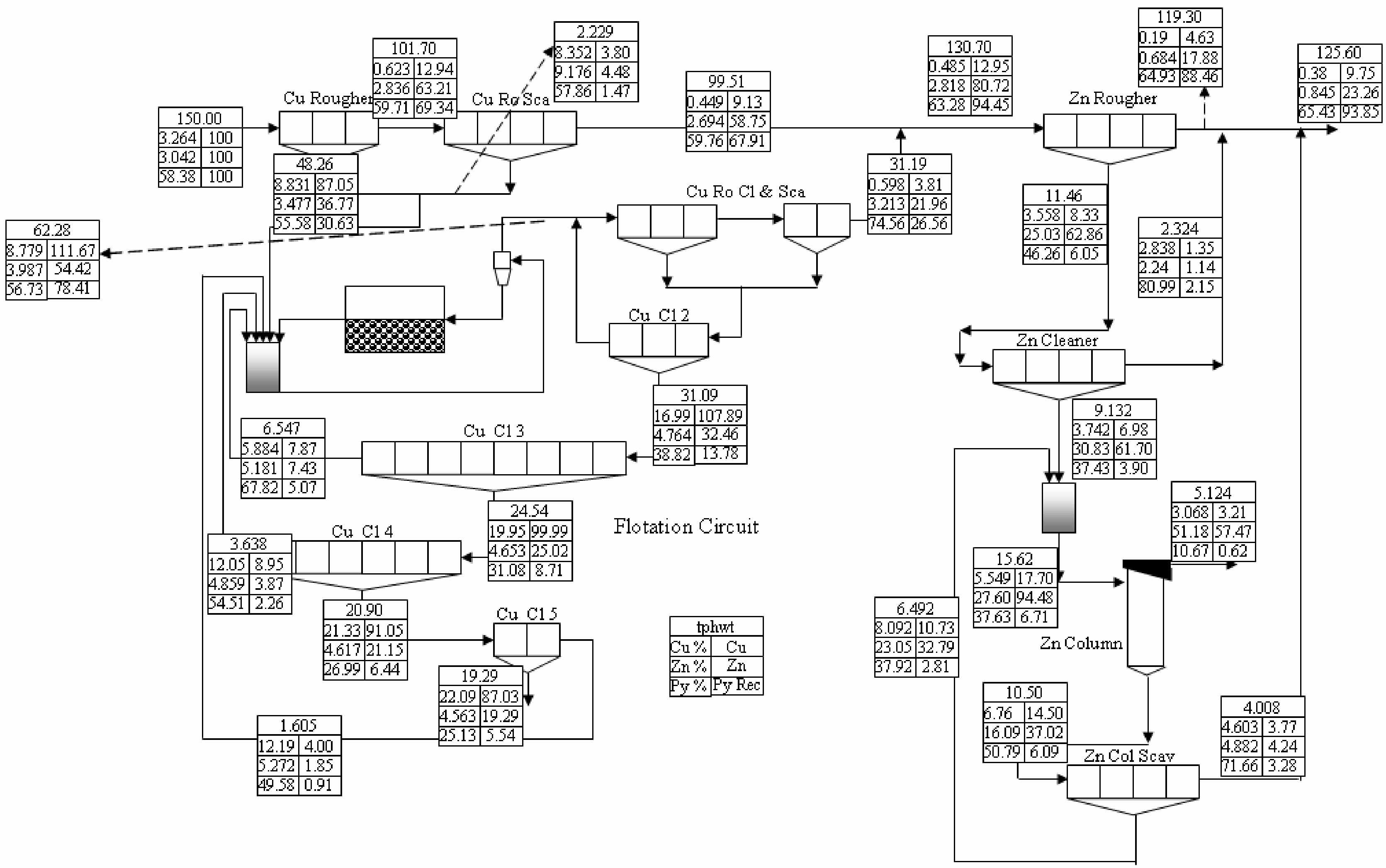

As can be seen from the figure, overall copper recovery was around 87% while overall zinc recovery was 57.47%. Zinc grade in copper concentrate was 4.56% which referred to 19.29% zinc loss whereas copper grade in zinc concentrate was 3.1% indicating that 3.2% of copper was lost in zinc concentrate. Copper metal losses were occured from two streams, Cu Rougher Scavenger tail which was responsible from 9.13% copper loss and Cu Cleaner 1 Scavenger tail which was responsible from 3.81% copper loss. At Zn Rougher stage, 22.15% of zinc metal was recovered as final tailing which composed of the other major part of zinc loss. Recovery of Zn Column stage is 60.79%. Final tail consisted of 0.38% Cu and 0.85% Zn. After having determined the flow rate of Cu regrinding cyclone overflow, by using particle size distribution and %solids of the streams around regrinding ball mill and cyclone mass balance study was performed to determine the mass and water flow rates of each stream. Calculated flowrates and particle size distributions after mass balancing is given in Figure 6-22 and Figure 6-23, respectively. By using mass balance results, efficiency curve and some important parameters of hydrocyclones was calculated and given in Figure 6-24.

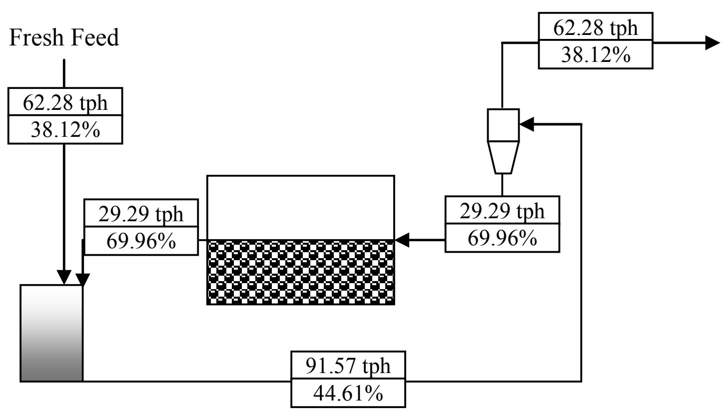

Figure 6-22. The result of mass balance calculation around regrinding circuit

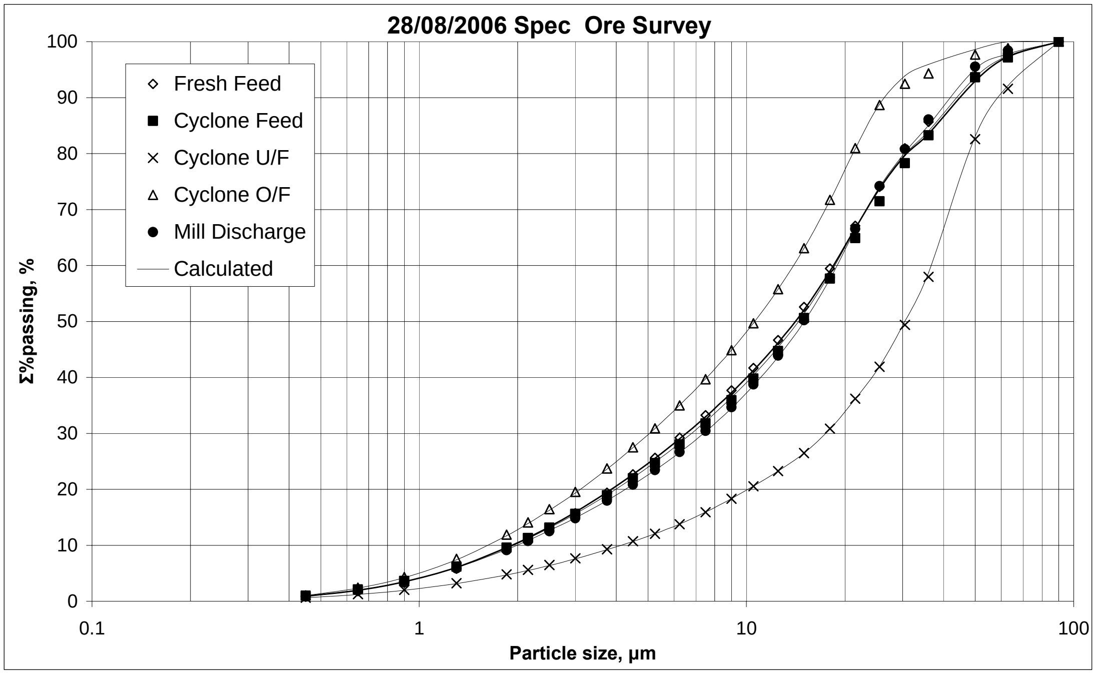

Figure 6-23. Calculated and experimental particle size distributions around regrinding circuit

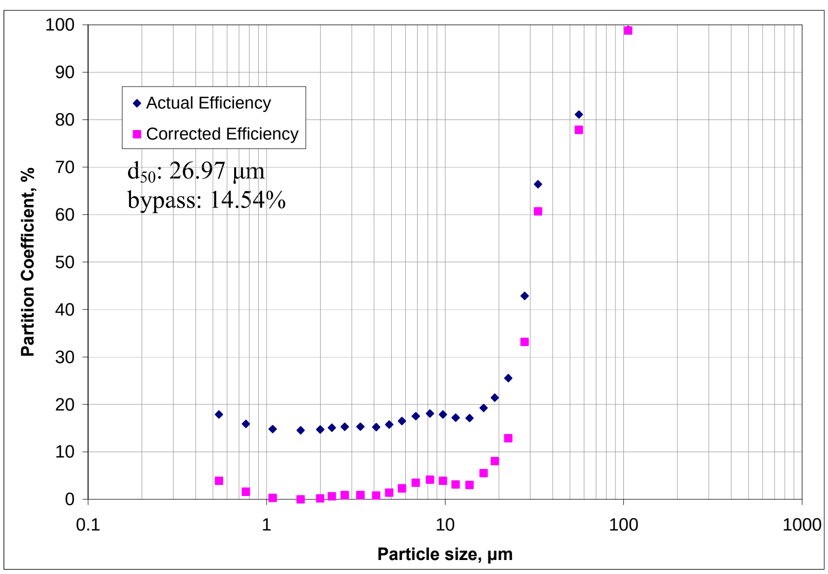

Figure 6-24. Efficiency curves of cyclones sampled on 28/08/2006

6.3.2. 06/09/2006 Copper and Zinc Flotation Circuit Survey – Non-Spec Ore

This survey was carried out when the fresh feed to the plant was 150 wmtph. Cyclone pressure was adjusted to 1.77 bar and kept constant during the survey. The observed parameters recorded in the control room are presented in Table 6-9.

Table 6-9. Parameters recorded in the control room during the survey

	Feed Tonnage (wet)	Cu Concentrate		Flotation Feed		Zn Concentrate		Final Tail	
		Cu%	Zn%	Cu%	Zn%	Cu%	Zn%	Cu%	Zn%
11:00	149.99	20.49	8.70	3.45	11.29	2.64	50.49	0.89	1.09
12:00	150.06	20.40	9.13	3.64	11.67	2.69	50.15	0.88	1.13
13:00	150.02	19.85	10.56	3.79	11.06	2.71	50.20	0.89	1.10

Mass balancing by using chemical assays in copper and zinc flotation circuit was done to calculate the flow rate of each stream. Flow rates and adjusted assays after mass balancing are given in Figure 6-25. The pyrite recoveries are presented instead of Fe recoveries for a better representation of performance.

As can be seen from the figure, overall copper recovery was around 57.50% while overall zinc recovery was 84.53%. Zinc grade in copper concentrate was 6.99% which refers to 5.64% zinc loss whereas copper grade in zinc concentrate was 2.62% indicating that 15.60% of copper was lossed in zinc concentrate. Copper metal losses were occured from two streams, Cu Rougher Scavenger tail which was responsible from 30.43% copper loss and Cu Cleaner 1 Scavenger tail which was responsible from 12.08% copper loss. At Zn Rougher stage, 6.07% of zinc metal was recovered as final tailing which composed of the other major part of zinc loss. Recovery of Zn Column stage was 61.60%. Final tail consisted of 0.98% Cu and 1.25% Zn.

Figure 6-25. 06/09/2006 - Mass balancing result of non-spec ore survey at copper and zinc flotation circuit

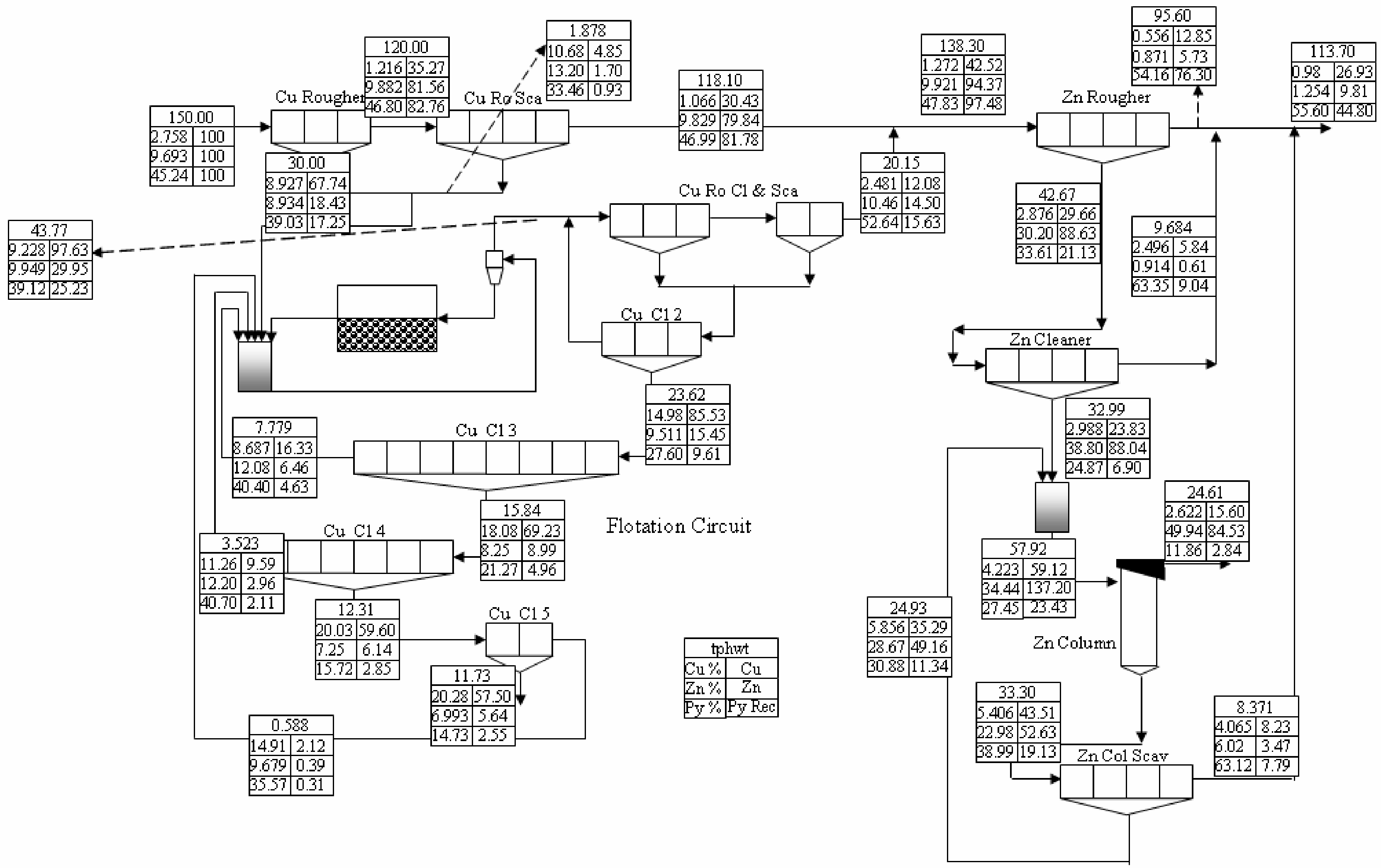

After having determined the flow rate of Cu regrinding cyclone overflow, by using particle size distribution and %solids of the streams around regrinding ball mill and cyclone mass balance study was performed to determine the mass and water flow rates of each stream. Calculated flowrates and particle size distributions after mass balancing is given in Figure 6-26 and Figure 6-27, respectively. By using mass balance results, efficiency curve and some important parameters of hydrocyclones was calculated and given in Figure 6-28.

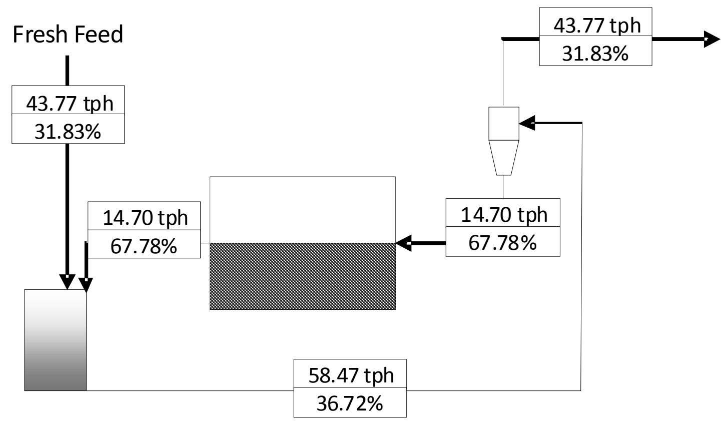

Figure 6-26. Calculated and experimental particle size distributions around regrinding circuit

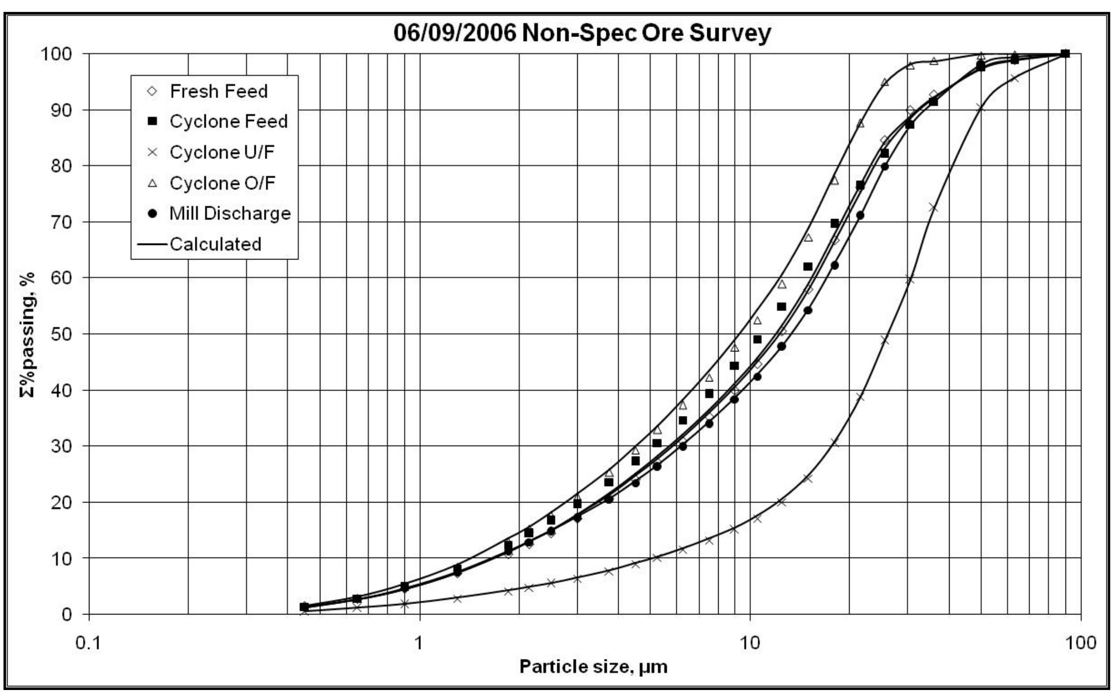

Figure 6-27. Calculated and experimental particle size distributions around regrinding circuit

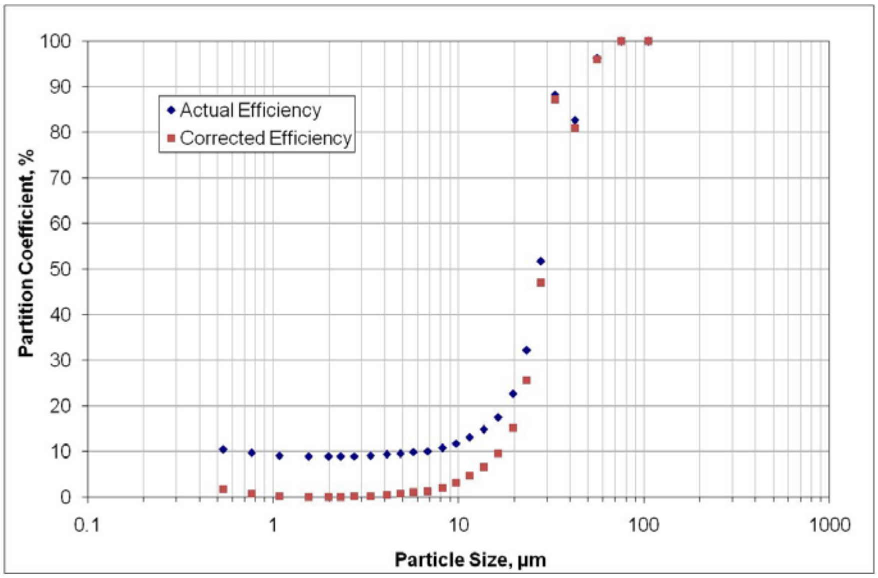

Figure 6-28. Efficiency curves of cyclones sampled on 06/09/2006

6.4. Performance Evaluation of Copper Regrinding Circuit

Mass-balanced data of flow rate and % solids of feed streams as well as operating pressures and figures indicating the separation efficiency of the regrinding cyclones obtained from 6 sampling periods are given in Table 6-10.

Table 6-10. Mass-balanced flowrates and figures relating to the separation efficiency of cyclones

Date of Survey	Flotation Feed Tonnage (wmtph)	Regrinding Circuit Tonnage (wmtph)	Cyclone Feed Tonnage (wmtph)	%solid of Cyclone Feed	Pressure (bar)	Circulating Load Ratio (%)	d_{50} (µm)	Bypass (%)
31/07/2006	150.00	50.40	77.13	41.56	1.45	53.04	27.47	14.08
04/08/2006	120.00	48.92	62.25	37.80	1.20	27.25	27.67	7.61
08/08/2006	140.00	35.08	55.58	37.82	1.85	58.44	22.65	15.43
09/08/2006	140.00	25.10	31.19	34.36	0.85	24.25	26.97	7.45
28/08/2006	150.00	62.28	91.57	44.61	1.31	47.03	26.97	14.54
06/09/2006	150.00	43.77	58.47	36.72	1.77	33.58	27.50	8.86

As can be seen from Table 6-10, there was a considerable variation in feed flow rates to cyclones. Operating pressure of cyclones could hardly be stabilised during operation because of the size of the sump feeding the cyclone cluster. In order to keep the pulp level as constant as possible and to avoid overflowing in that sump, the speed of the sump motor was automatically adjusted. However, this adjustment causes variation in cyclone pressure which fluctuates between 0 and 2 bars while they are in operation. For proper operation, this fluctuation should be avoided. During surveys, the number of operating cyclones was changed to between 8-10 to keep the pressure as constant as possible.

Comparison of size distribution of the streams around the cyclone is given in Figure 6-29. Increasing the plant feed to 150 wmtph cyclone resulted in coarser cyclone overflow while cyclone overflow for the other surveys were similar.

In Figure 6-30 and Figure 6-31, actual and corrected efficiency curves of the cyclones are given. d_{50} values were found to be very close to each other (approx. 27 µm) for all surveys excluding the one obtained from third sampling period (22.65 µm) in which the cyclone pressure was 1.85 bars being higher than the others.

In Table 6-10, the amount of bypass was about 15% for sampling periods of 1, 3 and 5. However, for the 2nd, 4th and 6th surveys, the bypass was about 8%. According to the available data, the bypass value evaluated as reasonable.

The circulating load was varied between 24-58% which was rather low. Increasing it may increase the energy efficiency. However, any attempt to increase circulating load would increase the load in cyclone feed sump which has already reached to its capacity.

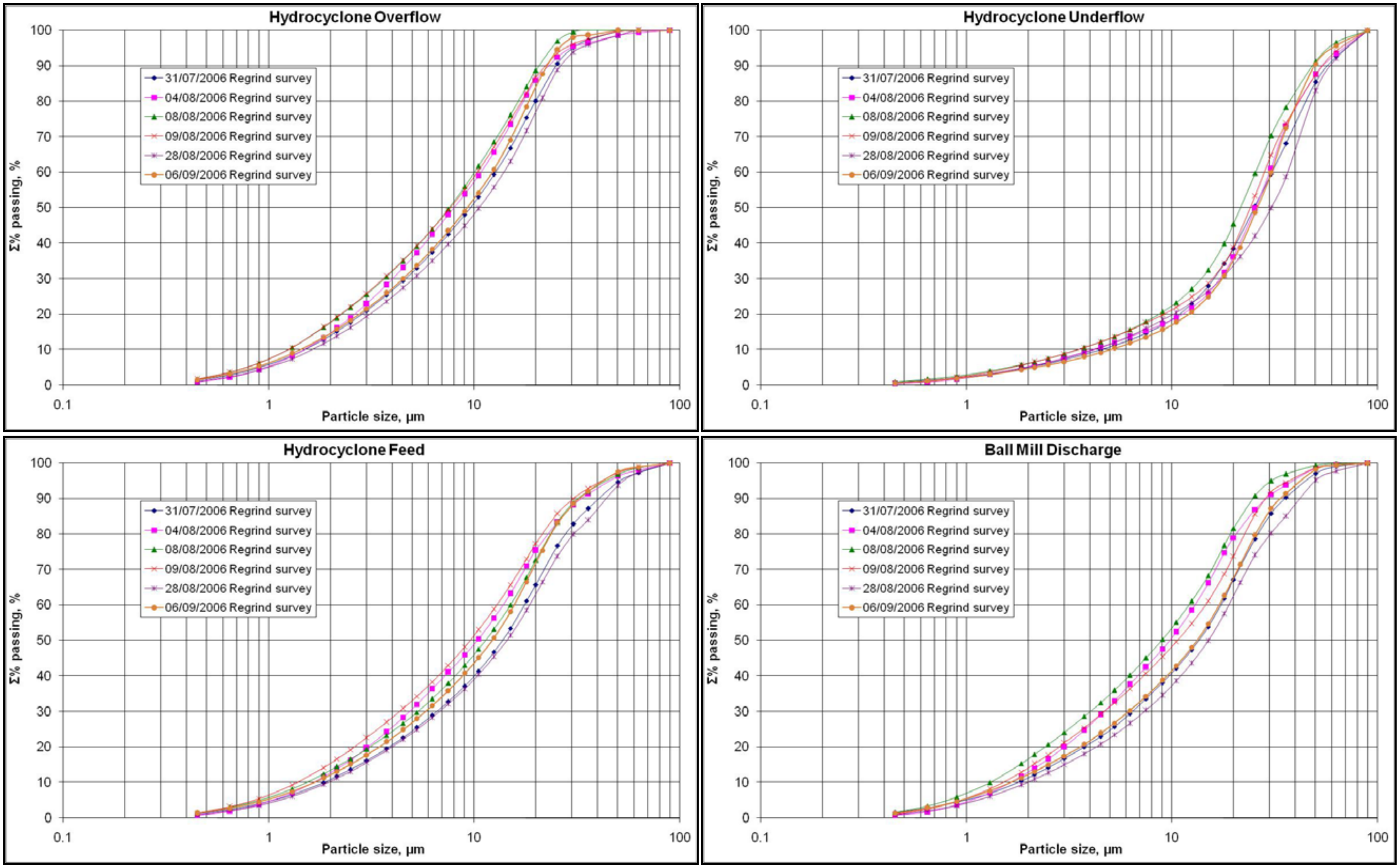

Figure 6-29. Comparison of the size distribution of streams around the regrinding cyclones obtained from 6 sampling periods

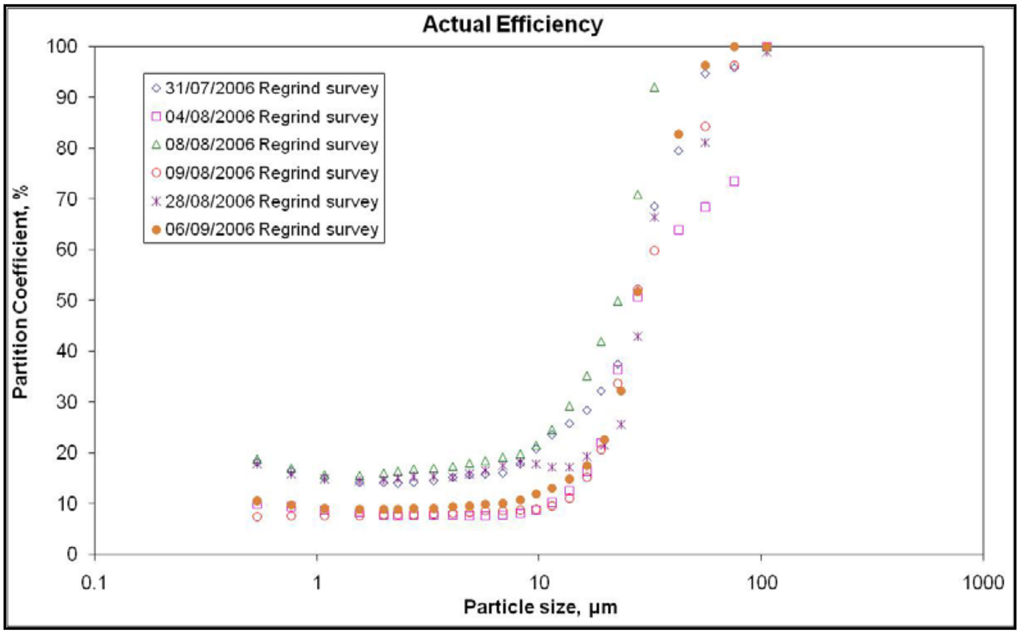

Figure 6-30. Actual efficiency curves of regrinding cyclones obtained from 6 sampling periods

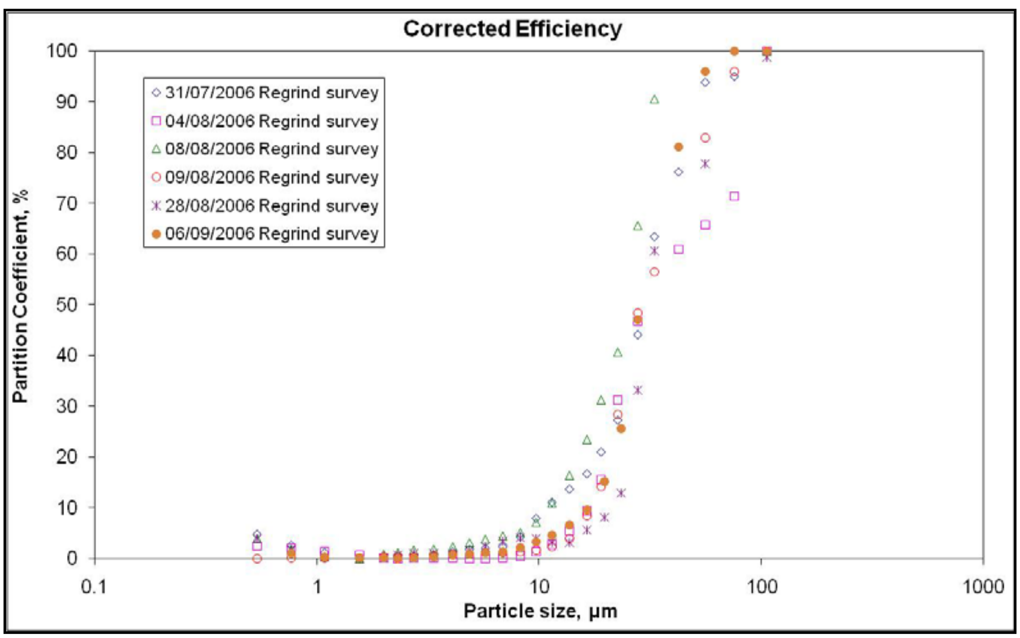

Figure 6-31. Corrected efficiency curves of regrinding cyclones obtained from 6 sampling periods

6.5. Mineralogical Studies

After completion of surveys for two different ore type (Spec and Non-Spec) processed in the plant, liberation analysis were done in order to evaluate the streams in terms of need for further grinding. For this purpose, all the samples taken from the predetermined streams were cyclosized to obtain 5 size fractions, namely +50, -50+36, -36+20, -20+9 and -9 µm. Then, chemical and liberation analysis were done for each size fraction. Chemical analysis and cyclosizing were carried out at ÇBI’s laboratory while mineralogical analysis of all samples were performed at Hacettepe University, Geological Engineering Department using scanning electron microscope (SEM) system. The images taken from SEM were used to determine the liberation degree of each fraction and hence that of each stream. Mineralogical analysis were carried out on streams given in Table 6-11 for both ore types.

Table 6-11. The streams where samples were taken for mineralogical analysis

Flotation Feed	Cu Rgh Concentrate	Zn Rgh Feed	Cu RG Cyclone O/F
Cu Concentrate	Cu Rgh Scav Concentrate	Cu Cl 3 Tail	Cu Cl 4 Tail
Cu Cl 5 Tail	Zn Rgh Concentrate	Final Tail	Zn Concentrate
Zn Column Tail	Zn Col Scav Concentrate		

Table 6-12 and Table 6-13 show %weight, chemical analysis, liberation degrees, tonnages of valuable metals in each size fraction and overall liberations of each stream given in Table 6-11 for Non-Spec and Spec ore, respectively. %weight of each fraction was determined from the results of laser sizing instead of using the cyclosizing results since the calculation regarding to liberation after stirred milling was based on laser sizer. It should be noted that mineralogical analysis of -9 µm fraction has not been performed and liberation of this fraction was assumed to be as same as that of -20+9 µm fraction in calculation of overall liberation.

Table 6-12. The results of mineralogical analysis of each stream for Non-Spec ore

Flotation Feed												
		Content, %			Liberation Degree			Tonnage (dmtph)		Overall Liberation		
	%wt	Cu	Zn	Fe	ZnS	$CuFeS_2$	FeS	Cu	Zn	ZnS	$CuFeS_2$	FeS
+50	12.61	2.30	8.90	15.40	43.87	61.35	71.33	0.422	1.633	75.86	82.06	88.45
+36	9.94	3.00	10.60	28.20	77.21	58.27	80.86	0.434	1.533			
+20	25.20	2.75	8.90	31.80	52.24	84.17	84.38	0.956	3.095			
+9	19.40	2.90	10.00	26.70	87.42	90.57	95.98	0.998	3.441			
-9	32.85	3.74	10.00	19.90				1.627	4.350			

Table 6-12 (Continuing). The results of mineralogical analysis of each stream for Non-Spec ore

Cu Rougher Concentrate												
		Content, %			Liberation Degree			Tonnage (dmtph)		Overall Liberation		
	%wt	Cu	Zn	Fe	ZnS	$CuFeS_2$	FeS	Cu	Zn	ZnS	$CuFeS_2$	FeS
+50	2.99	13.00	8.62	24.20	57.02	68.03	36.19	0.113	0.075	77.40	85.58	89.51
+36	5.85	11.60	8.80	29.20	53.76	79.22	77.37	0.197	0.150			
+20	21.71	8.14	7.48	31.20	62.35	81.76	83.86	0.499	0.459			
+9	30.37	8.82	9.15	30.10	84.97	88.06	94.6	0.838	0.870			
-9	39.08	9.95	9.82	24.10				1.084	1.070			
Zn Rougher Feed												
		Content, %			Liberation Degree			Tonnage (dmtph)		Overall Liberation		
	%wt	Cu	Zn	Fe	ZnS	$CuFeS_2$	FeS	Cu	Zn	ZnS	$CuFeS_2$	FeS
+50	13.57	1.71	11.60	18.00	59.35	44.71	51.56	0.311	2.112	77.58	66.10	88.35
+36	11.28	1.32	10.50	27.50	81.5	59.31	92.94	0.200	1.588			
+20	33.60	0.97	9.10	30.00	68.13	68.55	93.59	0.268	2.515			
+9	14.86	0.87	10.10	26.50	90.12	72.94	94.87	0.280	3.250			
-9	26.69	1.53	10.00	20.40				0.627	4.101			
Cu Concentrate												
		Content, %			Liberation Degree			Tonnage (dmtph)		Overall Liberation		
	%wt	Cu	Zn	Fe	ZnS	$CuFeS_2$	FeS	Cu	Zn	ZnS	$CuFeS_2$	FeS
+50	0.06	27.20	3.57	28.20	28.27	85.15	68.49	0.002	0.0002	64.48	91.07	87.27
+36	0.31	27.40	4.70	27.80	44.94	83.91	34.46	0.010	0.0017			
+20	12.41	21.80	6.58	26.50	54.55	87.58	81.83	0.346	0.1044			
+9	32.36	20.60	7.00	27.40	65.99	91.6	88.24	0.825	0.2803			
-9	54.86	21.50	7.10	25.20				1.235	0.4079			
Cu Rougher Scavenger Concentrate												
		Content, %			Liberation Degree			Tonnage (dmtph)		Overall Liberation		
	%wt	Cu	Zn	Fe	ZnS	$CuFeS_2$	FeS	Cu	Zn	ZnS	$CuFeS_2$	FeS
+50	6.51	19.80	10.20	26.70	59.44	64.55	43.91	0.022	0.011	84.28	88.08	91.73
+36	10.29	15.00	11.20	27.60	66.72	86.02	81.52	0.028	0.021			
+20	42.10	10.10	11.50	28.60	72.26	76.36	83.2	0.044	0.050			
+9	20.40	8.12	17.50	26.90	83.33	82.86	87.83	0.033	0.072			
-9	31.35	11.90	13.60	24.40				0.081	0.092			
Cu Cleaner 3 Tail												
		Content, %			Liberation Degree			Tonnage (dmtph)		Overall Liberation		
	%wt	Cu	Zn	Fe	ZnS	$CuFeS_2$	FeS	Cu	Zn	ZnS	$CuFeS_2$	FeS
+50	0.87	7.14	11.20	21.20	50.22	71.08	75.06	0.005	0.007	77.02	76.96	87.04
+36	1.45	12.10	10.60	28.50	52.92	67.49	64.34	0.013	0.012			
+20	17.36	9.81	10.20	29.90	66.00	82.44	86.95	0.097	0.100			
+9	37.78	8.16	12.40	29.70	78.71	74.66	86.05	0.277	0.420			
-9	43.99	8.01	14.20	24.70				0.240	0.426			
Cu Cleaner 4 Tail												
		Content, %			Liberation Degree			Tonnage (dmtph)		Overall Liberation		
	%wt	Cu	Zn	Fe	ZnS	$CuFeS_2$	FeS	Cu	Zn	ZnS	$CuFeS_2$	FeS
+50	0.16	19.90	9.02	25.20	49.34	71.03	60.34	0.001	0.001	75.34	80.86	88.03
+36	0.76	19.80	10.40	26.60	48.56	74.01	51.35	0.005	0.003			
+20	19.23	11.30	11.20	28.90	62.78	70.85	74.07	0.050	0.049			
+9	37.81	8.41	13.90	30.30	78.67	83.36	91.8	0.136	0.225			
-9	42.04	8.23	13.70	25.70				0.109	0.182			

Table 6-12 (Continuing). The results of mineralogical analysis of each stream for Non-Spec ore

Cu Cleaner 5 Tail												
		Content, %			Liberation Degree			Tonnage (dmtph)		Overall Liberation		
	%wt	Cu	Zn	Fe	ZnS	$CuFeS_2$	FeS	Cu	Zn	ZnS	$CuFeS_2$	FeS
+50	0.10	19.10	12.20	25.20	27.22	70.88	24.51	0.00011	0.00007	81.79	84.58	88.97
+36	0.41	21.10	8.28	26.40	57.08	79.73	54.35	0.00050	0.00020			
+20	13.94	15.30	8.75	30.00	63.42	83.23	81.52	0.00907	0.00519			
+9	34.97	13.20	10.70	30.20	84.96	84.84	90.43	0.03038	0.02463			
-9	50.58	14.90	11.10	25.50				0.04142	0.03086			
Cu RG Cyclone O/F												
		Content, %			Liberation Degree			Tonnage (dmtph)		Overall Liberation		
	%wt	Cu	Zn	Fe	ZnS	$CuFeS_2$	FeS	Cu	Zn	ZnS	$CuFeS_2$	FeS
+50	0.29	6.86	5.31	11.90	67.11	80.5	58.22	0.008	0.006	74.79	83.85	88.29
+36	0.96	11.50	9.27	21.90	63.77	81.54	70.19	0.047	0.038			
+20	17.94	9.10	9.80	29.30	59.35	79.51	89.15	0.693	0.746			
+9	37.47	8.54	10.20	30.10	78.38	84.85	88.42	1.359	1.623			
-9	43.35	9.87	10.30	24.70				1.817	1.896			
Zn Rougher Concentrate												
		Content, %			Liberation Degree			Tonnage (dmtph)		Overall Liberation		
	%wt	Cu	Zn	Fe	ZnS	$CuFeS_2$	FeS	Cu	Zn	ZnS	$CuFeS_2$	FeS
+50	8.99	4.13	39.40	12.40	57.10	55.25	24.67	0.154	1.466	88.72	68.31	79.17
+36	9.86	3.19	34.50	16.40	70.50	69.44	63.96	0.130	1.407			
+20	13.85	2.52	27.90	21.60	75.78	62.29	76.09	0.223	2.474			
+9	25.62	2.04	29.10	21.80	98.28	71.12	89.31	0.227	3.240			
-9	41.68	2.76	26.30	17.60				0.375	3.574			
Zn Concentrate												
		Content, %			Liberation Degree			Tonnage (dmtph)		Overall Liberation		
	%wt	Cu	Zn	Fe	ZnS	$CuFeS_2$	FeS	Cu	Zn	ZnS	$CuFeS_2$	FeS
+50	10.31	2.21	54.60	5.70	72.25	50.28	36.21	0.054	1.344	84.33	64.65	68.29
+36	9.58	2.28	53.20	6.85	84.06	46.86	51.63	0.052	1.217			
+20	16.51	2.59	49.10	9.45	80.91	63.02	54.89	0.104	1.977			
+9	26.32	2.63	49.20	9.55	87.22	70.08	79.47	0.189	3.534			
-9	37.28	3.42	46.60	8.20				0.271	3.688			
Zn Column Tail												
		Content, %			Liberation Degree			Tonnage (dmtph)		Overall Liberation		
	%wt	Cu	Zn	Fe	ZnS	$CuFeS_2$	FeS	Cu	Zn	ZnS	$CuFeS_2$	FeS
+50	6.93	5.96	37.00	14.80	54.85	69.8	36.65	0.133	0.828	62.82	78.94	69.97
+36	6.31	5.87	26.20	21.10	58.01	66.61	57.35	0.120	0.534			
+20	36.13	4.95	17.50	28.10	49.43	74.82	67.27	0.578	2.043			
+9	27.26	4.73	14.70	29.10	74.07	84.66	78.02	0.416	1.294			
-9	23.37	5.91	16.60	21.40				0.446	1.253			
Zn Column Scavenger Concentrate												
		Content, %			Liberation Degree			Tonnage (dmtph)		Overall Liberation		
	%wt	Cu	Zn	Fe	ZnS	$CuFeS_2$	FeS	Cu	Zn	ZnS	$CuFeS_2$	FeS
+50	7.57	4.96	40.60	12.50	62.59	47.69	29.69	0.091	0.743	67.27	74.17	63.58
+36	6.01	5.47	30.50	17.60	54.54	74.24	44	0.080	0.443			
+20	34.61	5.41	22.90	24.50	50.64	66.65	52.76	0.453	1.916			
+9	29.84	5.91	21.30	24.10	80.54	83.06	78.02	0.426	1.537			
-9	21.97	7.17	27.10	18.00				0.381	1.440			

Table 6-12 (Continuing). The results of mineralogical analysis of each stream for Non-Spec ore

Final Tail												
		Content, %			Liberation Degree			Tonnage (dmtph)		Overall Liberation		
	%wt	Cu	Zn	Fe	ZnS	$CuFeS_2$	FeS	Cu	Zn	ZnS	$CuFeS_2$	FeS
+50	14.39	2.49	4.16	22.40	31.83	67.11	70.82	0.395	0.660	39.73	65.04	89.65
+36	12.05	2.00	2.74	31.40	31.83	53.41	82.42	0.266	0.364			
+20	9.81	1.14	1.68	35.70	60.48	59.31	89.76	0.235	0.347			
+9	23.23	0.70	0.78	33.00	39.81	67.64	95.24	0.162	0.181			
-9	40.52	1.58	1.63	24.70				0.590	0.609			

Table 6-12 shows that 21.85% of the material in flotation feed is coarser than 36 µm indicating that fineness reached at primary grinding is not sufficient at 150 tph and liberation of these size fractions are relatively low which cause metal loss at coarse fractions. Similarly, some streams in the circuit such as Cu Rougher concentrate, Cu Rougher Scavenger concentrate, Zn Column tail and Zn Column Scavenger tail have significant amount of material above 36 µm and this constitutes one of the main reasons for metal loss due to low liberation of coarse size fractions of these streams.

Table 6-13. The results of mineralogical analysis of each stream for Spec ore

Flotation Feed												
		Content, %			Liberation Degree			Tonnage (dmtph)		Overall Liberation		
	%wt	Cu	Zn	Fe	ZnS	$CuFeS_2$	FeS	Cu	Zn	ZnS	$CuFeS_2$	FeS
+50	16.93	2.35	2.33	19.40	51.55	63.53	77.90	0.579	0.574	74.61	82.17	91.10
+36	10.49	3.18	3.02	33.10	68.22	56.77	84.95	0.485	0.461			
+20	18.26	2.91	2.50	38.20	79.15	81.45	90.47	0.918	0.789			
+9	21.12	3.33	3.08	31.80	81.51	93.13	96.61	1.130	1.045			
-9	33.20	3.65	3.32	24.20				1.465	1.332			
Cu Rougher Concentrate												
		Content, %			Liberation Degree			Tonnage (dmtph)		Overall Liberation		
	%wt	Cu	Zn	Fe	ZnS	$CuFeS_2$	FeS	Cu	Zn	ZnS	$CuFeS_2$	FeS
+50	6.33	11.40	2.70	28.60	30.97	79.19	84.07	0.338	0.080	57.57	84.16	94.85
+36	8.32	9.95	2.91	33.30	44.12	81.91	86.5	0.387	0.113			
+20	21.13	8.12	2.86	36.80	40.49	82.01	93.14	0.990	0.349			
+9	25.37	7.61	3.57	34.20	67.55	85.5	97.55	1.043	0.489			
-9	38.85	7.75	3.76	26.50				1.089	0.528			
Zn Rougher Feed												
		Content, %			Liberation Degree			Tonnage (dmtph)		Overall Liberation		
	%wt	Cu	Zn	Fe	ZnS	$CuFeS_2$	FeS	Cu	Zn	ZnS	$CuFeS_2$	FeS
+50	16.28	0.53	2.52	17.90	68.81	33.59	78.46	0.109	0.520	86.92	49.70	91.83
+36	10.98	0.54	3.08	32.60	64.5	40.32	84.12	0.075	0.429			
+20	16.40	0.45	2.38	38.30	82.21	37.81	95.15	0.123	0.651			
+9	22.37	0.34	2.85	33.20	97.89	59.64	96.23	0.101	0.848			
-9	33.97	0.53	3.21	25.10				0.186	1.127			

Table 6-13 (Continuing). The results of mineralogical analysis of each stream for Spec ore

Cu Concentrate												
		Content, %			Liberation Degree			Tonnage (dmtph)		Overall Liberation		
	%wt	Cu	Zn	Fe	ZnS	$CuFeS_2$	FeS	Cu	Zn	ZnS	$CuFeS_2$	FeS
+50	1.29	29.60	1.87	28.40	30.34	89.14	45.25	0.072	0.005	50.47	86.79	83.26
+36	4.43	29.10	2.38	28.60	32.45	86.78	62.48	0.241	0.020			
+20	23.70	22.80	3.34	30.50	36.58	84.3	78.88	1.032	0.151			
+9	30.64	20.60	4.48	31.20	56.64	87.59	86.73	1.381	0.300			
-9	39.94	21.90	4.09	29.50				1.404	0.262			
Cu Rougher Scavenger Concentrate												
		Content, %			Liberation Degree			Tonnage (dmtph)		Overall Liberation		
	%wt	Cu	Zn	Fe	ZnS	$CuFeS_2$	FeS	Cu	Zn	ZnS	$CuFeS_2$	FeS
+50	17.29	14.70	6.75	32.40	28.15	55.48	60.26	0.055	0.025	68.54	68.47	86.72
+36	14.40	9.17	7.05	34.90	42.66	57.52	77.21	0.029	0.022			
+20	17.87	5.94	7.80	37.60	57.82	45.94	87.97	0.030	0.040			
+9	20.29	4.92	11.20	33.50	93.58	84.03	98.07	0.021	0.048			
-9	30.15	8.55	10.00	27.10				0.046	0.054			
Cu Cleaner 3 Tail												
		Content, %			Liberation Degree			Tonnage (dmtph)		Overall Liberation		
	%wt	Cu	Zn	Fe	ZnS	$CuFeS_2$	FeS	Cu	Zn	ZnS	$CuFeS_2$	FeS
+50	3.07	21.60	4.05	29.20	42.75	69.59	36.22	0.042	0.008	69.83	63.79	90.03
+36	6.29	18.20	6.82	31.40	29.12	68.1	55.11	0.073	0.027			
+20	19.76	8.21	4.77	38.20	53.33	65.83	89.16	0.125	0.073			
+9	31.12	3.58	4.89	39.00	79.21	62.59	95.7	0.083	0.113			
-9	39.76	2.43	4.95	30.70				0.047	0.095			
Cu Cleaner 4 Tail												
		Content, %			Liberation Degree			Tonnage (dmtph)		Overall Liberation		
	%wt	Cu	Zn	Fe	ZnS	$CuFeS_2$	FeS	Cu	Zn	ZnS	$CuFeS_2$	FeS
+50	3.31	27.10	2.23	29.60	61.35	94.85	56.5	0.032	0.003	54.99	79.83	86.76
+36	7.44	26.80	3.22	29.40	46.59	88.4	71.03	0.070	0.008			
+20	31.12	16.90	4.11	33.30	42.92	78.49	79.15	0.190	0.046			
+9	32.32	8.60	4.97	36.10	62.17	78.6	94.57	0.113	0.065			
-9	25.81	4.32	4.72	31.60				0.031	0.034			
Cu RG Cyclone O/F												
		Content, %			Liberation Degree			Tonnage (dmtph)		Overall Liberation		
	%wt	Cu	Zn	Fe	ZnS	$CuFeS_2$	FeS	Cu	Zn	ZnS	$CuFeS_2$	FeS
+50	2.33	7.99	2.55	18.7	60.2	83.05	64.1	0.112	0.036	64.42	85.74	93.61
+36	3.34	11.2	4.45	28	45.99	86.07	82.11	0.226	0.090			
+20	24.70	7.81	3.64	36.6	53.79	89.55	91.51	1.165	0.543			
+9	33.14	6.96	3.76	36	69.22	84.47	95.89	1.393	0.753			
-9	36.49	7.88	4.2	27.8				1.737	0.926			
Zn Rougher Concentrate												
		Content, %			Liberation Degree			Tonnage (dmtph)		Overall Liberation		
	%wt	Cu	Zn	Fe	ZnS	$CuFeS_2$	FeS	Cu	Zn	ZnS	$CuFeS_2$	FeS
+50	10.36	4.87	32.80	17.40	80.11	40.88	69.55	0.056	0.378	87.76	47.99	89.03
+36	9.74	3.40	27.70	23.00	88.52	54.92	78.87	0.037	0.300			
+20	20.79	2.30	19.80	28.30	75.97	42.13	85.14	0.062	0.530			
+9	23.66	1.62	23.70	26.00	93.12	50.15	95.48	0.048	0.695			
-9	35.45	2.32	25.20	18.60				0.076	0.824			

Table 6-13 (Continuing). The results of mineralogical analysis of each stream for Spec ore

Final Tail												
		Content, %			Liberation Degree			Tonnage (dmtph)		Overall Liberation		
	%wt	Cu	Zn	Fe	ZnS	$CuFeS_2$	FeS	Cu	Zn	ZnS	$CuFeS_2$	FeS
+50	20.31	0.55	0.76	15.40	22.62	45.87	74.98	0.136	0.188	30.13	47.68	90.84
+36	12.04	0.57	0.73	31.00	27.06	62.02	81.76	0.084	0.107			
+20	18.77	0.50	0.49	38.50	21.55	47.56	94.67	0.126	0.123			
+9	19.58	0.32	0.32	31.70	37.31	44.94	98.2	0.085	0.085			
-9	29.30	0.67	1.85	24.70				0.205	0.567			
Zn Concentrate												
		Content, %			Liberation Degree			Tonnage (dmtph)		Overall Liberation		
	%wt	Cu	Zn	Fe	ZnS	$CuFeS_2$	FeS	Cu	Zn	ZnS	$CuFeS_2$	FeS
+50	8.44	2.68	56.40	5.30	64.74	20.66	32.85	0.011	0.237	86.51	45.38	65.03
+36	8.09	2.98	54.20	6.13	69.24	32.78	41.34	0.012	0.218			
+20	22.81	3.35	47.50	9.40	89.01	54.23	58.37	0.035	0.490			
+9	27.24	2.60	50.50	8.65	90.91	47.17	75.17	0.040	0.776			
-9	33.42	3.94	51.70	6.08				0.062	0.817			
Zn Column Tail												
		Content, %			Liberation Degree			Tonnage (dmtph)		Overall Liberation		
	%wt	Cu	Zn	Fe	ZnS	$CuFeS_2$	FeS	Cu	Zn	ZnS	$CuFeS_2$	FeS
+50	9.32	8.07	34.10	14.90	59.47	50.76	18.81	0.077	0.324	64.85	67.36	78.33
+36	9.50	9.02	25.70	21.00	63.3	73.43	51.11	0.087	0.249			
+20	27.96	7.87	13.00	29.60	59.83	67.11	82.39	0.254	0.420			
+9	27.83	5.35	8.82	34.00	68.7	69.32	91.48	0.156	0.256			
-9	25.39	5.47	18.00	29.40				0.117	0.384			
Zn Column Scavenger Concentrate												
		Content, %			Liberation Degree			Tonnage (dmtph)		Overall Liberation		
	%wt	Cu	Zn	Fe	ZnS	$CuFeS_2$	FeS	Cu	Zn	ZnS	$CuFeS_2$	FeS
+50	5.97	8.05	34.20	14.60	57.31	63.07	24.23	0.030	0.129	58.13	74.39	75.66
+36	6.54	9.37	27.00	20.00	58.34	78.13	54.58	0.039	0.111			
+20	34.38	8.61	14.00	27.70	51.91	66.12	72.11	0.210	0.342			
+9	28.15	7.07	11.80	30.20	62.2	80.55	86.33	0.164	0.274			
-9	24.96	6.92	28.80	17.40				0.051	0.214			

Table 6-13 shows that 27.42% of the material in flotation feed is coarser than 36 μm indicating that fineness reached at primary grinding is not sufficient at 150 tph for Spec ore and liberation of these size fractions are relatively low which cause metal loss at coarse fractions. Similarly, some streams in the circuit such as Cu Rougher concentrate, Cu Rougher Scavenger concentrate, Zn Column tail and Zn Column Scavenger tail have significant amount of material above 36 μm and this constitutes one of the main reasons for metal loss due to low liberation of coarse size fractions of these streams. In addition to these streams, tails of copper cleaner stages have also considerable amount of material at coarse fractions which needs further grinding.

6.5.1. Metallurgical Evaluations

The modal analysis of all streams sampled during the surveys are given in Appendix 3. Following evaluations were done according to these results.

Total copper recovery for Spec ore at 150 tph was 87.03%. Copper final concentrate also contained 19.29% of total zinc in flotation feed. The main reason of zinc loss to copper final concentrate was the liberated sphalerite particles mostly due to entrainment at fine size fractions (-20 µm). Besides the liberated sphalerite particles, significant amount of sphalerite was recovered to copper final concentrate through binary particles with chalcopyrite. There are two streams, where copper loss occurs, in copper flotation circuit. These streams are Cu Rougher Scavenger tail and Cu Cleaner 1 Scavenger tail. 9.13% of total copper in flotation feed reported to zinc flotation circuit through Cu Rougher Scavenger tail while the rest of copper was lost through Cu Cleaner 1 Scavenger tail. These two streams are combined and fed to zinc flotation circuit. Besides the liberated chalcopyrite particles in these streams, the other source of copper loss was the locked particles of chalcopyrite at coarse fractions which were in high quantity especially at high feed rates. Total zinc recovery in zinc flotation circuit was 71.20%. Zinc final concentrate also contained 3.21% of total copper in flotation feed. Copper loss to zinc final concentrate occured by binary particles of chalcopyrite especially with sphalerite and the liberated chalcopyrite. Zn content of Zinc Column Scavenger tail, which was sent to final tail, was found to be high although it had very low flowrate. Locked particles constituted the main reason of metal loss through this stream. Concentrate of the same stage which was recirculated to zinc column stage, consisted of high amount of locked particles as well. It does not seem to be possible to recover metal from this stream as long as liberation is low. However, this causes the accumulation of valuable metal in this stream. For Spec ore, final tail contained 9.75% of total copper and 23.26% of total zinc in flotation feed. The binary particles of chalcopyrite and sphalerite with pyrite were the main reason of metal loss in final tail.

Total copper recovery for Non-Spec ore at 150 tph was 57.50%. Copper final concentrate also contained 5.64% of total zinc in flotation feed. The main reason of zinc loss to copper final concentrate was the liberated sphalerite particles mostly due to entrainment at fine size fractions (-20 µm). Besides the liberated sphalerite particles, significant amount of sphalerite was recovered to copper final concentrate through binary particles with chalcopyrite. 30.43% of total copper in flotation feed reported to zinc flotation circuit through Cu Rougher Scavenger tail while 12.08% of total copper was lost through Cu Cleaner 1 Scavenger tail. These two streams are combined and fed to zinc flotation circuit. Besides the liberated chalcopyrite particles in these streams, the other source of copper loss was the locked particles of chalcopyrite at coarse fractions which were in high quantity especially at high feed rates. High metal loss at coarse fractions was occured because the desired fineness was not achieved in primary grinding due to the high flowrate. Total zinc recovery in zinc flotation circuit was 89.57%. Zinc final concentrate also contained 15.60% of total copper in flotation feed. Copper loss to zinc final concentrate occured by binary particles of chalcopyrite especially with sphalerite and the liberated chalcopyrite. The valuable metal content of Zinc Column Scavenger tail, which was sent to final tail, was found to be high although it had very low flowrate. Locked particles constituted the main reason of metal loss through this stream. Concentrate of the same stage which was recirculated to zinc column stage, consisted of high amount of locked particles at coarse size fractions as well as the liberated sphalerite particles whose flotabilities were probably low. The liberated sphalerite particles had another chance to float and report to final concentrate in Zinc column stage because of the recirculation of this stream. However, low liberation resulted in accumulation of valuable metal around Zinc Column stage. For Spec ore, final tail contained 26.93% of total copper and 9.81% of total zinc in flotation feed. Copper in final tail was in the form of chalcopyrite/pyrite binary particles and the liberated chalcopyrite particles. Similarly, zinc in final tail was in the form of sphalerite/pyrite binary particles and the liberated sphalerite particles at coarse size fractions.

The particle size distributions of the recirculating streams (Cu Cl 3 Tail, Cu Cl 4 Tail and Cu Cl 5 Tail) are very fine and less than 20% and 25 % of particles for Non-Spec ore and Spec ore respectively is finer than cut size of Cu RG Cyclone (Figure 6-32). Therefore, much of the particles in these streams are directly reported to cyclone overflow without grinding.

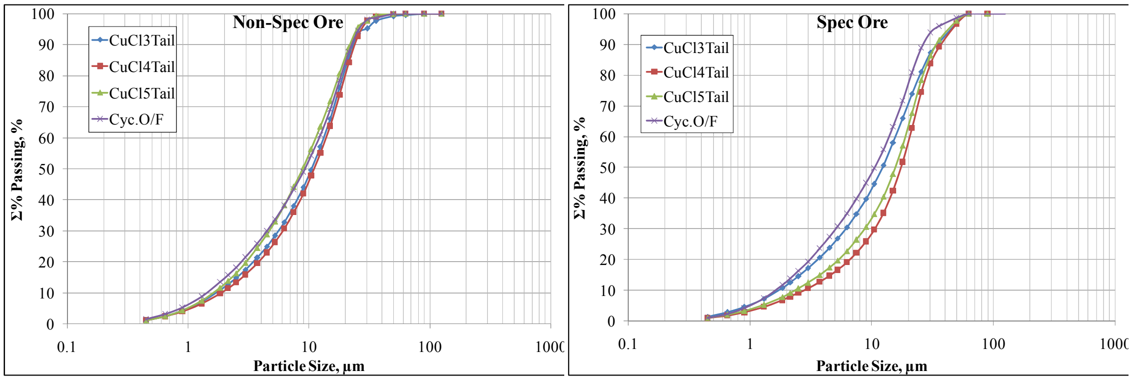

Figure 6-32. Comparison of particle size distributions of recirculating streams in Cu Regrind circuit and Cu RG Cyclone O/F

6.6. Evaluation of Alternative Circuit Design in CBI Flotation Plant

Detailed evaluation of existing regrinding and flotation circuit performance was described in previous sections. The most important findings and possible solutions are summarized as follows:

- One of the main reason of copper loss was that the locked particles of copper at coarse size fractions are directly reported to zinc circuit through the tails of Cu Rougher and Cu Rougher Scavenger streams. This situation became more pronounced at higher feed rates especially when the Non-Spec ore is being processed at the plant. In this case, 30% of copper in flotation feed was directly reported to zinc flotation circuit through copper rougher and copper rougher scavenger banks. On the other hand, copper loss to zinc flotation circuit through these stages was around 9% of copper in flotation feed for Spec ore. It is suggested at the first place that flotation feed fineness should be increased in primary grinding stage. On the other hand, grinding of Cu Rougher Tail stream seems a promising alternative without considering the mechanical aspects. The size of the ball mill originally used for copper regrinding is enough for this duty. After cycloning of Cu Rougher Tail, cyclone underflow can be ground in this mill and cyclone overflow can be fed to existing Cu Rougher Scavenger cells. The concentrate taken can be processed in existing flotation circuit. However, some extra flotation capacity may be needed and stirred ball mill can be used for regrinding purposes where necessary. Tailing of Cu Rougher Scavenger cells would have better liberated sphalerite which would improve the metallurgy in zinc circuit. The data obtained from sampling surveys showed that the tonnages of copper rougher tail were 101.70 and 120.00 tph for Spec and Non-Spec ore respectively at the plant feed of 150 tph. For the maximum tonnage, when the existing regrinding circuit was applied to this stream, circuit performance would be evaluated with simulation techniques. Based on the data obtained from 6 sampling surveys, the models of ball mill and hydrocyclone in the regrinding were fitted by the perfect mixing ball mill and the Whiten efficiency curve model respectively before simulation studies. For doing this, JKSimMet software was used. After having done the simulation, the predicted tonnages and %solids of each stream around the regrinding circuit is given in Figure 6-33. As can be seen from the figure, the tonnage passing through the ball mill is around 65 tph and the tonnage of hydrocyclone cluster is 185 tph. It is suggested that the number of hydrocyclones in the cluster should be increased in order to handle the high tonnage at this stage. Figure 6-34 also shows the measured particle size distribution of original copper rougher tail and the predicted particle size distribution of regrinding circuit product. As can be seen from the graph, 83% of total material is finer than 25 µm in original feed while the amount of material finer than 25 µm in the product is 94%. In addition, the amount of +36 µm material is significantly reduced. This situation leads to liberation of the locked particles at coarser sizes. Hence, it is suggested that the copper recovery should be increased and also the performance of the zinc flotation circuit would be improved.

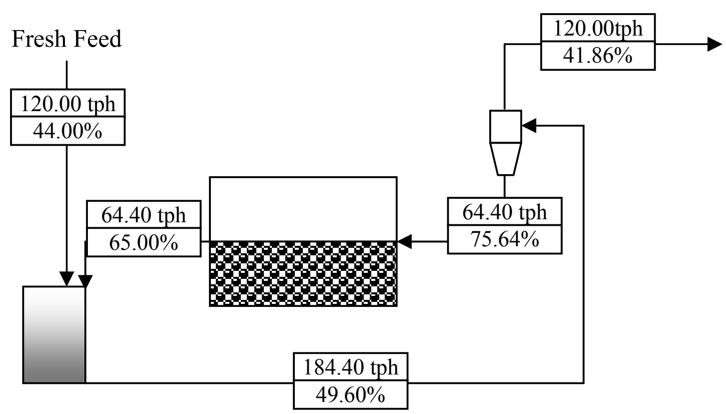

Figure 6-33. Simulated tonnages and %solids of the streams around regrinding circuit

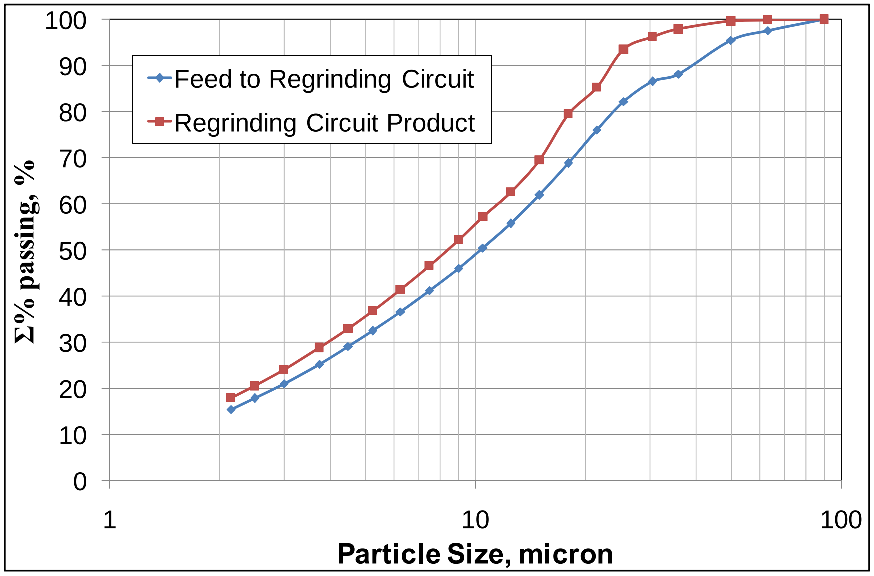

Figure 6-34. Simulated particle size distributions of the streams around regrinding circuit

- The results of the sampling surveys indicated that the particle size distribution of regrind hydrocyclone overflow fluctuated in a wide range depending on feed grade and feed rate. Figure 6-35 shows the coarsest and the finest particle size distribution of regrind hydrocyclone overflow obtained from sampling surveys in comparison with the particle size distributions of several streams in flotation circuit after ground in pilot stirred media mill. As can be seen clearly from the graph, it is possible to get much finer size distributions after comminution of the streams in stirred media mill than the finest regrinding hydrocyclone overflow available.

Cu Rougher concentrate constitutes the main part of the feed to regrind circuit. Pilot stirred ball mill test on this stream showed that open circuit stirred milling provides finer size distribution than hydrocyclone overflow. Table 6-14 shows the comparison between the values P_{95} and P_{80} of the available finest and coarsest regrinding hydrocyclone overflow and the stirred media mill product.

Table 6-14. The comparison between the values P_{95} and P_{80} of the available finest and coarsest regrinding hydrocyclone overflow and the stirred media mill product

	P_{95}	P_{80}
Stirred Media Mill Discharge	22.40	14.40
RG Cyclone Overflow (finest)	24.00	16.45
RG Cyclone Overflow (coarsest)	32.85	21.20

The elimination of coarse size fractions increases the amount of material having optimum flotability and would have positive effect on flotation performance. Overall liberation figures of Cu Rougher concentrate before and after grinding in stirred ball mill are given in Figure 6-36. Although coarser sizes were completely eliminated, the drastic differences in liberation should not be expected.

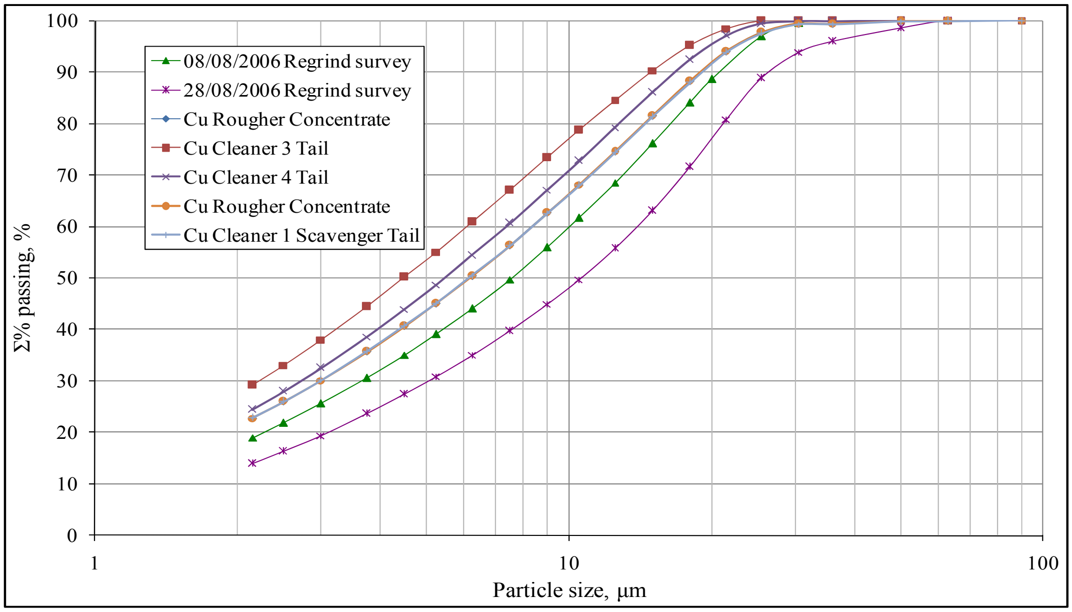

Figure 6-35. The comparison between the coarsest and the finest particle size distribution of regrind hydrocyclone overflow obtained from sampling surveys and the particle size distributions of several streams in flotation circuit after ground in pilot stirred ball mill

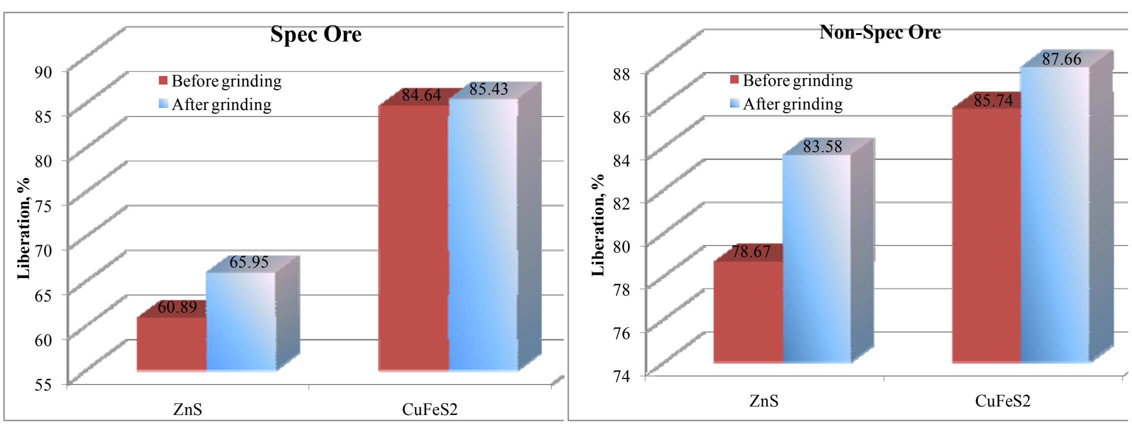

Figure 6-36. Overall liberation figures of Cu Rougher concentrate before and after grinding in stirred media mill

In Table 6-10, when the flotation feed tonnage was increased to 150 tph at the plant, the capacity of regrinding circuit reached to its highest tonnage which was 62.28 tph. In the case that the stream of copper rougher concentrate was ground in the pilot stirred media mill, the specific energy consumption of the mill was measured as 27.88 kWh/t. According to the assumption of energy-size reduction relation (Sepulveda, 1981), the motor power of the stirred media mill should be 1750 kW. In this condition, d_{50} of the product was 6.2 µm. Although the specific energy consumption seems to be high, in order to reach fine sizes the stirred media mills are the best options nowadays. The possible recovery improvement due to the high liberation can compansate the energy consumption in the fine grinding stage. The results shown in Table 6-15 are intended to demonstrate the range in results that can be obtained from different streams in the circuit. Power requirement is very sensitive to grind size and two results for each stream are shown as examples.

Table 6-15. Results from a test program and literature

Grinding Media	Specific Energy kWh/t	F_{80} µm	P_{80} µm
Copper Cleaner 4 Tail			
River Pebble	13.53	18.15	16.15
	25.00		15.20
Steel Ball	28.68		14.70
	60.60		12.75
Zinc Column Scavenger Concentrate			
Steel Ball	2.26	65.16	50.94
	13.09		32.07
Pyrite (Murphy et al., 2004)			
Ceramic	11.00	18.00	14.00
	34.00		11.00

- Overall liberation figures of the streams in zinc circuit indicated that the most suitable stream for regrinding is the tail of zinc column stage. At current situation, zinc column tail is fed to scavenger stage and tail of scavenger stage is sent to final tail. However, Zn Column Scavenger tail has very high metal content and bears the significant amount of locked particles. Concentrate of this stage which is recirculated to column stage contains considerable amount of locked particle as well. The tonnages of this stream for Non-Spec and Spec ore were 33.30 and 10.50 tph respectively. The amount of +36 µm material in this stream was around 13-19%. In addition, +36 µm material contained 20.5 % of zinc in this stream for Non-Spec ore while this value increased to 35.1% for Spec ore. In case that Zn Column Tail is ground finer in stirred ball mill, these locked particles could be liberated and this situation could reduce metal loss to final tail through Zn Column Scavenger tail and improve flotation at column stage.

7. CONCLUSIONS AND RECOMMENDATIONS

- In laboratory stirred milling tests, the results showed that there is preferential elimination of coarse size fractions in the mill and the major operating parameter is the impeller speed. An empirical model was developed to correlate product size with the operating variables (Section 5.1) . The results also suggested that the stirred media mills should be operated at highest possible impeller speed, ball charge and %solid with small balls in order to obtain finest product with acceptable capacity.

- The results of the pilot scale tests verified the findings obtained from laboratory scale tests. The major operating parameter affecting the power draw and product fineness was the impeller speed of the mill. The density of grinding media and the media load had also significant effect on power draw. It was found that it is possible to obtain finer products which are below the grinding limit of ball mill.

- Perfect mixing mill model was successfully applied to the pilot scale stirred mill data obtained from various streams in ÇBİ's flotation plant. The results of modelling studies indicated that r/d* values can be normalized with power draw of the mill which enables to predict the product size distribution for any size mill.

- Regarding to the regrinding requirements in ÇBİ flotation plant, the following conclusions were drawn:

  Six surveys carried out at the ÇBİ copper regrinding circuit showed that Cu regrinding circuit was operating at varying conditions due to changes in fresh feed tonnage and grade and ore type.

.

  Circulating load was found to be very low indicating possibility of increasing energy efficiency. However, the capacity of existing cyclone feed sump should be increased. This was also found to be necessary to avoid fluctuations in cyclone feeding.

  Locked particles at coarse sizes constituted the main reason of metal loss at the flotation plant. High metal loss at coarse fractions was occured because the desired fineness was not achieved in primary grinding due to the high flowrate.

In copper flotation circuit, tailing of rougher scavenger tailing was found to be responsible for the main losses particularly due to the locked particles at coarser sizes. At the same time, most of the cells were idle during the surveys. Therefore, grinding of copper rougher tailing in the existing regrinding circuit and then feed it to scavenger cells would improve the recovery. Regrinding requirement should be evaluated after implementation of these modifications. This modification would also improve the liberation of zinc flotation feed.

In zinc flotation circuit, column tail seemed the most promising stream for regrinding in the existing circuit. This application would improve the liberation in the column scavenger cells and may reduce the losses through scavenger tails.

- Although stirred mill was found to be performing very good, it is hard to predict the effects on flotation using only liberation data. Therefore, parallel flotation tests should be conducted for the investigation of chemical conditions of flotation and the type of grinding media used in stirred ball mill.

- For a particular plant, the performance of stirred milling could be predicted after making a testwork with a mill acoupled with a torquemeter. To generalize the relations obtained in this study, the effect of grindability should be quantified. Detailed experimental studies to develop a method to characterize the grindability of fine material is suggested.

REFERENCES

Austin, L.G., Klimpel, R.R. and Luckie, P.T., 1984, Process engineering of size reduction: Ball milling, SME, New York, 561p.

Baker, J.C., Barley, R.W., Williams, R.A., Clarke, A.J., Kostuch, J. and Parker, D.J., 1999, Investigation and model validation of media motion in a vertical stirred mill using positron emission particle tracking, 1st World Congress on Industrial Process Tomography, Buxton, Greater Manchester, April 14-17, 1999, pp.244-248.

Baker, J.C., Barley, R.W., Williams, R.A., Jia, X., Kostuch, J., McLoughlin, B. and Parker, D.J., 2002, Measurement of the motion of grinding media in a vertically stirred mill using positron emission particle tracking (PEPT), Minerals Engineering, 15, pp.53-59.

Belaroui, K., Pons, M.N., Vivier, H. and Meijer, M., 1999, Wet grinding of gibbsite in a bead mill, Powder Technology, 105, 369-405.

Bel-Fadhel, H. and Frances, C., 2001, Wet batch grinding of alumina hydrate in a stirred bead mill, Powder Technology, 119, 257-268.

Bel-Fadhel, H., Frances, C. ve Mamourian, A., 1999, Investigations on ultra-fine grinding of titanium dioxide in a stirred media mill, Powder Technology, 105, 362-373.

Bernhardt, C., Reinsch, E. and Husemann, K., 1999, The influence of suspension properties on ultra-fine grinding in stirred ball mills, Powder Technology, 105, 357-361.

Berthiaux, H., Varinot, C. and Dodds, J., 1996, Approximate calculation of breakage parameters from batch grinding tests, Chemical Engineering Science, vol.51, no.19, pp.4509-4516.

Blecher, L. and Schwedes, J., 1996, Energy distribution and particle trajectories in a grinding chamber of a stirred ball mill, Int. J. of Miner. Proc., 44-45, 617-627.

Blecher, L., Kwade, A. and Schwedes, J., 1996, Motion and stress intensity of grinding beads in a stirred media mill. Part 1: Energy density distribution and motion of single grinding beads, Powder Technology, 86, 59-68.

Clark, L.W. and Burford, B.D., 2004, Fine grinding and project enhancement, Innovative Mineral Development Symposium, October 6, Sydney, Australia.

CoBall® Brochure, frymakoruma.com/kcms/lib/download.php?id=1184232652681567&forcedownload=yes –

Curry, D.C. and Clermont, B., 2005, Improving the efficiency of fine grinding – Developments in ceramic media technology, Randol Conference, August 21-24, Perth, Australia.

Davies, E.G., Collins, E.W. and Feld, I.L., 1973, Large scale continuous attrition grinding of coarse kaolin, USBM R.I. 7771.

Davies, E.G., Hansen, J.P. and Sullivan, G.V., 1980, Attrition micro grinding, Proceedings of the International Symposium on Fine Particle Technology, AIME, Las Vegas, Nevada, February 24-28.

Dürr, H.M., 2002, "Maxxmill® - The Alternative to the drum mill", 10th European Symposium on Comminution, 2-5 September, Heidelberg, Germany.

Feld, I.L., Mcvay, T.N., Gilmore, H.L. and Clemmons, B.H., 1960, Paper coating clay from coarse Georgia kaloin by a new attrition grinding process, USBM R.I. 5697.

Gao, M., Young, M.F., Cronin, B. and Harbort, G., 2000, Isamill medium competency and its effect on milling performance, SME Annual Meeting, Feb. 28-March 1, Slat Lake City, Utah.

Gao, M.W. and Forssberg, E., 1993, A study on the effect of parameters in stirred ball milling, Int. J. of Miner. Proc., 37, 45-59.

Graves, G.A. and Boehem, T., 2007, Mill media considerations for high energy mills, Minerals Engineering, 20, pp.342-347.

Harbort, G., Murphy, M.F., Vargas, A. and Young, M., 1999, The introduction of the IsaMill for ultra-fine grinding in the Mt. Isa Lead/Zinc concentrator, Extemin99, September, Arequipa, Peru.

He, M. and Forssberg, E., 2007, Influence of slurry rheology on stirred media milling of quartzite, Int. J. Mineral Processing, 84, pp.240-251.

He, M., Wang, Y. and Forssberg, E., 2006, Parameter effects on wet ultrafine grinding of limestone through slurry rheology in a stirred media mill, Powder Technology, 161, pp.10-21.

Heim, A. and Leszczyniecki, R., 1985, A study on grinding and energy input in a vertical multi-disk batch pearl mill, Aufbereitung Technik, 10, pp.594-604.

Herbst, J.A. and Sepulveda, J.L., 1978, Fundamentals of fine and ultrafine grinding in a stirred ball mill, Proc. Int. Conf. Powder Bulk Handling Process., Rosemont Ill, Ind. Sci. Conf. Management, Chicago, pp.452-470.

Hively E.E., Jones S.M. Jr., 1983. Ultrafine Grinding in a Tower Mill, SME-AIME Annual Meeting Atlanta, Georgia, March 6-10.

Jankovic, A. and Morrell, S., 1998, Modelling of Stirred Mills, AMIRA Project P336A.

Jankovic, A. and Valery Jnr. W. (2005). Fine and Ultra fine grinding – the facts and myths, presented at the 6th Annual I.I.R. Crushing and Grinding Conference, Perth, Australia. 29-30 March 2004.

Jankovic, A., 2001, Media stress intensity analysis for vertical stirred mills, Minerals Engineering, 14, (10), 1177-1186.

Jankovic, A., 2003, Variables affecting the fine grinding of minerals using stirred mills, Minerals Engineering, 16, 337-345.

Kapur, P. and Agrawal, P.K., 1970, Approximate solutions to the discretized batch grinding equations, Chemical Engineering Science, 25, pp.1111-1113.

Kapur, P.C., Healy T.W., Scales, P.J., Boger, D.V. and Wilson, D., 1996, Role of dispersants in kinetics and energitics of stirred ball mill grinding, Int. J. of Miner. Proc., 47, 141-152.

Klimpel, R.R., 1999, The selection of wet grinding chemical additives based on slurry rheology control, Powder Technology, vol.105, Issues 1-3, pp.430-435.

Koka, V.R. and Trass, O., 1985, "Analysis of the Kinetics of Coal Breakage by Wet Grinding in the Szego Mill", Powder Technology, 43, pp.287-294.

Kwade, A. and Schwedes, J., 2002, Breaking characteristics of different materials and their effect on stress intensity and stress number in stirred media mills, Powder Technology, 122, 109-121.

Kwade, A., 1999 (a), Wet comminution in stirred media mills – Research and its practical application, Powder Technology, 105, 14-20.

Kwade, A., 1999 (b), Determination of the most important grinding mechanism in stirred media mills by calculating stress intensity and stress number, Powder Technology, 105, 382-388.

Kwade, A., 2004, Mill selection and process optimization using a physical grinding model, Int. J. Mineral Processing, 74S, pp.93-101.

Kwade, A., Blecher, L. and Schwedes, J., 1996, Motion and stress intensity of grinding beads in a stirred media mill. Part 2: Stress intensity and its effect on comminution, Powder Technology, 86, 69-76.

Lane, G., 1999, CFD modelling of a stirred bead mill for fine grinding, 2nd International Conference on CFD in the Minerals and Process Industries, CSIRO, Melbourne, Australia, 6-8 December, 449-454.

Mankosa, M.J., Adel, G.T. and Yoon, R.H., 1986, Effect of media size in stirred ball mill grinding of coal, Powder Technology, 49, 75-82.

Mankosa, M.J., Adel, G.T. and Yoon, R.H., 1989, Effect of operating parameters in stirred ball mill grinding of coal, Powder Technology, 59, 255-260.

Nesset, J.E., Radziszewski, P., Hardie, C. and Leroux, D.P., 2006, Assessing the performance and efficiency of fine grinding technologies, 38th Annual Meeting of the Canadian Mineral Processors, Jan. 17-19, Ottowa, Canada, pp.283-309.

Orumwense, O.A., 1992, Kinetics of fine grinding in an annular ball mill, Powder Technology, 73, pp.101-108.

Pease, J.D., Curry, D.C., Barns, K.E., Young, M.F. and Rule, C., 2006, Transforming flowsheet desing with inert grinding – the IsaMill, CMP 2006.

Pease, J.D., Young, M.F. and Curry, D.C., 2004, Fine grinding as enabling technology – The IsaMill, Sixth Annual Crushing and Grinding Conference, March 24-30, Perth, Australia.

Persson, H. ve Forssberg, E., 1994, Fine grinding of a magnetite ore with a stirred ball mill, Aufbereitung-Technik, 35, (6), 307-319.

Rao, B.V. and Datta, A., 2006, Analysis of non-linear batch grinding in stirred media mills using self-similarity solution, Powder Technology, 169, pp.41-48.

Schulz, N.F., 1970, Separation Efficiency, AIME Transactions, Vol 247, 81-87.

Sepulveda, J.L., 1981, A detailed study on stirred ball mill grinding, PhD Desertation, Department of Metallurgy and Metallurgical Engineering, The University of Utah.

Shinohara, K., Golman, B., Uchiyama, T. and Otani, M., 1999, Fine grinding characteristics of hard materials by attrition mill, Powder Technology, 103, pp.292-296.

Sinnott, M., Cleary, P:W. and Morrison, R., 2006(a), Analysis of stirred mill performance using DEM simulation: Part 1 – Media motion, energy consumption and collisional environment, Minerals Engineering, vol.19, no.15, pp.1537-1550.

Sinnott, M., Cleary, P:W. and Morrison, R., 2006(b), Analysis of stirred mill performance using DEM simulation: Part 2 – Coherent flow structures, linear stress and wear, mixing and transport, Minerals Engineering, vol.19, no.15, pp.1551-1572.

SMD® Brochure, http://www.metsominerals.com/inetMinerals/MaTobox7.nsf/DocsByID/53B338EE821BF913C1256C5A002E37C1/$File/Stirred_Media_Detritor_EN.pdf

Stanczyk, M.H. and Feld, I:L., 1963, Continuous attrition grinding of coarse kaolin. Part 1 – Open circuit tests, USBM R.I. 6327.

Stanczyk, M.H. and Feld, I:L., 1965, Continuous attrition grinding of coarse kaolin. Part 2 – Closed circuit tests, USBM R.I. 6694.

Stanczyk, M.H. and Feld, I:L., 1968, Investigation of operating variables in the attrition grinding process, USBM R.I. 7168.

Stehr, N., Mehta, R.K. and Herbst, J.A., 1987, Comparison of energy requirements for conventional and stirred ball milling of coal-water slurries, Coal Preperation, 4, pp.209.

Szegvari, A., 1956, Treatment of liquid systems and apparatus, U.S. Patent 2764359, Sept. 25.

Szegvari, A., 1961, Ball containing apparatus for finely grinding liquid suspended particles, U.S. Patent 3008657, Nov.14.

Szegvari, A., 1964(a), Method of an apparatus for grinding a solid in a liquid, U.S. Patent 3131875, May 5.

Szegvari, A., 1964(b), Continuous process of grinding particulate material, U.S. Patent 3149789, Sept. 22.

Szegvari, A., 1969, Agitator, U.S. Patent 3450356, June 17.

Theuerkauf, J. and Schwedes, J., 1999, Theoretical and experimental investigation on particle and fluid motion in stirred media mills, Powder Technology, 105, 406-412.

Tüzün, M.A., 1994, A study of comminution in a vertical stirred ball mill, PhD Desertation, Chemical Engineering Department, University of Natal.

Tüzün, M.A., Loveday, B.K. and Hinde, A.L., 1995, Effect of pin tip velocity, ball density and ball size on grinding kinetics in a stirred ball mill, Int. J. Mineral Processing, 43, pp.179-191.

Varinot, C., Berthiaux, H. and Dodds, J., 1999, Prediction of the product size distribution in associations of stirred bead mills, Powder Technology, 105, pp.228-236.

Varinot, C., Hiltgun, S., Pons, M.N. and Dodds, J., 1997, Identification of the fragmentation mechanisms in wet phase fine grinding in a stirred bead mill, Chemical Engineering Science, vol.52, no.20, pp.3605-3612.

VertiMill®Brochure, http://www.metsominerals.com/inetMinerals/MaTobox7.nsf/DocsByID/318FF33277D44D6CC1256DC800500D46/$File/Vertimill.pdf

Wang, Y. and Forssberg, E., 2000, Product size distribution in stirred media mills, Minerals Engineering, vol.13, no.4, pp.459-465.

Wang, Y., Forssberg, E. and Sachweh, J., 2004, Dry fine comminution in a stirred media mill - MaxxMill®, Int. J. Mineral Processing, 74S, pp.65-74.

Weller, K.R., Gao, M., Bowen, P., 1999, Scaling-up horizontal stirred mills from a 4-litre test mill to a 4000-litre IsaMill; Powder Technology Symposium, Pennsylvania State University, PA, USA.

Woodburn, E.T. and Skentzos, A.K., 1987, The investigation of the kinetics of breakage as a first step towards the assesment of the economics of ultra fine grinding of a British low rank, Powder Technology, 53, pp.137-143.

Young, J.D. and Gao, M., 2000, Performance of the IsaMills in the George Fisher flowsheet, Seventh Mill Operators' Conference, October 12-14, Kalgoorlie, Australia.

Yue, J. and Klein, B., 2004, Influence of rheology on the performance of horizontal stirred mills, Minerals Engineering, vol.17, Issues 11-12, pp.1169-1177.

Yue, J. and Klein, B., 2005, Particle breakage kinetics in horizontal stirred mills, Minerals Engineering, 18, pp. 325-331.

Zheng, J., 1997, Stirred Media Mills: Dynamics, performance and physico-chemical aspects, PhD desertation, Colombia University.

Zheng, J., Harris, C.C. and Somasundaran, P., 1996, A study on grinding and energy input in stirred media mills, Powder Technology, 86, 171-178.

Zheng, J., Harris, C.C. and Somasundaran, P., 1997, The effect of additives on stirred media milling of limestone, Powder Technology, 91, 173-179.

8. APPENDICES

8.1. Appendix 1

Particle size distributions of the laboratory and pilot scale tests carried out in this study are tabulated below.

Particle Size Distributions of Products from the Tests Carried Out at Hacettepe University

		Experiment 1					**Experiment 2**					**Experiment 3**				
Size (μm)	Feed	0.5 min	1 min	2 min	3 min	5 min	0.5 min	1 min	2 min	3 min	5 min	0.5 min	1 min	2 min	3 min	5 min
300	100.00	100.00	100.00	100.00	100.00	100.00	100.00	100.00	100.00	100.00	100.00	100.00	100.00	100.00	100.00	100.00
212	99.22	99.96	99.98	99.99	100.00	100.00	99.98	99.98	99.99	100.00	100.00	99.97	99.98	100.00	100.00	100.00
150	98.89	99.93	99.94	99.97	99.99	100.00	99.94	99.96	99.97	99.98	99.99	99.94	99.94	99.97	100.00	100.00
106	98.50	99.88	99.92	99.95	99.97	99.99	99.87	99.90	99.94	99.95	99.97	99.87	99.91	99.94	99.96	100.00
75	97.32	99.76	99.91	99.94	99.96	99.98	99.79	99.85	99.91	99.93	99.95	99.80	99.84	99.88	99.92	99.95
53	93.32	99.62	99.88	99.92	99.95	99.97	99.54	99.69	99.83	99.89	99.94	99.71	99.80	99.84	99.88	99.92
38	77.37	99.15	99.82	99.89	99.93	99.95	97.37	97.85	99.38	99.67	99.88	98.97	99.56	99.69	99.77	99.85
21.5	42.03	95.65	99.49	99.64	99.78	99.89	65.97	68.97	85.08	93.61	97.97	77.60	88.76	97.90	99.26	99.48
15	28.25	82.52	94.82	96.90	97.8	98.7	45.98	48.07	65.50	79.02	87.48	57.05	68.84	87.46	92.55	96.27
10.5	20.67	66.14	82.40	89.18	93.52	96.8	32.55	33.37	47.21	61.17	70.69	41.80	50.53	70.66	79.18	87.9
7.5	15.96	51.36	67.10	79.39	87.4	94.24	23.95	24.08	34.15	45.81	54.43	31.55	37.09	54.16	63.16	75.3
5.25	12.12	37.77	50.52	64.92	75.64	88.6	17.14	17.32	24.09	32.81	39.38	23.38	26.50	38.88	46.33	58.42
3	7.44	21.56	29.03	40.93	51.79	67.4	9.62	9.87	13.48	18.58	21.94	14.15	15.06	21.49	26.09	34.57

	Experiment 4				**Experiment 5**					**Experiment 6**				
Size (μm)	0.5 min	1 min	2 min	3 min	0.5 min	1 min	2 min	3 min	5 min	0.5 min	1 min	2 min	3 min	5 min
300	100.00	100.00	100	100	100.00	100	100.00	100.00	100.00	100.00	100.00	100.00	100.00	100.00
212	100.00	100.00	100	100	99.95	99.97	100.00	100.00	100.00	99.97	99.98	99.99	99.99	100.00
150	100.00	100.00	100	100	99.91	99.94	100.00	100.00	100.00	99.93	99.94	99.96	99.98	100.00
106	100.00	100.00	100	100	99.83	99.88	100.00	100.00	100.00	99.87	99.89	99.94	99.96	100.00
75	99.79	100.00	100	100	99.76	99.8	100.00	100.00	100.00	99.71	99.77	99.87	99.92	100.00
53	98.77	99.59	100	100	99.70	99.75	100.00	100.00	100.00	97.05	99.57	99.79	99.88	100.00
38	96.62	98.57	100	100	99.56	99.65	99.91	99.97	100.00	89.70	98.52	99.62	99.78	99.98
21.5	85.28	94.02	100	100	96.25	97.45	99.29	99.64	99.91	58.38	77.91	90.47	96.31	98.19
15	71.51	86.56	98.24	98.66	83.51	88.6	98.14	99.27	99.78	40.55	56.84	70.98	83.89	92.05
10.5	55.89	73.19	92.07	94.92	67.18	74.86	94.19	97.99	99	28.60	40.40	51.79	66.05	79.04
7.5	42.71	58.25	81.18	87.52	52.42	61.5	85.97	91.85	95.4	20.76	29.18	37.37	49.71	63.04
5.25	30.69	42.90	66.02	75.21	38.94	46.52	71.86	79.00	86.34	14.84	20.61	26.12	35.50	46.39

	Experiment 7					Experiment 8					Experiment 9			
Size (µm)	0.5 min	1 min	2 min	3 min	5 min	0.5 min	1 min	2 min	3 min	5 min	1 min	2 min	3 min	5 min
300	100.00	100.00	100.00	100.00	100.00	100.00	100.00	100.00	100.00	100.00	100.00	100.00	100.00	100.00
212	99.98	100.00	100.00	100.00	100.00	99.97	100.00	100.00	100.00	100.00	100.00	100.00	100.00	100.00
150	99.95	99.97	100.00	100.00	100.00	99.94	99.95	99.96	99.97	100.00	100.00	100.00	100.00	100.00
106	99.91	99.93	100.00	100.00	100.00	99.87	99.88	99.90	99.92	99.94	100.00	100.00	100.00	100.00
75	99.87	99.91	99.95	100.00	100.00	99.61	99.82	99.85	99.88	99.91	99.97	100.00	100.00	100.00
53	99.84	99.89	99.92	99.95	100.00	96.05	99.70	99.74	99.82	99.87	99.26	99.89	99.97	100.00
38	99.76	99.85	99.90	99.93	99.96	87.67	99.22	99.51	99.70	99.79	96.63	99.55	99.75	100.00
21.5	81.74	89.40	97.71	98.85	99.61	55.70	76.12	84.90	92.50	98.11	80.97	98.16	98.72	99.02
15	59.86	70.50	87.98	92.18	96.45	38.09	53.52	66.89	75.84	88.41	63.94	88.38	93.55	93.89
10.5	43.29	49.77	70.78	77.75	85.53	27.11	37.29	48.67	56.97	73.10	46.83	73.1	82.43	83.74
7.5	32.06	36.22	54.59	62.88	74.56	20.12	26.91	34.98	41.74	56.49	34.42	56.51	66.31	70.05
5.25	23.23	25.56	39.28	46.70	58.81	14.53	18.90	24.52	29.22	40.51	24.68	40.51	48.74	53.09
3	13.55	14.24	21.74	26.86	34.86	8.27	10.46	13.62	15.87	22.50	14.38	22.35	27.78	29.78

	Experiment 10					Experiment 11					Experiment 12				
Size (µm)	0.5 min	1 min	2 min	3 min	5 min	0.5 min	1 min	2 min	3 min	5 min	0.5 min	1 min	2 min	3 min	5 min
300	100.00	100.00	100.00	100.00	100.00	100.00	100.00	100.00	100.00	100.00	100.00	100.00	100.00	100.00	100.00
212	99.96	99.98	100.00	100.00	100.00	100.00	100.00	100.00	100.00	100.00	100.00	100.00	100.00	100.00	100.00
150	99.88	99.90	99.93	99.95	100.00	100.00	100.00	100.00	100.00	100.00	99.72	100.00	100.00	100.00	100.00
106	99.66	99.71	99.78	99.89	99.96	100.00	100.00	100.00	100.00	100.00	98.69	100.00	100.00	100.00	100.00
75	99.49	99.65	99.72	99.81	99.93	99.04	99.68	100.00	100.00	100.00	97.25	99.79	99.87	99.96	100.00
53	99.16	99.49	99.64	99.75	99.88	95.32	98.22	99.54	99.8	99.97	92.62	97.87	98.55	99.24	99.63
38	96.21	98.84	99.34	99.60	99.73	86.20	93.68	97.81	98.54	99.01	81.23	91.49	95	97.2	98.46
21.5	72.14	87.99	96.73	97.07	97.54	57.32	71.59	84.74	90.79	95.62	49.95	65.82	84.5	89.4	93.88
15	55.29	72.95	90.41	93.06	94.85	40.91	54.10	68.79	79.39	90.25	35.21	48.97	68.56	77.2	85.56
10.5	41.63	57.24	77.18	83.46	88.94	29.36	39.13	52.48	63.57	78.41	25.95	36.46	52.05	61.75	71.09
7.5	30.77	43.25	62.23	69.99	79.03	21.74	28.59	39.53	48.86	62.86	20.24	28.31	40.46	48.54	56.88
5.25	21.49	30.75	46.84	53.74	64.22	15.58	20.05	28.65	35.86	46.53	15.43	21.30	30.88	36.71	43.56
3	11.53	16.88	27.45	31.68	39.94	8.66	10.87	16.56	20.78	26.12	9.51	12.84	19.01	22.37	27.18

	Experiment 13					Experiment 14					Experiment 15				
Size (μm)	0.5 min	1 min	2 min	3 min	5 min	0.5 min	1 min	2 min	3 min	5 min	0.5 min	1 min	2 min	3 min	5 min
300	100.00	100.00	100.00	100.00	100.00	100.00	100.00	100.00	100.00	100.00	100,00	100,00	100,00	100,00	100,00
212	99.99	100.00	100.00	100.00	100.00	100.00	100.00	100.00	100.00	100.00	100,00	100,00	100,00	100,00	100,00
150	99.94	99.95	99.95	100.00	100.00	100.00	100.00	100.00	100.00	100.00	100,00	100,00	100,00	100,00	100,00
106	99.83	99.85	99.86	99.97	100.00	100.00	100.00	100.00	100.00	100.00	100,00	100,00	100,00	100,00	100,00
75	99.71	99.75	99.79	99.86	99.97	99.70	99.84	99.98	100.00	100.00	99,97	99,98	100,00	100,00	100,00
53	99.52	99.60	99.68	99.82	99.91	97.26	99.10	99.75	100.00	100.00	98,94	99,51	99,94	100,00	100,00
38	98.39	98.75	99.40	99.69	99.84	90.29	97.45	99.34	100.00	100.00	92,87	96,06	98,82	99,41	100,00
21.5	74.62	78.05	95.88	98.05	98.95	63.06	78.00	96.92	99.17	99.80	66,87	74,09	94,36	96,00	99,55
15	53.77	57.96	81.30	88.46	95.60	45.44	61.83	84.80	92.93	97.78	49,29	57,65	81,05	83,52	95,23
10.5	38.83	42.17	62.60	72.35	85.69	32.02	47.44	68.20	79.34	90.04	36,83	43,85	64,27	69,35	84,58
7.5	28.71	30.74	46.83	55.48	70.63	23.16	35.62	52.83	63.82	76.58	28,81	34,08	49,82	55,67	71,01
5.25	20.56	21.75	33.52	39.77	52.95	16.08	25.23	38.55	47.29	58.33	22,13	26,07	37,26	43,04	56,12
3	11.57	12.19	18.80	22.11	29.99	8.50	13.64	21.63	26.62	32.73	13,56	16,25	22,38	27,15	35,41

	Experiment 16					Experiment 17					Experiment 18				
Size (μm)	0.5 min	1 min	2 min	3 min	5 min	0.5 min	1 min	2 min	3 min	5 min	0.5 min	1 min	2 min	3 min	5 min
300	100,00	100,00	100,00	100,00	100,00	100,00	100,00	100,00	100,00	100,00	100,00	100,00	100,00	100,00	100,00
212	100,00	100,00	100,00	100,00	100,00	100,00	100,00	100,00	100,00	100,00	100,00	100,00	100,00	100,00	100,00
150	100,00	100,00	100,00	100,00	100,00	100,00	100,00	100,00	100,00	100,00	100,00	100,00	100,00	100,00	100,00
106	100,00	100,00	100,00	100,00	100,00	100,00	100,00	100,00	100,00	100,00	100,00	100,00	100,00	100,00	100,00
75	100,00	100,00	100,00	100,00	100,00	100,00	100,00	100,00	100,00	100,00	100,00	99,99	100,00	100,00	100,00
53	100,00	100,00	100,00	100,00	100,00	99,61	99,83	100,00	99,97	100,00	99,20	99,73	100,00	99,99	100,00
38	97,57	99,00	99,99	100,00	100,00	97,93	99,14	99,87	99,77	99,95	95,72	97,71	99,81	99,90	100,00
21.5	79,32	88,55	98,49	100,00	100,00	89,70	94,71	97,92	98,70	99,31	76,55	86,01	95,48	98,04	99,99
15	62,02	74,39	91,79	97,00	98,35	76,07	86,56	93,93	96,87	97,92	60,25	71,91	87,54	93,88	99,11
10.5	47,41	58,82	78,93	91,08	93,67	60,41	73,09	85,19	92,00	95,36	46,53	56,48	75,31	84,53	94,72
7.5	37,11	46,20	64,71	77,17	85,41	47,48	59,21	73,20	83,51	90,64	36,77	44,15	62,57	72,24	86,54
5.25	28,71	35,60	50,39	60,32	72,72	36,57	45,96	58,93	70,74	81,78	28,73	33,96	49,67	58,20	73,63
3	18,24	22,65	31,52	36,58	48,92	23,22	28,86	37,62	47,34	59,68	18,46	21,58	31,85	37,51	49,23

	Experiment 19					Experiment 20					Experiment 21				
Size (µm)	0.5 min	1 min	2 min	3 min	5 min	0.5 min	1 min	2 min	3 min	5 min	0.5 min	1 min	2 min	3 min	5 min
300	100,00	100,00	100,00	100,00	100,00	100,00	100,00	100,00	100,00	100,00	100,00	100,00	100,00	100,00	100,00
212	100,00	100,00	100,00	100,00	100,00	100,00	100,00	100,00	100,00	100,00	100,00	100,00	100,00	100,00	100,00
150	100,00	100,00	100,00	100,00	100,00	100,00	100,00	100,00	100,00	100,00	100,00	100,00	100,00	100,00	100,00
106	100,00	100,00	100,00	100,00	100,00	100,00	100,00	100,00	100,00	100,00	100,00	100,00	100,00	100,00	100,00
75	99,95	100,00	100,00	100,00	100,00	99,87	100,00	100,00	100,00	100,00	99,98	100,00	100,00	100,00	100,00
53	99,41	99,83	100,00	100,00	100,00	99,04	99,80	100,00	100,00	100,00	99,56	99,84	99,97	100,00	100,00
38	96,74	99,10	99,81	99,87	100,00	96,92	99,07	99,94	99,98	100,00	95,54	98,27	99,44	99,76	100,00
21.5	79,80	91,14	97,57	98,65	98,99	84,55	94,23	99,76	99,86	99,96	74,24	87,80	96,20	98,38	99,73
15	63,16	78,69	92,69	96,19	97,39	70,22	85,18	97,48	98,70	99,27	56,49	72,85	87,85	94,59	98,21
10.5	48,62	63,86	83,55	90,40	94,59	55,65	72,18	90,74	94,30	97,05	42,52	56,90	74,05	85,50	93,95
7.5	38,14	51,04	72,41	81,77	90,31	44,07	59,48	80,31	85,16	94,04	33,10	44,72	60,32	73,34	85,85
5.25	29,24	39,61	59,59	69,67	82,11	33,93	47,24	66,64	74,35	87,04	25,62	34,90	47,69	59,33	73,02
3	17,99	25,07	39,51	47,33	60,35	21,05	30,59	44,16	51,82	65,73	16,36	22,69	31,24	38,42	48,95

	Experiment 22					Experiment 23					Experiment 24				
Size (µm)	0.5 min	1 min	2 min	3 min	5 min	0.5 min	1 min	2 min	3 min	5 min	0.5 min	1 min	2 min	3 min	5 min
300	100,00	100,00	100,00	100,00	100,00	100,00	100,00	100,00	100,00	100,00	100,00	100,00	100,00	100,00	100,00
212	100,00	100,00	100,00	100,00	100,00	100,00	100,00	100,00	100,00	100,00	100,00	100,00	100,00	100,00	100,00
150	100,00	100,00	100,00	100,00	100,00	100,00	100,00	100,00	100,00	100,00	100,00	100,00	100,00	100,00	100,00
106	100,00	100,00	100,00	100,00	100,00	100,00	100,00	100,00	100,00	100,00	100,00	100,00	100,00	100,00	100,00
75	99,48	99,95	100,00	100,00	100,00	99,99	100,00	100,00	100,00	100,00	100,00	100,00	100,00	100,00	100,00
53	98,55	99,43	99,64	100,00	100,00	99,40	99,96	100,00	100,00	100,00	99,40	99,86	99,96	100,00	100,00
38	93,42	97,18	99,02	99,79	99,96	96,73	99,40	99,89	100,00	100,00	96,36	99,02	99,69	99,97	100,00
21.5	69,55	80,84	92,20	97,61	99,00	79,68	91,90	97,98	99,38	99,58	78,78	92,27	97,61	97,91	99,75
15	52,30	64,45	80,32	89,88	95,69	62,71	79,33	92,47	96,55	98,68	61,39	81,03	92,75	95,61	99,15
10.5	39,81	50,40	64,84	76,28	87,50	47,88	63,82	81,33	89,41	96,00	46,39	66,54	82,89	89,46	96,93
7.5	31,66	40,68	52,42	63,04	76,31	37,24	50,57	68,36	78,73	90,15	36,09	53,79	70,82	79,79	92,35
5.25	24,96	32,64	42,20	51,25	63,32	28,66	39,35	54,95	64,93	79,57	27,82	42,50	57,41	66,49	83,06
3	16,13	21,67	28,65	35,21	42,80	18,15	25,47	36,07	42,54	56,26	17,52	27,74	37,49	43,77	59,95

	Experiment 25					Experiment 26					Experiment 27				
Size (μm)	0.5 min	1 min	2 min	3 min	5 min	0.5 min	1 min	2 min	3 min	5 min	0.5 min	1 min	2 min	3 min	5 min
300	100,00	100,00	100,00	100,00	100,00	100,00	100,00	100,00	100,00	100,00	100,00	100,00	100,00	100,00	100,00
212	100,00	100,00	100,00	100,00	100,00	100,00	100,00	100,00	100,00	100,00	100,00	100,00	100,00	100,00	100,00
150	100,00	100,00	100,00	100,00	100,00	100,00	100,00	100,00	100,00	100,00	100,00	100,00	100,00	100,00	100,00
106	100,00	100,00	100,00	100,00	100,00	100,00	100,00	100,00	100,00	100,00	100,00	100,00	100,00	100,00	100,00
75	100,00	100,00	100,00	100,00	100,00	99,82	100,00	100,00	100,00	100,00	99,93	100,00	100,00	100,00	100,00
53	99,97	100,00	100,00	100,00	100,00	99,42	99,97	100,00	100,00	100,00	99,45	99,99	100,00	100,00	100,00
38	99,44	99,94	100,00	100,00	100,00	98,12	99,73	99,96	100,00	100,00	98,28	99,76	99,98	100,00	100,00
21.5	90,98	97,25	99,43	99,76	100,00	86,88	96,64	99,06	99,84	99,95	88,11	97,06	99,25	99,83	99,96
15	78,50	91,62	97,40	98,77	99,29	72,38	88,36	96,05	98,53	99,10	73,92	89,90	96,61	98,79	98,95
10.5	63,76	82,17	92,78	96,30	97,41	56,92	74,26	87,87	94,28	96,89	58,08	77,33	89,45	94,97	97,21
7.5	51,04	71,25	85,64	92,03	94,93	44,77	60,09	76,05	86,26	93,28	45,45	64,09	78,84	87,64	93,99
5.25	39,77	59,00	74,58	83,78	89,86	34,88	47,25	61,83	73,74	85,34	35,13	51,17	65,37	75,88	87,03
3	25,31	39,69	51,97	61,90	70,78	22,72	30,92	40,18	49,90	63,14	22,60	33,48	43,34	52,47	65,90

	Experiment 28				
Size (μm)	0.5 min	1 min	2 min	3 min	5 min
300	100,00	100,00	100,00	100,00	100,00
212	100,00	100,00	100,00	100,00	100,00
150	100,00	100,00	100,00	100,00	100,00
106	99,99	100,00	100,00	100,00	100,00
75	99,75	99,83	100,00	100,00	100,00
53	99,28	99,57	99,84	100,00	100,00
38	97,87	99,23	99,58	99,94	100,00
21.5	88,72	96,79	98,64	99,41	99,58
15	77,55	91,57	96,91	98,43	98,69
10.5	64,42	81,62	92,67	96,19	96,37
7.5	52,58	69,63	85,38	91,85	93,88
5.25	41,42	56,36	73,90	83,21	89,24
3	26,54	36,73	51,01	60,96	70,44

Particle Size Distributions of Products from the Tests Carried Out at Çayeli Bakır İşletmeleri A.Ş.

	Experiment 1					**Experiment 2**					**Experiment 3**				
Size (μm)	0.5 min	1 min	2 min	3 min	5 min	0.5 min	1 min	2 min	3 min	5 min	0.5 min	1 min	2 min	3 min	5 min
50	100.00	100.00	100.00	100.00	100.00	100.00	100.00	100.00	100.00	100.00	100.00	100.00	100.00	100.00	100.00
36	99.95	99.95	100.00	100.00	100.00	99.86	99.97	99.98	100.00	100.00	99.53	99.91	100.00	100.00	100.00
20	99.25	99.70	99.94	100.00	100.00	92.54	98.55	99.73	99.79	99.90	86.28	95.78	99.38	99.83	99.93
18	96.52	98.98	99.73	99.77	100.00	88.64	97.11	99.03	99.24	99.62	82.38	93.30	98.60	99.34	99.69
15	89.73	96.73	98.95	99.09	99.67	81.01	93.32	97.03	97.68	98.79	75.56	88.06	96.13	97.82	98.82
12.5	83.59	93.05	97.49	97.93	99.04	73.20	88.20	93.97	95.41	97.55	68.70	82.08	92.28	95.33	97.22
10.5	77.34	88.35	95.40	96.40	98.19	66.02	82.43	90.03	92.55	96.01	62.14	76.00	87.53	92.00	95.05
9	71.76	83.45	92.90	94.63	97.21	60.04	76.83	85.77	89.36	94.26	56.49	70.46	82.64	88.28	92.56
7.5	65.11	76.95	89.02	91.83	95.63	53.40	69.82	79.82	84.56	91.49	50.16	63.83	76.13	82.90	88.64
6.25	58.60	70.09	84.14	88.06	93.42	47.28	62.72	73.14	78.66	87.75	44.35	57.28	69.16	76.68	83.56
5.25	52.54	63.36	78.55	83.37	90.45	41.81	56.02	66.28	72.03	83.05	39.19	51.13	62.21	70.09	77.57
4.5	47.37	57.42	72.97	78.32	87.00	37.27	50.29	60.04	65.55	78.00	34.90	45.85	55.95	63.90	71.50
3.75	41.51	50.53	65.78	71.34	81.83	32.24	43.82	52.66	57.39	71.02	30.11	39.77	48.50	56.33	63.61
3	34.83	42.51	56.61	61.87	74.16	26.60	36.53	44.01	47.34	61.59	24.68	32.76	39.65	47.12	53.55
2.5	29.79	36.40	49.11	53.81	67.03	22.44	31.14	37.42	40.10	53.64	20.64	27.45	32.89	39.89	45.46
2.15	25.88	31.64	42.98	47.09	60.61	19.24	27.02	32.30	34.29	47.06	17.56	23.35	27.70	34.18	38.99
1.85	22.20	27.15	37.02	40.50	53.86	16.30	23.20	27.53	28.88	40.64	14.72	19.56	22.96	28.82	32.90

	Experiment 4					Experiment 5					Experiment 6				
Size (µm)	0.5 min	1 min	2 min	3 min	5 min	0.5 min	1 min	2 min	3 min	5 min	0.5 min	1 min	2 min	3 min	5 min
50	100.00	100.00	100.00	100.00	100.00	100.01	100.00	100.00	100.00	100.00	100.00	100.01	100.00	100.00	100.00
36	100.00	100.00	100.00	100.00	100.00	100.02	100.00	99.99	99.99	100.00	100.00	100.02	100.01	100.00	100.00
25.5	98.98	100.00	100.00	100.00	100.00	98.10	99.38	100.00	100.00	100.00	96.44	98.19	99.03	99.90	100.00
20	94.63	97.76	98.74	99.80	99.87	91.28	95.07	97.13	97.92	99.46	87.41	91.50	94.47	97.32	99.09
18	91.63	95.82	97.54	99.29	99.52	87.16	91.68	94.90	96.19	98.72	82.62	87.35	91.27	94.74	97.98
15	85.51	91.11	94.44	97.31	98.41	79.59	84.63	89.89	92.14	96.36	74.47	79.60	84.75	88.91	94.77
12.5	78.80	85.09	90.18	93.88	96.54	72.19	77.10	83.85	87.02	92.74	66.96	71.98	77.68	82.32	90.19
10.5	72.20	78.60	85.13	89.43	93.92	65.41	69.98	77.50	81.35	88.30	60.41	65.14	70.82	75.80	84.87
9	66.40	72.61	79.98	84.72	90.80	59.65	63.92	71.64	75.88	83.67	55.01	59.45	64.86	69.97	79.55
7.5	59.68	65.47	73.19	78.30	85.99	53.15	57.05	64.56	69.01	77.36	49.02	53.06	58.04	63.06	72.66
6.25	53.28	58.53	66.09	71.33	80.09	47.14	50.60	57.62	62.04	70.48	43.45	47.07	51.62	56.33	65.49
5.25	47.45	52.17	59.24	64.37	73.58	41.82	44.79	51.23	55.46	63.55	38.46	41.70	45.86	50.13	58.61
4.5	42.53	46.78	53.29	58.17	67.34	37.42	39.93	45.83	49.80	57.36	34.31	37.21	41.05	44.88	52.62
3.75	37.00	40.72	46.48	50.93	59.65	32.49	34.50	39.76	43.36	50.12	29.68	32.20	35.64	38.96	45.75
3	30.71	33.82	38.64	42.45	50.30	26.93	28.37	32.88	35.99	41.69	24.48	26.55	29.51	32.25	37.83
2.5	25.98	28.63	32.68	35.93	42.94	22.76	23.81	27.73	30.42	35.27	20.62	22.34	24.94	27.21	31.85
2.15	22.30	24.60	28.03	30.81	37.06	19.55	20.31	23.76	26.09	30.27	17.67	19.13	21.43	23.34	27.22
1.85	18.86	20.83	23.66	25.99	31.45	16.57	17.08	20.08	22.03	25.59	14.94	16.17	18.18	19.73	22.93

	Experiment 7					Experiment 8					Experiment 9				
Size (μm)	0.5 min	1 min	2 min	3 min	5 min	0.5 min	1 min	2 min	3 min	5 min	0.5 min	1 min	2 min	3 min	5 min
50	100.00	100.00	100.00	100.00	100.00	100.00	100.00	100.00	100.00	100.00	100.00	100.00	100.00	100.00	100.00
36	100.00	100.00	100.00	100.00	100.00	100.00	100.00	100.00	100.00	100.00	100.00	100.00	100.00	100.00	100.00
25.5	100.00	100.00	100.00	100.00	100.00	99.51	100.00	100.00	100.00	100.00	99.09	100.00	100.00	100.00	100.00
20	97.68	99.15	99.80	99.72	99.98	95.68	97.94	99.39	99.84	99.87	93.62	97.54	99.02	99.52	99.48
18	95.77	98.14	99.28	99.21	99.88	92.64	96.17	98.61	99.37	99.53	89.63	95.32	97.75	98.69	98.87
15	91.35	95.33	97.82	97.60	99.39	86.37	91.82	96.20	97.90	98.59	81.84	89.93	94.08	96.02	97.32
12.5	85.92	91.45	95.65	95.32	98.40	79.70	86.19	92.54	95.44	97.20	73.98	83.21	89.03	92.18	95.22
10.5	80.15	86.96	92.89	92.54	97.03	73.27	80.06	88.05	92.19	95.30	66.82	76.20	83.43	87.71	92.50
9	74.75	82.40	89.81	89.51	95.47	67.55	74.31	83.38	88.59	93.01	60.85	69.90	78.04	83.12	89.36
7.5	68.08	76.33	85.26	85.12	93.06	60.75	67.29	77.08	83.37	89.46	54.17	62.59	71.18	76.92	84.58
6.25	61.38	69.81	79.81	80.00	89.90	54.13	60.32	70.25	77.29	85.01	47.93	55.66	64.04	70.20	78.78
5.25	55.03	63.29	73.81	74.48	85.93	48.05	53.80	63.45	70.83	79.83	42.35	49.33	57.20	63.48	72.43
4.5	49.53	57.45	68.03	69.21	81.57	42.92	48.24	57.38	64.78	74.51	37.70	43.99	51.34	57.50	66.36
3.75	43.23	50.54	60.78	62.65	75.33	37.17	41.94	50.28	57.44	67.52	32.53	37.98	44.72	50.46	58.85
3	35.96	42.37	51.77	54.52	66.51	30.70	34.84	42.02	48.64	58.60	26.76	31.24	37.09	42.09	49.66
2.5	30.47	36.08	44.57	47.98	58.73	25.92	29.60	35.75	41.82	51.38	22.54	26.26	31.25	35.59	42.42
2.15	26.23	31.17	38.78	42.66	52.08	22.28	25.60	30.88	36.45	45.51	19.34	22.48	26.71	30.51	36.66
1.85	22.30	26.56	33.25	37.49	45.41	18.91	21.91	26.34	31.38	39.79	16.42	19.03	22.49	25.80	31.21

Particle Size Distributions of Pilot Stirred Ball Mill Tests

Size (µm)	Feed	Test 2	Test 3	Test 4	Test 5	Test 6	Test 7	Test 8	Test 9	Test 10	Test 11	Test 12	Test 13	Test 14	Test 15
90	100.00	100.00	100.00	100.00	100.00	100.00	100.00	100.00	100.00	100.00	100.00	100.00	100.00	100.00	100.00
63	78.24	96.84	96.86	88.33	89.25	96.59	94.35	92.44	87.90	87.32	97.61	98.70	96.12	93.70	87.98
50	66.62	93.65	93.78	80.08	81.03	93.77	90.71	86.89	79.58	79.28	96.28	97.05	92.05	88.60	79.10
36	48.86	82.09	82.56	61.98	63.38	82.37	76.50	71.41	59.92	62.69	87.91	90.65	76.98	75.08	62.35
30.5	43.14	78.69	79.58	57.61	59.76	79.03	72.99	67.36	56.33	56.87	85.19	88.34	73.44	71.64	55.61
25.5	37.85	72.13	73.44	51.75	53.63	72.41	66.42	60.89	50.57	50.28	79.20	82.82	66.46	65.31	49.18
21.5	32.91	64.58	66.04	45.59	46.91	64.65	59.00	53.74	44.24	43.76	71.58	75.35	58.35	58.24	42.96
18	28.65	57.06	58.43	39.95	40.69	56.78	51.67	47.02	38.34	37.93	63.47	67.09	50.57	51.30	37.33
15	25.27	50.53	51.73	35.33	35.61	49.87	45.34	41.39	33.47	33.19	56.09	59.46	44.03	45.30	32.67
12.5	22.64	45.17	46.19	31.65	31.58	44.18	40.16	36.85	29.60	29.41	49.86	52.98	38.74	40.39	28.93
10.5	20.60	40.84	41.71	28.72	28.39	39.59	36.02	33.23	26.55	26.42	44.75	47.65	34.52	36.43	25.94
9	19.03	37.44	38.19	26.43	25.92	36.02	32.80	30.40	24.20	24.09	40.75	43.46	31.23	33.34	23.64
7.5	17.36	33.77	34.40	23.94	23.30	32.23	29.39	27.40	21.72	21.64	36.49	38.98	27.77	30.03	21.22
6.25	15.86	30.42	30.92	21.64	20.95	28.85	26.37	24.71	19.53	19.47	32.70	34.97	24.69	27.06	19.08
5.25	14.53	27.45	27.82	19.58	18.92	25.92	23.78	22.40	17.65	17.60	29.45	31.51	22.07	24.50	17.25
4.5	13.41	24.96	25.21	17.84	17.25	23.53	21.70	20.51	16.12	16.07	26.81	28.69	19.97	22.40	15.76
3.75	12.13	22.12	22.21	15.85	15.40	20.89	19.39	18.39	14.43	14.39	23.93	25.59	17.69	20.07	14.12
3	10.61	18.86	18.75	13.56	13.30	17.91	16.82	15.98	12.51	12.47	20.71	22.10	15.19	17.43	12.25
2.5	9.40	16.35	16.13	11.80	11.71	15.66	14.91	14.13	11.04	11.00	18.32	19.48	13.34	15.42	10.81
2.15	8.42	14.39	14.11	10.43	10.46	13.90	13.43	12.66	9.88	9.82	16.46	17.42	11.92	13.85	9.67
1.85	7.45	12.54	12.21	9.12	9.25	12.21	12.00	11.22	8.73	8.67	14.67	15.44	10.57	12.32	8.56
1.55	6.33	10.51	10.15	7.66	7.88	10.31	10.41	9.58	7.42	7.35	12.65	13.19	9.05	10.58	7.29
1.3	5.28	8.67	8.31	6.33	6.61	8.57	8.90	8.03	6.19	6.11	10.75	11.08	7.65	8.94	6.09
1.1	4.36	7.11	6.76	5.19	5.49	7.07	7.57	6.67	5.11	5.03	9.07	9.23	6.42	7.49	5.05
0.9	3.38	5.48	5.17	4.00	4.30	5.48	6.08	5.21	3.96	3.88	7.23	7.23	5.08	5.92	3.93
0.75	2.62	4.24	3.95	3.09	3.35	4.24	4.87	4.06	3.07	2.99	5.73	5.67	4.01	4.66	3.05
0.65	2.10	3.40	3.15	2.47	2.71	3.41	4.01	3.27	2.46	2.39	4.69	4.59	3.27	3.78	2.45
0.55	1.58	2.56	2.35	1.85	2.05	2.57	3.10	2.48	1.85	1.79	3.61	3.48	2.50	2.89	1.85
0.45	1.06	1.72	1.57	1.24	1.39	1.73	2.15	1.68	1.25	1.20	2.49	2.37	1.72	1.97	1.25

Size (µm)	Test 16 Feed	Test 16	Test 17	Test 18	Test 19 Feed	Test 19	Test 20	Test 21	Test 22	Test 23	Test 24 Feed	Test 24	Test 25	Test 26	Test 27	Test 28
90	100.00	100.00	100.00	100.00	100.00	100.00	100.00	100.00	100.00	100.00	100.00	100.00	100.00	100.00	100.00	100.00
63	93.73	99.88	99.77	99.70	99.83	100.00	100.00	100.00	100.00	100.00	100.00	100.00	100.00	100.00	99.75	99.93
50	88.62	99.64	99.43	99.14	99.44	99.97	99.99	99.98	99.96	99.99	99.54	99.99	99.99	99.96	99.69	99.90
36	70.48	98.34	97.40	96.21	97.82	99.81	99.90	99.91	99.80	99.88	98.20	99.94	99.96	99.92	99.46	99.61
30.5	54.81	96.10	93.11	92.45	97.13	99.81	99.90	99.91	99.80	99.88	97.80	99.94	99.96	99.92	99.46	99.61
25.5	42.99	90.39	85.12	84.99	93.52	98.14	99.45	99.38	98.20	98.27	94.74	98.56	98.96	98.48	96.49	96.75
21.5	33.86	82.25	75.88	75.99	86.61	94.35	97.27	97.18	94.42	94.80	88.23	95.39	96.38	95.24	91.23	91.61
18	27.22	72.89	66.31	66.51	77.68	88.33	92.31	92.44	88.24	89.30	79.67	90.17	91.77	89.94	84.25	84.70
15	22.70	63.94	57.64	57.91	68.88	81.20	85.61	86.05	80.84	82.62	71.23	83.61	85.72	83.32	76.71	77.17
12.5	19.59	56.11	50.30	50.66	61.22	74.06	78.56	79.22	73.45	75.66	63.84	76.60	79.14	76.32	69.47	69.93
10.5	17.34	49.59	44.31	44.77	54.88	67.51	72.00	72.76	66.73	69.09	57.60	69.87	72.69	69.61	63.00	63.45
9	15.66	44.44	39.65	40.19	49.86	61.97	66.39	67.16	61.11	63.42	52.56	64.02	66.99	63.79	57.60	58.06
7.5	13.91	38.95	34.75	35.33	44.41	55.68	59.95	60.66	54.79	56.91	46.99	57.29	60.32	57.06	51.57	52.06
6.25	12.34	34.07	30.42	31.01	39.40	49.75	53.84	54.41	48.88	50.77	41.82	50.95	53.96	50.72	45.96	46.47
5.25	10.98	29.91	26.73	27.30	34.96	44.43	48.30	48.74	43.60	45.27	37.26	45.30	48.23	45.06	40.99	41.52
4.5	9.86	26.59	23.78	24.32	31.29	39.99	43.68	43.96	39.22	40.69	33.50	40.65	43.48	40.43	36.89	37.43
3.75	8.63	23.01	20.59	21.09	27.24	35.04	38.48	38.60	34.35	35.60	29.36	35.56	38.21	35.33	32.35	32.91
3	7.27	19.10	17.10	17.55	22.73	29.46	32.60	32.52	28.86	29.89	24.78	29.95	32.36	29.70	27.31	27.85
2.5	6.27	16.26	14.57	14.96	19.41	25.30	28.19	27.97	24.79	25.68	21.39	25.84	28.04	25.57	23.59	24.11
2.15	5.50	14.10	12.65	13.01	16.85	22.09	24.78	24.44	21.64	22.46	18.79	22.73	24.72	22.42	20.74	21.23
1.85	4.79	12.12	10.87	11.20	14.49	19.08	21.56	21.12	18.69	19.48	16.33	19.82	21.61	19.47	18.05	18.51
1.55	4.02	9.97	8.96	9.25	11.92	15.81	18.01	17.50	15.48	16.22	13.63	16.63	18.19	16.27	15.11	15.50
1.3	3.32	8.07	7.27	7.51	9.65	12.89	14.81	14.24	12.60	13.31	11.18	13.75	15.08	13.38	12.43	12.78
1.1	2.73	6.49	5.86	6.07	7.76	10.44	12.09	11.51	10.19	10.87	9.11	11.30	12.41	10.93	10.16	10.46
0.9	2.12	4.89	4.43	4.60	5.84	7.92	9.26	8.70	7.71	8.32	6.96	8.73	9.62	8.38	7.80	8.04
0.75	1.65	3.69	3.35	3.49	4.40	6.02	7.10	6.59	5.86	6.38	5.32	6.76	7.45	6.44	5.99	6.19
0.65	1.32	2.90	2.64	2.76	3.45	4.76	5.65	5.21	4.62	5.09	4.22	5.42	5.98	5.14	4.77	4.94
0.55	1.00	2.13	1.95	2.04	2.53	3.52	4.23	3.84	3.41	3.81	3.14	4.08	4.51	3.85	3.57	3.70
0.45	0.68	1.40	1.29	1.35	1.65	2.34	2.82	2.53	2.26	2.55	2.09	2.75	3.04	2.57	2.39	2.47

Size (µm)	Test 29	Test 30 Feed	Test 30	Test 31 Feed	Test 31	Test 32 Feed	Test 32	Test 33 Feed	Test 33	Test 34 Feed	Test 34	Test 35 Feed	Test 35	Test 36 Feed	Test 36
90	100.00	100.00	100.00	100.00	100.00	100.00	100.00	100.00	100.00	100.00	100.00	100.00	100.00	100.00	100.00
63	99.94	96.46	99.94	85.23	99.84	97.88	100.00	98.61	99.91	97.61	99.97	99.63	100.00	99.82	100.00
50	99.87	94.07	99.87	78.96	99.35	96.50	99.77	97.32	99.80	95.49	99.87	99.26	99.97	99.43	99.96
36	99.50	84.81	99.52	63.73	97.33	91.43	99.30	92.67	99.27	88.23	99.39	97.39	99.91	97.97	99.76
30.5	99.50	83.36	99.52	58.87	97.02	91.02	99.30	91.74	99.27	86.57	99.39	96.82	99.91	97.21	99.76
25.5	97.20	78.66	98.62	52.19	94.21	88.55	98.94	88.34	97.56	82.22	97.73	93.62	99.91	94.01	99.09
21.5	92.79	71.52	95.79	45.32	87.89	83.58	96.91	82.58	93.84	75.99	94.06	87.30	98.42	88.11	96.78
18	86.50	63.54	90.46	39.15	79.30	77.08	92.16	75.45	88.06	68.82	88.29	79.12	95.16	80.47	92.24
15	79.33	56.35	83.72	34.16	70.61	70.49	85.60	68.33	81.27	61.91	81.46	71.13	90.30	72.75	86.32
12.5	72.22	50.41	76.84	30.21	62.84	64.39	78.64	61.85	74.40	55.75	74.55	64.14	84.58	65.76	80.10
10.5	65.72	45.58	70.52	27.07	56.24	58.88	72.08	56.17	68.04	50.43	68.13	58.26	78.74	59.69	74.22
9	60.26	41.78	65.19	24.62	50.93	54.17	66.40	51.46	62.59	46.05	62.64	53.47	73.44	54.69	69.06
7.5	54.09	37.68	59.17	22.02	45.17	48.76	59.83	46.18	56.37	41.18	56.35	48.15	67.08	49.08	62.97
6.25	48.34	33.93	53.51	19.69	39.99	43.59	53.54	41.23	50.49	36.60	50.41	43.18	60.84	43.86	56.93
5.25	43.23	30.62	48.46	17.66	35.53	38.90	47.85	36.78	45.18	32.49	45.08	38.73	55.06	39.19	51.27
4.5	39.02	27.89	44.25	16.01	31.93	34.95	43.07	33.06	40.75	29.09	40.64	35.03	50.14	35.30	46.37
3.75	34.34	24.83	39.53	14.19	28.03	30.48	37.72	28.87	35.80	25.29	35.69	30.90	44.51	30.94	40.69
3	29.08	21.33	34.15	12.14	23.73	25.45	31.71	24.14	30.20	21.02	30.11	26.22	38.01	26.00	34.11
2.5	25.17	18.68	30.08	10.60	20.57	21.72	27.26	20.65	26.05	17.85	25.96	22.71	33.05	22.30	29.12
2.15	22.14	16.61	26.88	9.42	18.16	18.88	23.86	18.02	22.86	15.43	22.76	19.99	29.16	19.44	25.27
1.85	19.28	14.63	23.81	8.29	15.90	16.27	20.71	15.60	19.88	13.19	19.77	17.44	25.47	16.75	21.68
1.55	16.12	12.41	20.32	7.04	13.42	13.49	17.29	13.01	16.63	10.79	16.49	14.63	21.38	13.82	17.82
1.3	13.26	10.36	17.08	5.89	11.16	11.03	14.23	10.73	13.71	8.68	13.54	12.09	17.65	11.21	14.40
1.1	10.83	8.59	14.24	4.89	9.24	8.98	11.65	8.81	11.23	6.95	11.04	9.92	14.48	9.02	11.58
0.9	8.29	6.70	11.19	3.83	7.18	6.88	8.96	6.83	8.65	5.20	8.45	7.66	11.15	6.80	8.71
0.75	6.35	5.22	8.77	3.00	5.60	5.28	6.91	5.30	6.66	3.90	6.47	5.92	8.59	5.12	6.57
0.65	5.05	4.21	7.11	2.42	4.52	4.22	5.53	4.27	5.33	3.05	5.16	4.74	6.87	4.03	5.17
0.55	3.77	3.20	5.40	1.84	3.43	3.15	4.15	3.23	4.00	2.23	3.85	3.57	5.16	2.96	3.80
0.45	2.52	2.17	3.68	1.26	2.33	2.11	2.79	2.20	2.69	1.45	2.56	2.41	3.46	1.93	2.49

8.2. Appendix 2

Experimental and mass-balanced asseys and particle size distributions obtained from the sampling surveys carried out at the plant are tabulated below.

Experimental and Mass-Balanced Assays and Tonnages of 6 Regrind Surveys

31/07/2006 Cu RG Survey

	TPH Solids (Bal)	Component Cu (Exp)	Component Cu (Bal)	Component Zn (Exp)	Component Zn (Bal)	Component Fe (Exp)	Component Fe (Bal)
Flotation Feed	150.00	3.760	3.762	5.440	5.493	28.80	28.95
Copper Concentrate	18.39	25.90	25.90	3.280	3.273	29.50	29.48
Feed to Zn Circuit	131.6	0.67	0.668	5.85	5.803	29.00	28.87
Cu RG Cyclone O/F	50.40	11.70	11.67	5.100	5.213	32.60	32.49
Cu Rgh Concentrate	11.34	13.50	13.49	4.990	5.015	31.80	31.78
Cu Cl 1 Total Feed	67.38	9.3	11.44	5.650	5.299	32.80	32.55
Cu Cl 1 Concentrate	38.29	18.80	18.80	4.500	4.513	31.80	32.08
Cu Cl 1 Tail	29.09	1.720	1.753	5.970	6.332	33.10	33.16
Cu Cl 2 Concentrate	32.65	20.80	21.14	4.080	4.147	31.10	31.65
Cu Cl 2 Tail	5.643	5.240	5.250	6.550	6.632	34.60	34.60
Cu Rgh Scav Tail	102.5	0.410	0.360	5.820	5.653	27.70	27.65

04/08/2006 Cu RG Survey

	TPH Solids (Bal)	Component Cu (Exp)	Component Cu (Bal)	Component Zn (Exp)	Component Zn (Bal)	Component Fe (Exp)	Component Fe (Bal)
Flotation Feed	120.00	3.730	3.731	6.270	6.021	23.50	23.06
Copper Concentrate	13.91	25.70	25.70	6.070	6.099	25.80	25.85
Feed to Zn Circuit	106.1	0.850	0.849	6.07	6.01	22.30	22.69
Cu Rgh Scav Tail	77.55	0.580	0.500	5.860	5.313	20.30	22.21
Cu RG Cyclone O/F	48.92	9.930	9.953	7.850	7.759	25.40	25.24
Cu Cl 1&2 Concentrate	20.36	21.40	21.39	7.520	7.558	26.90	26.97
Cu Cl 1&2 Tail	28.55	1.840	1.797	8.050	7.902	23.20	24.00

08/08/2006 RG Survey

	TPH Solids (Bal)	Component Cu (Exp)	Component Cu (Bal)	Component Zn (Exp)	Component Zn (Bal)	Component Fe (Exp)	Component Fe (Bal)
Flotation Feed	140.00	2.87	2.895	6.50	7.217	27.6	28.36
Copper Concentrate	11.74	23.30	23.30	4.80	4.740	30.10	30.04
Feed to Zn Circuit	128.30	1.050	1.027	8.10	7.443	28.90	28.21
Cu Rgh Scav Tail	112.80	0.850	0.815	7.870	7.303	28.00	27.67
Cu RG Cyclone O/F	35.08	10.30	10.30	6.920	6.925	31.50	31.49
Cu Cl 1&2 Concentrate	19.60	19.10	16.40	6.000	5.711	30.30	30.95
Cu Cl 1&2 Tail	15.48	2.580	2.575	8.770	8.464	31.70	32.17

09/08/2006 RG Survey

	TPH Solids (Bal)	Component Cu (Exp)	Component Cu (Bal)	Component Zn (Exp)	Component Zn (Bal)	Component Fe (Exp)	Component Fe (Bal)
Flotation Feed	140.0	3.14	3.097	5.85	7.040	25.6	25.94
Copper Concentrate	15.74	19.20	19.20	6.95	6.649	29.4	29.36
Feed to Zn Circuit	124.3	1.02	1.058	7.10	7.089	25.80	25.50
Cu RG Cyclone O/F	25.10	7.530	7.521	10.20	10.21	29.60	29.52
Cu Rgh Concentrate	45.15	7.860	7.844	7.670	7.683	29.40	29.26
Cu Cl 1 Total Feed	78.50	7.210	7.238	8.650	8.665	28.90	29.48
Cu Cl 1 Concentrate	38.17	13.30	12.95	8.100	8.085	30.60	30.32
Cu Cl 1 Tail	40.33	1.850	1.831	9.250	9.214	28.70	28.68
Cu Cl 2 Concentrate	29.92	15.70	15.68	7.800	7.737	30.00	30.27
Cu Cl 2 Tail	8.257	4.070	3.065	9.800	9.346	31.90	30.48
Cu Rgh Scav Tail	83.97	0.700	0.687	6.100	6.069	24.20	23.97

28/08/2006 Spec Ore Survey

	TPH Solids (Bal)	Component Cu (Exp)	Component Cu (Bal)	Component Zn (Exp)	Component Zn (Bal)	Component Fe (Exp)	Component Fe (Bal)
Flotation Feed	150.00	3.270	3.264	3.000	3.042	30.20	30.04
Cu Rougher Concentrate	48.26	8.990	8.831	3.700	3.477	33.90	33.63
Cu Rougher Tail	101.7	0.640	0.623	3.030	2.836	28.60	28.34
Cu Rgh Scav Concentrate	2.229	8.380	8.352	9.200	9.176	34.30	34.27
Cu Rgh Scav Tail	99.51	0.350	0.449	2.910	2.694	28.40	28.21
Feed to Zn Circuit	130.7	0.460	0.485	3.010	2.818	30.20	29.88
Cu RG Cyclone O/F	62.28	8.400	8.779	4.100	3.987	34.30	34.12
Cu Cl 1&2 Total Concentrate	31.09	17.10	16.99	5.000	4.764	33.10	33.00
Cu Cl 1&2 Total Tail	31.19	0.660	0.598	3.140	3.213	35.10	35.23
Cu Cl 3 Concentrate	24.54	19.70	19.95	4.890	4.653	31.60	32.00
Cu Cl 3 Tail	6.547	5.900	5.884	5.120	5.181	36.70	36.74
Cu Cl 4 Concentrate	20.90	21.40	21.33	4.500	4.617	31.40	31.31
Cu Cl 4 Tail	3.638	12.10	12.05	4.790	4.859	36.00	35.96
Cu Cl 5 Concentrate	19.29	22.20	22.09	4.220	4.563	31.10	31.11
Cu Cl 5 Tail	1.605	12.20	12.19	5.250	5.272	33.80	33.79
Zn Rougher Concentrate	11.46	2.420	3.558	24.70	25.03	24.10	24.66
Zn Rougher Tail	119.3	0.240	0.190	0.330	0.684	30.00	30.39
Zn Rgh Cleaner Concentrate	9.132	4.890	3.742	29.30	30.83	21.60	20.71
Zn Rgh Cleaner Tail	2.324	3.070	2.838	2.300	2.240	40.30	40.19
Zn Col Total Feed	15.62	5.330	5.549	29.60	27.60	21.10	22.39
Zn Column Concentrate	5.124	3.010	3.068	51.50	51.18	7.800	7.661
Zn Column Tail	10.50	6.750	6.760	17.10	16.09	28.60	29.58
Zn Col Scav Concentrate	6.492	8.190	8.092	21.60	23.05	25.90	24.76
Zn Col Scav Tail	4.008	4.560	4.603	4.700	4.822	37.90	37.40
Final Tail	125.6	0.430	0.380	0.550	0.845	30.20	30.79

06/09/2006 Non-Spec Ore Survey

	TPH Solids (Bal)	Component Cu (Exp)	Component Cu (Bal)	Component Zn (Exp)	Component Zn (Bal)	Component Fe (Exp)	Component Fe (Bal)
Flotation Feed	150.00	2.850	2.758	9.300	9.693	23.00	23.48
Cu Rougher Concentrate	30.00	9.170	8.927	8.920	8.934	26.50	26.01
Cu Rougher Tail	120.0	1.200	1.216	9.980	9.882	22.50	22.85
Cu Rgh Scav Concentrate	1.878	10.70	10.68	13.20	13.20	25.00	24.96
Cu Rgh Scav Tail	118.1	0.750	1.066	9.820	9.829	22.60	22.81
Feed to Zn Circuit	138.3	1.150	1.272	9.780	9.921	23.30	23.38
Cu RG Cyclone O/F	43.77	9.100	9.228	9.920	9.949	26.00	26.32
Cu Cl 1&2 Total Concentrate	23.62	14.80	14.98	9.520	9.511	24.30	26.01
Cu Cl 1&2 Total Tail	20.15	2.320	2.481	10.50	10.46	26.40	26.68
Cu Cl 3 Concentrate	15.84	17.90	18.08	8.600	8.250	25.90	25.79
Cu Cl 3 Tail	7.779	8.770	8.687	12.08	12.08	27.06	26.44
Cu Cl 4 Concentrate	12.31	20.70	20.03	7.250	7.121	25.10	24.92
Cu Cl 4 Tail	3.523	11.34	11.26	12.12	12.20	29.10	28.84
Cu Cl 5 Concentrate	11.73	19.80	20.28	6.650	6.993	25.20	24.68
Cu Cl 5 Tail	0.588	14.89	14.91	9.660	9.679	29.69	29.66
Zn Rougher Concentrate	42.67	2.490	2.876	29.90	30.20	17.40	18.17
Zn Rougher Tail	95.60	0.520	0.556	0.750	0.871	25.20	25.70
Zn Rgh Cleaner Concentrate	32.99	3.260	2.988	39.70	38.80	14.00	14.20
Zn Rgh Cleaner Tail	9.684	2.580	2.496	0.970	0.914	31.80	31.68
Zn Col Total Feed	57.92	4.240	4.223	33.30	34.44	16.90	16.49
Zn Column Concentrate	24.61	2.710	2.622	50.00	49.94	8.450	7.823
Zn Column Tail	33.30	5.550	5.406	22.80	22.98	23.90	22.90
Zn Col Scav Concentrate	24.93	5.740	5.856	29.30	28.67	18.60	19.52
Zn Col Scav Tail	8.371	4.030	4.065	6.050	6.020	32.80	32.95
Final Tail	113.7	1.370	0.980	1.720	1.254	28.30	26.74

Experimental and Mass-Balanced Particle Size Distributions of 6 Regrind Surveys

EXPERIMENTAL PARTICLE SIZE DISTRIBUTIONS																
	31/07/2006				04/08/2006				08/08/2006				09/08/2006			
Size (µm)	Cyclone Feed	Cyclone U/F	Cyclone O/F	Mill Discharge	Cyclone Feed	Cyclone U/F	Cyclone O/F	Mill Discharge	Cyclone Feed	Cyclone U/F	Cyclone O/F	Mill Discharge	Cyclone Feed	Cyclone U/F	Cyclone O/F	Mill Discharge
90	100.00	100.00	100.00	100.00	100.00	100.00	100.00	100.00	100.00	100.00	100.00	100.00	100.00	100.00	100.00	100.00
63	97.42	92.52	99.75	99.07	97.88	93.35	99.48	99.49	99.55	96.27	99.95	99.82	98.90	94.21	99.89	99.58
50	94.95	85.26	99.43	97.02	95.77	87.56	98.96	98.59	98.40	90.68	99.88	99.29	97.25	87.46	99.65	98.69
36	86.78	68.30	97.52	90.28	89.95	73.18	97.45	93.90	94.78	77.31	99.58	96.85	91.22	74.05	98.86	94.56
30.5	82.70	59.50	95.20	85.80	87.10	61.42	96.27	91.10	91.30	69.50	99.30	94.90	88.70	65.17	97.13	91.88
25.5	76.70	50.39	90.69	78.60	82.70	49.87	92.90	86.90	84.23	59.30	97.59	90.80	84.70	53.53	94.30	85.57
20	66.60	38.12	79.47	67.12	75.30	36.19	85.98	79.00	72.42	45.49	89.90	81.60	77.70	38.87	86.36	73.80
18	63.16	33.59	74.12	61.78	71.60	31.73	81.36	74.75	67.59	39.93	85.31	76.77	74.00	34.21	81.62	68.80
15	55.55	27.14	65.43	53.81	63.30	25.83	73.30	66.09	60.18	32.38	77.06	68.20	67.35	28.41	73.44	61.20
12.5	49.12	22.16	57.80	47.33	56.07	21.82	65.82	58.54	53.79	26.87	69.18	61.10	60.40	24.53	65.92	54.86
10.5	43.88	18.47	51.44	42.14	50.14	19.10	59.34	52.35	48.34	22.97	62.14	55.17	54.42	21.70	59.40	49.61
9	39.70	15.99	46.44	38.08	45.56	17.25	54.07	47.56	43.92	20.23	56.25	50.34	49.56	19.56	54.10	45.38
7.5	35.06	13.82	41.07	33.57	40.66	15.39	48.22	42.45	39.12	17.51	49.77	45.05	44.23	17.29	48.33	40.71
6.25	30.79	12.08	36.16	29.33	36.02	13.69	42.71	37.61	34.75	15.18	43.99	40.23	39.38	15.27	43.11	36.38
5.25	27.13	10.59	31.87	25.73	31.62	12.16	37.67	33.01	30.89	13.26	39.00	35.99	35.14	13.49	38.48	32.47
4.5	24.20	9.38	28.36	22.96	27.80	10.87	33.41	29.03	27.69	11.77	34.95	32.48	31.62	12.05	34.61	29.16
3.75	20.98	8.11	24.51	20.04	23.58	9.40	28.63	24.62	24.18	10.21	30.51	28.56	27.68	10.46	30.27	25.41
3	17.32	6.76	20.21	16.74	19.09	7.76	23.29	19.93	20.27	8.51	25.53	24.08	23.20	8.71	25.35	21.08
2.5	14.60	5.80	17.04	14.20	15.88	6.56	19.35	16.57	17.41	7.24	21.77	20.65	19.79	7.41	21.64	17.79
2.15	12.54	5.07	14.61	12.22	13.46	5.66	16.38	14.06	15.22	6.28	18.83	17.93	17.15	6.40	18.74	15.23
1.85	10.68	4.39	12.38	10.42	11.23	4.83	13.65	11.73	13.16	5.40	16.07	15.35	14.66	5.45	16.03	12.85
1.3	7.11	3.03	7.96	6.94	6.80	3.10	8.34	7.10	8.89	3.68	10.46	10.00	9.56	3.55	10.46	8.12
0.9	4.43	1.93	4.64	4.39	3.53	1.74	4.49	3.68	5.44	2.36	6.16	5.83	5.60	2.10	6.14	4.61
0.65	2.74	1.22	2.67	2.78	1.71	0.93	2.34	1.78	3.26	1.50	3.57	3.31	3.19	1.22	3.52	2.55
0.45	1.41	0.63	1.24	1.46	0.62	0.38	0.96	0.65	1.58	0.79	1.67	1.52	1.47	0.59	1.63	1.13

Experimental and Mass-Balanced Particle Size Distributions of 6 Regrind Surveys (Continuing)

EXPERIMENTAL PARTICLE SIZE DISTRIBUTIONS										
	28/08/2006					**06/09/2006**				
Size (μm)	Fresh Feed	Mill Discharge	Cyclone Feed	Cyclone U/F	Cyclone O/F	Fresh Feed	Mill Discharge	Cyclone Feed	Cyclone U/F	Cyclone O/F
90	100.00	100.00	100.00	100.00	100.00	100.00	100.00	100.00	100.00	100.00
63	98.60	98.42	97.15	91.59	98.85	98.90	99.41	98.86	95.61	99.90
50	93.90	95.54	93.60	82.59	97.67	97.52	98.28	97.60	90.40	99.71
36	85.68	86.08	83.26	57.96	94.33	92.74	91.59	91.39	72.50	98.76
30.5	80.94	80.80	78.30	49.40	92.50	89.94	87.57	87.40	59.71	97.89
25.5	74.06	74.20	71.50	41.90	88.69	84.54	79.89	82.10	48.82	95.04
21.5	67.08	66.56	64.90	36.20	80.97	76.11	71.04	76.40	38.84	87.62
18	59.46	57.83	57.65	30.85	71.74	66.66	62.13	69.60	30.48	77.40
15	52.59	50.21	50.61	26.48	63.11	57.91	54.26	62.06	24.29	67.25
12.5	46.67	43.89	44.70	23.25	55.76	50.54	47.70	54.93	19.99	58.91
10.5	41.68	38.73	39.82	20.56	49.68	44.58	42.43	49.02	17.08	52.48
9	37.66	34.69	35.95	18.33	44.86	40.01	38.33	44.33	15.10	47.56
7.5	33.27	30.44	31.79	15.90	39.68	35.21	33.89	39.25	13.19	42.23
6.25	29.23	26.68	28.02	13.79	35.01	30.88	29.82	34.62	11.54	37.30
5.25	25.64	23.45	24.69	12.07	30.91	27.08	26.29	30.55	10.11	32.92
4.5	22.66	20.82	21.96	10.73	27.53	24.00	23.48	27.23	8.97	29.29
3.75	19.39	17.97	18.94	9.29	23.75	20.67	20.48	23.61	7.74	25.29
3	15.74	14.83	15.60	7.68	19.55	17.05	17.19	19.60	6.44	20.91
2.5	13.10	12.53	13.15	6.49	16.45	14.45	14.77	16.68	5.50	17.71
2.15	11.11	10.76	11.29	5.60	14.09	12.51	12.91	14.44	4.80	15.28
1.85	9.31	9.13	9.57	4.80	11.91	10.75	11.17	12.36	4.15	13.05
1.3	5.82	5.87	6.19	3.23	7.58	7.28	7.58	8.15	2.83	8.51
0.9	3.28	3.39	3.66	2.02	4.32	4.57	4.71	4.88	1.79	5.01
0.65	1.81	1.92	2.12	1.25	2.41	2.83	2.86	2.85	1.11	2.87
0.45	0.81	0.88	1.01	0.63	1.07	1.44	1.42	1.35	0.57	1.32

Experimental and Mass-Balanced Particle Size Distributions of 6 Regrind Surveys (Continuing)

MASS-BALANCED PARTICLE SIZE DISTRIBUTIONS															
	31/07/2006					04/08/2006					08/08/2006				
Size (µm)	Fresh feed	Mill Discharge	Cyclone Feed	Cyclone U/F	Cyclone O/F	Fresh feed	Mill Discharge	Cyclone Feed	Cyclone U/F	Cyclone O/F	Fresh feed	Mill Discharge	Cyclone Feed	Cyclone U/F	Cyclone O/F
90	100.00	100.00	100.00	100.00	100.00	100.00	100.00	100.00	100.00	100.00	100.00	100.00	100.00	100.00	100.00
63	96.38	99.07	97.31	92.56	99.82	97.66	99.49	98.05	93.32	99.34	98.10	99.82	98.74	96.57	100.00
50	93.43	97.02	94.67	85.36	99.61	95.57	98.59	96.22	87.47	98.61	95.32	99.29	96.78	91.27	100.00
36	85.54	90.28	87.18	68.17	97.26	90.63	93.90	91.33	72.89	96.36	89.18	96.85	92.01	78.33	100.00
30.5	81.19	85.80	82.79	59.48	95.14	87.31	91.10	88.12	61.21	95.46	85.28	94.90	88.83	70.41	99.59
25.5	75.72	78.60	76.72	50.39	90.68	82.31	86.90	83.29	49.75	92.43	78.81	90.80	83.24	59.67	97.01
20	64.88	67.12	65.66	38.45	80.09	74.30	79.00	75.31	36.19	85.97	67.44	81.60	72.67	45.40	88.60
18	60.84	61.78	61.17	34.28	75.43	70.07	74.75	71.08	31.84	81.77	62.53	76.77	67.79	39.86	84.10
15	53.12	53.81	53.36	27.90	66.86	62.41	66.09	63.20	25.85	73.38	55.24	68.20	60.02	32.44	76.14
12.5	46.44	47.33	46.75	22.98	59.35	55.65	58.54	56.26	21.78	65.67	48.67	61.10	53.26	27.07	68.55
10.5	40.98	42.14	41.38	19.34	53.08	49.98	52.35	50.49	19.02	59.06	43.09	55.17	47.55	23.27	61.74
9	36.79	38.08	37.24	16.85	48.05	45.49	47.56	45.93	17.17	53.77	38.63	50.34	42.95	20.59	56.02
7.5	32.46	33.57	32.84	14.59	42.52	40.58	42.45	40.98	15.32	47.97	33.86	45.05	37.99	17.93	49.70
6.25	28.63	29.33	28.87	12.75	37.42	35.95	37.61	36.30	13.63	42.49	29.65	40.23	33.55	15.63	44.03
5.25	25.27	25.73	25.43	11.18	32.99	31.69	33.01	31.97	12.08	37.39	26.05	35.99	29.72	13.70	39.08
4.5	22.47	22.96	22.64	9.92	29.38	28.06	29.03	28.27	10.77	33.04	23.17	32.48	26.60	12.17	35.04
3.75	19.35	20.04	19.59	8.59	25.42	24.01	24.62	24.14	9.28	28.19	20.07	28.56	23.20	10.57	30.59
3	15.88	16.74	16.18	7.16	20.96	19.53	19.93	19.61	7.65	22.88	16.68	24.08	19.41	8.83	25.59
2.5	13.38	14.20	13.66	6.13	17.66	16.25	16.57	16.32	6.47	19.01	14.21	20.65	16.59	7.55	21.87
2.15	11.49	12.22	11.74	5.35	15.13	13.77	14.06	13.83	5.58	16.09	12.35	17.93	14.41	6.58	18.98
1.85	9.76	10.42	9.99	4.63	12.83	11.50	11.73	11.55	4.76	13.40	10.63	15.35	12.37	5.69	16.27
1.3	6.35	6.94	6.56	3.22	8.32	7.04	7.10	7.05	3.05	8.14	7.13	10.00	8.19	3.94	10.67
0.9	3.73	4.39	3.96	2.09	4.95	3.77	3.68	3.75	1.69	4.32	4.39	5.83	4.92	2.55	6.31
0.65	2.15	2.78	2.37	1.35	2.91	1.94	1.78	1.91	0.89	2.19	2.69	3.31	2.92	1.63	3.67
0.45	1.01	1.46	1.16	0.72	1.40	0.78	0.65	0.75	0.35	0.86	1.33	1.52	1.40	0.86	1.72

Experimental and Mass-Balanced Particle Size Distributions of 6 Regrind Surveys (Continuing)

MASS-BALANCED PARTICLE SIZE DISTRIBUTIONS															
	09/08/2006					**28/08/2006**					**06/09/2006**				
Size (µm)	Fresh feed	Mill Discharge	Cyclone Feed	Cyclone U/F	Cyclone O/F	Fresh feed	Mill Discharge	Cyclone Feed	Cyclone U/F	Cyclone O/F	Fresh feed	Mill Discharge	Cyclone Feed	Cyclone U/F	Cyclone O/F
90	100.00	100.00	100.00	100.00	100.00	100.00	100.00	100.00	100.00	100.00	100.00	100.00	100.00	100.00	100.00
63	98.65	99.58	98.83	94.23	99.95	97.29	97.80	97.45	92.12	99.96	98.75	99.36	98.91	95.65	100.00
50	96.92	98.69	97.26	87.46	99.64	92.94	95.09	93.63	83.04	98.61	97.32	98.21	97.56	90.48	99.93
36	92.48	94.56	92.88	73.73	97.53	83.55	85.08	84.03	58.72	95.94	92.29	91.44	92.09	72.48	98.67
30.5	89.55	91.88	90.00	64.92	96.09	79.69	80.21	79.86	50.05	93.88	88.89	87.22	88.48	59.79	98.11
25.5	85.70	85.57	85.67	53.34	93.52	73.72	74.04	73.82	41.95	88.81	84.19	79.77	83.09	48.69	94.63
20	78.20	73.80	77.34	38.94	86.66	66.62	66.35	66.53	36.13	80.83	76.79	71.26	75.41	38.86	87.67
18	74.06	68.80	73.03	34.40	82.40	58.99	57.61	58.55	30.79	71.60	67.86	62.52	66.53	30.85	78.49
15	66.86	61.20	65.75	28.72	74.73	52.06	49.96	51.39	26.48	63.11	59.11	54.65	58.00	24.91	69.09
12.5	59.86	54.86	58.88	24.83	67.15	46.19	43.67	45.38	23.26	55.78	51.68	48.07	50.78	20.65	60.88
10.5	53.84	49.61	53.01	21.98	60.54	41.26	38.54	40.39	20.57	49.71	45.80	42.83	45.06	17.67	54.24
9	48.96	45.38	48.25	19.82	55.16	37.30	34.52	36.41	18.35	44.91	41.29	38.75	40.65	15.60	49.05
7.5	43.64	40.71	43.07	17.52	49.27	32.98	30.31	32.13	15.93	39.74	36.49	34.31	35.94	13.59	43.44
6.25	38.86	36.38	38.37	15.47	43.93	29.04	26.59	28.25	13.81	35.05	32.13	30.23	31.65	11.87	38.29
5.25	34.66	32.47	34.23	13.67	39.22	25.55	23.41	24.86	12.06	30.89	28.28	26.68	27.87	10.38	33.74
4.5	31.18	29.16	30.78	12.22	35.29	22.67	20.83	22.08	10.69	27.44	25.12	23.84	24.79	9.21	30.02
3.75	27.29	25.41	26.92	10.61	30.88	19.48	18.01	19.01	9.23	23.61	21.66	20.80	21.43	7.96	25.96
3	22.91	21.08	22.55	8.84	25.88	15.92	14.92	15.60	7.59	19.37	17.87	17.45	17.75	6.63	21.50
2.5	19.59	17.79	19.24	7.52	22.08	13.33	12.64	13.10	6.40	16.26	15.13	14.98	15.08	5.67	18.25
2.15	17.01	15.23	16.66	6.50	19.13	11.37	10.88	11.21	5.51	13.89	13.06	13.08	13.06	4.96	15.78
1.85	14.59	12.85	14.25	5.53	16.36	9.58	9.26	9.47	4.71	11.71	11.17	11.30	11.20	4.30	13.52
1.3	9.58	8.12	9.29	3.60	10.67	6.08	5.99	6.05	3.15	7.42	7.39	7.61	7.44	2.97	8.95
0.9	5.66	4.61	5.45	2.13	6.26	3.50	3.49	3.50	1.97	4.21	4.47	4.67	4.52	1.91	5.40
0.65	3.26	2.55	3.12	1.23	3.58	1.97	2.00	1.98	1.22	2.34	2.66	2.79	2.69	1.21	3.19
0.45	1.52	1.13	1.44	0.60	1.65	0.90	0.92	0.91	0.62	1.05	1.29	1.36	1.30	0.63	1.53

8.3. Appendix 3

The modal analysis of the streams around the flotation circuit are given below.

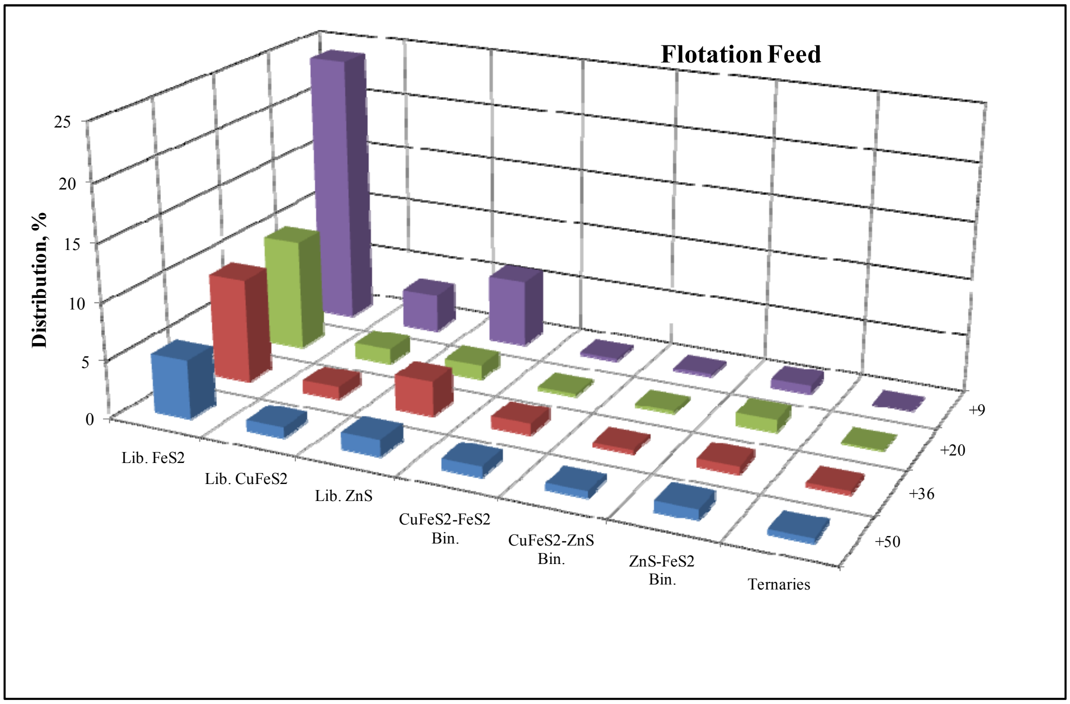

Modal analysis of the plant feed for different size fractions for Non-Spec ore

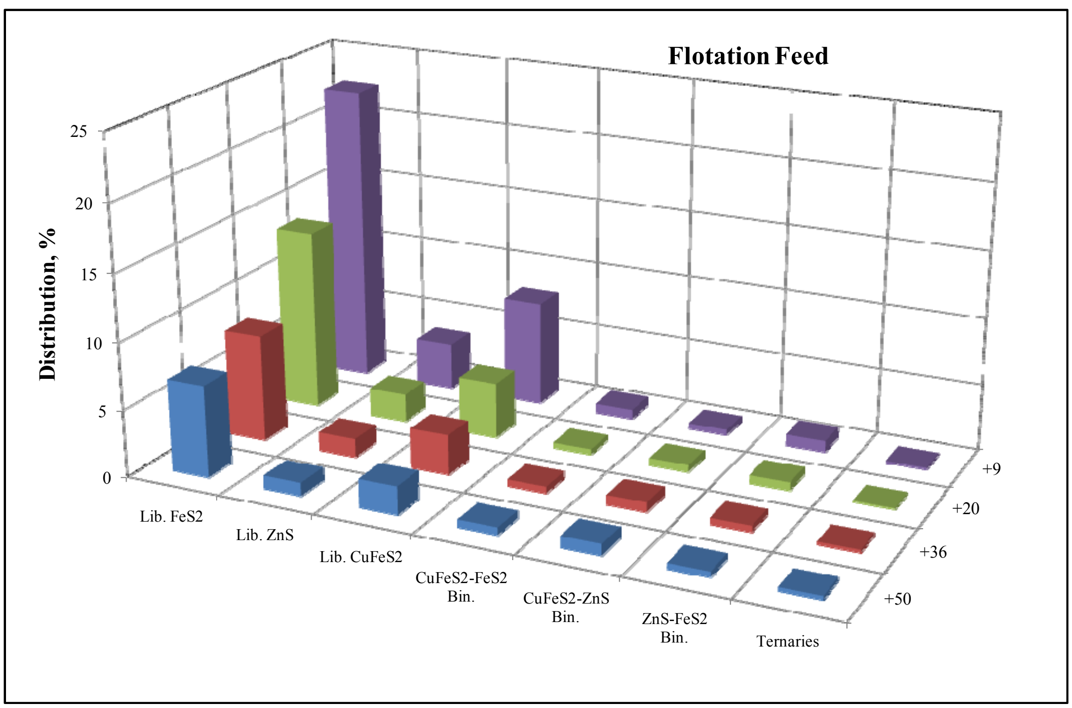

Modal analysis of the plant feed for different size fractions for Spec ore

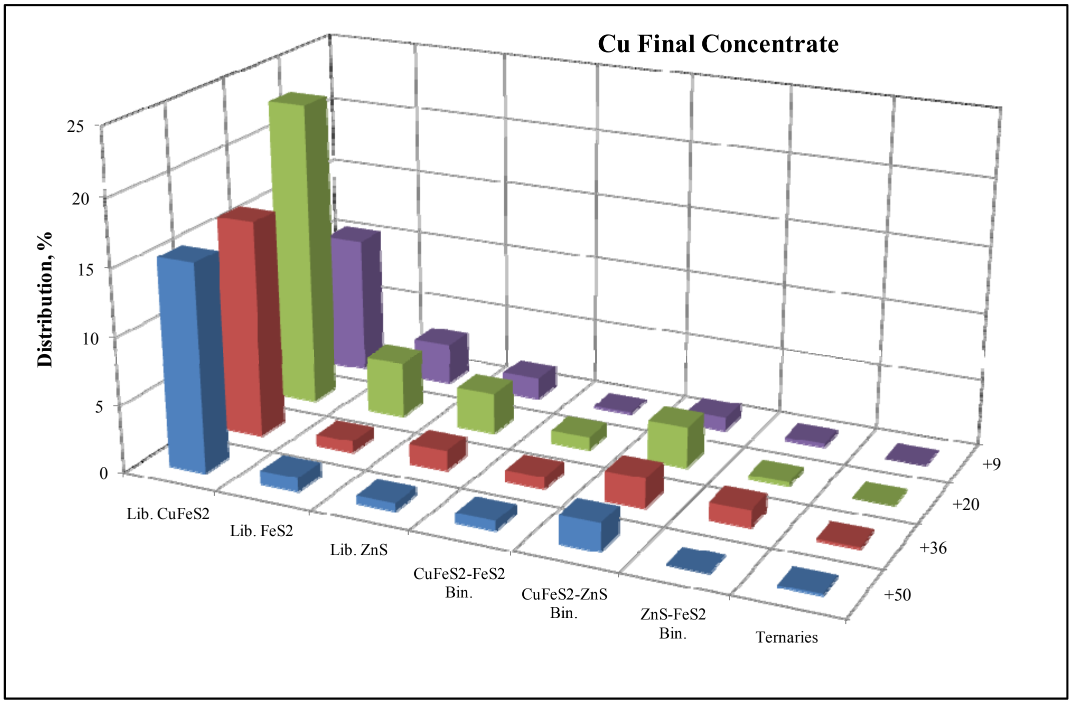

Modal analysis of Cu final concentrate for different size fractions for Non-Spec ore

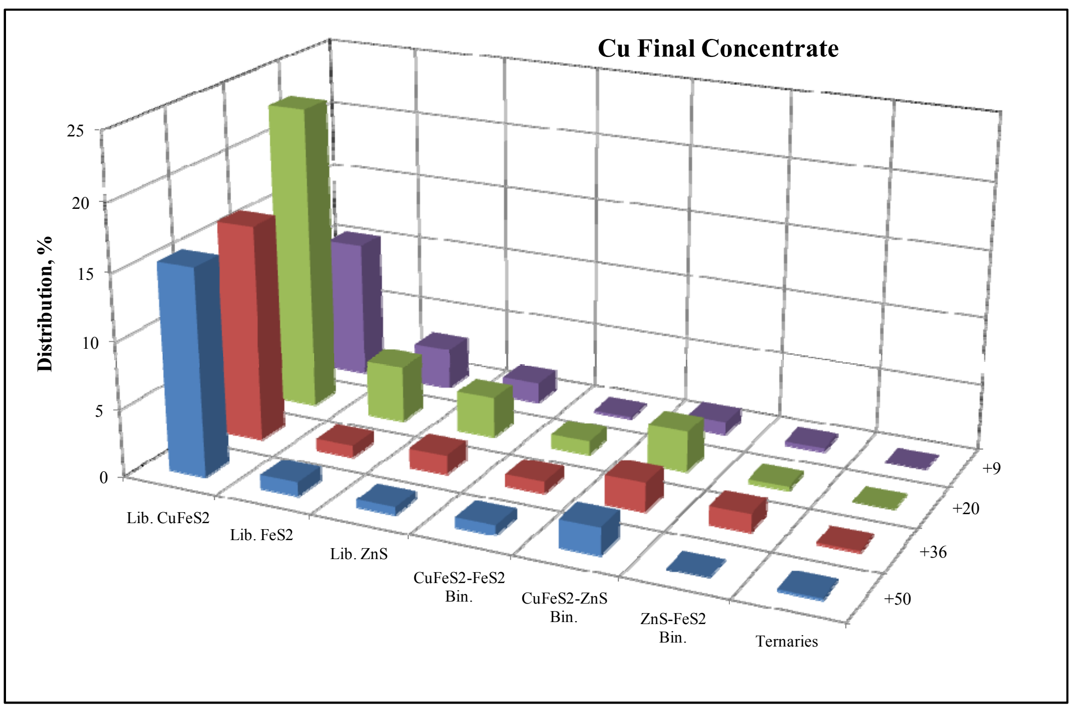

Modal analysis of Cu final concentrate for different size fractions for Spec ore

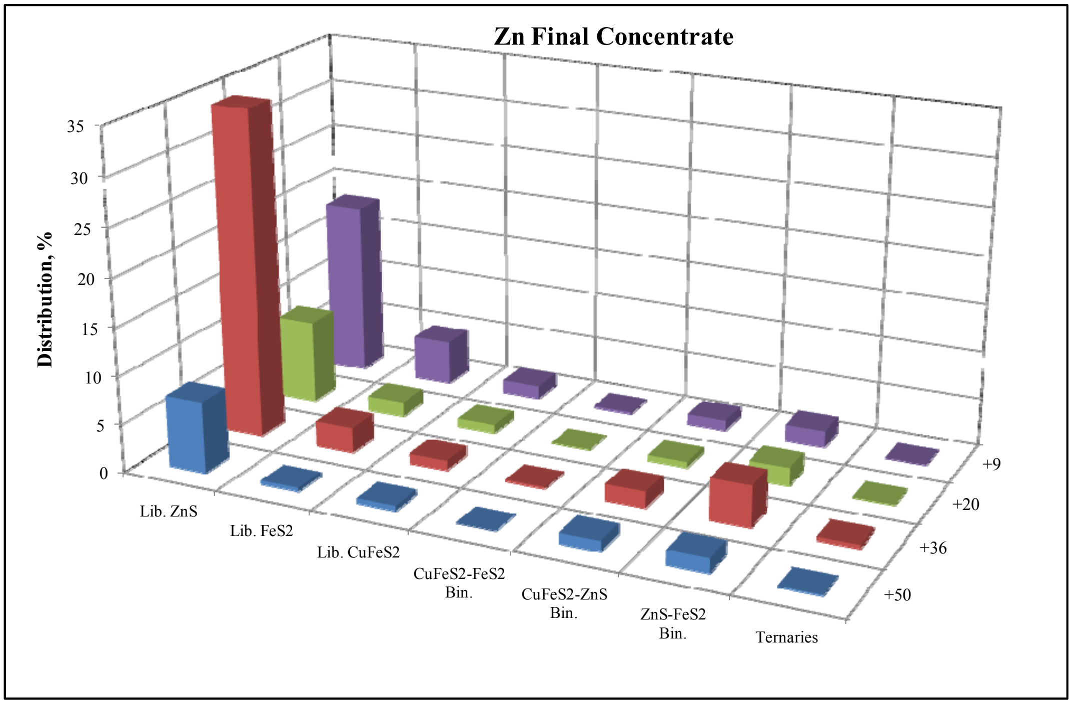

Modal analysis of Zn final concentrate for different size fractions for Non-Spec ore

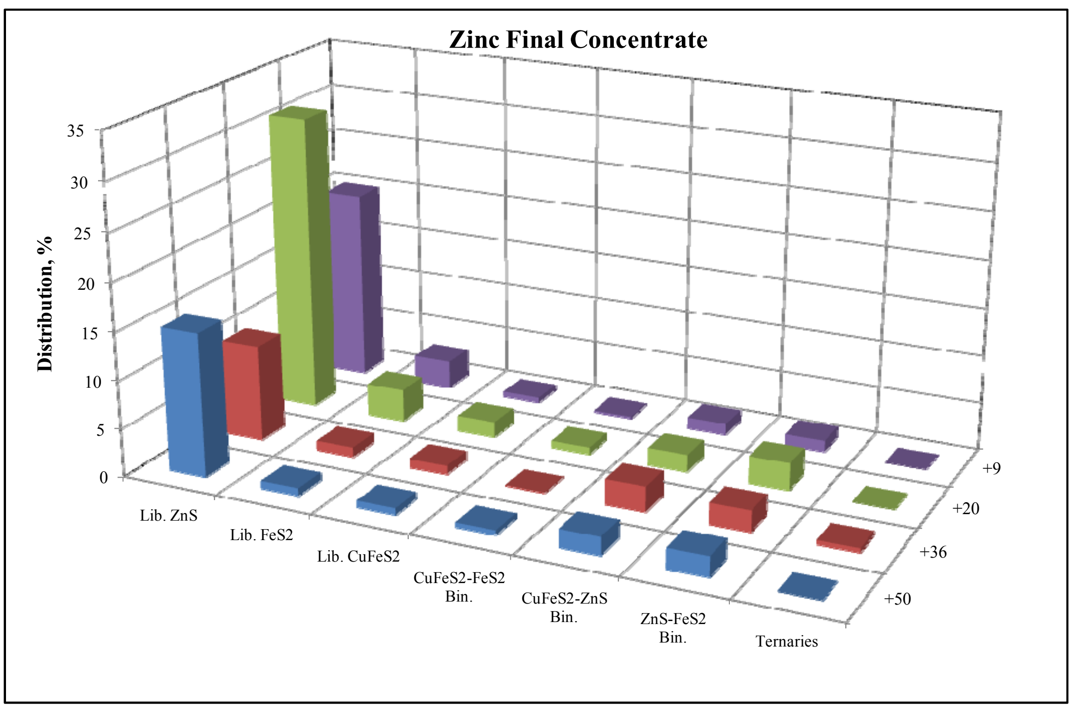

Modal analysis of Zn final concentrate for different size fractions for Spec ore

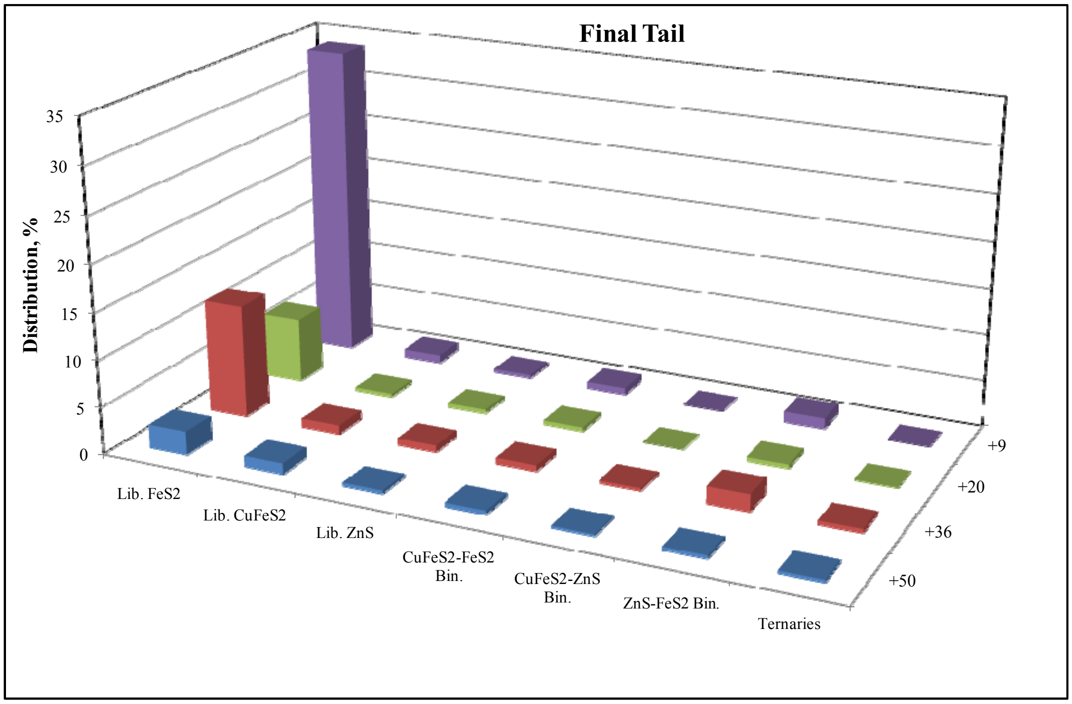

Modal analysis of final tail for different size fractions for Non-Spec ore

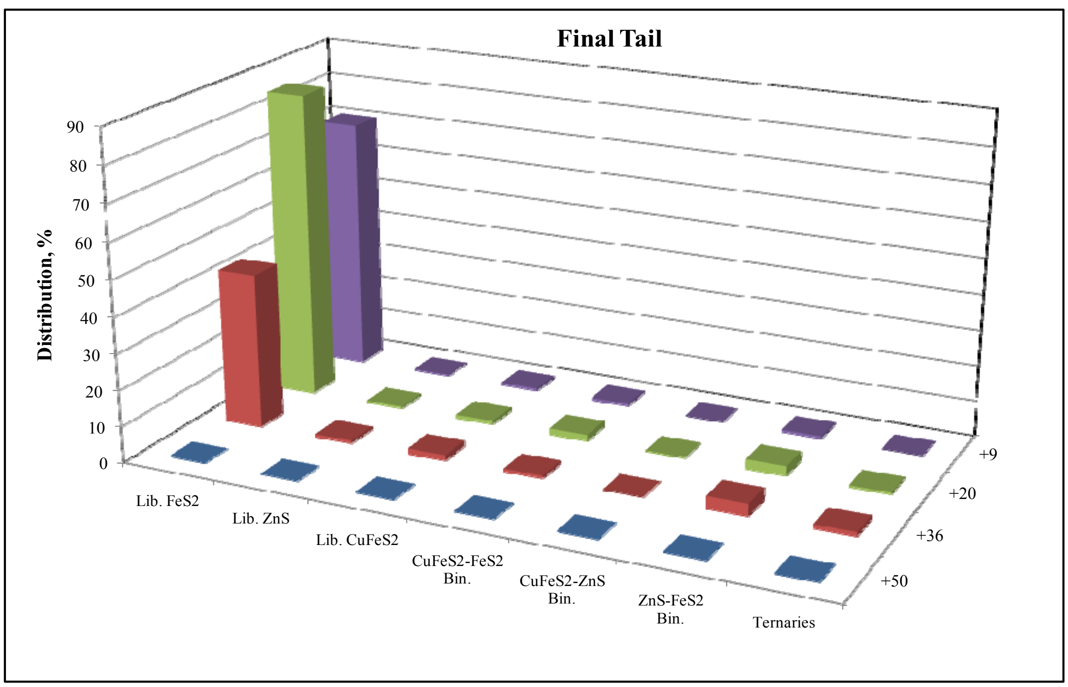

Modal analysis of final tail for different size fractions for Spec ore

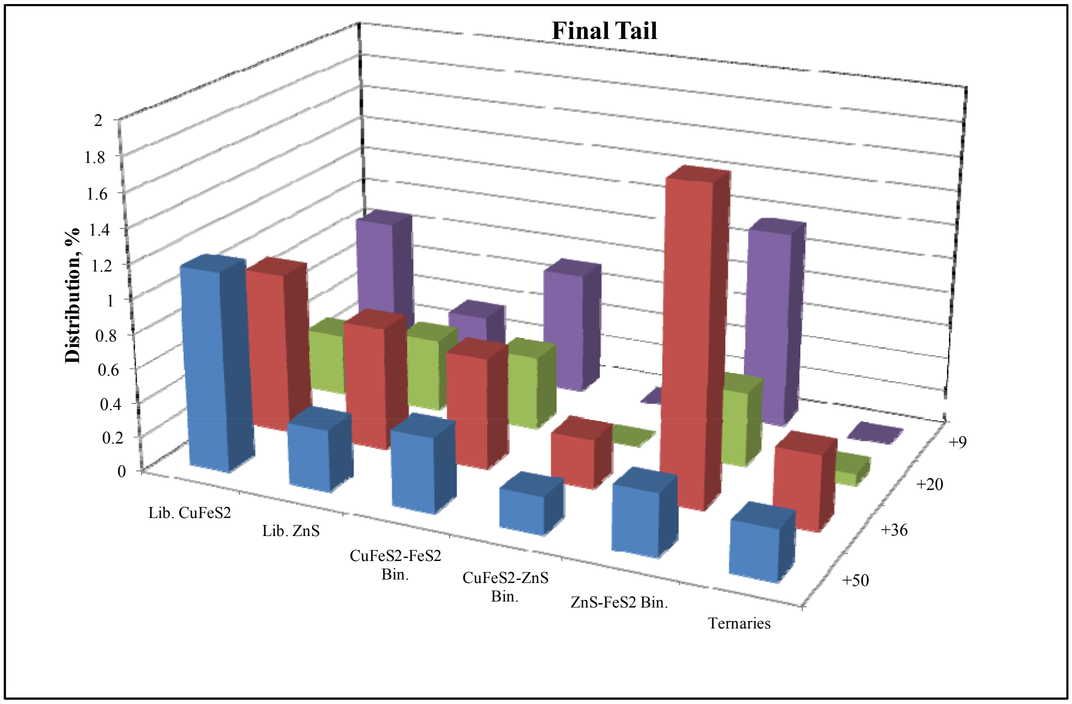

Modal analysis of final tail in the absence of pyrite for Non-Spec ore

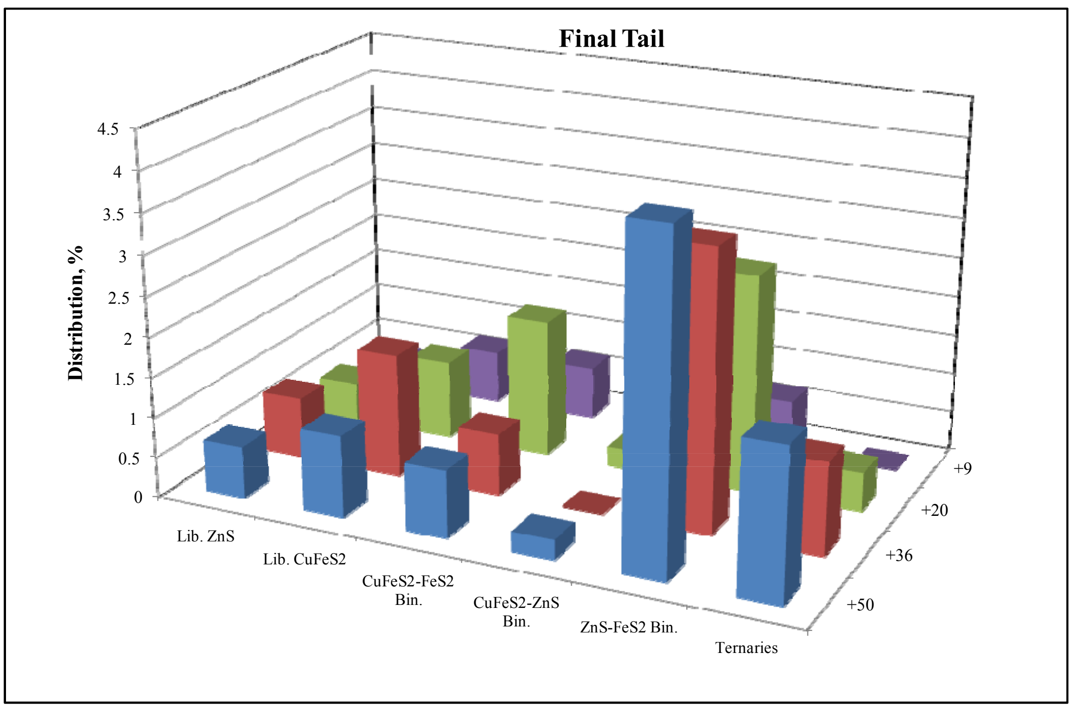

Modal analysis of final tail in the absence of pyrite for Spec ore

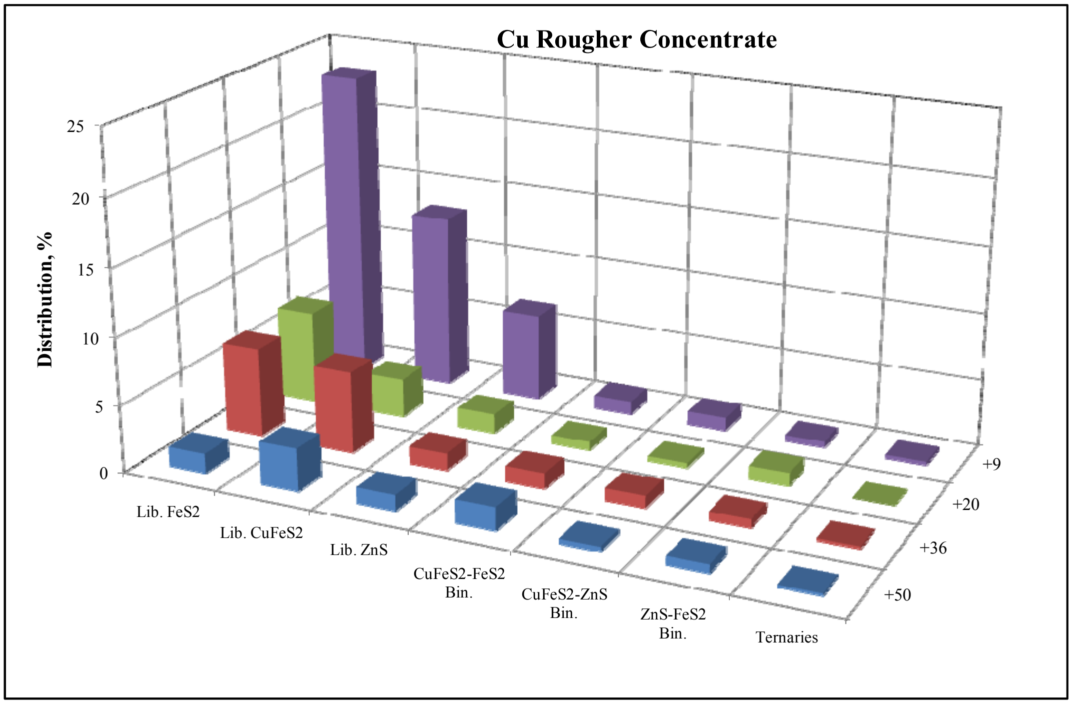

Modal analysis of Cu Rgh concentrate for different size fractions for Non-Spec ore

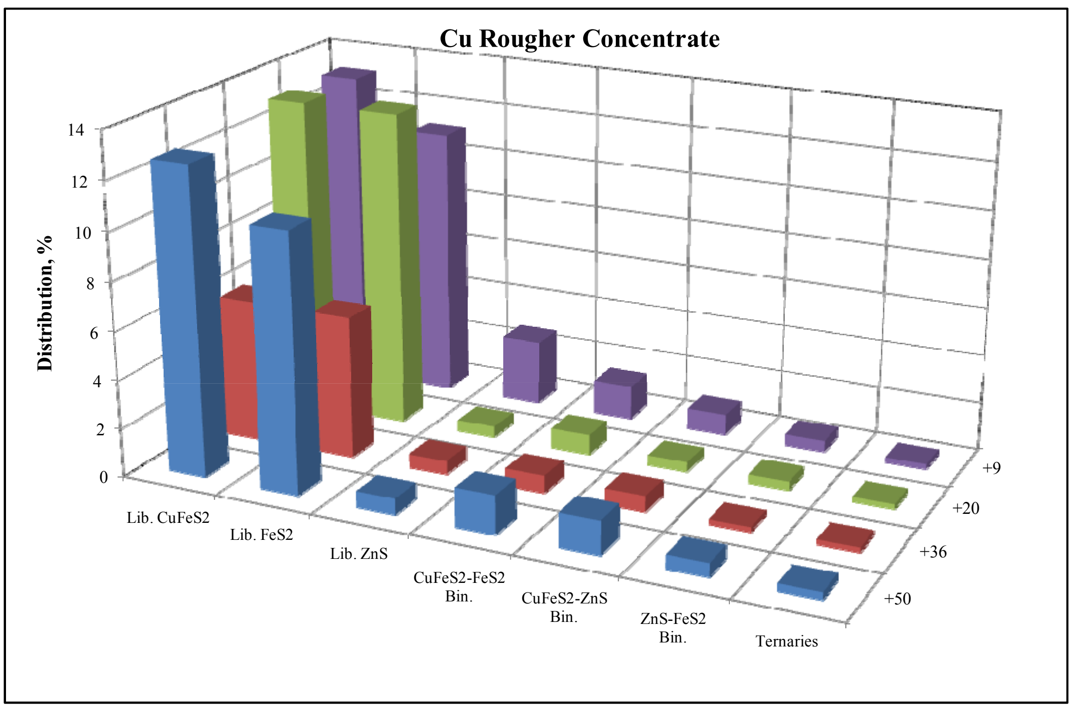

Modal analysis of Cu Rgh concentrate for different size fractions for Spec ore

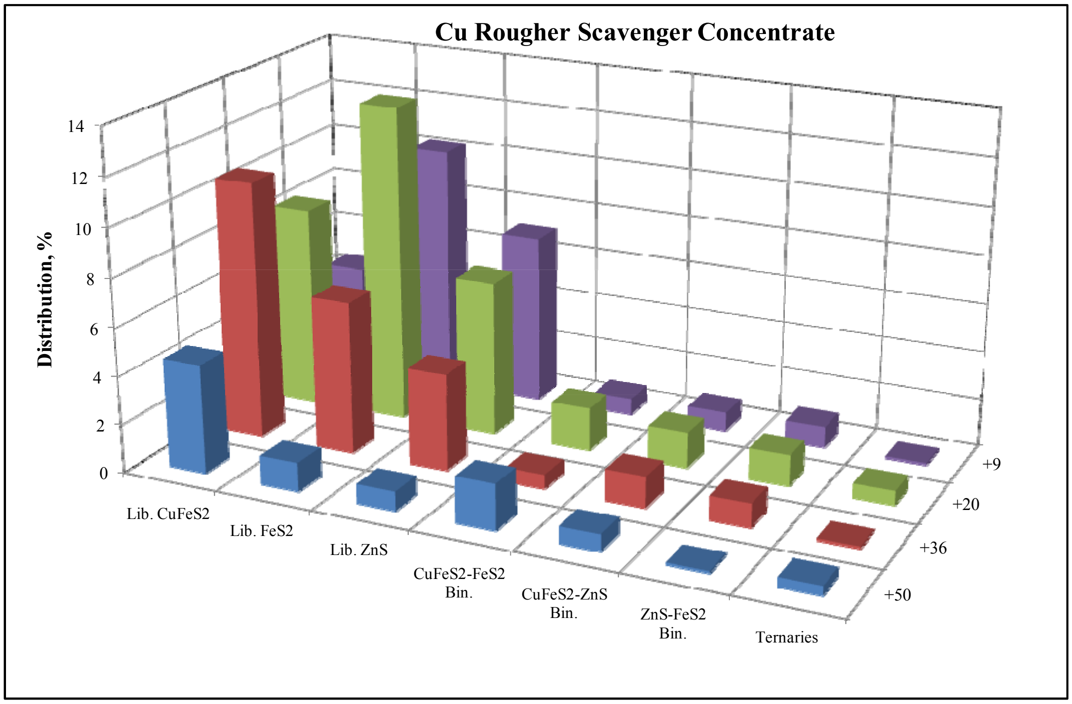

Modal analysis of Cu Rgh Scav concentrate for different size fractions for Non-Spec ore

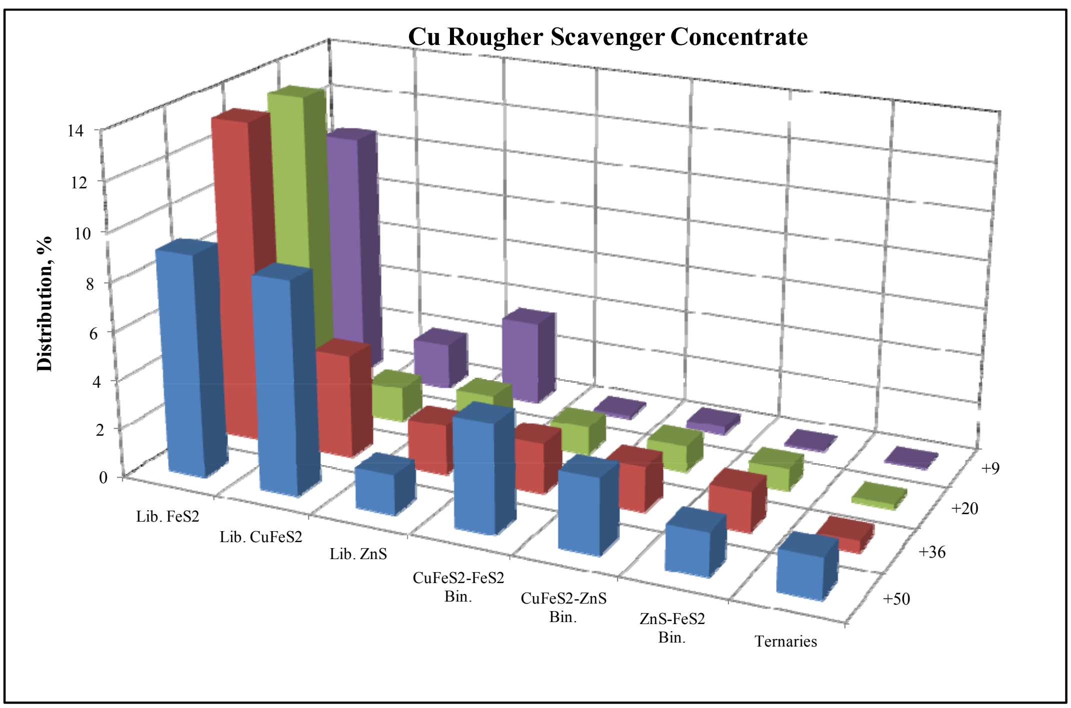

Modal analysis of Cu Rgh Scav concentrate for different size fractions for Spec ore

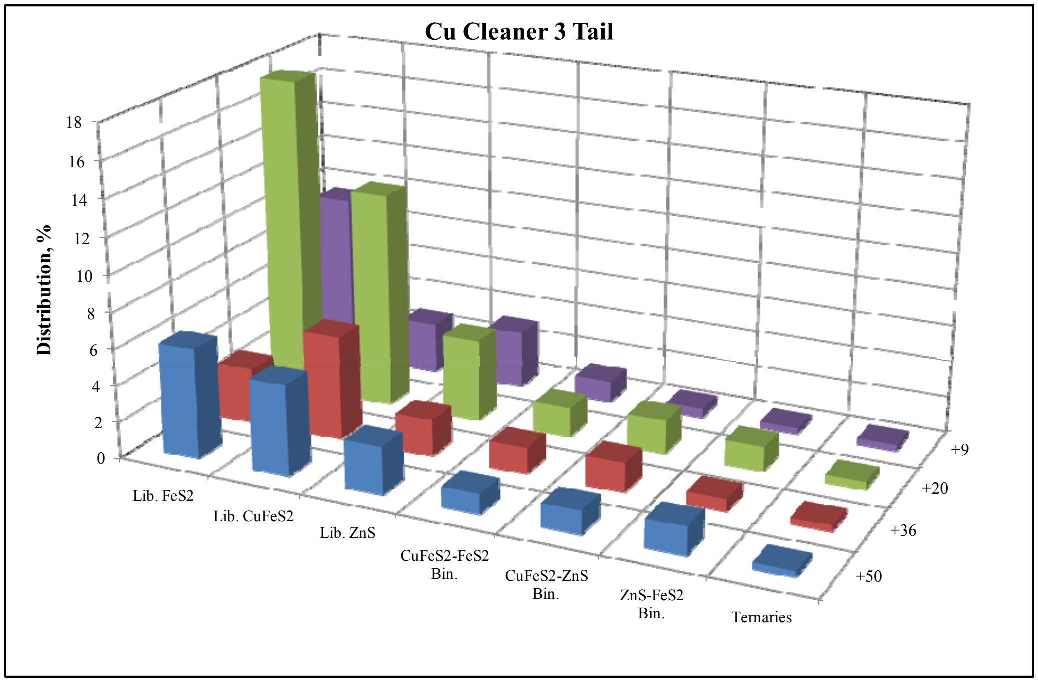

Modal analysis of Cu Cl 3 Tail for different size fractions for Non-Spec ore

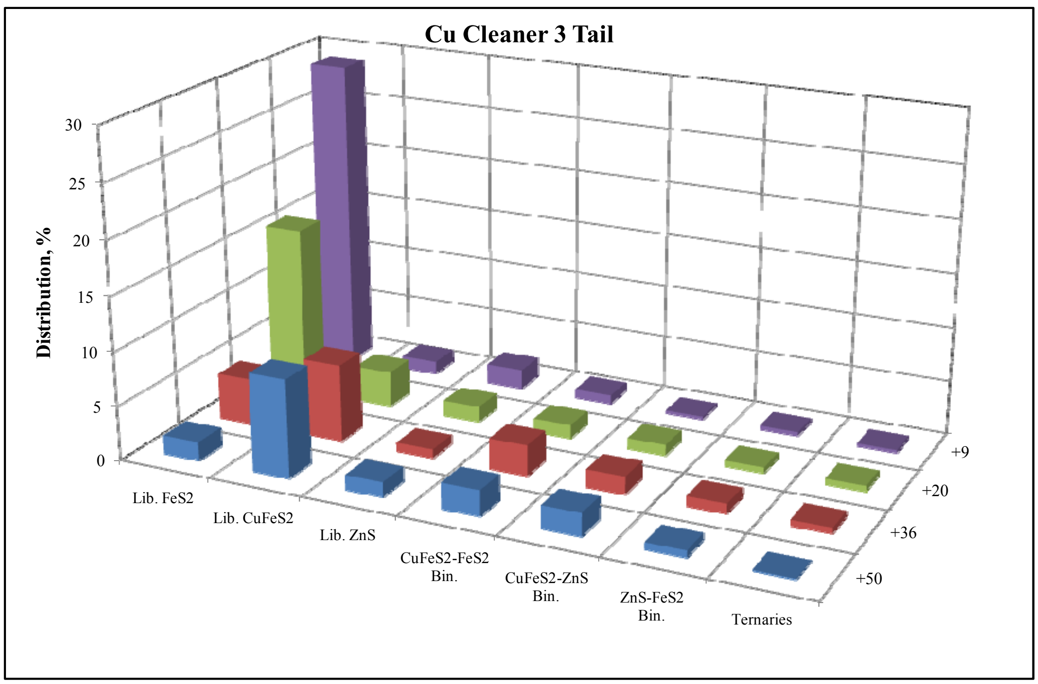

Modal analysis of Cu Cl 3 Tail for different size fractions for Spec ore

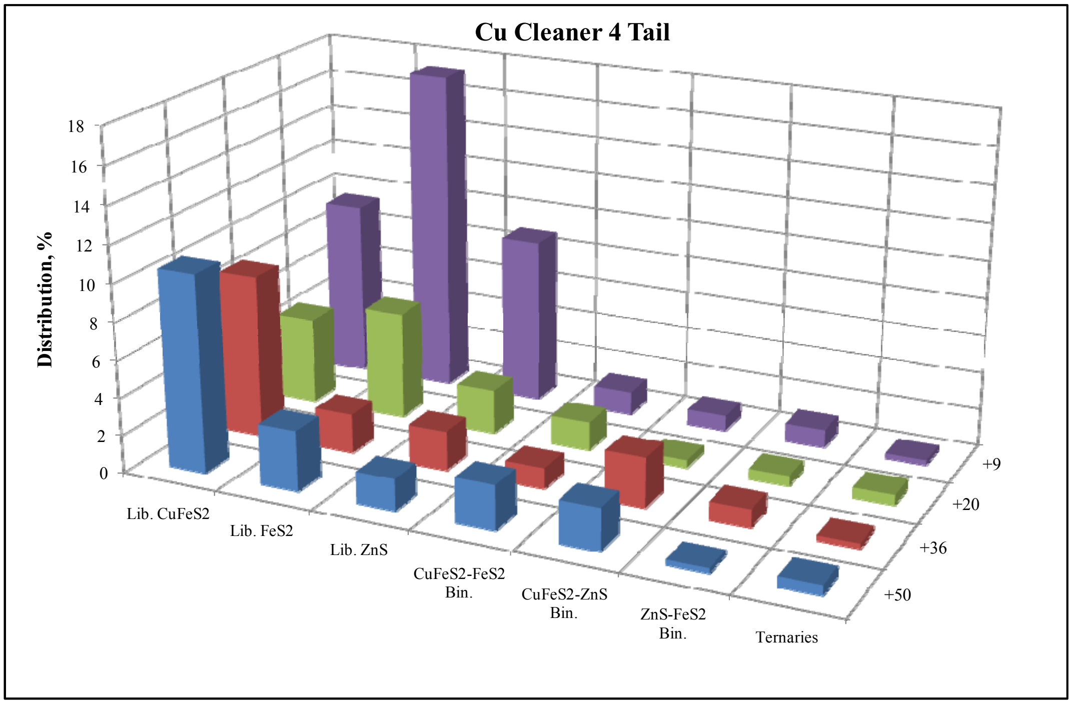

Modal analysis of Cu Cl 4 Tail for different size fractions for Non-Spec ore

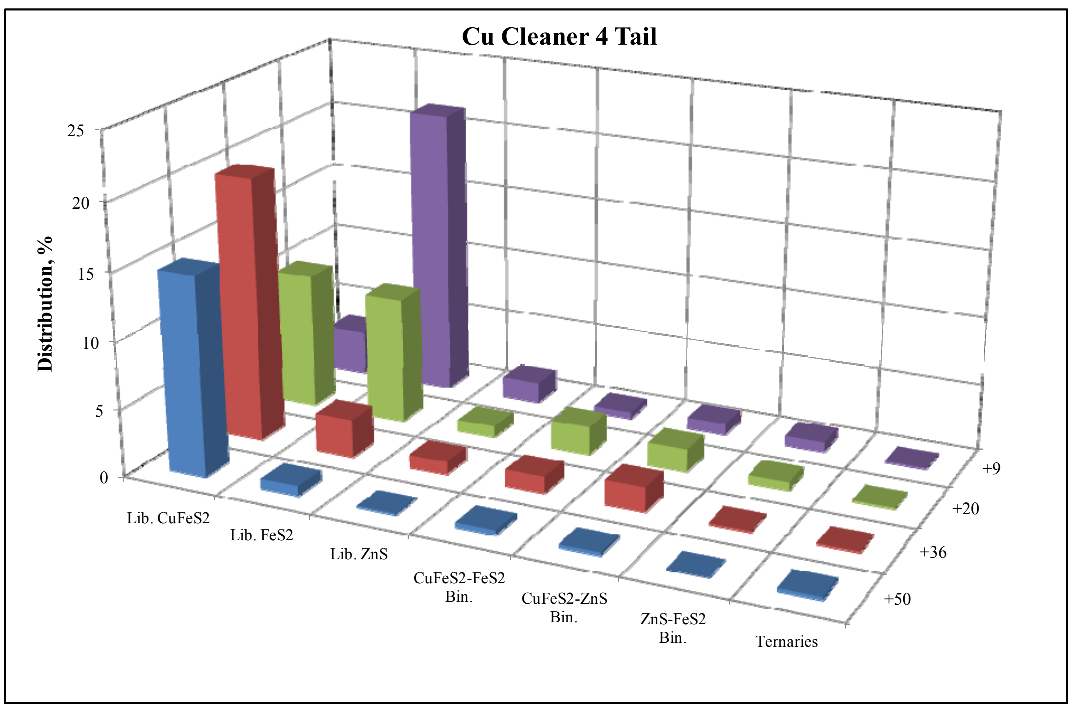

Modal analysis of Cu Cl 4 Tail for different size fractions for Spec ore

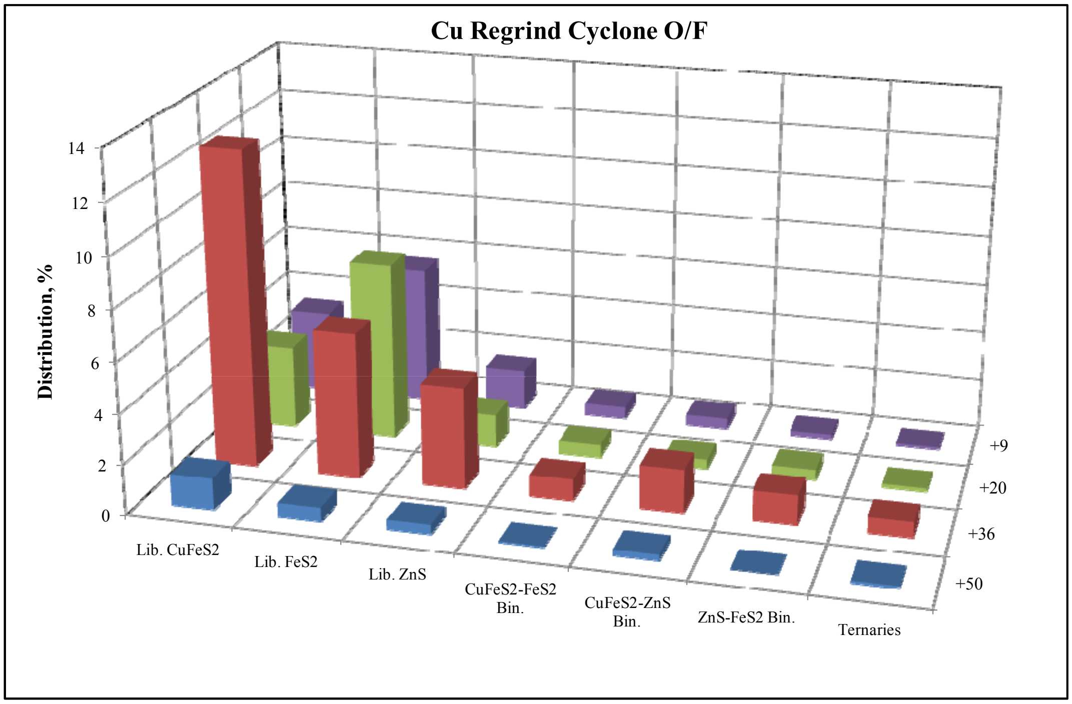

Modal analysis of Cu RG Cyclone O/F for different size fractions for Non-Spec ore

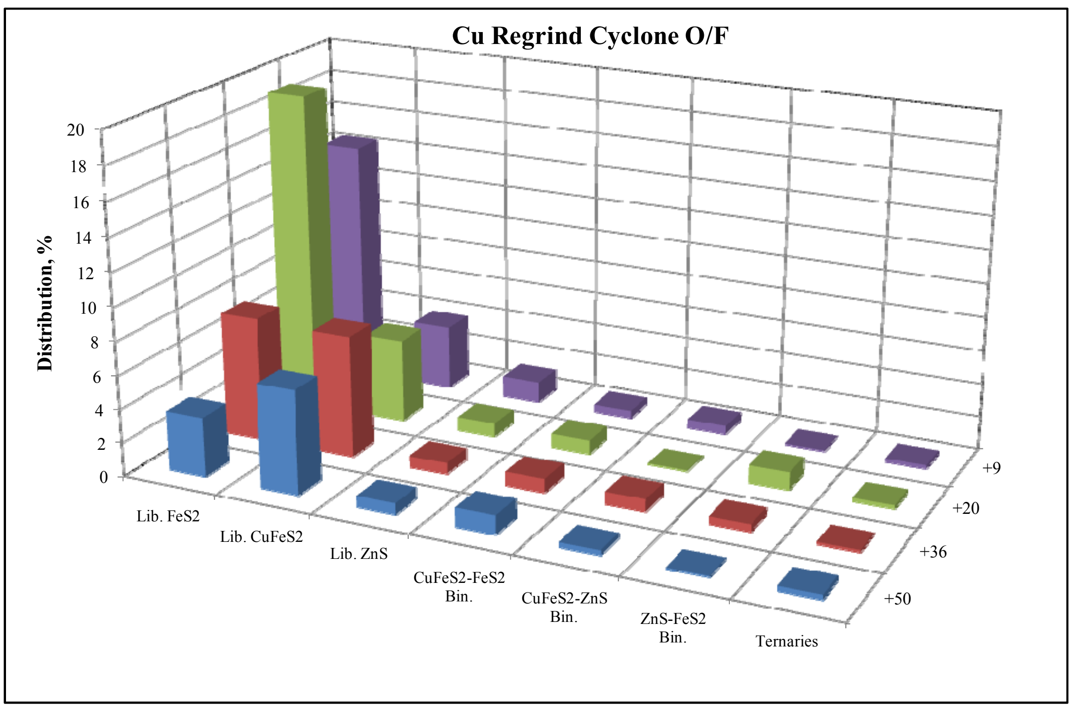

Modal analysis of Cu RG Cyclone O/F for different size fractions for Spec ore

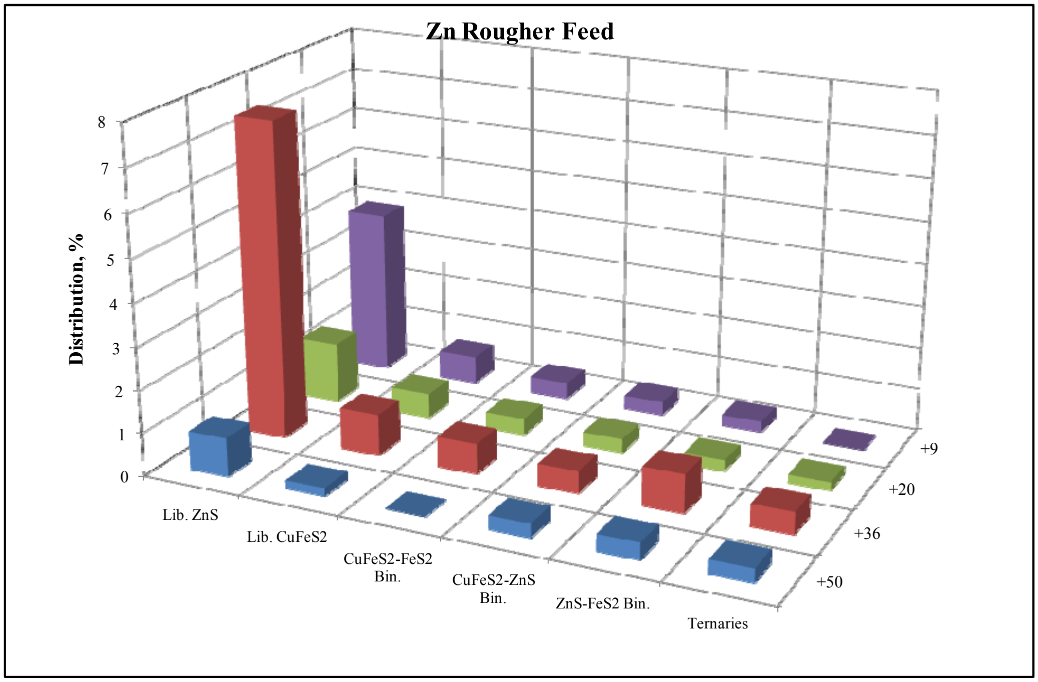

Modal analysis of Zn Rougher Feed for different size fractions for Non-Spec ore

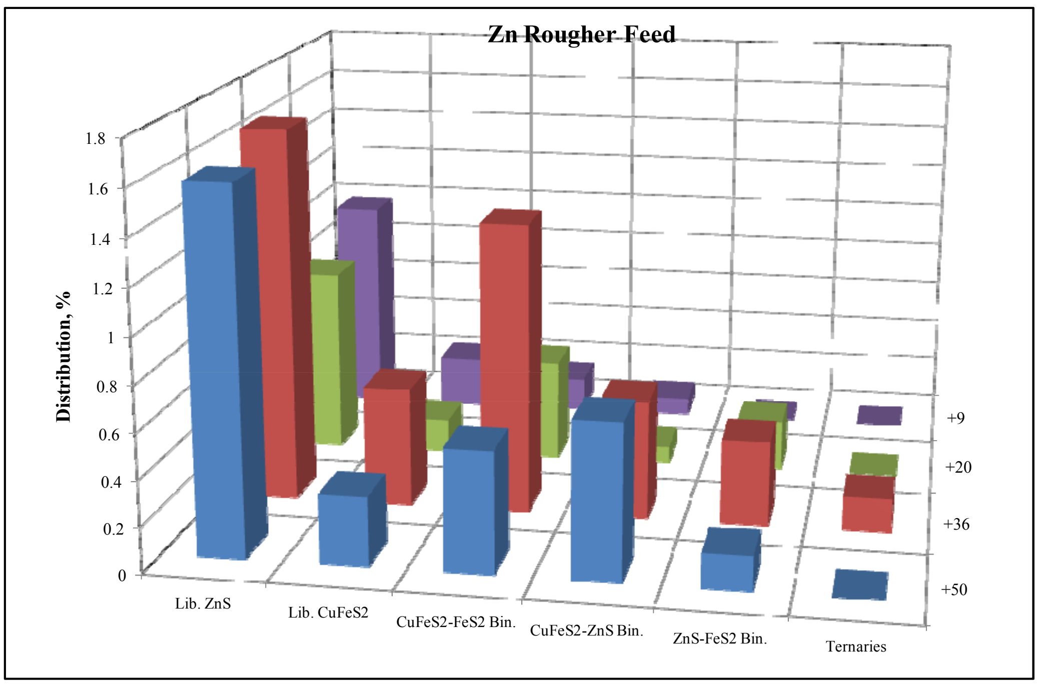

Modal analysis of Zn Rougher Feed for different size fractions for Spec ore

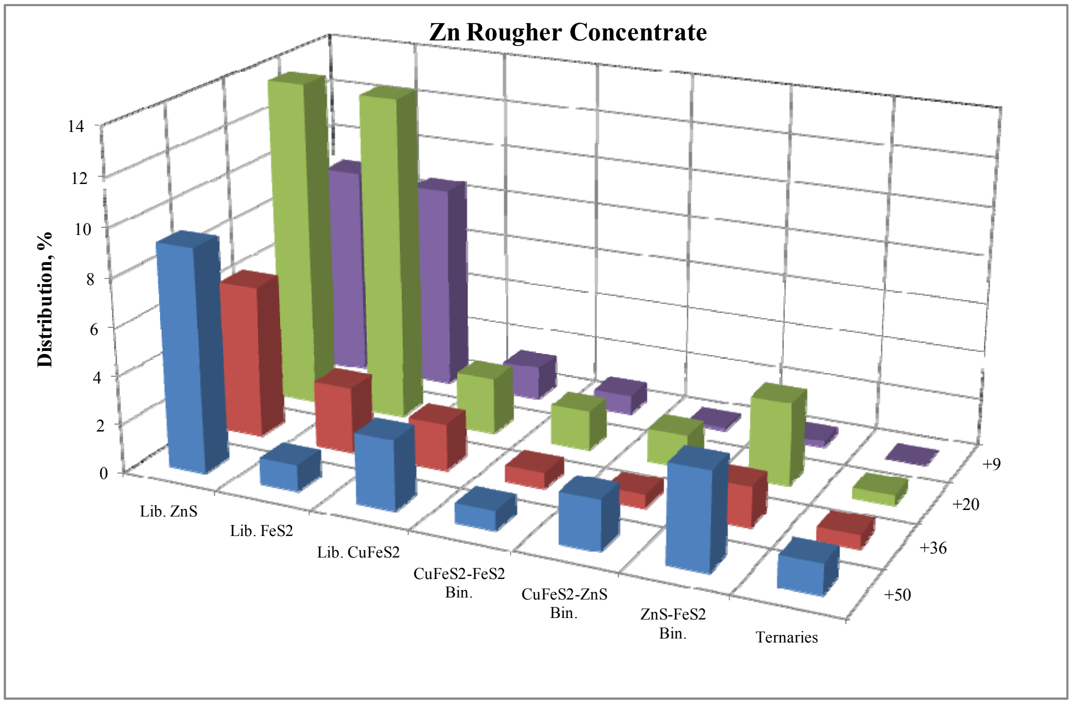

Modal analysis of Zn Rougher Concentrate for different size fractions for Non-Spec ore

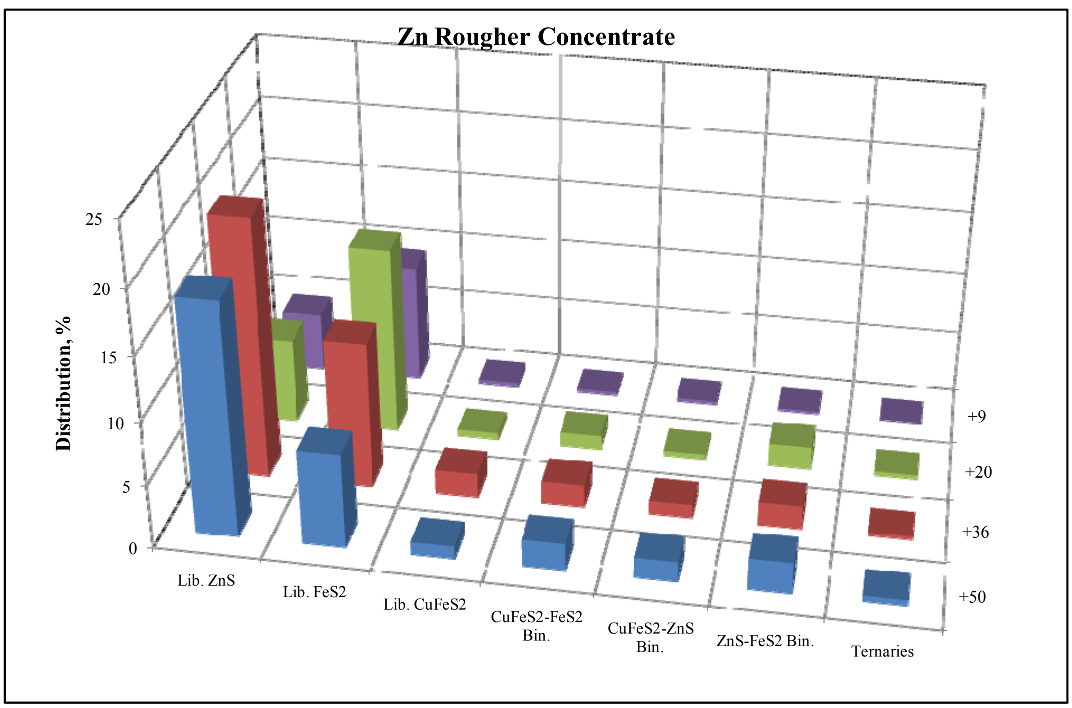

Modal analysis of Zn Rougher Concentrate for different size fractions for Spec ore

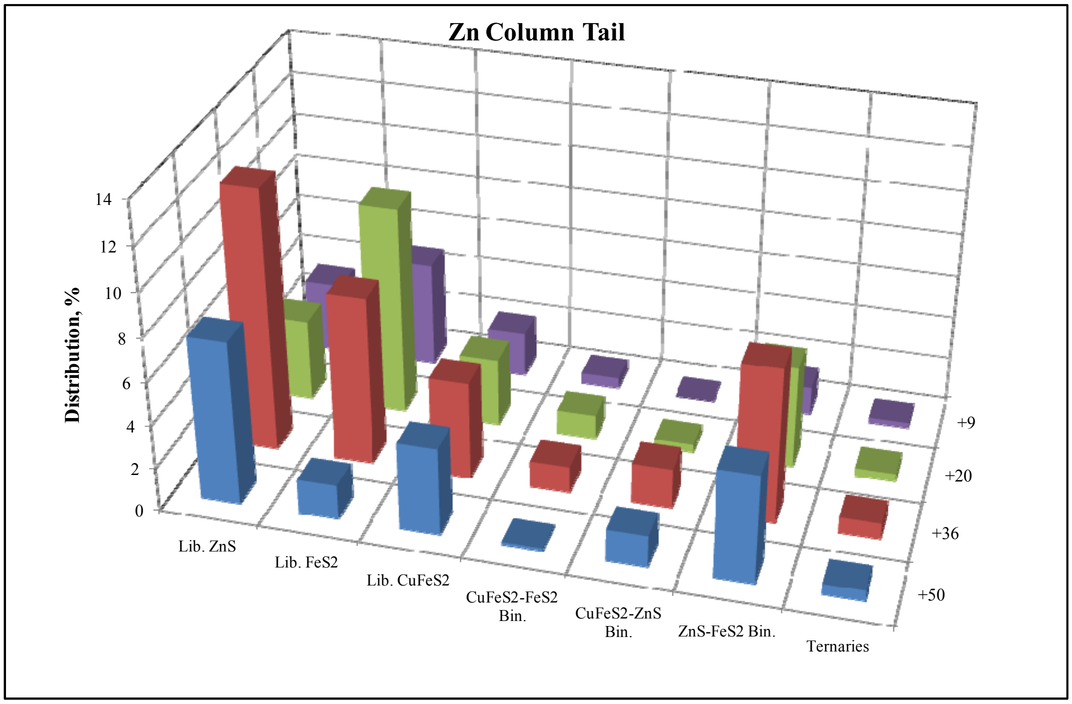

Modal analysis of Zn Column Tail for different size fractions for Non-Spec ore

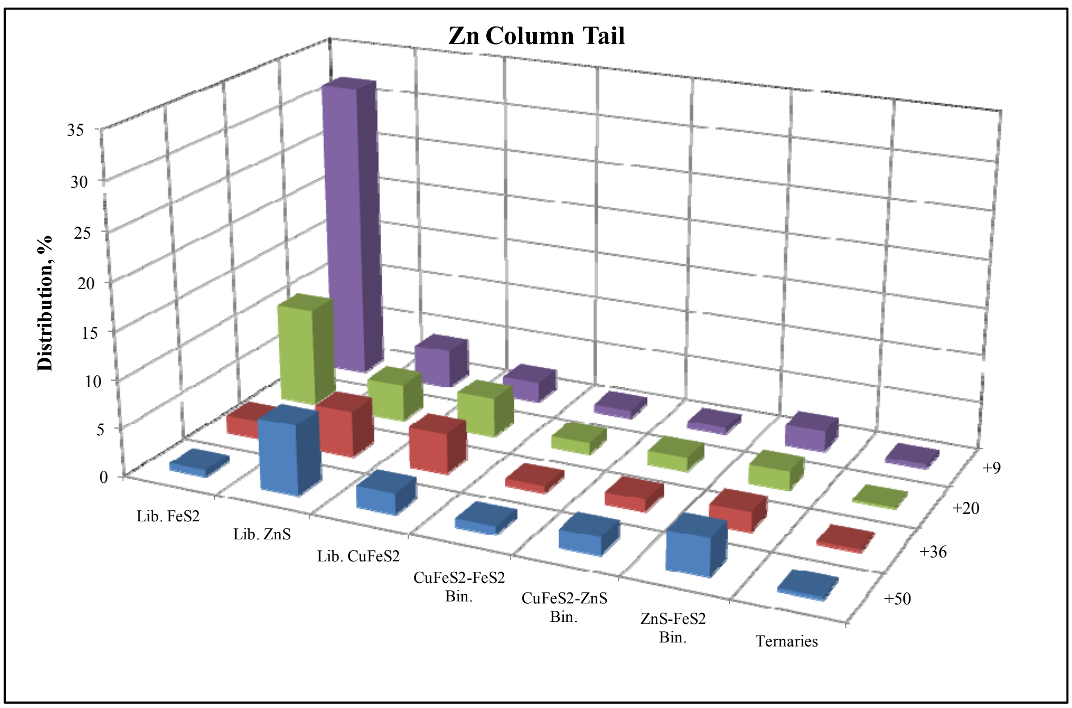

Modal analysis of Zn Column Tail for different size fractions for Spec ore

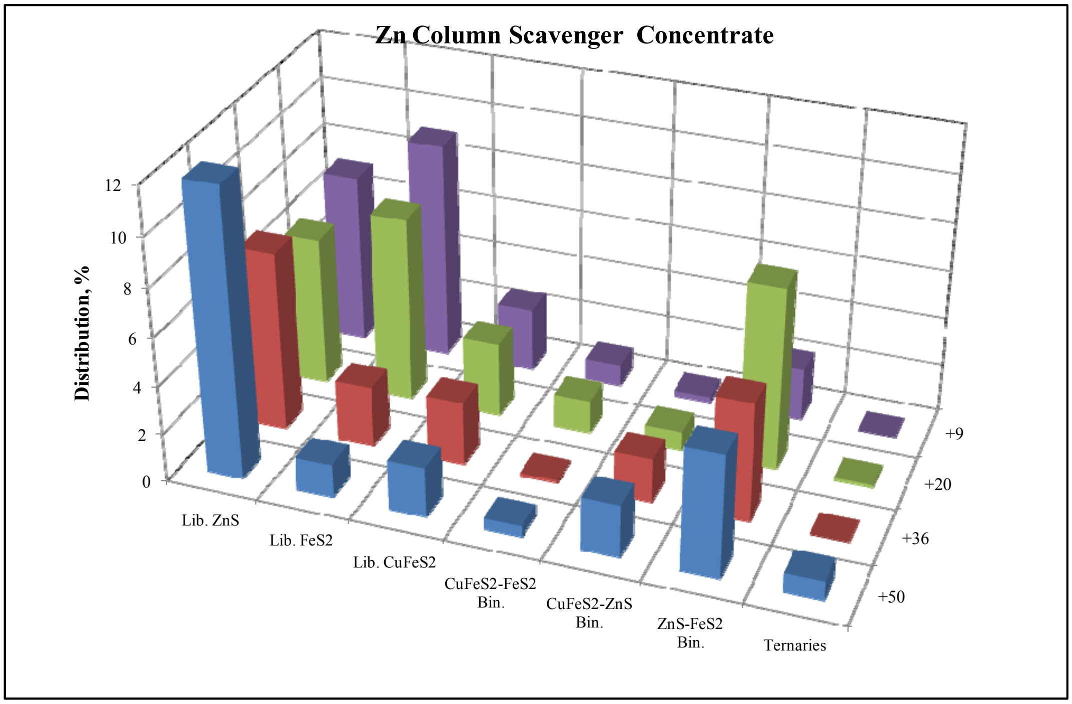

Modal analysis of Zn Column Scavenger Concentrate for different size fractions for Non-Spec ore

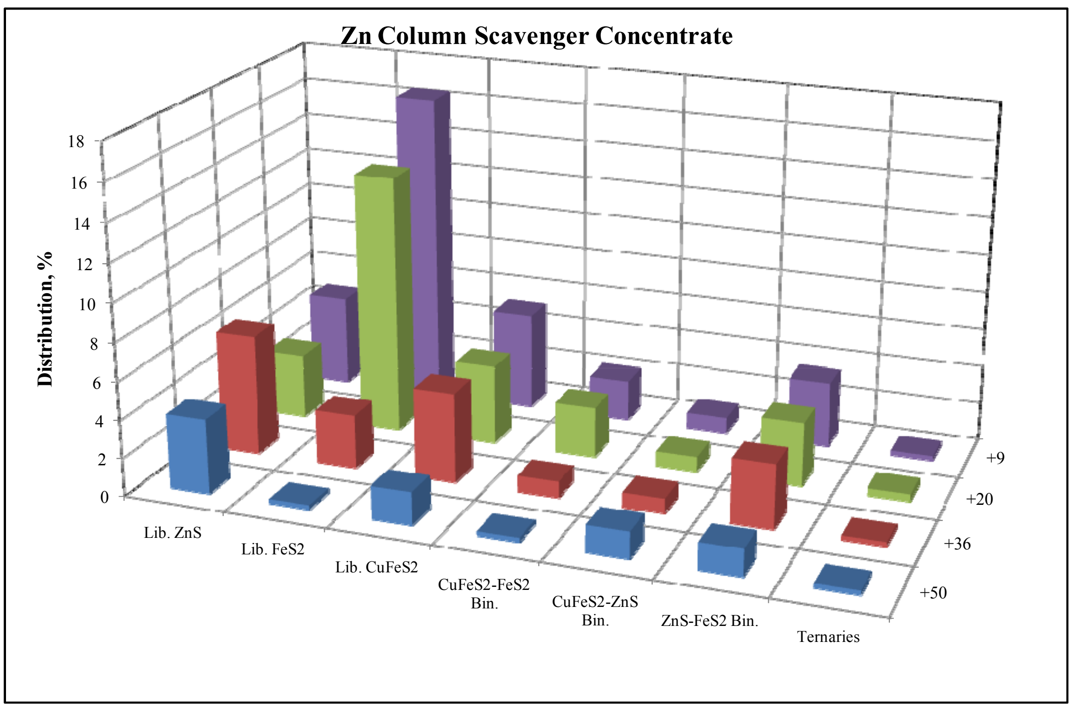

Modal analysis of Zn Column Scavenger Concentrate for different size fractions for Spec ore

RESUMÈ

Name Surname	:	Serkan Dikmen
Birth Place	:	Ankara
Date of Birth	:	17-08-1976
Marital Status	:	Single

Education:

High School	1990.-1993	Ankara Atatürk Lisesi
Graduate	1993-1998	Hacettepe University Mining Engineering Department

Language: English

Job Experience:

1999-2008 Research Assistant, Hacettepe University Mining Engineering Department